Dune dynamics under specific constrains of flow discharge and sediment supply

Dissertation

submitted to and approved by the

Department of Architecture, Civil Engineering and Environmental Sciences
University of Braunschweig – Institute of Technology

and the

Department of Civil and Environmental Engineering
University of Florence

in candidacy for the degree of a
Doktor-Ingenieur (Dr.-Ing.) /
Dottore di Ricerca in Mitigation of Risk due to Natural Hazards on Structures and Infrastructures[*)]

by
Andrea Corridori
Born 16 December 1982
from Grosseto, Italy

Submitted on	15 January 2013
Oral examination on	23 April 2013
Professorial advisors	Prof. Enio Paris Prof. Andreas Dittrich

2013

*) Either the German or the Italian form of the title may be used.

Contents

List of symbols

c	Speed of the crest of the dunes
$c_{adim} = \frac{c}{D_{50}}$	Dimensionless celerity of bed features
$C = \frac{U}{u_*}$	Chézy coefficient
$C' = 5.75 \log\left(\frac{12Rid}{ks}\right)$	Grain related Chézy coefficient
D_{50}	Characteristic particle diameter of bed material *(50th percentile of distribution)*
D_m	Mean particle diameter of bed material
$D_* = D_{50}(\frac{(s-1)g}{\nu^2})^{\frac{1}{3}}$	Dimensionless grain size
e	Void ratio
g	Gravitational acceleration
k_S	Equivalent sand roughness height
Ql	Flow discharge
ql	Flow discharge per unit of width
$ql_* = \frac{ql}{\sqrt{g \cdot D_{50}^3}}$	Dimensionless flow discharge per unit of width
Qs	Sediment supply
qs	Sediment supply per unit of width
q_{tf}	Feed rate per unit of width
R_{Hyd}	Hydraulic radius
Rb	Hydraulic mean radius of bed (side wall correction applied)
Re	Reynolds number
$s = \frac{\rho_s}{\rho_w}$	Specific gravity
S_f	Energy slope
$T = \frac{\tau' - \tau_{cr}}{\tau_{cr}}$	Bed shear stress (Van Rijn) parameter
u_*	Shear velocity
u'_*	Grain related shear velocity
u_{*cr}	Critical shear velocity
U	Mean flow velocity
$U_{adim} = \frac{U}{D_{50}}$	Dimensionless mean flow velocity
Y	Mean water depth
$Y_{adim} = \frac{Y}{D_{50}}$	Dimensionless mean water depth

Continued on next page

γ_S	Specific weight of sediment
γ_W	Specific weight of water
Δ	Height of bed features
$\Delta_{adim} = \frac{\Delta}{D_{50}}$	Dimensionless height of bed features
$\theta = \frac{\tau}{(\rho_s - \rho_W) g d}$	Shields parameter
λ	Wavelength of bed features
$\lambda_{adim} = \frac{\lambda}{D_{50}}$	Dimensionless wavelength of bed features
μ	Dynamic viscosity
ν	Kinematic viscosity coefficient
ρ_s	Density of sediment
ρ_w	Density of water
τ	Shear stress
τ_b	Bed shear stress
τ_{cr}	Critical shear stress
τ'	Shear stress based on grain roughness
τ''	Shear stress based on shape of bed forms
ϕ	Porosity of the bed material

SUMMARY

Rivers have always been a necessary aid for the development of civilizations and cities. The proximity of a river has always delivered vital support to populations for their livelihood as well as for commercial and civil transportation. Human presence over the years has increased its impact on rivers due to the increase in activities and urbanization along its flow. This phenomenon brings two consequences which complicate the co-existence between man and river. On the one hand, the river is more controlled, the natural "flooding" areas around it are reduced and confined by embankments; on the other hand, there is an increase in the damage from floods. It is important to improve our knowledge of river processes in order to increase the quality of modelling for reliable predictions, design and maintenance of the river system itself. In particular, these factors require an increase of the resistance that a bed provides to the liquid flow. The drag can be subjected to a significant change, in time and space, especially in movable bed conditions because, in addition to the resistance of the transported grains, an additional resistance due to the configuration assumed by the bed can arise; often this resistance can be crucial in the determination of the total resistance. The total resistance can vary considerably since it may be strongly affected by bedform geometrical characteristics such as size and shape. For this reason, compared to unerodable riverbeds, the uncertainties on the evaluation of flow resistance, and consequently of the depth of the water, grows significantly in the case of a movable bed. The aim of this thesis is to analyse bed form dynamics under the condition of imposed constraints of independent variables. In particular, the response of dunes to changes in sediment supply is investigated through laboratory experiments carried out by varying sediment supply under constant water discharge. Complementary experiments have been conducted by varying water discharge under constant sediment supply. In this way two attempts are made: to better understand the processes involving the development of bed forms and flow resistance, and to decrease uncertainty in friction factor predictions. Experiments conducted in a sand bed flume allowed us to observe the behaviour of the dunes in terms of changes of the celerity, height and length, and the average slope of the bottom was also observed. The experiments were conducted in simplified conditions: the flow was steady and uniform on average, the sediment transport of almost uniform sand was exclusively bed load, with a bottom covered by two-dimensional dunes. Two types of experimental

cycles were used based on whether the flow rate or the sediment supply was kept constant: each experimental cycle starts in a state of sedimentological and hydraulic equilibrium; then a variation of the liquid flow or of the sediment supply is imposed. In this way the equilibrium between solid transport and sediment transport capacity was modified. As a consequence to the imposed unbalance, the flow and bed geometry adjust their characteristics such as bed slope, water depth, size and celerity of bed forms until a new equilibrium condition is reached. Each cycle is characterized by a number of imposed variations in liquid flow or sediment supply and, therefore, by an equal number of equilibrium states: Measurements related to the transition conditions together with those characterizing the equilibrium states were recorded. In this work, only data concerning the equilibrium states are considered. The analysis of experimental data highlights the role played by the dune dynamics as a response to the imposed change of flow over a movable bed. A physically based model was implemented to reproduce the phenomena observed during the laboratory experiments, in an attempt to a extend the understanding of the dune dynamics. The physically based model is referred to steady and spatially averaged uniform flow, using the basic equations of mechanics, such as momentum and mass conservation. Furthermore, the model was applied to give a definition of the existence conditions of the dunes and to define, in this way, the extent of the channel's potential adaptive behaviour in response to an imbalance between the sediment transport capacity of the liquid flow and the effective availability of solid material.

SOMMARIO

I fiumi sono sempre stati un necessario aiuto per lo sviluppo di civiltà e città. La vicinanza di un fiume ha sempre consegnato alla popolazione un aiuto per la propria sussistenza oltre ad un valido mezzo di trasporto commerciale e civile. La presenza umana, negli anni, ha aumentato il proprio impatto sul fiume, causato da un aumento di attività e abitazioni lungo il suo scorrere. Questo fenomeno porta con se una duplice conseguenza che complica la convivenza tra uomo e fiume. Il fiume vede diminuita la sua capacità naturale di ridurre il suo carico idraulico e la sua velocità durante gli eventi di piena; tratti meandriformi utilizzati dal fiume per esondare naturalmente spesso vengono eliminati rettificandoli e arginandoli. Inoltre aumentando le attività e le abitazioni nei terreni limitrofi al fiume aumenta il danno che una esondazione produrrebbe. Entrambi questi fattori richiedono un aumento della capacità di previsione di un corso d'acqua ed in particolare del valore della resistenza che un alveo offre alla corrente. La resistenza al moto puó subire, nel tempo e nello spazio, una notevole variazione del suo valore, questo fenomeno accentuato sopratutto in condizioni di fondo mobile; infatti oltre ai grani che vengono trasportati, la configurazione che il fondo può assumere, contribuisce alla generazione di una resistenza aggiuntiva e spesso determinante all'interno della resistenza complessiva o totale. Dunque, si deduce che la resistenza totale varia notevolmente nel tempo dipendendo, come ne sono dipendenti le forme di fondo, dalle caratteristiche idrauliche e di apporto sedimentologico del fiume; inoltre, rispetto ad alvei inerodibili le incertezze sulla valutazione delle resistenze al moto crescono notevolmente. Lo scopo di questa tesi è quello di analizzare le dinamiche delle forme di fondo al variare dell'apporto solido o al variare della portata liquida. In particolare, è stata investigata la risposta delle dune mediante due cicli di esperimenti, ogni ciclo è costituito da una successione di fasi di equilibrio: nel primo ciclo, è stato variato, per ogni fase, l'apporto solido della canaletta mentre la portata liquida viene tenuta costante, nel secondo ciclo, inversamente, viene tenuto costante l'apporto solido mentre viene fatta variare la portata liquida. Per entrambi i cicli si parte da una condizione di equilibrio e successivamente, si impone una variazione della portata liquida o della portata solida; la canaletta viene lasciata libera di adattarsi alle sue nuove condizioni di portata liquida o portata solida fin quando si raggiunge una nuova situazione di equilibrio. Durante il passaggio tra una condizione di equilibrio ad un' altra si registrano variazioni delle carat-

teristiche sedimentologiche ed idrauliche della canaletta diverse a seconda che si esegua un ciclo rispetto che un'altro. Durante i cicli sperimentali sono stati registrati i valori quali: la pendenza del fondo, la profondità dell'acqua, le dimensioni e celerità delle forme di fondo; le misure son relative alle condizioni di transizione e a quelle che caratterizzano gli stati di equilibrio. In questo lavoro solo i dati relativi agli stati di equilibrio sono stati considerati.

Gli esperimenti sono stati eseguiti in un canale rettilineo artificiale di tipo feed flume con letto sabbioso. Sono stati osservati e misurati il comportamento delle dune, in termini di cambiamenti dei valori medi della celerità, altezza e lunghezza, inoltre è stata misurata la pendenza media del fondo. Gli esperimenti sono stati condotti in condizioni semplificate: il flusso è stato stazionario e mediamente uniforme, il trasporto solido, con sabbia uniforme, è stato esclusivamente al fondo e le dune formatesi hanno avuto caratteristiche bidimensionali. L'analisi dei dati sperimentali sottolinea il ruolo svolto dalla dinamica dunale come risposta al cambiamento imposto dal flusso solido o liquido su un letto mobile. Per analizzare i dati raccolti sperimentalmente, per riprodurre gli esperimenti e per incrementarli, è stato implementato un modello matematico basandosi su relazioni fisiche e sperimentali fornite dalla letteratura e sulle prove sperimentali compiute. Inoltre, il modello è stato applicato per definire le condizioni di esistenza della dune e definire, in questo modo, le condizioni di esistenza di un potenziale comportamento adattativo del canale, fortemente influenzato dalle caratteristiche che assumono le dune, in risposta ad uno squilibrio tra la capacità di trasporto solido e la disponibilità effettiva di materiale solido.

Part I

INTRODUCTION

Chapter 1

River dunes and associated flow resistance

In alluvial rivers, whenever the average shear stress exceeds the critical value, bed particles start to move and the process of sediment transport begins. Depending on the interaction between flow and sediment characteristics, the bed and water surfaces assume various forms. Among these, dunes can be considered the most important bed forms developed in sub-critical flows in sand beds. In fact, their dynamics may deeply affect the velocity distributions, resistance to flow and sediment transport processes. Yalin (1973),Garde and Ranga Raju (1985),Guy et al. (1966),Southard and Boguchwal (1990),Van Den Berg and Van Gelder (1993). Dunes have a relatively low height to length ratio and their dimensions are strongly related to the water depth van Rijn (1984b), Yalin (1973). The dune length is several times the water depth and dunes reach heights of up to one third of the water depth. The dunes become washed out when the flow regime is still subcritical. As the Froude number increases, an upper plane bed condition may be reached, followed by bed forms developing in a supercritical regime, such as standing waves and antidunes. Predictions of dune geometry are generally based on empirical models Gill (1971), Engelund and Fredsøe (1982), Yalin (1985), van Rijn (1984b). These models, which predict the bed states and the bedform dimensions, have been developed assuming uniform sediments and uniform flow conditions, i.e. the bedform formation is not limited by the amount of available sediment. Bed state prediction for a non-uniform sediment, also known as a graded sediment, is more complex than for a uniform sediment. Furthermore the critical shear stress for the initiation of motion of each size fraction in uni-modal grain size mixtures is approximately equal to that of the average grain size of the mixture. For bimodal sediments, the critical shear stress varies with grain size Kleinhans and Van Rijn (2002),Wilcock (1993),Kuhnle et al. (2006).

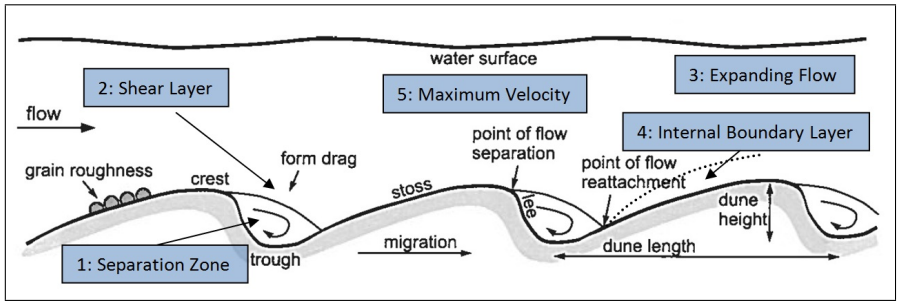

Figure 1.1: Schematic diagram of the principal regions of flow over symmetrical dunesPaarlberg (2008), Best (2005);

Steady and unidirectional flow over two dimensional dunes can be divided into five main regions Best (2005), figure 1.1: (1) A region of flow separation is formed on the lee-side of the dune, with a reattachment which occurs approximately 4-6 times the height of the dune crest downstream. (2) A shear layer is generated above the separation zone and divides this recirculation flow from the free stream fluid above. Large scale turbulence is formed along this shear layer in the form of Kelvin-Helmholtz instability, and as the free shear expands, it creates a wake zone that grows and dissipates downstream. (3) The third region is one of expanding flow over the dune lee-side.(4) Downstream from the reattachment region, a new internal boundary layer grows and there is a more logarithmic velocity distribution of the flow velocity. (5) The maximum horizontal velocity of the flow occurs over the dune crest and bed shear stresses here may be sufficient to generate upper stage plane bed conditions; The flow conditions on the crest will determine the entity and the frequency of the sediment supply to the dune's lee-side and the nature of the sediment sorting in the lee-side deposits. Further complexities arise from the three-dimensional bed form geometry and the curvature of the crest Allen (1968),Maddux et al. (2003a,b), Best (2005), Parsons et al. (2005), Venditti et al. (2005a),Venditti (2007), a non uniformity of the bed sediment, the coalescence of dunes with different geometric scales Driegen (1986), Julien et al. (2002), Wilbers and Ten Brinke (2003), Jerolmack and Mohrig (2005), Fernandez et al. (2006).

1.1 Bed roughness and hydraulic risk

The flow over river dunes generates important implications in the resistance to flow, in bed shear stress and in sediment transport (A.S.C.E. (2002), Fedele and Garcia (2006). For example, the different pressures generated by the flow separation and the accelerations/decelerations associated with the shape of the dunes, generate a strength on the dunes called form drag; this resistance is in addition to the resistance offered by the grains and makes the morphology of the dunes fundamental in the valuation of the resistance to flow and loss of energy

over the dunes Vanoni and Hwang (1967), Ogink (1988), Wijbenga (1990), Julien et al. (2002), Maddux et al. (2003a,b). Many criteria which attempt to predict flow resistance are based on the division into two components of the total shear stress at the bottom: the first component is created by the surface roughness due to the grain size, the second is generated by the difference in pressure between the lee side and the stoss side of the dune Yalin (1964), Engelund and Hansen (1967), Engelund (1977).

$$\tau = \tau' + \tau'' \tag{1.1}$$

where τ is the total shear stress, τ' is the component due to the grain roughness and τ'' is the component due to the shape of bed forms. Several empirical and semi-empirical models provide a prediction of the bed roughness requiring as an input the size of the bedforms Yalin (1964), Engelund (1977), van Rijn (1984b), Van der Mark (2009) or implicitly, including the geometry of bed forms Engelund and Hansen (1967) The variation of the two components of the total bed shear stress is well represented in figure1.2, originally proposed by Vanoni and Brooks (1957), where the behaviour of the form drag and grain drag is shown as a function of flow velocity. The graph shows a gradual increase of the shear stress generated by the roughness of the grains, called surface or grain drag here denoted τ', while the shear stress induced by the form drag ,τ'', increases significantly and very rapidly increase particularly in the region of dunes. Similar behaviour is created by the friction factor. Where the friction factor (f) is defined as:

$$f = 8 \cdot \left(\frac{u_*}{U} \right)^2 \tag{1.2}$$

The u_* represents the shear velocity, and U the liquid flow velocity. In natural rivers, flow resistance is also influenced by the presence of structures, vegetation or water course irregularities. Often the resistance of a channel is estimated by linking the measures of levels and flow rates in the field with those estimated by a model Wijbenga et al. (1998), Udo et al. (2007). In this way the estimation of flow resistance is probably more reliable even if it is not based on physical knowledge of the phenomena Morvan et al. (2008). Models which use calibrated hydraulic resistance parameters can produce inaccurate water levels when they are applied to fields where the model had not been calibrated. Field measurements reveal the complex behaviour of the bed forms and their correlation with resistance to flow during floods Peters (1978), Shen et al. (1978), Klaassen et al. (1988), Brownlie (1981),Raslan (1991), and Bridge (2003),Julien and Wargadalam (1995), Julien et al. (2002), Wilbers and Ten Brinke (2003), Holmes and Garcia (2008).

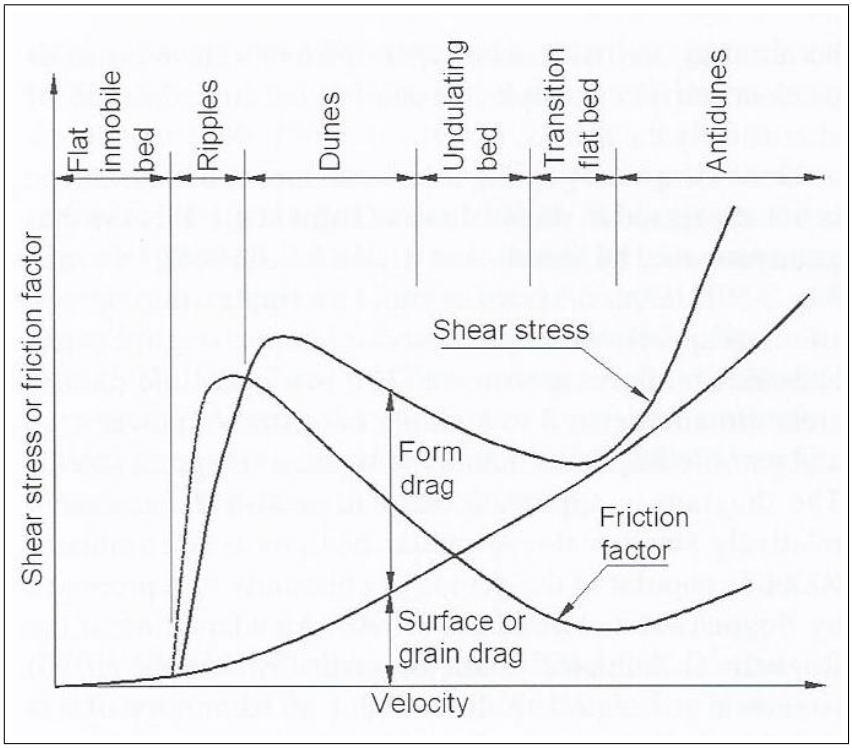

Figure 1.2: Variation of bed shear stress (τ_0) and Darcy-Weisbach friction factor f with mean velocity U of flow over a fine sand bed Raudkivi (1998);

Moreover, the behaviour of flow and bed form dynamics becomes more complex in an unsteady flow Wijbenga (1990). In fact, hysteresis effects have been observed in the dune heights during the rising and the falling stage of the flood wave, as described in figure 1.3. In particular, the height and the propagation speed of the dunes can vary from 2-10 times between the rising and falling stage of the flood wave Znamenskaya (1963). Subsequent measurements carried out on the river Rhine in the Netherlands show, in fact, an hysteresis between the height of the dune and the water discharge Julien and Klaassen (1995), Julien et al. (2002), Wilbers and Ten Brinke (2003). The existence of this hysteresis is also confirmed by laboratory experiments Wijbenga and Klaassen (1993), Wijbenga and Van Nes (1986). It was registered that dunes do not reach their maximum height during the peak of the flow hydro-graph but shortly after, when the flow rate begins to decrease. This delay is due to the time required by bed forms to adapt to flow condition changes. It was also observed that the flow resistance is out of phase as regards liquid flow in a similar way to the trend of the dunes' geometries Julien et al. (2002).

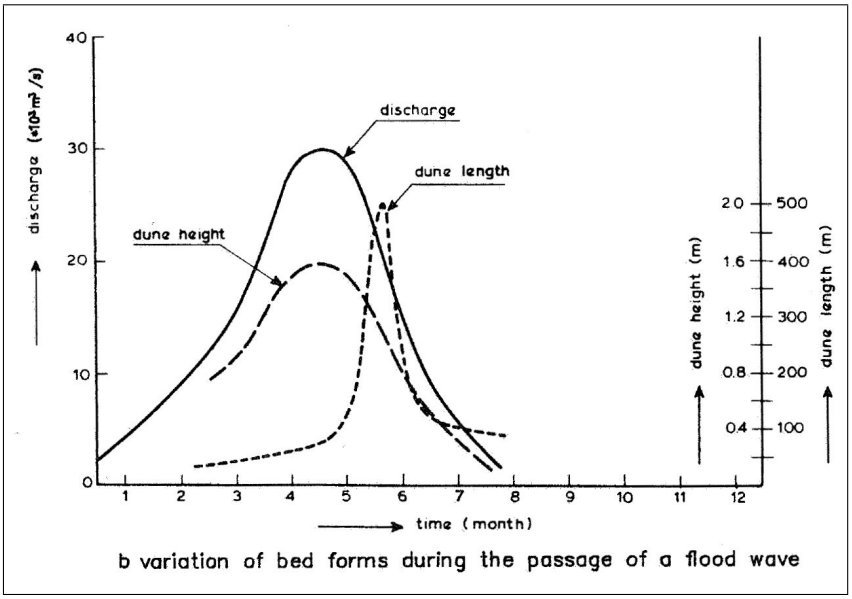

Figure 1.3: Variation of bed forms during the passage of a flood wave Znamenskaya (1963);

Flow resistance induced by bed forms may have a remarkable influence on flow depth, thereby it can affect the risk derived from flooding in natural rivers. Hydraulic risk arises from the possibility of damage to persons or property, which can occur as a consequence of intense water and/or sediment transport discharges. In the hydraulic risk can be considered the **risk from flooding**, i.e. the risk related to liquid discharge and the **risk from river bed dynamics**, i.e. the risk connected to the transport of solid mass. A correct prediction of hydraulic risk should be based on a sound knowledge of the several processes occurring in a river flow over a movable bed. For instance, the definition of the rating curve depends enormously on the bed resistance, and therefore on the bedform dynamics. An incorrect estimate of the roughness can lead to a not accurate association between the return period which identifies a flood event and the expected value of the water depths. This, finally, can lead to an incorrect association between a single flood event and its hydraulic risk. The hydraulic risk associated with a certain event can be defined as the product of the hazard, the elements at risk and their vulnerability Varnes et al. (1984).

$$Risk = H \cdot R \cdot V \tag{1.3}$$

where:

V=Vulnerability: Is the degree of loss to a given element or set of elements within the area affected by a hazard. It is expressed on a scale of 0 (no loss) to

1 (total loss).
R=Elements at risk: The Population, buildings and engineering works, infrastructure, environmental features and economic activities in the area affected by a hazard.
H=Hazard: The probability that a particular danger (threat) occurs within a given period of time.
The evaluation of damages (Elements at risk x Vulnerability) is strongly affected by a reliable estimation of flood water elevation which in turn is directly dependent on bed roughness and its variations during floods.

Chapter 2

State of the Art

After the first significant experiments conducted by Guy et al. (1966), many attempts have been made to describe bedform dynamics by adopting experimental and theoretical approaches. After the early approaches primarily based on dimensional analysis and empiricism A.S.C.E. (2008), appreciable advances in understanding basic bedform processes have been achieved with reference to the **origin of dunes** Kennedy (1963, 1969), Raudkivi (1966),Engelund and Fredsøe (1974, 1982), Yalin (1973, 1992), Richards (1980), Nelson and Smith (1989), McLean (1990), Bennett and Best (1995), Gyr and Kinzelbach (2004), their **stability and development** Leeder (2009), Bennett and Best (1995), Robert and Uhlman (2001), Schindler and Robert (2005), **their role in determining flow resistance** Ogink (1988), Vionnet and Serra (2005), Yoon and Patel (1996), Julien et al. (2002), Wilbers (2004) and bed load transport Engel and Lau (1980), van Rijn (1984b), Mohring and Smith (1996). Additionally, these studies have been conducted both in increasingly sophisticated and quantitative laboratory studies Van Mierlo and de Ruiter (1988), Mendoza and Shen (1990), Lyn (1993), McLean et al. (1994, 1996, 1999b,a),Nelson et al. (1993), Bennett and Best (1995), Bennet and Venditti (2000), Kadota and Nezu (1999), Nelson et al. (2001), Best and Kostaschuk (2002) , Maddux et al. (2003a,b),Best (2005) and a growing quantification of dune form and process within the natural environment Kostaschuk et al. (1989), Gabel (1993), Julien and Klaassen (1995), Kostaschuk and Church (1993),Kostaschuk and Ilersich (1995), Kostaschuk and Villard (1996), Roden (1998), Villard and Kostaschuk (1998), Carling et al. (2000a,b), Best et al. (2001, 2007),Williams et al. (2003), Sukhodolov et al. (2006), Parsons et al. (2005). Most of this work has been summarized in several review articles, reports and books, including those by Engelund and Fredsøe (1982),Ikeda and Parker (1989),McLean (1990),Southard (1991),Kennedy and Odgaard (1991),Seminara (1995),Best (1995),Seminara and Blondeaux (2001),Yalin and da Silva (2001), A.S.C.E. (2002),Bridge (2003),Best (2005),Parker and Garcia (2006). Notwithstanding the many contributions, several aspects still remain to be completely understood. Among these, a process

which has scarcely been investigated is the behaviour of bed forms in conditions of **limited sediment supply**. In literature, this condition has been investigated with reference to experiments where the development of bed forms is inhibited by the limited availability of sand in a bed where sediments present a bimodal size distribution, with a significant coarse fraction. The graded sediments in the bed material is often the cause of permanent supply limitation Dietrich et al. (1989), Klaassen et al. (1988), Kuhnle et al. (2006), Dreano et al. (2010). In fact, the coarser sediments which form the bed can create, through the phenomenon of vertical sorting, a static layer of coarse particles which prevent the underlying finer particles to be put in motion, as is described in Blom et al. (2003), Wilcock and McArdell (1997), Koll and Dittrich (2001). A limited quantity of sediment supplied leads either to smaller dimensions sediment-starved bedforms Tuijnder et al. (2009) or fewer isolated bedforms Carling et al. (2000b), Kleijwegt (1992). Although with the same amount of sediments both of the two dune forms can be reached, in the condition of limited sediment supply, mainly sediment-starved bedforms arise Kuhnle et al. (2006), Dreano et al. (2010),Tuijnder (2010). The degree of limitation of the sediment supplied is expressed in literature in several ways: by using the ratio of the layer thickness of the bedload sediment to the layer thickness required for alluvial conditions Struiksma (1985) or the alluvial bedform height Tuijnder et al. (2009) or the ratio of the actual, supply-limited sediment transport rate to the transport capacity Van der Zwaard (1974) e Dietrich et al. (1989). It must be noted that most of the literature data have been obtained using recirculating flumes. Very few data have been obtained using feed flumes. At this point it is worth explaining the difference between recirculating and feed flume and their implication on dune experiments. In a **recirculating flume**, the water and the sediment are recirculated through a pump; thus the discharge and the flow depth are set by the flume operator, and the total volume sediment transport rate and the bed slope evolve to equilibrium accordingly. In a **feed flume**, however, the water and the sediment are fed in upstream and allowed to wash out at the downstream end; so in a feed flume, the equilibrium value of discharge and of the total volume sediment transport rate are set by the flume operator, and the equilibrium flow depth and bed slope evolve accordingly. Conditions identical to either flume system at equilibrium are rare in the field, indeed, most natural rivers show both feed and recirculating components, Parker and Wilcock (1993). Which variables can be considered as independent or dependent in a stream modelling experiments is a hard question. Several authors, White et al. (1982),Guy et al. (1966),Wilcock and Southard (1989), have reviewed this issue. Parker and Wilcock assert in Parker and Wilcock (1993) that the recirculating flume approaches the field case for short time and space scales whereas the feed flume approaches the field case for long time and space scales with constant water and sediment input. In Parker and Wilcock (1993),the authors consider negligible suspension load and bed forms, and affirm that: "The equilibrium themselves are equivalent in that they obey the same laws of flow and sediment transport. It is shown here that if the sediment is of uniform size, the asymptotic

equilibrium flows obtained for both types of flume are completely equivalent and independent of initial conditions". In Wilcock and Southard (1989) the case of heterogeneous sediment is investigated with the aim of analysing the equilibrium conditions reached in the feed or recirculating flume. The Authors conclude that under the same initial conditions, completely different equilibrium states can be reached depending on whether a feed flume or a recirculating flume is used. It can be observed that a feed flume tends to reach equilibrium state mainly by adjusting the bed slope, while this process is much less evident in a recirculating flume.

Chapter 3

Thesis Outline

The present study aims to investigate the response of bed morphology to variations in sediment or water supply. In particular, sediment supply, water discharge and grain size are assumed to be independent variables, while water depth, bed slope and bedform characteristics are dependent variables. Using a laboratory flume with movable bed, experiments were carried out by imposing changes on one of the independent variables while the remaining two were kept constant. The grain size was assumed as constant in all the experiments. In this way, two distinct experimental cycles were obtained: one cycle was performed at constant water discharge and variable sediment supply, while the other cycle was carried out under constant sediment supply and varying water discharge. In each cycle variations of the independent variable were imposed following a succession of steps. At each step bed morphology and flow characteristics were allowed to adjust until average steady and uniform flow conditions were reached. At this point, a new change was imposed to proceed with the next step. This experimental procedure differs considerably from the one followed by Tuijnder (2010) who investigated the case of a reduction of sediment supplied induced by the presence of an armoured layer underlying the sand bed; this configuration, though realistic, leads to totally different results from those found in this study since the bed has no capacity to adjust the slope in reaching a new equilibrium. To investigate this type of response an extensive experimental study was carried out in a sand flume having no restriction in the bed adjustment capacity, as will be described in Part II. The experimental cycles were constituted by a variable number of steps under stationary conditions of uniform flow.
Two types of cycle were performed:

- one that reproduces the situation where at each step in sedimentological equilibrium conditions, the amount of sediment supplied is varied while the liquid flow rate remains constant; the channel and the bed forms characteristics are left free to vary;

- the other cycle reproduces the situation where at each step in sedimen-

tological equilibrium conditions, the liquid flow is varied, giving, in this way, an input to the variation of the sediment transport capacity, keeping the amount of sediment supplied constant; also in this case the geometric characteristics of the channel and of the bed forms are left free to vary;

The analysis of the collected experimental data, chapter 7, leads to a new interpretation of bed morphodynamics that can explain both the conditions of imbalance caused by an excess/defect of the solid material supplied as well as an excess/defect of the sediment transport capacity. A mathematical model based on the physical relations is developed and tested against the experimental data. Within this framework, it is possible to carry out a physical interpretation of the experimental results and to attempt to extend the data patterns beyond the experimental range, chapter 9. In particular, the mathematical model allows the definition of the existence of the conditions of the dune regime. A comparison with the criteria available in literature shows satisfactory results. Furthermore, the mathematical model is used to identify the hydraulic conditions under which bed forms are able to perform their response when the existing equilibrium condition is modified by variations imposed on the independent variables, chapter 10.

Finally, the experimental activity carried out in the present study contributes to increasing the limited amount of data available from feed flumes in literature. This is despite the fact that several physical processes can only be simulated in feed flumes, such as the sedimentological imbalance unless one uses the phenomena of armoured layer or vertical sorting, such as some experiments in limited supply conditions have illustrated.

Part II

THE EXPERIMENTS

Abstract

This section describes experiments conducted to observe the adaptation of the channel system with bed covered by bedforms to a situation of imbalance between sediment transport capacity and available solid material. In particular: In chapter 4 there is a description of the flume and the instruments used to carry out the experiments, section 4.1, and the procedure used, section 4.2; The data resulting from the experiments in mobile-bed equilibrium were collected and are listed in the tables in chapter 5; In chapter 6 the collected data obtained from the experiments are compared with data available in literature. Comparisons are also made with the most meaningful relationships between the experimental data, section 6.1.2.

Chapter 4

Experiments Design

4.1 Channel Description

In order to highlight the flume's and the bedforms' response to a situation of imbalance between sediment transport capacity and the sediment available, some experiments were conducted at the Laboratory of Hydraulics at the Department of Civil and Environmental Engineering at the University of Florence. The experiments were conducted in a straight tilting flume, of 10 m in length and 0.105 m in width (see figures 4.1, 4.2, 4.3). The experiments were conducted in conditions of uniform and sub-critical flow, while the sediment used for the movable bed was of two types, one with the $D_{50} = 0.79\ mm$ and the other $D_{50} = 1.25\ mm$, both sediment distributions are quite homogeneous as is demonstrated by their standard deviation, respectively, 0.49 and 0.6 (see Appendix C). The experimental channel is a **feed flume** (see figure 4.4) which differs from a recirculating flume because only the water is completely recirculated by a pump and not the sediment. The constraints on a feed flume are the water discharge and the upstream sediment discharge. In fact all the water and all the sediment are fed in upstream and allowed to wash out at the downstream end. Water is introduced into the channel at the desired rate, and sediment is fed into the channel using a sediment feeder at the desired rate. In addition to the sediment itself, the operator is thus free to specify two parameters in the operation of the flume: the water discharge per unit width q_W and the sediment discharge per unit width q_S. Once the final equilibrium condition is reached, sediment transport and water discharge along the flume must be equal to the feed rate q_{tf}. Thus, in a feed flume, equilibrium q_W and q_S are set by the flume operator and equilibrium flow depth H and bed slope S evolve accordingly Parker (2004). The flume is a straight canal with a rectangular section, the bottom is made of slabs of steel and the walls of glass. The channel is supported by a steel structure which is connected to a wheel control for adjusting the bed slope. Water discharge is fed into the flume by a centrifugal pump connected to three water tanks. The pump draws the water from the tanks and releases

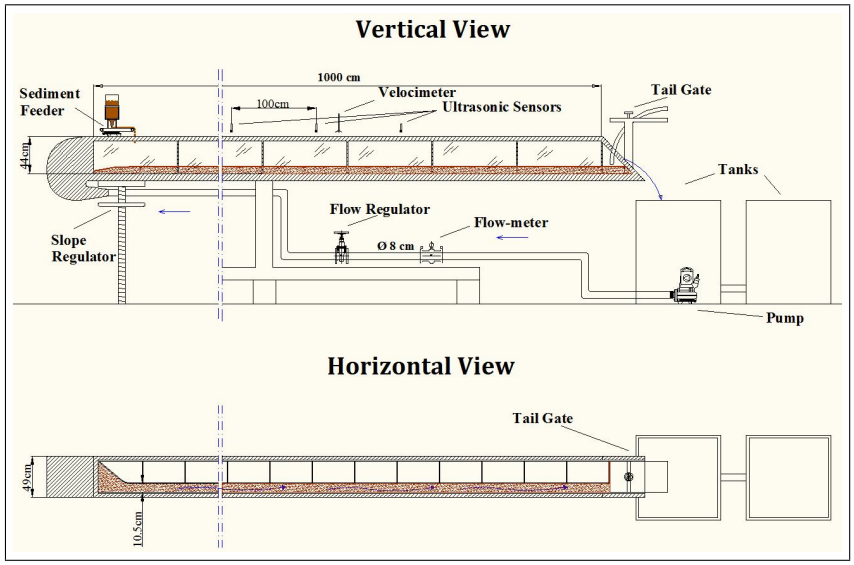

Figure 4.1: The Flume: Vertical and Horizontal view;

it through a feed tube at the beginning of the channel. The three tanks are interconnected with a total capacity of 2.1 m^3. The channel was later modified including along its length a plexiglass septum which reduces the width from a value of 0.49 m to that of 0.105 m. The shape of the initial part of the septum is made in order to dump the perturbation produced at the flume entrance. The liquid flow rate is adjusted manually through a valve, while an electromagnetic flow meter provides the value of instantaneous water discharge.

The channel was equipped with several ultrasonic **probes**, Honeywell 943-F4V-2D-1C0-330E (see figures 4.5, 4.6), to measure the water free surface elevation, by which estimation of the mean slope was made . The number and the location of probes were kept constant for all the experiments, except for the first seven runs, as shown in figures 4.7,4.8, the slope of the channel was determined by a wheel in the upper side and verified by two probes placed as shown in figure 4.9.

As shown in figure 4.6, the ultrasonic probes take the measure of the piezometric head by providing the water surface elevation of the piezometers installed along the flume. Piezometers consist of a cylindrical plexiglass tube of an inner diameter of 17 cm and a height of 40 cm; The piezometer are hydraulically connected to the channel flow by a small plastic tube of inner diameter 4 mm placed under the layer of bed sediment. The sediment feeder is placed at the beginning of the channel and provides a known amount of sediment flow rate, figure 4.10. The instrument is composed of a conveyor belt whose velocity can be regulated by a rheostat. Sediments loaded in a cylindrical holder are conveyed by a hopper over the conveyor belt and then discharged at the inlet of

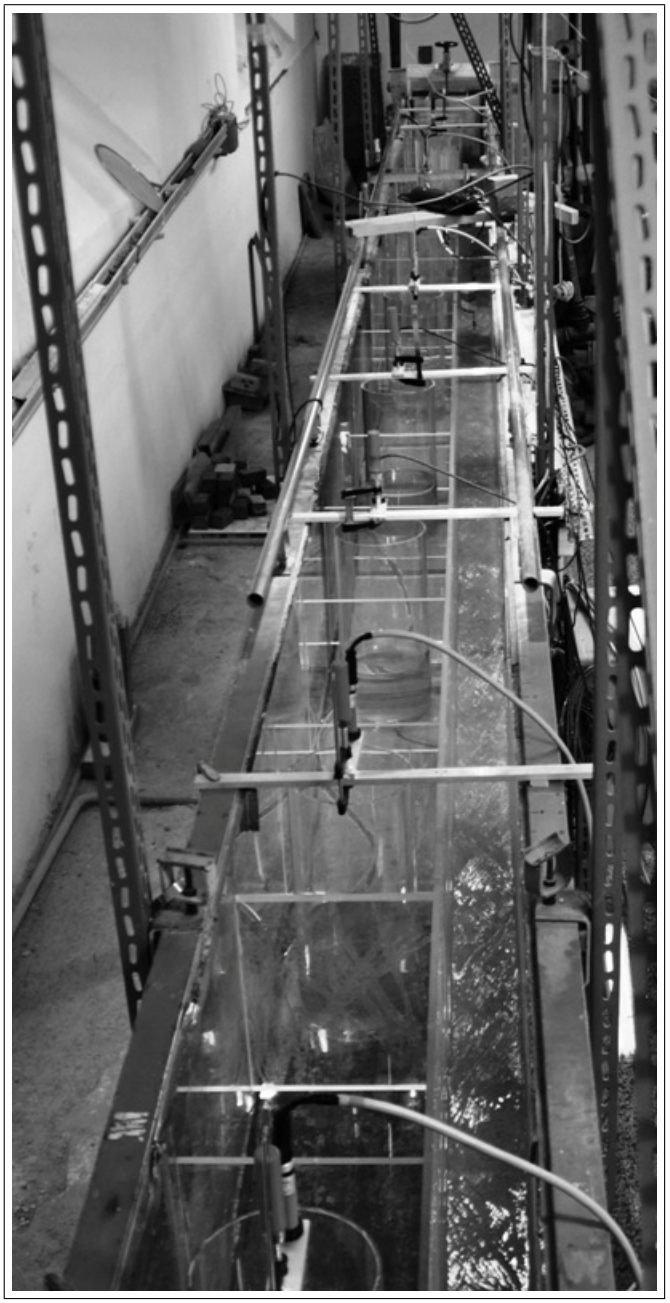

Figure 4.2: The Flume-Central Detail (upper view);

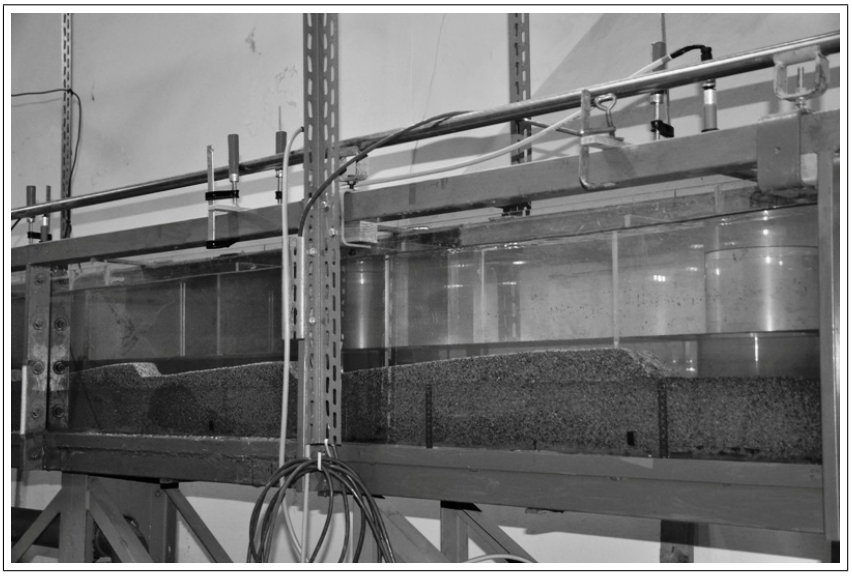

Figure 4.3: The Flume-Central Detail (lateral view);

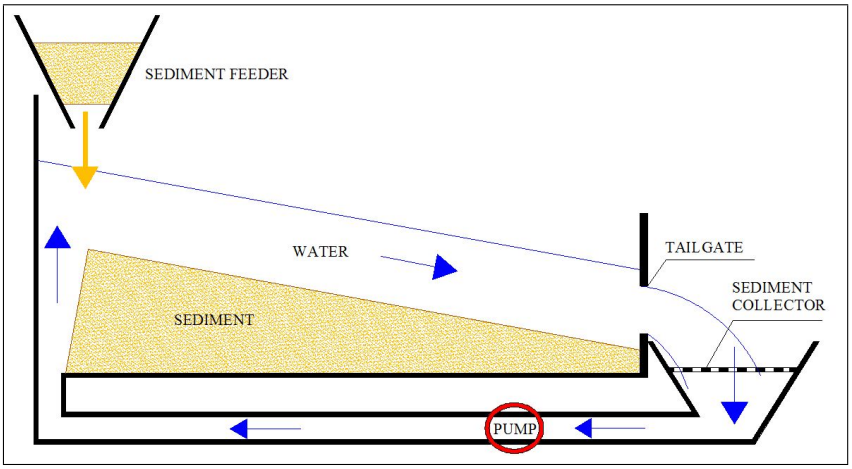

Figure 4.4: Feed Flume Schema Parker (2004);

Figure 4.5: Probe Honeywell 943-F4V-2D-1C0-330E;

Figure 4.6: Probes and piezometers along the side of the channel;

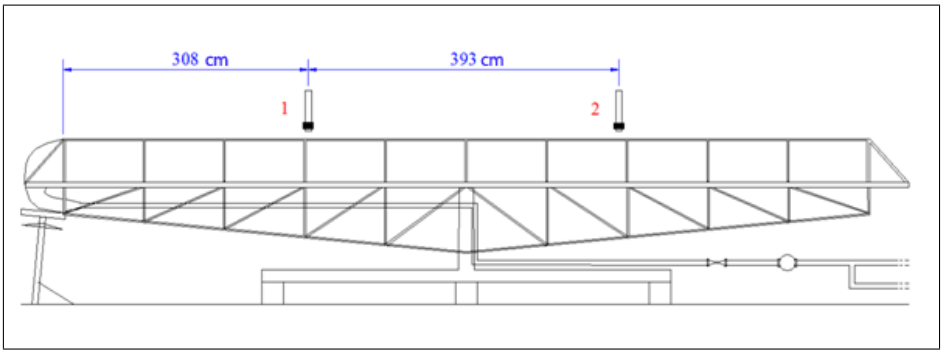

Figure 4.7: Experiments 1 to 7-sediment type A: position of the probes for water elevation measurements;

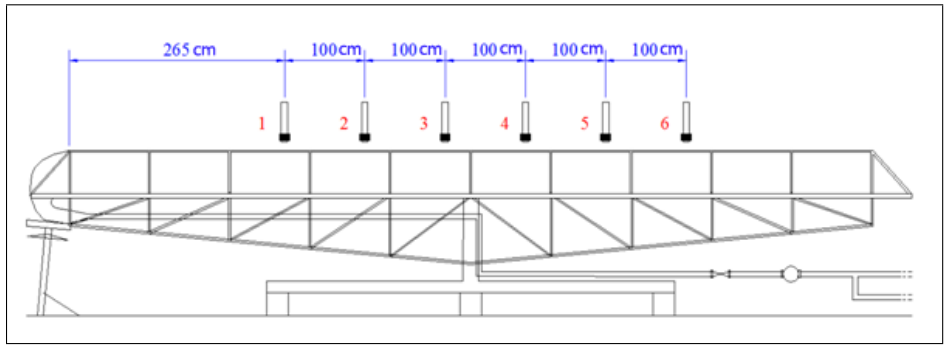

Figure 4.8: Experiments 8 to 32-sediment type A and all experiment-sediment type B: position of the probes for water elevation measurements;

the flume. The sediment accumulates inside a net above the first tank, to the outlet of the channel, figure 4.11; The net has a mesh size of less than 0.5 mm.

Measurements of flow velocity were carried out by using an acoustic doppler velocimeter, see figure 4.12 mounted on a support which allows it to move vertically through the flow section. In order to not disturb the monitored area, the ADV instrument, is displaced from the middle of the channel, as is shown in figure 4.13.

4.2 Experimental Procedure

The experimental procedure can be divided into two phases: a first preparatory phase and the experiment.

PREPARATORY PHASE

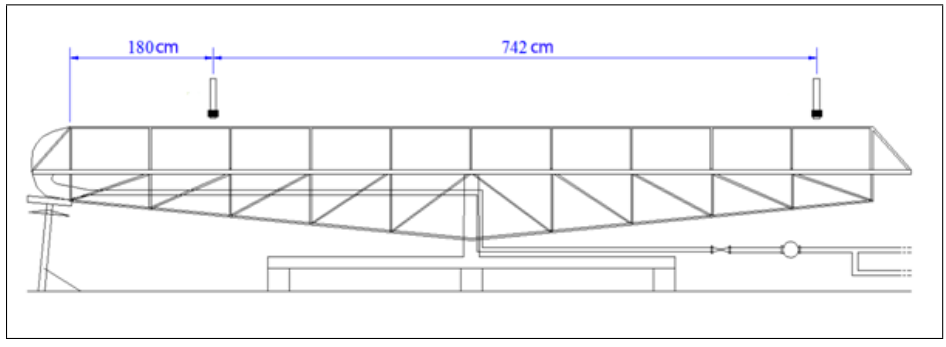

Figure 4.9: Probes position to determine the channel slope;

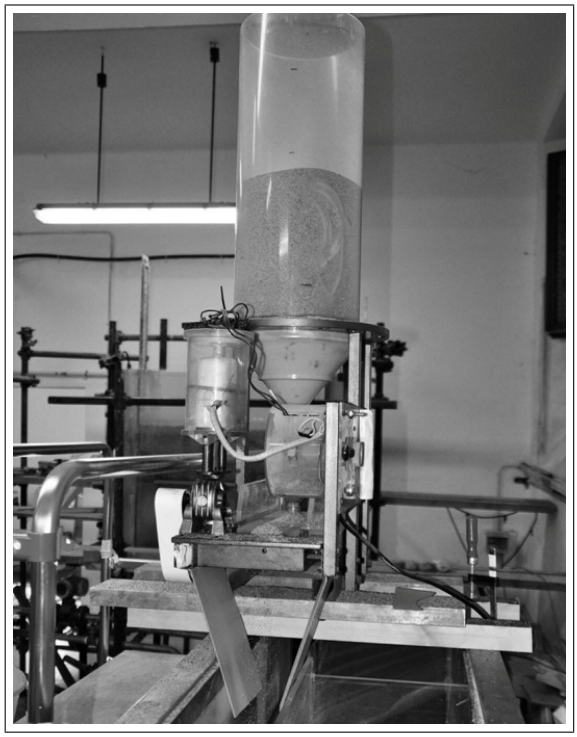

Figure 4.10: The sediment feeder;

Figure 4.11: The outlet of the channel;

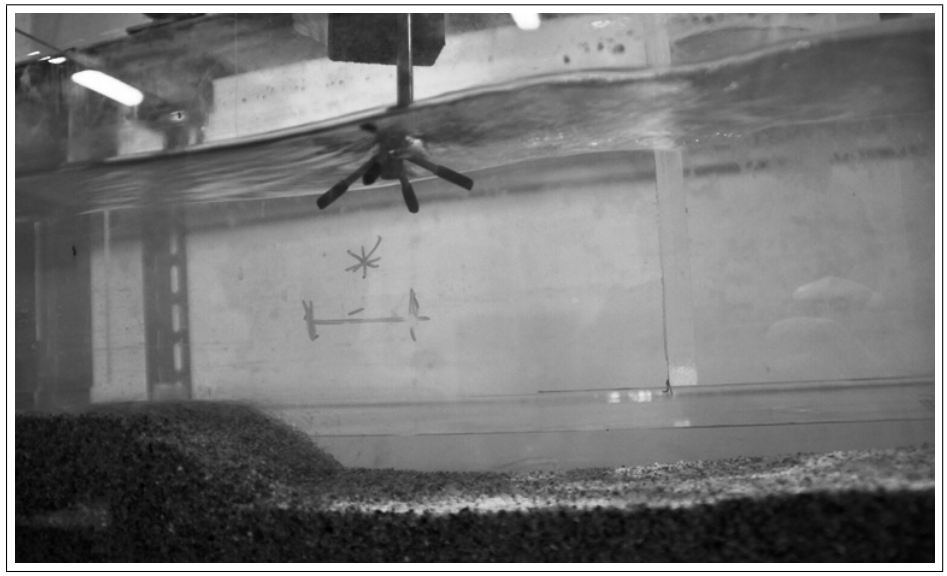

Figure 4.12: Acustic Doppler Velocimeter during an experiment;

The bottom of the channel is formed by a layer of sediments 10 cm in thickness. At the beginning of the experiment, a very low water discharge (generally between 0.2 - 0.3 l/s) was fed into the flume to slowly saturate the sand bed in order to prevent the formation of internal air bubbles. Then the liquid flow was gradually increased until the established value. At this time the sediment feeder was switched on. The testing reach is 3 m long and was chosen at about 4 meters downstream from the flume entrance, see figure 4.14. The velocity measurements were taken at downstream of the testing reach, by placing the acoustic doppler velocimeter in the centre of the flume width and in the way

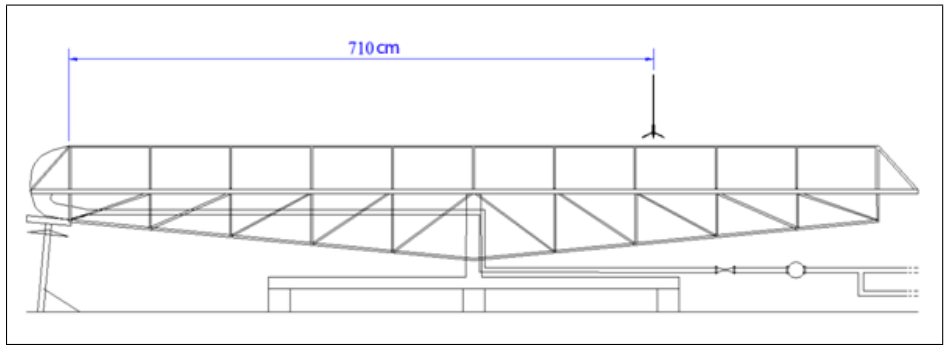

Figure 4.13: Position of Doppler Acoustic Sensor along the channel;

that the sampling volume should be approximately in the middle of the water depth. These measurements were assumed to be representative of the average flow velocity. A video camera was also used to film the water flow and the bed dynamics in the testing reach.

The preparatory phase continued until the flow condition in the flume could be assumed, on average, to be steady and uniform. The time required to attain this condition could vary in a wide range depending on how far the initial conditions were from the equilibrium stage. The starting condition was a plane bed which turned into an undulated bed as soon as the water discharge and the sediment supply was progressively increased. Uniform water depth was then reached by adjusting the tailgate. In all the experiments, the observed bed forms were dunes. After this preparatory phase, a balance between the sediment transport capacity and the sediment supply was assumed to be achieved. Although the long-term equilibrium approached in a recirculating flume should be dynamically equivalent to that obtained in a sediment-feed flume Parker and Wilcock (1993), feed flumes reach mobile-bed equilibrium faster than recirculating flumes Parker (2004).

The achievement of the equilibrium stage was verified by checking that the sediment supply was the same as the sediment transport along the flume bed and as the rate of sediment collected in the trap at the end of the channel. To this purpose two criteria were used: one based on measuring the height and celerity of the dunes and applying the continuity sediment equation:

$$Qs = \frac{1-e}{2} \cdot c \cdot \Delta \cdot B \qquad (m^3/s) \tag{4.1}$$

Where the symbols represent:
Qs = Sediment Supply or Sediment Transport (m^3/s);
e = Void ratio of the sediment $(-)$;
Δ = The height of dunes (m);
c = The celerity of dunes (m/s);
B = The width of the flume (m);
The explanation of the shape of equation 4.1 is given in Appendix D
The other criterion consists of the weight of the sediment collected in the final trap in a known time.

THE EXPERIMENTS

Once the preparatory phase was completed, two distinct cycles of experiments were carried out. Each cycle developed through successive states of morphodynamic equilibrium, spaced out by a transitional phase between one state and another. The first cycle, indicated as CFD (Constant Flow Discharge), was conducted by imposing a constant water discharge and by varying the sediment supply following a succession of steps. Each step represented an equilibrium stage during which the sediment transport capacity balanced the sediment supply. Conversely, in the second cycle, indicated as CSS, a constant sediment

supply was imposed while the water discharge was varied following a succession of steps during which equilibrium conditions were obtained before proceeding to the next step. During the experimental cycles, the dependent variables of the channel, such as water depth, dune characteristics and average bed slope were free to adjust until morphodynamic equilibrium was reached. The time required to achieve the equilibrium condition was different in the two cycles: experiments carried out under constant sediment supply (cycle CSS) reached the equilibrium steps faster then the experiments carried out under constant flow discharge (cycle CFD). In conclusion it should be noted that every 15 minutes for the entire duration of the experiment, the geometry of the bed forms (in particular, the dune height and length and the speed of the crest) were recorded: The values are an average of a number varying from four to eight sets of dunes. The dunes were measured in the testing reach, see figure 4.14.

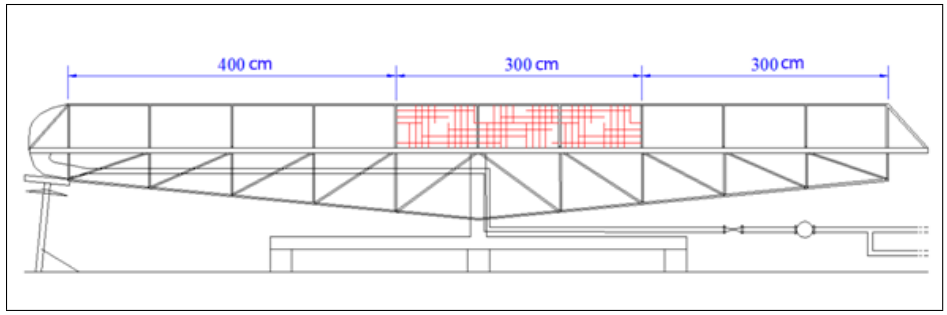

Figure 4.14: Testing reach;

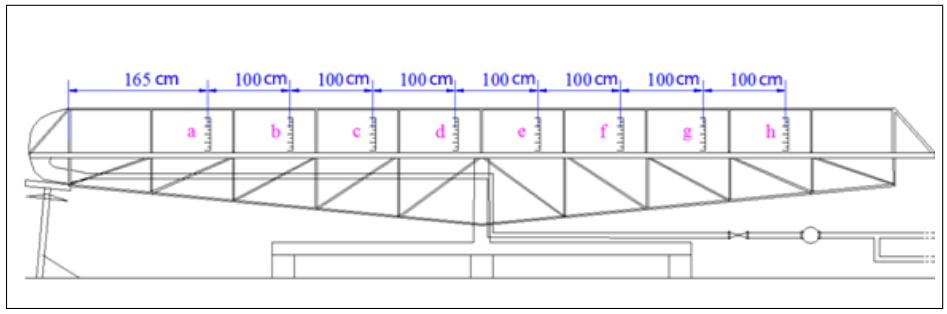

Figure 4.15: Manual detection points of the sediment heights and the water depths;

The testing reach is placed in the middle of the channel in order to avoid the perturbations of the flow in the input and output of the flume. All these measurements were made by hand along the glass wall. Furthermore, again every 15 minutes, the height of the sediment which constituted the bottom and the depth of the water were measured using the same method, all along the channel in the sections shown in figure 4.15.

Chapter 5

Equilibrium Data Base

As described in the previous chapter, each experimental cycle develops through sequential phases of equilibrium. Each equilibrium phase is assumed to be reached when hydraulic and sedimentological variables do not show appreciable variation in time and space. Only the data collected as described in section 4.2, which corresponds to an equilibrium phase have been listed in table 5.1 and table 5.2 for sediment type-A, and type-B respectively. For both tables the first column shows the **code** of each experimental cycle and, for each equilibrium step the following was reported: flow discharge per unit width (**ql**), the sediment supply/sediment transport per unit width (**qs**), the average bed slope (**S**), the mean flow velocity (**U**), the height (Δ), the length (λ) and the speed of the dunes crest (**c**). All experiments are quoted in full in Appendix **??**. The acronym U.P.B. means Upper Plane Bed.

Table 5.1: Equilibrium Data-Sediment Type A

CODE	**ql** (m^2/s) $\times 10^{-2}$	**qs** (m^2/s) $\times 10^{-2}$	**S** $(-)$ $\times 10^{-3}$	**U** (m/s) $\times 10^{-1}$	Δ (m) $\times 10^{-2}$	λ (m) $\times 10^{-1}$	**c** (m/s) $\times 10^{-3}$
A2	4.808	9.149	6.347	5.808	3.000	2.400	8.330
A3	4.808	5.769	3.785	6.750	1.500	2.200	7.630
A3	4.808	1.818	4.976	5.900	1.400	5.150	4.795
A4	7.212	5.769	3.957	7.490	2.300	4.650	3.480
A4	7.212	4.691	5.012	7.330	2.000	6.500	5.720
A4	7.212	4.079	4.157	7.330	2.000	6.200	5.000
A4	7.212	3.089	4.269	7.200	1.630	4.000	3.960
A4	7.212	1.818	4.092	6.770	1.800	4.075	3.840
A6	4.952	3.671	7.033	5.455	1.050	2.217	6.565
A6	4.952	4.254	6.278	5.455	1.400	1.900	8.320
A6	4.952	3.089	6.389	5.270	9.300	3.600	1.054

Continued on next page

Continued from previous page

CODE	**ql** (m^2/s) $\times 10^{-2}$	**qs** (m^2/s) $\times 10^{-5}$	**S** $(-)$ $\times 10^{-3}$	**U** (m/s) $\times 10^{-1}$	Δ (m) $\times 10^{-2}$	λ (m) $\times 10^{-1}$	**c** (m/s) $\times 10^{-3}$
A6	4.952	1.399	5.660	5.221	1.050	3.700	6.200
A7	8.750	7.343	8.454	8.760	1.675	4.050	8.220
A7	7.404	7.343	7.439	8.300	2.000	3.000	7.690
A8	4.808	6.002	1.044	7.310	2.143	2.467	6.860
A8	4.808	3.671	8.726	7.140	2.130	2.750	6.190
A9	4.837	1.195	3.886	5.840	1.523	5.663	2.320
A10	6.202	1.195	3.811	6.210	1.675	4.961	1.980
A11	6.202	1.818	3.920	6.630	1.677	5.897	2.560
A12	6.202	2.477	5.388	6.930	1.292	5.144	4.516
A14	6.202	3.112	6.590	7.150	1.218	4.210	7.210
A15	6.202	2.477	5.858	7.030	1.365	5.120	5.072
A20	6.519	0.991	3.828	6.180	1.575	4.750	1.180
A21	4.808	4.336	5.725	6.860	1.030	2.300	6.070
A21	4.808	6.579	7.823	7.230	1.735	2.500	6.950
A21	4.808	8.846	9.814	7.420	2.400	2.350	6.045
A22	5.769	19.848	1.261	9.800	U.P.B.	U.P.B.	U.P.B.
A22	5.769	21.591	14.640	10.160	U.P.B.	U.P.B.	U.P.B.
A25	3.750	0.886	2.566	4.970	1.799	6.833	1.308
A27	6.731	0.886	2.193	5.270	2.650	5.255	1.163
A29	8.654	0.886	2.123	5.340	2.838	5.123	1.035
A31	10.580	0.886	2.544	5.830	3.323	5.750	1.051

Concluded from previous page

Table 5.2: Equilibrium Data-Sediment Type B

CODE	**ql** (m^2/s) $\times 10^{-2}$	**qs** (m^2/s) $\times 10^{-2}$	**S** $(-)$ $\times 10^{-3}$	**U** (m/s) $\times 10^{-1}$	Δ (m) $\times 10^{-2}$	λ (m) $\times 10^{-1}$	**c** (m/s) $\times 10^{-3}$
B1	4.856	0.390	1.580	5.030	1.039	9.394	1.101
B2	4.856	2.535	5.290	6.390	0.731	4.531	7.570
B4	4.856	2.535	4.980	6.550	0.653	4.911	7.398
B5	4.856	0.390	2.360	5.240	0.992	7.767	1.375
B6	3.846	0.866	3.200	5.420	0.556	7.550	3.180
B8	7.837	0.866	2.490	5.830	1.701	8.296	1.981
B10	11.683	0.866	3.380	6.690	2.681	7.857	0.978
B11	7.837	0.866	2.740	5.750	1.818	9.245	1.328
B12	3.846	0.866	3.700	5.330	0.638	9.125	2.580

Continued on next page

Continued from previous page

CODE	**ql** (m^2/s) $\times 10^{-2}$	**qs** (m^2/s) $\times 10^{-5}$	**S** $(-)$ $\times 10^{-3}$	**U** (m/s) $\times 10^{-1}$	Δ (m) $\times 10^{-2}$	λ (m) $\times 10^{-1}$	**c** (m/s) $\times 10^{-3}$
B17	2.837	0.973	3.730	5.310	0.465	5.418	4.749
B20	5.769	0.973	2.870	5.740	1.292	7.650	3.161
B22	8.558	0.973	2.510	6.170	2.410	8.944	1.134
B24	11.394	0.973	2.780	6.270	3.006	6.660	1.253
B26	8.558	0.973	2.710	6.220	2.267	7.304	1.577
B27	5.769	0.973	3.190	5.690	1.322	5.978	2.448
B29	2.356	0.973	4.670	5.410	0.333	5.400	5.458
B31	9.615	1.445	3.520	6.690	3.008	8.758	1.413
B33	9.615	2.273	3.940	7.140	2.478	6.725	3.074
B36	9.615	3.409	4.370	7.750	2.072	6.060	4.722
B38	3.846	0.565	3.830	5.46	0.906	9.842	2.328
B40	7.596	0.565	3.020	5.970	1.856	0.792	1.193

Concluded from previous page

Chapter 6

Comparison with literature data

6.1 Data Comparison

6.1.1 Data base from literature

Experimental data of flow over dunes were collected from literature for comparison with the present experimental data. To this purpose, experiments conducted by Guy et al. (1966), Klaassen (1979), Mancini and Menduni (1986), Wang and White (1993), Wijbenga and Klaassen (1993), Venditti et al. (2005b) were observed and a total amount of 56 equilibrium states were collected.

- In particular, the first fifteen sets of figures were taken from the experiments described in Guy et al. (1966). This data had been collected in a recirculating flume with a mobile bed and with three-dimensional bedform shape measuring 2.44 m wide, 0.61 m deep, and 45.72 m long. The slope could be adjusted from 0 to 1.5 percent. The bed materials were selected from natural river sand.

- Eight sets of figures, which represent the initial condition of stationary equilibrium, were taken from the work described in Wijbenga and Klaassen (1993). Flume tests had been carried out at the Delft Hydraulics Laboratory to study the changes in bedform dimensions and the resistances to flow for unsteady flow conditions. The tests were carried out in a straight recirculating flume with uniform bed material $D_m = 0.77$ mm. Results are presented for a sudden increase or decrease of the discharge. The flume dimensions were 50 m length, 1.50 m width and the maximum water depth without sediment 1.00 m.

- The Klaassen (1979) experiments were conducted in the same laboratory

from which twelve sets of figures were drawn in sedimentological and hydraulic equilibrium conditions.

- Thirteen sets of figures were taken from the work Wang and White (1993). A set of experiments was carried out at the Sediment Research Laboratory of Tsinghua University, Beijing, China. The experiments were performed in a recirculating, tilting flume 60 m long and 1.2 m wide. The sediment used in the experiments was a fine sand with a D_{50} size of 0.076 mm and a value for D_{84}/D_{16} of 1.44.

- In Venditti et al. (2005b) some experiments conducted at the National Sedimentation Laboratory, United States Department of Agriculture, Oxford, Mississippi, using a tilting, recirculating flume 15.2 m long, 1 m wide, and 0.30 m deep, are described. The flume was filled with 2250 kg of narrowly graded, unimodal, washed and sieved white quartz sand with a median grain size $D_{50} = 0.5$ mm. The flow was both subcritical and fully turbulent, and three sets of figures were taken from these tests that describe the equilibrium condition.

- The only examples collected in a feed flume are those by Mancini and Menduni in Mancini and Menduni (1986). The experiments were carried out in dune regime and sediment transport as bedload only in a tilting flume feed, 6m long and 12 cm wide, and five sets of figures were taken, in sedimentological and hydraulic equilibrium.

Below are two tables; for both tables, the first column shows the **source** of the data and the second column indicates the code of each state, specified as the **Run**; In the first table, table 6.1, the following are also listed: the flow discharge per unit width (**ql**), the suspended load transport per unit of width, (**qss**), the sediment supply/sediment transport per unit width, (**qs**), the width of the channel, (**B**) and the average bed slope, (**S**). In the second table, table 6.2, further values have been taken into account, measured in the same experiments and in the same equilibrium states: the mean flow depth, (**Y**), the characteristic diameter of the sediment, (D_{50}), the height, (Δ), the length, (λ) and the speed of the crest, (**c**) of the dunes, **n.m.** means that the variable is not measured.

Table 6.1: Literature Data-A;

SOURCE	Run	ql (m^2/s)	qss (m^2/s)	qs (m^2/s)	B (m)	S $(-)$
	1	1.56E-01	5.88E-08	1.23E-06	2.44	3.70E-04
	2	1.69E-01	6.37E-08	1.78E-06	2.44	3.70E-04
	3	1.89E-01	2.92E-07	4.63E-06	2.44	5.90E-04
	4	8.61E-02	3.25E-08	2.05E-06	2.44	7.10E-04
	5	8.22E-02	3.10E-08	2.26E-06	2.44	8.00E-04
	6	1.96E-01	8.86E-07	1.03E-05	2.44	1.12E-03

Continued on next page

Continued from previous page

SOURCE	Run	ql (m^2/s)	qss (m^2/s)	qs (m^2/s)	B (m)	S ($-$)
Guy,	7	8.87E-02	3.35E-08	6.73E-06	2.44	1.30E-03
Simons,	8	1.95E-01	2.21E-06	1.56E-05	2.44	1.36E-03
Richiardson	9	9.50E-02	5.02E-07	9.07E-06	2.44	1.45E-03
(1966)	10	1.91E-01	5.75E-06	2.21E-05	2.44	1.83E-03
	11	8.01E-02	3.63E-07	1.36E-05	2.44	1.92E-03
	12	1.04E-01	2.20E-06	2.04E-05	2.44	3.04E-03
	13	2.59E-01	2.75E-05	5.25E-05	2.44	3.13E-03
	14	2.58E-01	5.98E-05	1.15E-04	2.44	3.93E-03
	15	1.30E-01	1.54E-05	7.31E-05	2.44	4.30E-03
	1	3.80E-02	0.00	9.12E-06	1.20E-01	3.90E-03
Mancini,	2	2.00E-02	0.00	3.77E-06	1.20E-01	4.00E-03
Menduni	3	4.00E-02	0.00	9.43E-06	1.20E-01	4.10E-03
(1986)	4	1.90E-02	0.00	3.77E-06	1.20E-01	4.40E-03
	5	3.80E-02	0.00	1.07E-05	1.20E-01	4.30E-03
Venditti,	1	7.59E-02	0.00	1.02E-05	1.00	1.20E-03
Church,	2	7.23E-02	0.00	5.09E-06	1.00	1.10E-03
Bennett (2005)	3	6.96E-02	0.00	3.95E-06	1.00	7.00E-04
	1	7.59E-02	0.00	1.02E-05	1.00	1.20E-03
	2	1.50E-01	0.00	7.43E-06	1.50	1.26E-03
	3	2.00E-01	0.00	7.31E-06	1.50	9.63E-04
	4	2.27E-01	0.00	7.60E-06	1.50	8.91E-04
	5	2.87E-01	0.00	7.68E-06	1.50	7.55E-04
Klaassen	6	3.67E-01	0.00	7.76E-06	1.50	6.24E-04
(1979)	7	1.80E-01	0.00	1.37E-05	1.50	1.62E-03
	8	3.17E-01	0.00	1.42E-05	1.50	1.10E-03
	9	2.03E-01	0.00	1.54E-06	1.50	3.84E-04
	10	2.07E-01	0.00	6.44E-05	1.50	3.99E-03
	11	2.27E-01	0.00	7.72E-06	1.50	8.79E-04
	12	4.23E-01	0.00	6.26E-05	1.50	2.70E-03
	1	7.59E-02	0.00	1.02E-05	1.00	1.20E-03
	2	1.77E-01	0.00	1.46E-05	1.50	1.64E-03
	3	9.70E-02	0.00	7.29E-06	1.50	1.60E-03
Wijbenga,	4	1.77E-01	0.00	1.41E-05	1.50	1.56E-03
Klaassen	5	9.80E-02	0.00	7.32E-06	1.50	1.65E-03
(1993)	6	2.67E-01	0.00	2.01E-05	1.50	1.53E-03
	7	9.80E-02	0.00	7.34E-06	1.50	1.61E-03
	8	1.77E-01	0.00	1.38E-05	1.50	1.68E-03
	1	4.34E-02	0.00	n.m.	9.17E-01	4.22E-04
	2	4.34E-02	0.00	n.m.	9.17E-01	4.22E-04
	3	4.56E-02	0.00	n.m.	9.17E-01	1.37E-03

Continued on next page

Continued from previous page

SOURCE	Run	ql (m^2/s)	qss (m^2/s)	qs (m^2/s)	B (m)	S ($-$)
Wang, White (1990)	4	4.89E-02	0.00	n.m.	9.17E-01	1.67E-03
	5	5.49E-02	0.00	n.m.	9.17E-01	1.99E-03
	6	5.81E-02	0.00	n.m.	9.17E-01	2.88E-03
	7	6.68E-02	0.00	n.m.	9.17E-01	3.22E-03
	8	5.62E-02	0.00	n.m.	9.17E-01	4.01E-03
	9	7.45E-02	0.00	n.m.	9.17E-01	3.33E-03
	10	7.88E-02	0.00	n.m.	9.17E-01	4.12E-03
	11	8.43E-02	0.00	n.m.	9.17E-01	4.45E-03
	12	8.97E-02	0.00	n.m.	9.17E-01	4.77E-03
	13	9.47E-02	0.00	n.m.	9.17E-01	5.10E-03

Concluded from previous page

Table 6.2: Literature Data-B;

SOURCE	Run	Y (m)	D_{50} (m)	Δ (m)	λ (m)	c (m/s)
Guy, Simons, Richiardson (1966)	1	3.08E-01	9.30E-04	1.22E-02	6.40E-01	3.05E-04
	2	3.17E-01	9.30E-04	1.52E-02	1.13	3.56E-04
	3	3.29E-01	9.30E-04	2.74E-02	1.00	7.11E-04
	4	1.77E-01	9.30E-04	6.10E-03	8.84E-01	6.10E-04
	5	1.65E-01	9.30E-04	6.10E-03	8.84E-01	6.10E-04
	6	3.17E-01	9.30E04	4.88E-02	1.10	6.60E-04
	7	1.62E-01	9.30E-04	1.83E-02	8.84E-01	1.02E-03
	8	3.05E-01	9.30E-04	5.49E-02	1.07	9.14E-04
	9	1.71E-04	9.30E-04	2.44E-02	1.01	9.14E-04
	10	2.83E-01	9.30E-04	8.53E-02	1.58	8.64E-04
	11	1.40E-01	9.30E-04	3.66E-02	1.19	1.22E-03
	12	1.68E-01	9.30E-04	3.96E-02	1.07	1.63E-03
	13	3.17E-01	9.30E-04	9.45E-02	1.77	2.29E-03
	14	2.80E-01	9.30E-04	9.75E-02	2.26	3.05E-03
	15	1.74E-01	9.30E-04	5.18E-02	1.80	3.00E-03
Mancini, Menduni (1986)	1	7.80E-02	8.80E-04	1.10E-02	4.82E-01	n.m.
	2	4.80E-02	8.80E-04	4.00E-03	3.51-01	n.m.
	3	8.00E-02	8.80E-04	9.00E-03	4.78E-01	n.m.
	4	4.90E-02	8.80E-04	4.00E-03	3.42E-01	n.m.
	5	7.80E-02	8.80E-04	9.00E-03	5.10E-01	n.m.
Venditti, Church, Bennett (2005)	1	1.52E-01	5.00E-04	4.77E-02	1.17	6.50E-04
	2	1.53E-01	5.00E-04	4.16E-02	8.60E-01	3.71E-04
	3	1.53E-01	5.00E-04	3.59E-02	9.50E-01	3.34E-04

Continued on next page

Continued from previous page

SOURCE	Run	Y (m)	D_{50} (m)	Δ (m)	λ (m)	c (m/s)
Klaassen (1979)	1	2.84E-01	7.50E-04	8.90E-02	1.66	n.m.
	2	3.63E-01	7.50E-04	9.30E-02	1.81	n.m.
	3	3.97E-01	7.50E-04	9.70E-02	1.91	n.m.
	4	4.89E-01	7.50E-04	1.04E-01	1.89	n.m.
	5	5.92E-01	7.50E-04	1.02E-0	1.65	n.m.
	6	3.01E-01	7.50E-04	9.30E-02	1.57	n.m.
	7	4.88E-01	7.50E-04	1.12E-01	1.82	n.m.
	8	4.51E-01	7.50E-04	1.01E-01	2.45	n.m.
	9	2.63E-01	7.50E-04	1.17E-01	1.90	n.m.
	10	4.05E-01	7.50E-04	1.00-01	1.79	n.m.
	11	4.89E-01	7.503-04	1.65-01	2.19	n.m.
Wijbenga, Klaassen (1993)	1	3.02E-01	7.50E-04	7.70E-02	1.20	6.75E-04
	2	2.00E-01	7.50E-04	7.10E-02	1.38	3.83E-04
	3	3.01E-01	7.50E-04	8.70E-02	1.45	6.61E-04
	4	2.00E-01	7.50E-04	7.10E-02	1.39	4.00E-04
	5	4.05E-01	7.50E-04	1.04E-01	1.59	8.00E-04
	6	2.01E-01	7.50E-04	6.90E-02	1.25	5.36E-04
	7	3.01E-01	7.50E-04	8.60E-02	1.41	6.83E-04
Wang, White (1990)	1	1.13E-01	7.60E-04	3.50E-02	6.00E-01	1.68E-04
	2	1.09E-01	7.60E-04	3.50E-02	6.00E-01	1.68E-04
	3	1.13E-01	7.60E-04	4.50E-02	1.00	3.05E-04
	4	1.18E-01	7.60E-04	5.00E-02	1.00	6.47E-04
	5	1.13E-01	7.60E-04	5.00E-02	1.00	1.28E-03
	6	1.22E-01	7.60E-04	5.50E-02	1.00	1.83E-03
	7	1.00E-01	7.60E-04	5.50E-02	1.00	1.92E-03
	8	1.27E-01	7.60E-04	6.00E-02	1.00	2.08E-03
	9	1.27E-01	7.60E-04	6.50E-02	1.10	2.61E-03
	10	1.32E-01	7.60E-04	7.003E-02	1.20	2.95E-03
	11	1.35E-01	7.60E-04	7.00E-02	1.20	3.20E-03
	12	1.35E-01	7.60E-04	7.00E-02	1.40	3.61E-03

Concluded from previous page

The tables 6.3 and 6.4 show the summaries of the experimental data collected in the present work and in literature.

Table 6.3: Summary of experimental data-A: Range (Maximum and minimum value) observed;

SOURCE	Run	ql (m^2/s)	qss (m^2/s)	qs (m^2/s)	B (m)	S $(-)$
Guy,Simons, Richiardson (1966)	**15**	8.01E-02	3.10E-08	1.23E-06	2.44	3.70E-04
		2.59E-01	5.98E-05	1.15E-04	2.44	4.30E-03
Mancini, Menduni (1986)	**5**	1.90E-02	0.00	3.77E-06	0.12	3.90E-03
		4.00E-02	0.00	1.07E-05	0.12	4.40E-03
Venditti,Church, Bennett (2005)	**3**	6.96E-02	0.00	3.95E-06	1.00	7.00E-04
		7.59E-02	0.00	1.20E-03	1.00	1.20E-03
Klaassen (1979)	**11**	1.50E-01	0.00	1.54E-06	1.50	3.84E-04
		4.23E-01	0.00	6.44E-05	1.50	3.99E-03
Wijbenga, Klaassen (1993)	**7**	9.70E-02	0.00	7.29E-06	1.50	1.53E-03
		2.67E-01	0.00	2.01E-05	1.50	1.68E-03
Wang, White (1990)	**12**	9.47E-02	0.00	1.74E-05	0.92	5.10E-03
		4.34E-02	0.00	7.46E-04	0.92	4.22E-04
DICeA 2009	**32**	3.75E-02	0.00	9.21E-07	0.10	2.12E-03
		1.06E-01	0.00	2.25E-05	0.10	1.46E-02
DICeA 2011	**23**	2.36E-02	0.00	0.00	0.10	1.58E-03
		1.17E-01	0.00	3.55E-06	0.10	5.29E-03

Table 6.4: Summary of experimental data-B: Range (Maximum and minimum value) observed;

SOURCE	Run	Y (m)	D_{50} (m)	Δ (m)	λ (m)	c (m/s)
Guy,Simons, Richiardson (1966)	**15**	0.140	9.40E-04	6.10E-03	6.30E-01	3.05E-04
		0.320	9.30E-04	9.75E-02	2.26	3.05E-03
Mancini, Menduni (1986)	**5**	0.048	8.80E-04	4.00E-03	3.42E-01	n.m.
		0.080	8.80E-04	1.10E-02	5.10E-01	n.m.
Venditti,Church, Bennett (2005)	**3**	0.152	5.00E-04	3.59E-02	8.60E-01	3.34E-04
		0.153	5.00E-04	4.77E-02	1.17	6.50E-04
Klaassen (1979)	**11**	0.263	7.50E-04	8.90E-02	1.57	n.m.
		0.592	7.50E-04	1.65E-01	2.45	n.m.
Wijbenga, Klaassen (1993)	**7**	0.200	7.50E-04	6.90E-02	1.20	3.83E-04
		0.405	7.50E-04	1.04E-01	1.59	8.00E-04
Wang, White (1990)	**12**	0.135	7.60E-04	7.00E-02	1.40	3.61E-03
		0.100	7.60E-04	3.50E-02	6.00E-01	1.68E-04
DICeA 2009	**32**	0.057	7.90E-04	9.30E-03	1.90E-01	1.04E-03
		0.181	7.90E-04	3.32E-02	6.83E-01	1.05E-02
DICeA 2011	**23**	0.044	1.25E-03	2.50E-03	4.53E-01	2.84E-04
		0.197	1.25E-03	3.01E-02	1.13	7.57E-03

6.1.2 Graphical Comparison

The present experimental data have been compared with literature data. For clarity, the present data have been classified according to the following sets:

- - **DICeA 2009 C.S.S.**, are the data collected from the experiments described in this thesis in a condition of constant sediment supply conducted with the sediment type A
- - **DICeA 2009 C.F.D.**, are the data collected from the experiments described in this thesis in a condition of constant flow discharge conducted with the sediment type A
- - **DICeA 2010 C.S.S.**, are the data collected from the experiments described in this thesis in a condition of constant sediment supply conducted with the sediment type B
- - **DICeA 2010 C.F.D.**, are the data collected from the experiments described in this thesis in a condition of constant flow discharge conducted with the sediment type B
- - **Literature**, are the data collected from the literature

Furthermore, the following dimensionless variables have been introduced:

- $Y_{adim} = \frac{Y}{D_{50}}$
- $\Delta_{adim} = \frac{\Delta}{D_{50}}$
- $\lambda_{adim} = \frac{\lambda}{D_{50}}$
- $c_{adim} = \frac{c}{\sqrt{g \cdot D_{50}}}$

Comparisons are shown in the following graphs. In particular, the dimensionless dune height (Δ_{adim}) against the dimensionless mean flow velocity (Y_{adim}) is shown in figure 6.1. A very similar pattern can be seen between literature and the present data, in which dune height increases with water depth. Analogous results are obtained by plotting the dimensionless dune length, λ_{adim} as shown in figure 6.2.

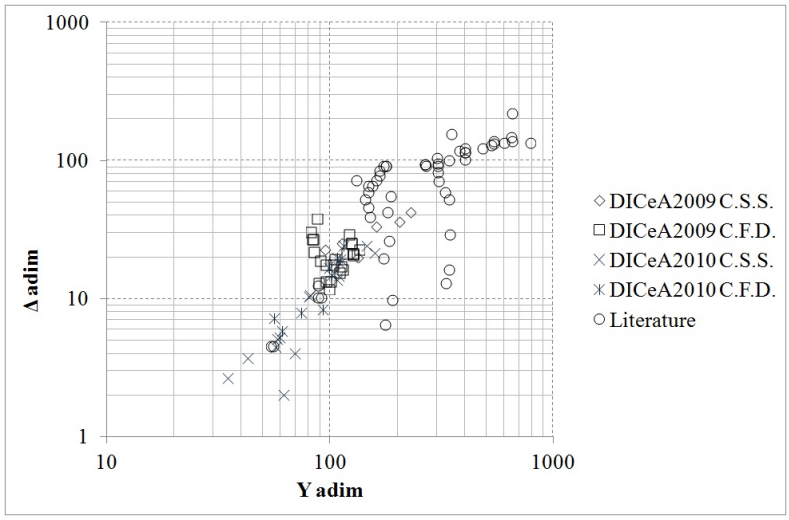

Figure 6.1: Height of Dune Behaviour: $\Delta_{adim} - Y_{adim}$;

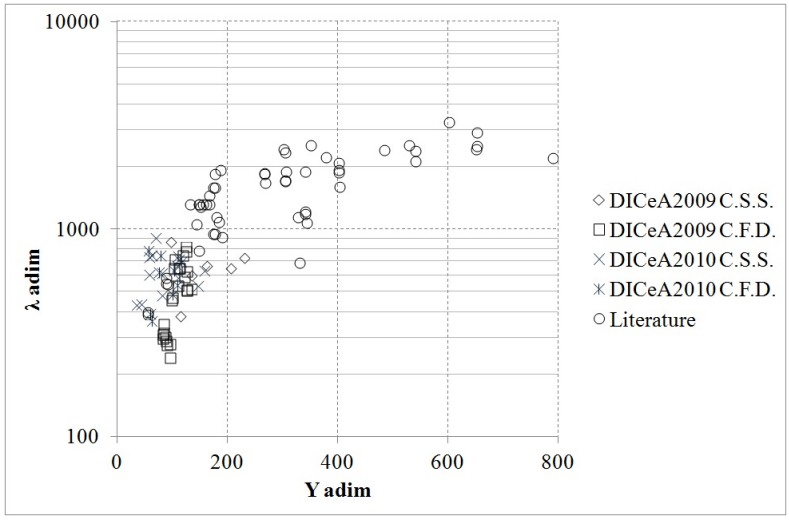

Figure 6.2: Length of Dune Behaviour: $\lambda_{adim} - Y_{adim}$;

The dimensionless dune length has also been plotted against the Froude number, as shown in figure 6.3, where one can see a general decreasing trend of dimensionless dune length as the Froude number increases.

Finally, the dune crest celerity, in figure 6.4, is plotted against the dimensionless water depth and the relation shows a decreasing trend, whereas in figure 6.5, an increasing trend when the Froude number increases is apparent;

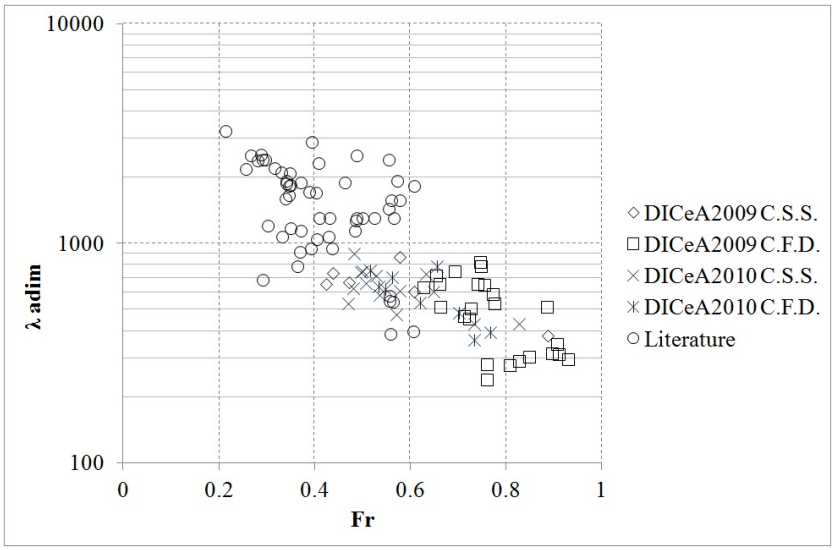

Figure 6.3: Length of Dune Behaviour: $\lambda_{adim} - Fr$;

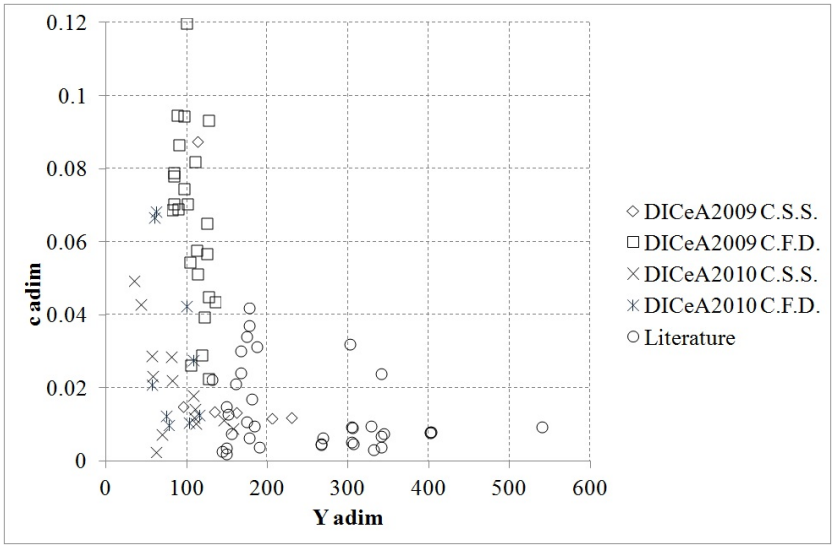

Figure 6.4: Celerity of Dune Behaviour: $c_{adim} - Y_{adim}$;

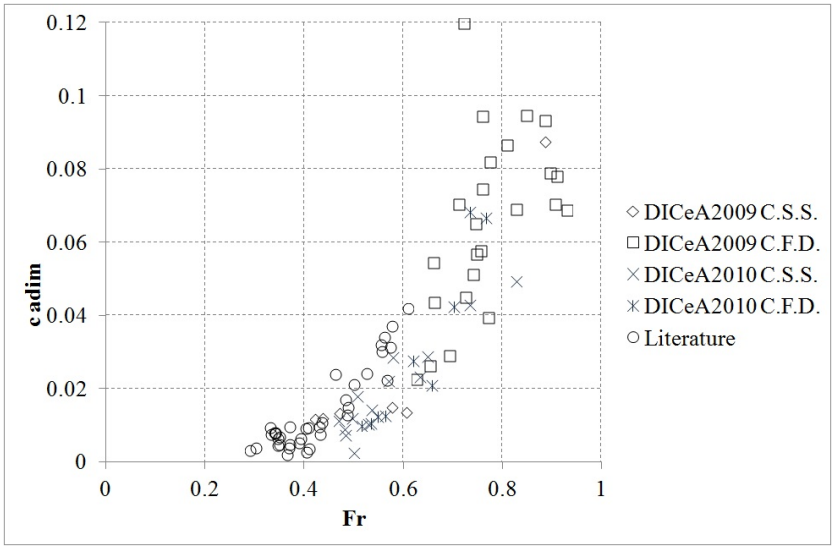

Figure 6.5: Celerity of Dune Behaviour: $c_{adim} - Fr$;

By considering the dunes as the "footprints" of the eddies on the bed,Yalin (1973), derived a theoretical relationship for the dune length:

$$\lambda \simeq 2 \cdot \pi \cdot Y \tag{6.1}$$

which appears to agree substantially with the empirical relationship derived from Yalin (1964) experimental data:

$$\lambda \simeq 5 \cdot Y \tag{6.2}$$

The relation 6.2 is at the same time very near to the "prevailing dune length" of Hino (1969):

$$\lambda \simeq 7 \cdot Y \tag{6.3}$$

The A.S.C.E. (2008) suggest a lower and upper limit considering this relation:

$$k = \frac{2 \cdot Y}{\lambda} \tag{6.4}$$

with a value of the dimensionless wave number k: $0.25 < k < 4.0$

The relationships 6.1,6.2,6.3,6.4 have been plotted in figure 6.6 together with the experimental data from literature and from the present study

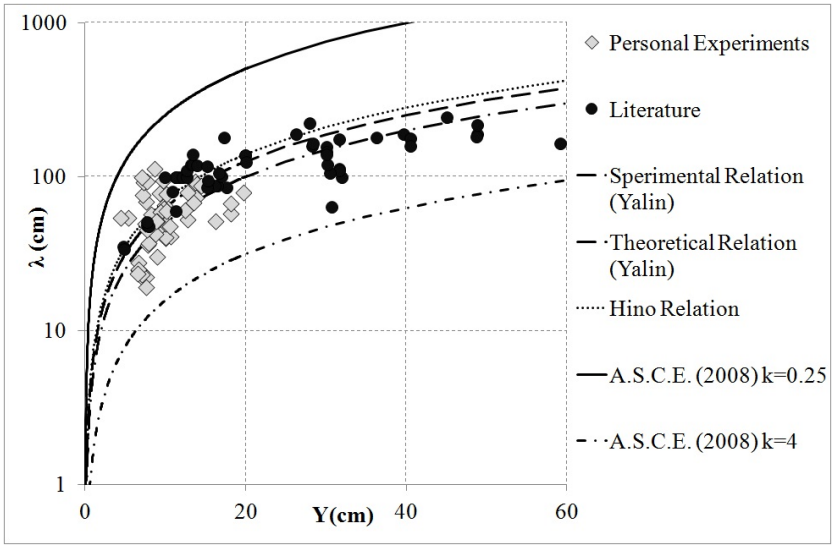

Figure 6.6: Comparison with Yalin Relation;

Kondap and Garde (1973) suggested an empirical relationship between the celerity of the dunes, the mean water depth and the Froude number of the flow, which seems to fit the experimental data quite well, as shown in figure 6.7.

$$c = 0.021 \cdot Fr^4 \cdot \sqrt{g \cdot Y} \tag{6.5}$$

From the comparison shown in figure 6.6 and figure 6.7 has been found a good agreement between the literature data and the present data. It is noteworthy to point out that the data collected in the literature were collected in flume type recirculating flume while present data were collected in a channel-type feed flume. **This result suggests that the behaviour of dune celerity and dune wavelength do not seem dependent on the type of flume and on the experimental cycle.**

Now it is logical to ask: **Does the height of dunes assume an independent behaviour of the flume and of the experimental cycle too?**
Parker and Wilcock (1993) asserts that in a condition of plane bed or for small-scale bed forms "*If the sediment is of uniform size, the asymptotic equilibrium flows obtained for both types of flumes are completely equivalent and independent of initial conditions.*"
Does this assumption continue to be valid for a bed covered by well developed dunes?

In order to answer these two questions in figure 6.8, present data and the literature data are compared in terms of dune height: In the abscissa is plotted the ratio between the sediment transport or sediment supply and the flow discharge (Qs/Ql), whereas in the y-axis is plotted the ratio between the dune height and the mean water depth (Δ/Y).

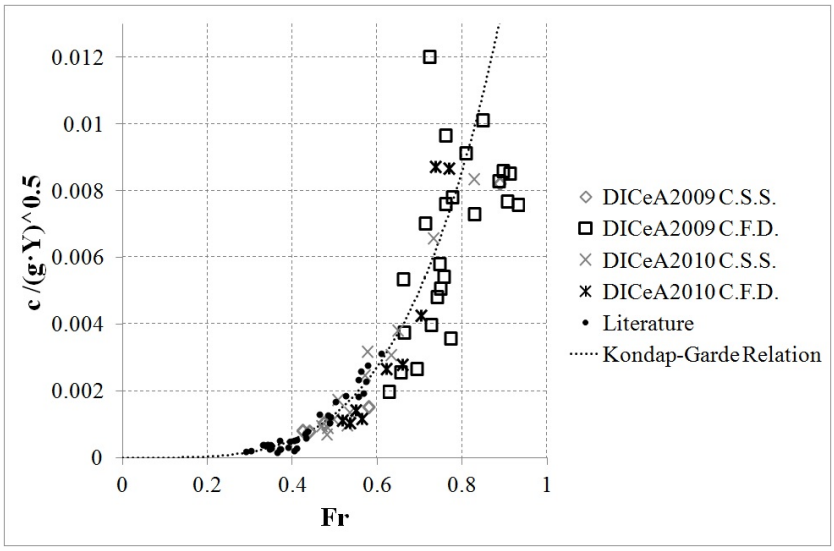

Figure 6.7: Comparison with the Kondap-Garde Relation;

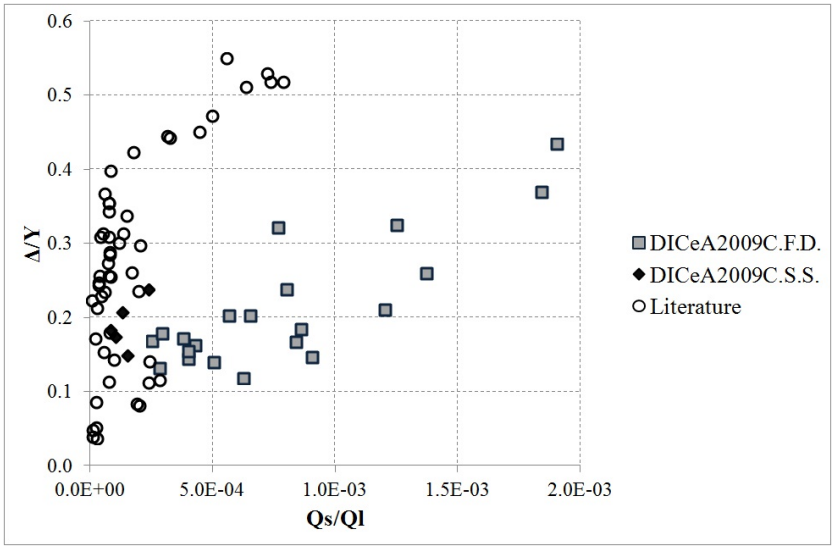

Figure 6.8: Comparison of dimensionless dunes height from experiments in CFD and CSS cycle conducted in a feed flume and literature experiments conducted in a recirculating flume;

The figure 6.8 seems to show a very interesting trend of the variables. In fact, the behaviour of the dimensionless dune height seem to be similar in the experiments in CSS cycle conducted in a feed flume and in the experiments conducted in recirculating flume. The trend shown by the dimensionless dune height in the experiments in CFD cycle conducted in a feed flume is very different from the other two.

The comparisons in figures 6.6, 6.7, 6.8 show that while the behaviour of dune celerity and dune wavelength do not seem to be dependent on the type of flume and on the experimental cycle the behaviour of the dune height is strongly dependent on the type of flume and on the experimental cycle used for the experiments

In particular, in a channel type feed flume, the behaviour of the dune height seems to be completely different in a CSS cycle respect to that in a CFD cycle; this concept will be better analysed in the part III. Moreover, the behaviour of the dune height, in experiments conducted in a channel type recirculating flume, is similar to that conducted in a channel type feed flume during a CSS cycle but it is very different from the behaviour of dune height during a CFD cycle, as demonstrated by the comparison shown in figure 6.7.

The hypothesis of this different behaviour will be analyzed and reported in the conclusions as a result of the considerations that will be made in the following part.

Part III

DATA ANALYSIS

Abstract

In this part, the data of the experimental cycle conducted and described in the previous part II are analysed. As has been stated previously, the experimental cycles consist of two types: one where, in addition to the composition of the sediment and to the geometry of the experimental channel, the sediment transport/sediment supplied also remains fixed while the liquid flow rate, for each step, is varied by the operator, section 7.1; while for the other type, in addition to the composition of the sediment and to the geometry of the flume, the liquid flow rate also remains fixed while the sediment transport/sediment supplied is varied, for each step, by the operator, section 7.2.

In both cycles, other quantities relating to the flume were free to change, and in this way the flume reaches a new equilibrium. Particular attention was given in the cycle to the behaviour offered of the average slope of the bed, the speed and the height of the dunes. In caption 8, an "interpretation" of the behaviour of these observed quantities has been provided, and of their response diametrically opposed to depending on whether the cycle is type CSS or CFD.

In chapter 9, a numerical model was presented, based on both the physical relationships that governed the experiments and the results that the experiments produced.

The model is designed to reproduce the experiments already conducted in this work, section 9.3, and also to extend the set of combinations obtained through personal experiments.

In chapter 10, the physically based model was also used to define a condition of existence of the dunes. This defined field, in addition to adapting to the limits proposed in the literature, gives a more accurate definition of the field of existence of the dunes, and then defines the field of the adaptive behaviour that the dunes can provide to the channel.

Chapter 7

Experiment analysis

As can be seen in section 4.2, each experimental cycle is constituted by a series of steps in dynamic equilibrium and starts by imposing some constraints, which were considered the **independent variables**:

- 1. The sediment supply;
- 2. The liquid discharge;
- 3. The grain size and the void ratio;
- 4. The channel width;

the following physical quantities were considered as **dependent variables** of the physical system:

- 1. The water depth;
- 2. The sand wave height;
- 3. The sand wave length;
- 4. The velocity of the propagation of sand waves;
- 5. The channel slope;

Then two sets of experimental cycles were carried out:

- **The Constant Sediment Supply (C.S.S.) experiments**, where the behaviour of the dependent variables were analysed at several equilibrium conditions obtained at different flow discharges maintaining the value of sediment supply constant, for the whole duration of the cycle;

- **The Constant Fluid Discharge (C.F.D.) experiments**, where the behaviour of the dependent variables were analysed at several equilibrium conditions obtained at different sediment supply values, maintaining the value of flow discharge constant, for the whole duration of the cycle;

To give a better explanation of the two sets of experiments, two experimental cycles are presented: one in a CSS condition and the other in a CFD condition. Both experiments start in a condition of sedimentological equilibrium and then this equilibrium is upset by an increase of the liquid discharge (in a C.S.S. condition) or by an increase of the sediment supply (in a C.F.D. condition); in both the experiments it is observed how the flume reaches another sedimentological equilibrium, changing freely the bed slope, the water depth, the flow velocity and the geometric features and the celerity of the bed forms along the channel.

7.1 C.S.S.Cycle

The first example was derived from the experimental cycle 17-29 (B.5), conducted with the sediment type B; the time duration of this experiment was of 76 hours; In figure 7.1 and 7.2 plotted in the x-axis are the number of sedimentogical equilibria during the cycle and in the y-axis the values of some independent and dependent variables. The experimental cycle started in a condition of sedimentological equilibrium with a value of liquid flow equal to 6 l/s and a sediment supply of 1.67 g/s; then the liquid discharge was increased up to a value of 8.9 l/s and the experimental channel, freely varying its parameters, reached another sedimentological equilibrium. Proceeding in this way, the flow discharge was increased up to the value of 11.85 l/s and it then decreased as far as the initial value while the sediment supply remained constant for the all the experiments with a total number of 5 sedimentological equilibria.

Observations concerning the behaviour of the dependent variables:

- Figure 7.1, shows the trend of the independent variables, the sediment transport/sediment supply and the liquid discharge; it also shows, as the dependent variable, the variation of the bed slope; It can be seen that with a large variation of the independent variable, the liquid flow, there was a weak response of the bed slope (variation range of the bed slope 0.0025-0.0032);

- In figure 7.2 the trend of the height of the dunes and of the celerity in the experimental cycle is plotted. In particular the height of the dunes has a large variation and increases (1.3-3 cm) when the liquid discharge increases. Similarly, the height of the dunes decreases (3-1.32 cm) when the liquid discharge decreases. As regards the dune celerity, it decreases slowly (3.1-1.1 mm/s) when the liquid discharge increases. In contrast, it increases in the same way (1.25-2.45 cm), when the liquid discharge decreases.

Therefore it can be summarized that the main change in the CSS cycles is sustained by the height of the dune in the same direction as the variation of liquid flow, while the average slope of the bed and the velocity of the dune undergo a small change in a direction discordant with the variation of liquid flow.

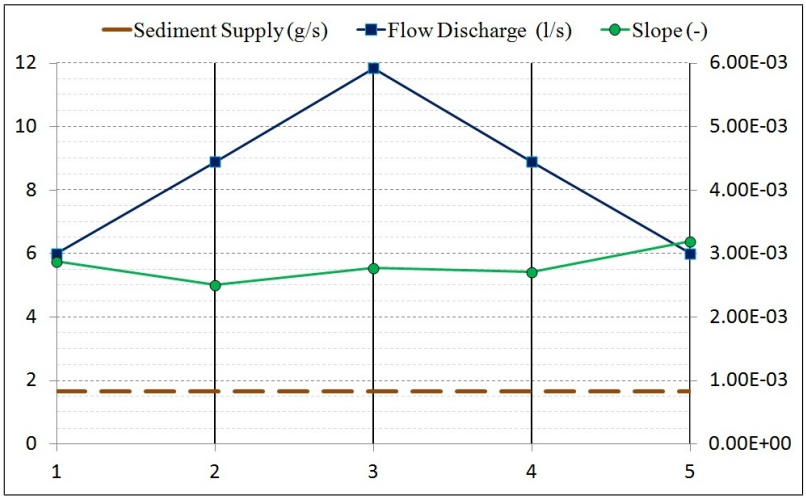

Figure 7.1: Variables' behaviour in a C.S.S. cycle through 5 equilibrium phases: sediment supply, flow discharge (left y-axis), channel slope (right y-axis);

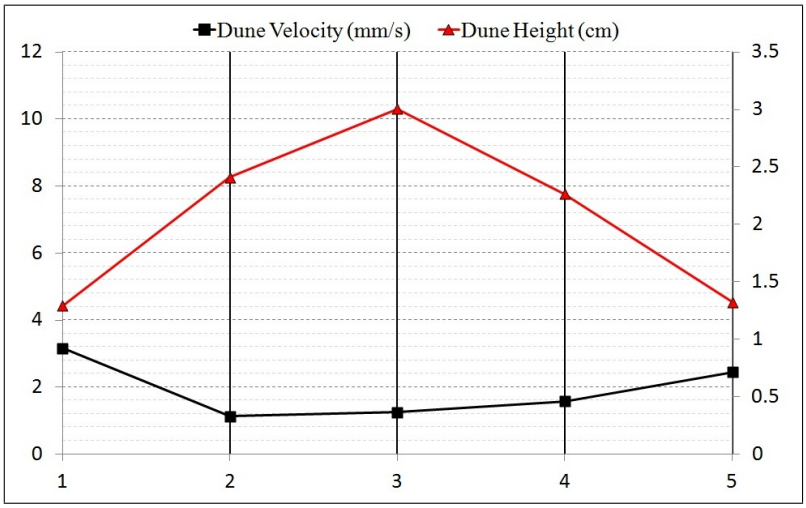

Figure 7.2: Variables' behaviour in a C.S.S. cycle through 5 equilibrium phases: dune height, dune velocity;

7.2 C.F.D.Cycle

The second example was derived from the experimental cycle 1-5 (B.1); it was conducted with the sediment type B; the time duration of this experiment was of 36 hours; The experimental cycle started in a condition of sedimentological equilibrium with a value of flow discharge of 5.05 l/s and a sediment supply of 0.67 g/s; then the sediment supply was increased up to a value of 4.35 g/s and then the experimental channel, freely varying its parameters, reached another sedimentological equilibrium. Proceeding in this way, the sediment supply was increased up to the value of 6.1 g/s and then decreased as far as the initial value, while the flow discharge remained constant for the whole of the experiment with a total number of 5 sedimentological equilibria.
Observations concerning dependent variable behaviour:

- Figure 7.3 shows the trend of the independent variables, the sediment transport/sediment supply and the liquid discharge; it also shows, as the dependent variable, the variation of the bed slope; It can be seen that with a large variation of the independent variable, sediment transport/sediment supply, the response of bed slope was significant (variation range of the bed slope 0.0015-0.0055);

- In figure 7.4 the trend of the height of the dunes and of the celerity in the experimental cycle is plotted. In particular, the height of the dunes decreases slowly (1.04-0.41 cm) when the sediment supply increases and, in contrast, the height of the dunes increases slowly (0.41-1 cm) when the sediment supply decreases. As regards the dune celerity, it has significant variations; in fact, it is much increased (1.1-11.4 mm/s) when the sediment supply increases and it is much decreased (11.4-1.3 cm) when the sediment supply decreases.

In CFD cycles, the main change is experienced by the average slope of the bottom and the speed of the dune, in the same direction with the variation of sediment supplied and the height of the dune undergoes a small change in direction discordant with the variation of the sediment supplied.

7.3 Orthogonal Behaviour in C.F.D. and C.S.S. cycles

In addition, the choice it has been made to display the main changes of the channel in its free process of adaptation, using the graphs below. To best view these changes only data from complete cycles have been used, where both the ascending and descending phases of the chosen independent variable are present. Specifically, the experimental cycles are: A.13, B.2, B.5 e A.9, B.1, B.6.

Variables in the graphics are defined as follows:

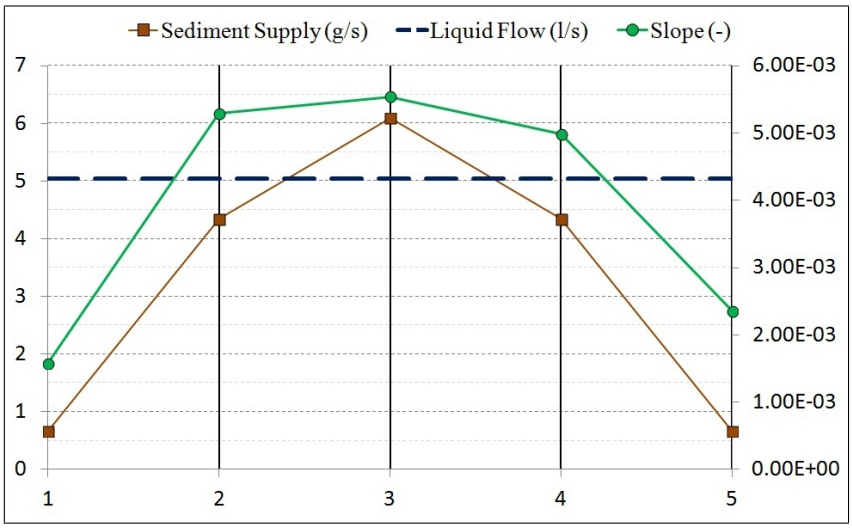

Figure 7.3: Variables' behaviour in a C.F.D. cycle through 5 equilibrium phases: sediment supply, flow discharge (left y-axis), channel slope (right y-axis);

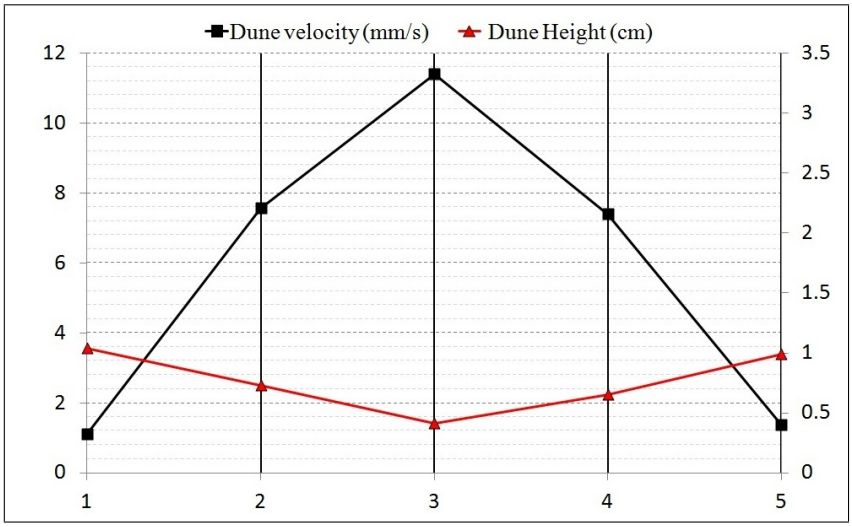

Figure 7.4: Variables' behaviour in a C.F.D. cycle through 5 equilibrium phases: dune height, dune velocity;

$Ql_* = \frac{Ql_i}{Ql_1}$

$Qs_* = \frac{Qs_i}{Qs_1}$

$S_* = \frac{S_i}{S_1}$

$\Delta_* = \frac{\Delta_i}{\Delta_1}$

$c_* = \frac{c_i}{c_1}$

$\tau'_* = \frac{\tau'_i}{\tau'_1}$

Ql is the liquid flow in the channel, Qs the sediment transport, Δ the height of the dune, c the velocity of the dune crest, S the mean slope of the bottom and τ' the value of the effective shear stress calculated as $\tau' = \rho \cdot (u*')^2 \mapsto u*' = U/C' \mapsto C' = 5.75 \cdot \log(12 \cdot R_b/Ks)$; Where $Ks = 2 \cdot D_{50}$ is the equivalent (sand grain) roughness height and R_b is the hydraulic mean radius of the bed (side wall correction applied) The subscripts **1** and **i** indicate the sizes records at the beginning of the cycle and in subsequent stages of the cycle. Qs_* and Ql_* are always placed on the abscissa, respectively, for cycles: Constant Flow Discharge, and Constant Sediment Supply. In figure 7.5, a orthogonal trend of the height of the dunes is evident depending on whether the cycle has a liquid or a solid discharge variable.
In particular: in the experiments at **constant sediment supplied CSS**, the height of the dune shows great sensitivity to the variation of the liquid flow rate, and also grows in accordance. In the experiments at **constant flow discharge CFD**, the height of the dune behaves in the opposite way, in fact it shows a small change and it also decreases with an increasing sediment supply. In figure 7.6, the trend of the celerity of dunes in both cycles is plotted, and in this graph too, the completely different behaviour of a dependent variable is evident depending on the type of cycle. In particular, the response of the dune celerity is opposite to the height of the dunes, in fact: In the experiments at **constant sediment supplied CSS**, the celerity of the dune shows a small change and it also decreases with an increasing flow discharge. In the experiments at **constant flow discharge CFD**, the dune celerity behaves in the opposite way, in fact, it shows great sensitivity to the variation of the sediment supply, and also grows in accordance with it. In figure 7.7, the trend of the mean bed slope in both cycles is plotted; even in this case, different variations of trends and amount are clear, depending on the cycles. In particular, one can observe a much more relevant variation of bed slope, in accordance with the sediment supply variation, for an experimental cycle in a condition of constant flow discharge. From the graph in figure 7.8, it can be seen that τ'_*, during the experiment at a constant sediment supply CSS is much more constant than during the experiment at constant flow discharge CFD where it grows with the increasing sediment supply.

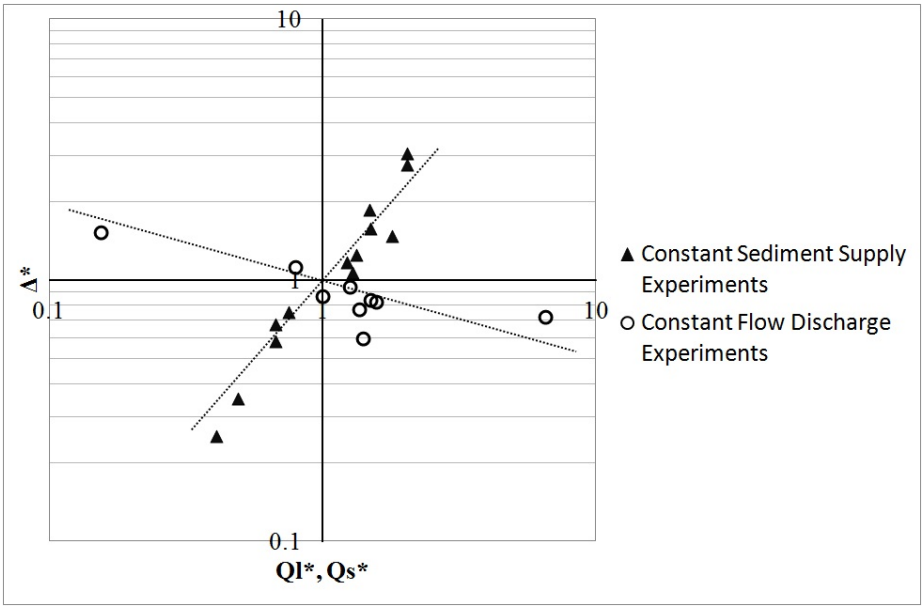

Figure 7.5: Δ_* in C.S.S. (C.F.D.) experiments versus $Ql_*(Qs_*)$;

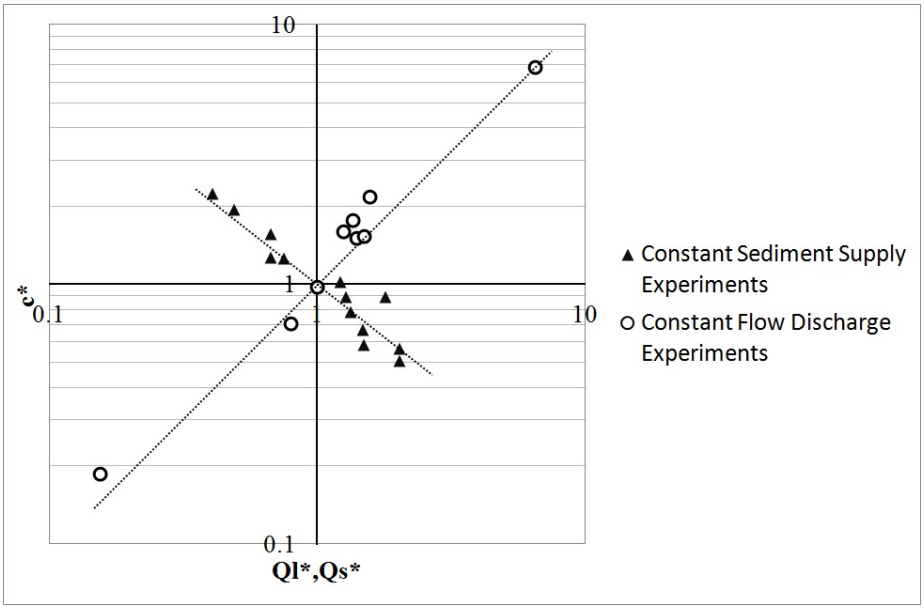

Figure 7.6: c_* in C.S.S. (C.F.D.) experiments versus $Ql_*(Qs_*)$;

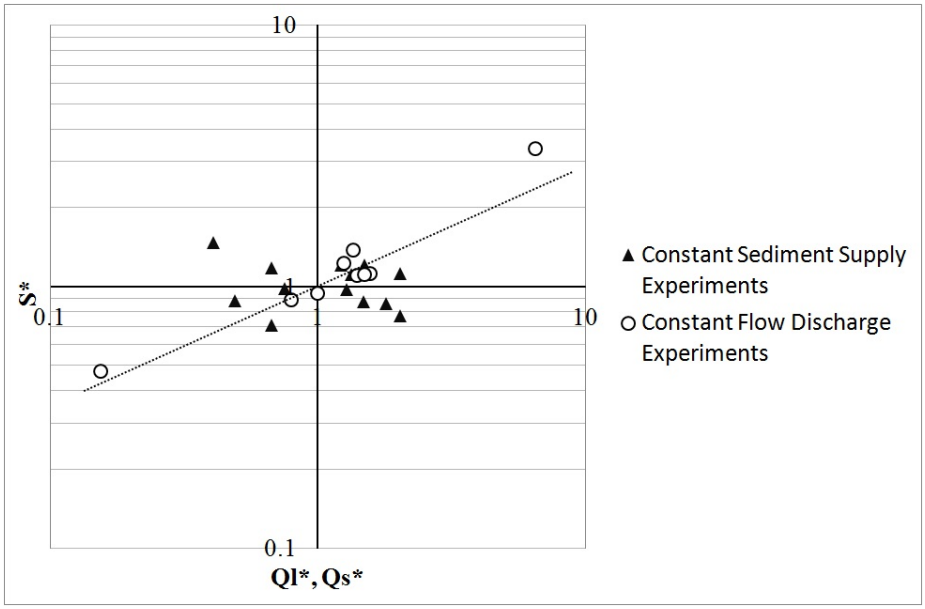

Figure 7.7: S_* in C.S.S. (C.F.D.) experiments versus $Ql_*(Qs_*)$;

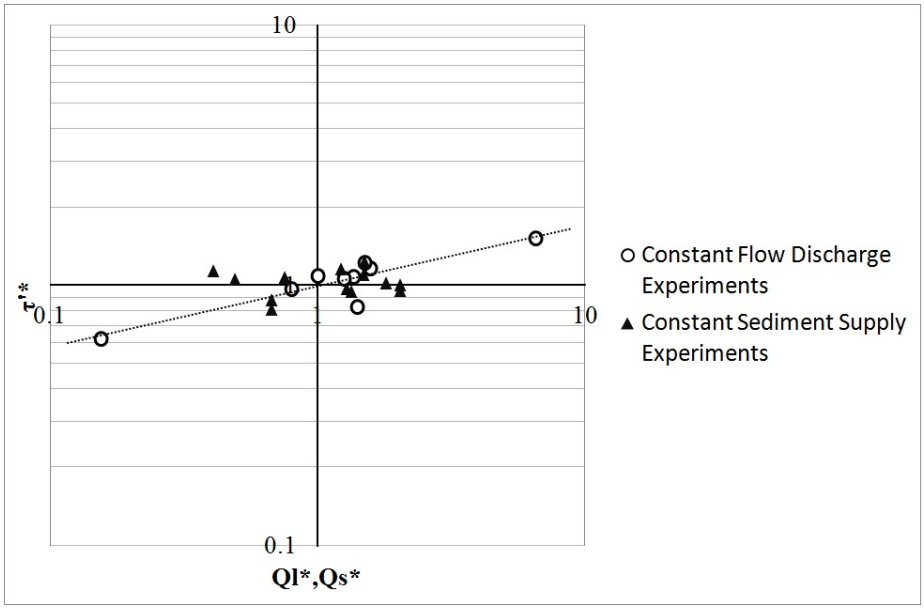

Figure 7.8: τ'_* in C.S.S. (C.F.D.) experiments versus $Ql_*(Qs_*)$;

Chapter 8

An interpretation of dunes' behaviour - The adaptive process of the bedforms

From the previous chapter, it is clear that the dependent variables such as bed slope, height and velocity of dune evolve through different patterns depending on whether the cycle is CFD or CSS. The different response of a dependent variable within different cycles conducts the physical system to a different dynamic equilibrium of the channel. In this chapter, an attempt is made to give a physical interpretation of these processes. First of all, it is necessary to estimate the sediment transport capacity of the channel. To this aim, the equation proposed by van Rijn (1984a) has been considered since it provides the best fit with experimental data. The equation estimates the bed load transport in terms of effective bed shear stress.

$$qs = 0.053 \cdot [(s-1) \cdot g]^{0.5} \cdot D_{50}^{1.5} \cdot D_*^{-0.3} \cdot T^{2.1} \qquad (m^2/s) \tag{8.1}$$

The formula 8.1 is for particles in the range of 200-2000 μm, and qs represents the bed load transport per unit width, s represents the specific gravity, g the gravitational acceleration, D_{50} the characteristic particle diameter of bed material, D_* dimensionless grain size, T the Van Rijn parameter defined as $\frac{\tau' - \tau_{cr}}{\tau_{cr}}$.

The sediment transport capacity can be considered as dependent on the effective shear stress and on the water depth as well as on the liquid discharge, as can be seen in equations 8.2, 8.3, 8.4:

$$\tau' = \rho_w \cdot (u'_*)^2 \tag{8.2}$$

$$u'_* = \left(\frac{U}{C'}\right) \tag{8.3}$$

$$C' = 5.75 \cdot Log_{10}\left(\frac{12 \cdot R_{Hyd}}{2.5 \cdot D_{50}}\right) \tag{8.4}$$

Furthermore, according to equation 1.1 the total bed shear stress (τ) is given by the sum of the effective bed shear stress (τ') and the component due to the drag of the bed forms (τ''), Yalin (1992),Garde and Ranga Raju (1985),Raudkivi (1998).

With these assumptions, the experiments described in the previous chapter were analysed. It seems that when a sedimentological imbalance occurs in the channel (i.e. its sediment transport capacity is not equal to the sediment supplied) the behaviour of the slope of the channel, of the height of dunes and of the velocity of the dune crests are different, depending on whether the imbalance is due to a variation of sediment supply or of liquid discharge.
In particular, in a CSS cycle the sediment supply remains constant whereas the liquid discharge is variable and consequently also the channel sediment transport capacity. In this condition, experiments show that the bed slope does not change significantly. Similar behaviour is also shown by the velocity of the dune crests. In contrast, the height of the dunes seems to vary much more greatly.
In the CFD cycle, the dependent variables exhibit a dual behaviour with respect to the CSS cycle. In fact, under constant flow discharge, sediment supply is variable. The experiments, in this case, have shown a significant change of bed slope and dune velocity as an to adjustment to the sediment transport capacity. In contrast, the height of the dunes does not vary greatly.

In the table of figure 8.1, the above concepts are summarized in terms of variation of the dependent variables within each equilibrium phase.

	Channel slope Variation	Dune Celerity Variation	Dune Height Variation
C.F.D. Experiments	**> 100%**	**> 100%**	< 100%
C.S.S. Experiments	< 100%	< 100%	**> 100%**

Figure 8.1: Variation of the dependent variables in the experiments;

This behaviour can be interpreted with reference to the adaptive process of the dunes in the channel, which develops in the physical system when changes are imposed to the independent variables. In particular, between two sequential equilibrium phases, a transient phase occurs during which the system adjusts its dependent variables. It is considered the results obtained by de Vries (1969) to analyse the behaviour of the dependent variables in the transient phase.

In a condition of flow over a mobile bed, three kind of celerity are defined:

- M1 = (1+$\frac{1}{Fr}$) Celerity of small water surface waves moving in the flow direction.
- M2 = (1-$\frac{1}{Fr}$) Celerity of small water surface waves moving against the flow direction.
- M3 = $\frac{\Psi_2}{(1-Fr^2)}$ Celerity for the propagation of disturbances at the bed, it is largely influenced by the sediment transport.

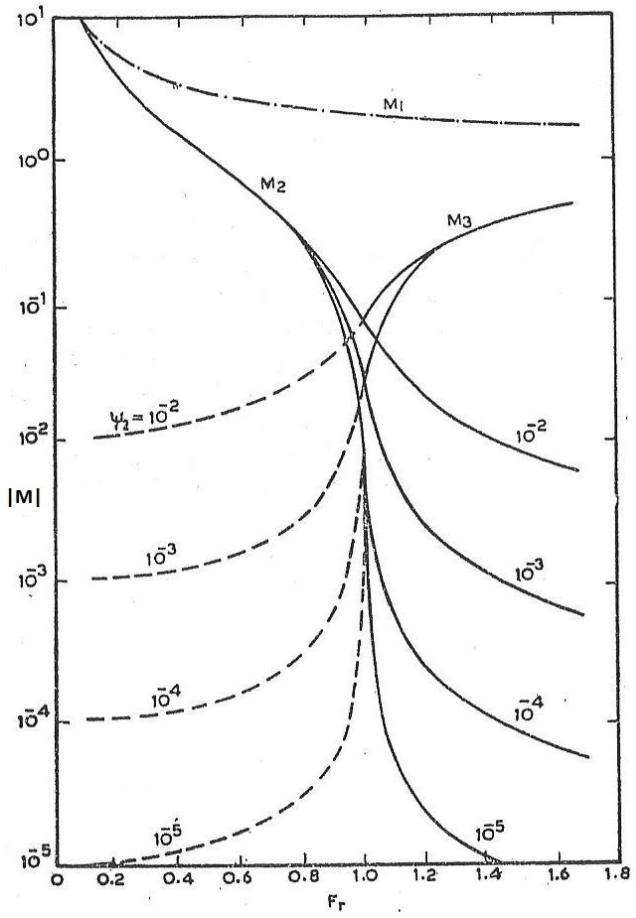

Figure 8.2: Characteristic velocities in alluvial channel, de Vries (1969)

;

In figure 8.2 the characteristic velocities are plotted against the Froude number, and for different values of the non dimensional sediment transport Ψ_2. Where the definition of Ψ_2 is:
$\Psi_2 = \frac{b}{1-\phi} \cdot \gamma_S \cdot \frac{qt}{q}$;

considering the following variables:
γ_S=Specific weight of sediment;
qt= Sediment transport per unit width = $a \cdot U^b$;
U = Flow velocity;
q = Flow discharge per unit width;
ϕ= porosity of the bed material;

It is noteworthy that for subcritical flow, Froude number less than 1, the values of M1 and M2 are much larger than M3.
Taking in regard the theory of de Vries (1969), here it tried to give an interpretation to the phenomena observed during the experiments conducted: From observations of the experiments it was noted that in the C.F.D. cycle, the relevant process of channel adaptation is associated to the bed evolution. In a CFD cycle, the channel passes through several equilibrium phases by modifying essentially the bed slope; For this reason the velocity of the channel adaptation is low and comparable with M3. In particular it was observed in the personal experiments that if the sediment supply increases, the bed slope increases accordingly. At the same time, the dune height tends to decrease. Decreasing the height of dunes increase the effective bed shear stress and the sediment transport capacity (see equation 8.1). However, as mentioned before, it was observed in personal experiments that the relative variation of the dune height is not comparable to that of the bed slope. This behaviour can be explained by observing that the dune height is mainly dependent on the water depth. In contrast, the dune celerity is more susceptible to the variation of sediment supply and it increases its value, balancing the reduction of the dune height in order to satisfy the bed sediment continuity equation 8.5:

$$Qs = \frac{1-e}{2} \cdot c \cdot \Delta \cdot B \qquad (m^3/s) \tag{8.5}$$

where **e** is the void ratio of the sediment, **c** the speed of the crest of the dunes, Δ is the height of dunes and **B** is the width of the channel. The derivation of this equation is given in Appendix D.
Finally, it is worth noting the consistency of this result with the empirical relationships for dune celerity (see equation 6.5).
From observations of the personal experiments it was noted that in the C.S.S. cycle the change of flow discharge under constant sediment supply generates an adjustment process faster and deeply different than it is activated in the CSS cycles. The speed of the adaptation process is now comparable with M1, M2. In fact the velocity of the changes of the water depth and dune height (comparable with M1 and M2) is much faster than the velocity of changes of the bed slope (comparable with M3)and in the CSS cycle the relevant process of channel adaptation is associated to the liquid discharge evolution. In particular, if the flow discharge increases, the water depth and the height of the dunes increase. In this way, the drag form increases and, consequently, so does the total roughness. On the other hand, the effective bed shear stress seems to remain almost constant in order to preserve the sediment transport capacity (see equation 8.1).

Analogously, the bed slope seems to show small relative variations. The most evident aspects of this adaptation process is the role played by the dune height. In this cycle, dune height shows relevant changes occurring at a celerity comparable to that of water depth and no significant variation of dune celerity has been observed. A graphical representation of the processes previously described can be made in terms of bed shear stress. In figures 8.3 and 8.4, the effective and total shear stress are plotted according to the sequential equilibrium phases, in analogy with the previous graphical representation of the experimental data (see figures 7.1 and 7.3). The graphs 8.3 and 8.4 show the trend of the total bed shear stress τ, calculated with the equation 8.6 and the effective shear stress τ', calculated with equation 8.2 in C.S.S. and C.F.D. experiments.

$$\tau = \rho_w \cdot (u_*)^2 \tag{8.6}$$

where u_* is shear velocity:

$$u_* = \sqrt{g \cdot S \cdot R_{Hyd}} \tag{8.7}$$

In the C.S.S experiments the sediment supply remains constant and the results of the behaviour of the dependent variables is that of keeping the effective shear stress almost constant, and, similarity, also the sediment transport capacity. In the first part of the experiment, the total bed shear stress increases because of an increase in the flow discharge but the effective shear stress is not increased although it will be an addend of the total shear stress, as shown in the equation 1.1. This is possible because of the increase in the height of the dune and, consequently, of the τ''.

In the C.F.D experiments the flow discharge remains constant, the effective shear stress can vary together with the value of the sediment supply and the total bed shear stress changes with the effect of the channel slope.

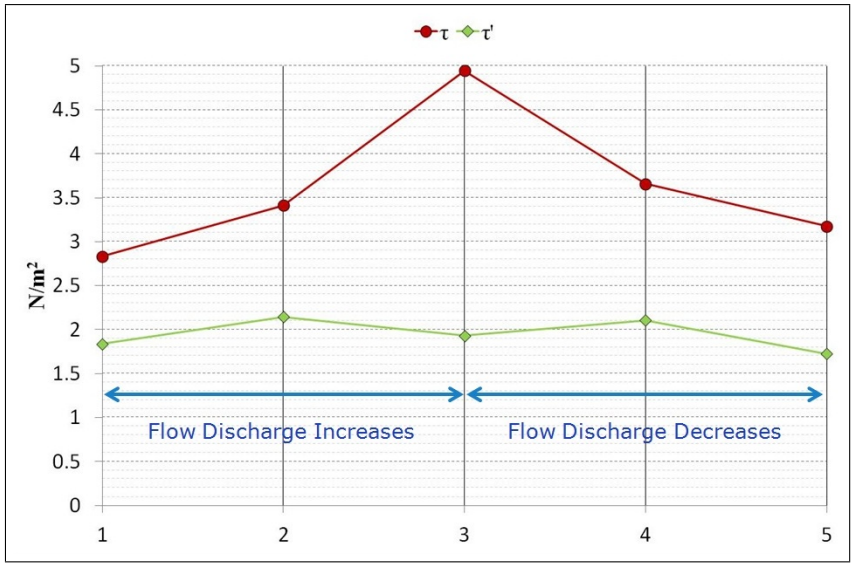

Figure 8.3: τ and τ' behaviour through 5 equilibrium phases in a C.S.S. cycle;

Figure 8.4: τ and τ' behaviour through 5 equilibrium phases in a C.F.D. cycle;

Chapter 9

The Physically Based Model

A physically based model was implemented to reproduce the phenomena observed during the laboratory experiments, in an attempt to a extend the understanding of the dune dynamics. The physically based model is referred to steady and spatially averaged uniform flow, using the basic equations of mechanics, such as momentum and mass conservation. The physical system is schematised by assuming the following set of independent and dependent variables, according to the schema shown in figure 9.1.

The independent variables used as input in the model are:

- 1. Sediment Supply $(m^3/s) = Qs$
- 2. Liquid Discharge $(m^3/s) = Ql$
- 3. Grain Size (m) = D_{50}
- 4. Channel width (m) = B
- 5. Void Ratio = e $\begin{matrix} 0.41 & (D_{50}\text{=1.25 mm}) \\ 0.39 & (D_{50}\text{=0.79 mm}) \end{matrix}$

The dependent variables produced by the model as output are:

- 1. Y = Water Depth (m)
- 2. Δ = Sand Wave Height (m)
- 3. λ = Sand Wave Length (m)
- 4. c = Velocity of propagation of sand waves (m/s)
- 5. S = Slope (-)

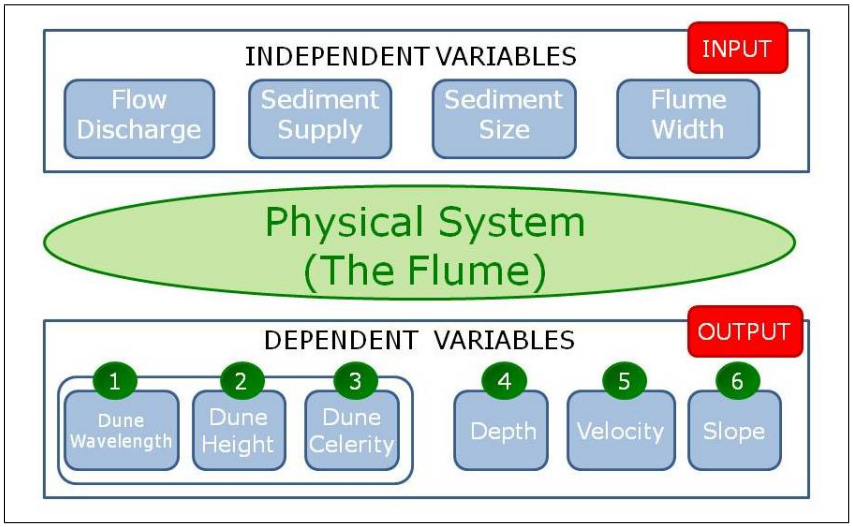

Figure 9.1: Physically Based Schema;

9.1 Development of the model

To implement the model, the following equations were used:

- 1. Continuity Equation for water

$$Ql = U \cdot A \qquad (m^3/s) \tag{9.1}$$

  Where U is the mean water velocity and A the section area, considering the flow completely developed and the channel constant in width.

- 2. Continuity Sediment Equation

$$Qs = \frac{1-e}{2} \cdot c \cdot \Delta \cdot B \qquad (m^3/s) \tag{9.2}$$

- 3. Bed Load Transport, van Rijn (1984a)

$$qs = 0.053 \cdot [(s-1) \cdot g]^{0.5} \cdot D_{50}^{1.5} \cdot D_*^{-0.3} \cdot T^{2.1} \qquad (m^2/s) \tag{9.3}$$

- 4. Momentum Conservation Law

  The momentum equation in vectorial form is:

$$\bar{\mathbf{I}} + \bar{\mathbf{G}} + \bar{\mathbf{M}}in - \bar{\mathbf{M}}out + \bar{\Pi} = 0 \tag{9.4}$$

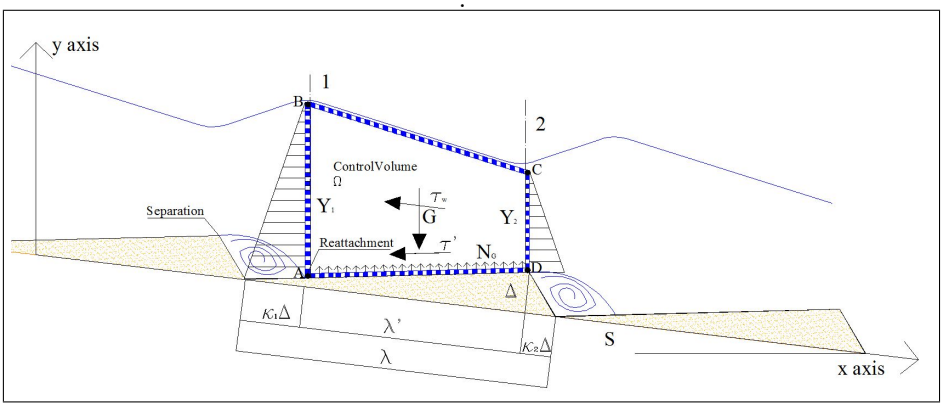

Figure 9.2: Conservation of Momentum Sketch;

With reference to figure 9.2, equation 9.4 has been applied to the control volume ABCD along the x-axis:

$$I_x + G_x + Min_x - Mout_x + \Pi_x = 0 \tag{9.5}$$

where:
I_x: x-component of inertial term, null for steady flow;
G_x: x-component of the water weight within the control volume, equation 9.6;
Π_x: x-component of the forces acting on the control surface, equation 9.10;
$Min_x, Mout_x$: x-component of momentum rate entering and leaving the control volume, respectively, equations 9.19, 9.20.

$$Gx = Y \cdot \lambda' \cdot B \cdot \gamma_W \cdot S \tag{9.6}$$

where λ' is the length of the control volume measured along the dune lee side between the reattachment point and the crest, i.e.:

$$\lambda' = \lambda - K_1 \cdot \Delta - K_2 \cdot \Delta = \lambda - K_3 \cdot \Delta \tag{9.7}$$

The constants K1 and K2 are assumed to be 3 and 1 respectively. Moreover, denoting by Y1 and Y2 the water depth at sections 1 and 2, the following has been assumed:

$$Y1 \approx Y + \frac{\Delta}{2} \tag{9.8}$$

$$Y2 \approx Y - \frac{\Delta}{2} \tag{9.9}$$

Where Y is the mean depth in the channel, Δ the height of the dunes and Y1 and Y2 are, respectively, the depth of the water at the beginning and at the end of the control volume. The x-component of the surface forces is:

$$\Pi_x = \Pi_{x-thrust} + \Pi_{x-wall} + \Pi_{x-bed} + \Pi_{x-normal} \tag{9.10}$$

where:
$\Pi_{x-thrust}$: the resultant hydrostatic pressure along section 1 and 2;
Π_{x-wall}: the resultant wall shear stress;
Π_{x-bed}: the resultant effective bed shear stress;
$\Pi_{x-normal}$: the force due to the normal pressure along the dune stoss side, hydrostatic pressure.
Each term is computed as follows:

$$\Pi_{x-thrust} = Y \cdot \gamma_w \cdot B \cdot \Delta \tag{9.11}$$

$$\Pi_{x-wall} = -2 \cdot \tau_{wall} \cdot Y \cdot (\lambda - K_3 \cdot \Delta) \tag{9.12}$$

where:

$$\tau_{wall} = \rho_w \left(\frac{U}{C_w} \right)^2 \tag{9.13}$$

$$C_{wall} = \frac{\sqrt[6]{R_{Hyd}}}{n_{wall} \cdot \sqrt{g}} \tag{9.14}$$

n_{wall} is the Manning coefficient related to a glass surface, 0.011.

$$\Pi_{x-bed} = -\tau_b \cdot B \cdot (\lambda - K_3 \cdot \Delta) \cos\left(\frac{\Delta}{\lambda} - S \right) \tag{9.15}$$

Assuming the bed slope is negligible with respect to $\frac{\Delta}{\lambda}$: The equation 9.15 can be rewritten:

$$\Pi_{x-bed} = -\tau_b \cdot B \cdot (\lambda - K_3 \cdot \Delta) \cos\left(\frac{\Delta}{\lambda} \right) \tag{9.16}$$

To better explain the computation of Π_{x-bed}, reference is made to figure 9.3:

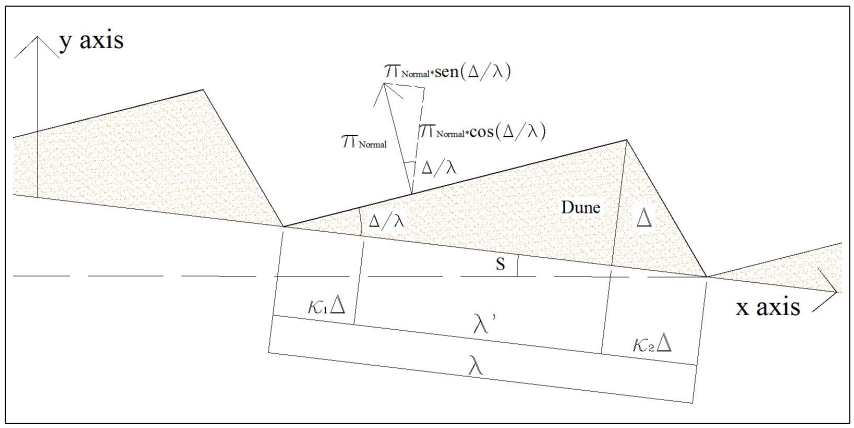

Figure 9.3: Scheme for $\Pi_{x-normal}$ computation;

$$\Pi_{x-normal} = -\gamma_w \cdot \frac{(Y_1 + Y_2)}{2} \cdot (\lambda - K_3 \cdot \Delta) \cdot sin\left(\frac{\Delta}{\lambda} - S\right) \tag{9.17}$$

Considering the relations 9.8 and 9.9 and assuming the bed slope is negligible with respect to $\frac{\Delta}{\lambda}$, we can rewrite the equation 9.17:

$$\Pi_{x-normal} = -\gamma_w \cdot Y \cdot (\lambda - K_3 \cdot \Delta) \cdot sin\left(\frac{\Delta}{\lambda}\right) \tag{9.18}$$

The x-components of the momentum flux are:

$$Min_x = \rho_w \cdot Ql \cdot \frac{Ql}{B \cdot Y_1} \tag{9.19}$$

$$Mout_x = \rho_w \cdot Ql \cdot \frac{Ql}{B \cdot Y_2} \tag{9.20}$$

After some algebraic arrangements, the difference between entering and leaving momentum flux becomes:

$$Min_x - Mout_x = -\rho_W \cdot \frac{Ql^2}{B} \cdot \frac{\Delta}{Y^2 - \Delta^2/4} \tag{9.21}$$

In addition to the above equations, the following empirical relations have been used:

- 5. Relationship for dune celerity Kondap and Garde (1973)

$$c = 0.021 \cdot Fr^4 \cdot \sqrt{g \cdot Y} \tag{9.22}$$

- 6. Relationship for dune length Yalin (1964)

$$\lambda = 5 \cdot Y \tag{9.23}$$

9.2 Details of the proposed model

1. The values of the following independent variable must be assigned:

   Input Values = qs, ql, D_{50}, B, e;

2. From the D_{50} value, the critical Shields parameter can be calculated as follows, Shields (1936):

$$\begin{cases} Rg = \nu \cdot \sqrt{g \cdot D_{50}^3} \\ Ym = (1.28 \cdot Rg)^{-0.6} \\ \theta_{cr} = 0.22 \cdot Ym + 0.06 \cdot (10^{-7.7 \cdot Ym}) \end{cases} \tag{9.24}$$

Then, the critical shear velocity is:

$$u_{*cr} = \sqrt{\theta_{cr} \cdot D_{50} \cdot (s-1) \cdot g} \tag{9.25}$$

Finally, the Van Rijn parameter can be computed:

$$T = \frac{u_*^2 - u_{*cr}^2}{u_{*cr}^2} \tag{9.26}$$

Introducing the equivalent sand roughness height (Ks) and the dimensionless sediment diameter D_*.

$$Ks = 2.5 \cdot D_{50} \tag{9.27}$$

$$D_* = D_{50} \cdot \sqrt[3]{\frac{(S_g - 1) \cdot g}{\nu^2}} \tag{9.28}$$

3. Deriving T from the Van Rijn equation 8.1

$$T = \left(\frac{Q_S}{(0.053 \cdot ((s-1) \cdot g)^{0.5} \cdot D_{50}^{1.5} \cdot D_*^{-0.3} \cdot B)} \right)^{\frac{1}{2.1}} \tag{9.29}$$

Where $(s-1) = \frac{\rho_s - \rho}{\rho}$ is the apparent roughness.

4. From the definition of T (equation 9.26) the shear velocity in terms of effective bed shear stress can be obtained:

$$u'_* = u_{*cr} \cdot \sqrt{T+1} \tag{9.30}$$

5. Since the dune lee side can be considered a roughly flat bed, the Chézy coefficient can be computed as follows:

$$\begin{cases} C' = 5.75 \log_{10} \left(\frac{12 \cdot R_{Hyd}}{Ks} \right) \\ U = u'_* \cdot C' \end{cases} \tag{9.31}$$

$$Y = \frac{ql}{U} \tag{9.32}$$

$$Fr = \frac{U}{\sqrt{g \cdot Y}} \tag{9.33}$$

6. The value of the crest velocity of dunes was calculated with the empirical relation 9.22.

7. The value of sand wave height was calculated from the continuity of sediment equation 8.5.

$$\Delta = \frac{K \cdot qs}{c \cdot (1 - e)} \tag{9.34}$$

where K is a constant depending on the form of the dunes, varying between 1.5 and 2. In the present study the value of 1.5 is assumed:

$$\Delta = \frac{1.5 \cdot qs}{c \cdot (1 - e)} \tag{9.35}$$

8. The value of the sand wave length was calculated with the empirical relation 6.1.

9. In the equation 9.21 the Boussinesq coefficient (β) was added. The coefficient β depends on the velocity distribution and can vary between 1 and 1.1. In the present study, the value of 1 has been assumed for section 2 where the velocity distribution is almost uniform, while for section 1, a value of 1.05 has been assumed.

The difference of momentum fluxes is:

$$Min_x - Mout_x = -\rho_W \cdot \frac{Ql^2}{B} \cdot \frac{Y \cdot (\beta - 1) - \frac{\Delta}{2} \cdot (\beta + 1)}{Y^2 - \Delta^2/4} \tag{9.36}$$

Finally, from the equation 9.5 an unknown variable can be computed. By solving the equation 9.5in terms of the slope (S) we obtain the computed values of bed slope, S_{mod}:

$$A_1 = \frac{\rho_W \cdot \frac{Ql^2}{B} \cdot \frac{Y \cdot (\beta - 1) - \frac{\Delta}{2} \cdot (\beta + 1)}{Y^2 - \Delta^2/4}}{\gamma_W \cdot B \cdot Y \cdot (\lambda - K_3 \cdot \Delta)}$$

$$A_2 = \frac{-Y \cdot \gamma_W \cdot B \cdot \Delta}{\gamma_W \cdot B \cdot Y \cdot (\lambda - K_3 \cdot \Delta)}$$

$$A_3 = \frac{2 \cdot \tau_W \cdot Y \cdot (\lambda - K_3 \cdot \Delta)}{\gamma_W \cdot B \cdot Y \cdot (\lambda - K_3 \cdot \Delta)}$$

$$A_4 = \frac{\tau_b \cdot B \cdot (\lambda - K_3 \cdot \Delta) \cos(\frac{\Delta}{\lambda})}{\gamma_W \cdot B \cdot Y \cdot (\lambda - K_3 \cdot \Delta)}$$

$$A_5 = \frac{\gamma_W \cdot B \cdot Y (\lambda - K_3 \cdot \Delta) \sin(\frac{\Delta}{\lambda})}{\gamma_W \cdot B \cdot Y \cdot (\lambda - K_3 \cdot \Delta)}$$

$$S_{mod} = (A_1 + A_2 + A_3 + A_4 + A_5) \tag{9.37}$$

Equation 9.37 can be considered as the "output" of the proposed model. Obviously, since no model calibration has been made so far, it is to be expected that equation 9.37 needs to be corrected. This has been done by comparing

the slope values predicted by equation 9.37 with the observed values of the experimental data (see tables 5.1 and 5.2) and from literature (see tables 6.3 and 6.4).

Figure 9.4 shows the comparison of predicted values with the whole set of experimental values. As can be observed, predicted slope values show a correct trend even if shifted systematically. This discrepancy can be removed by introducing a correction factor as follows:

$$Slope_{corrected} = 0.1554 \cdot \left(\frac{Qs \cdot B}{Ql \cdot D_{50}} \right)^{-0.213} \cdot Slope \tag{9.38}$$

It must be noted that the calibration factor is only a function of the independent variables.

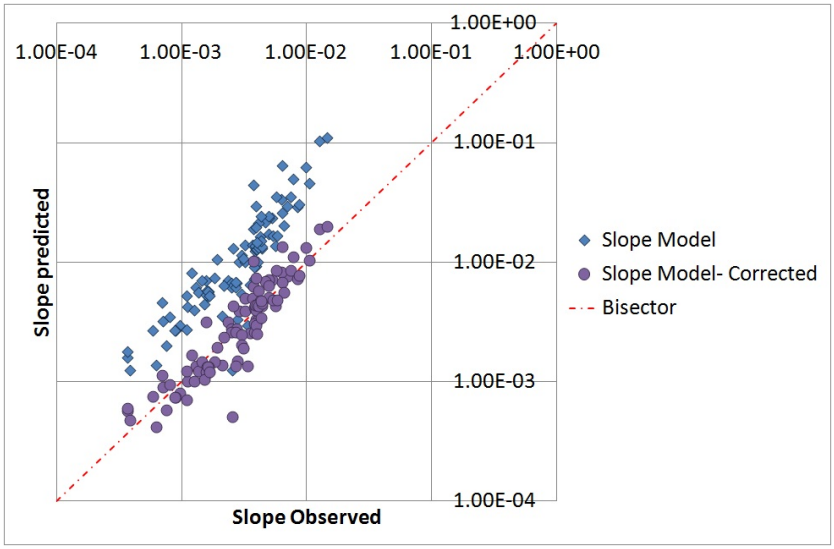

Figure 9.4: Comparison between observed and predicted slope values;

The other dependent variables have been computed through steps 1-11 and shown in the Figures 9.5, 9.6,9.7,9.8,9.9.

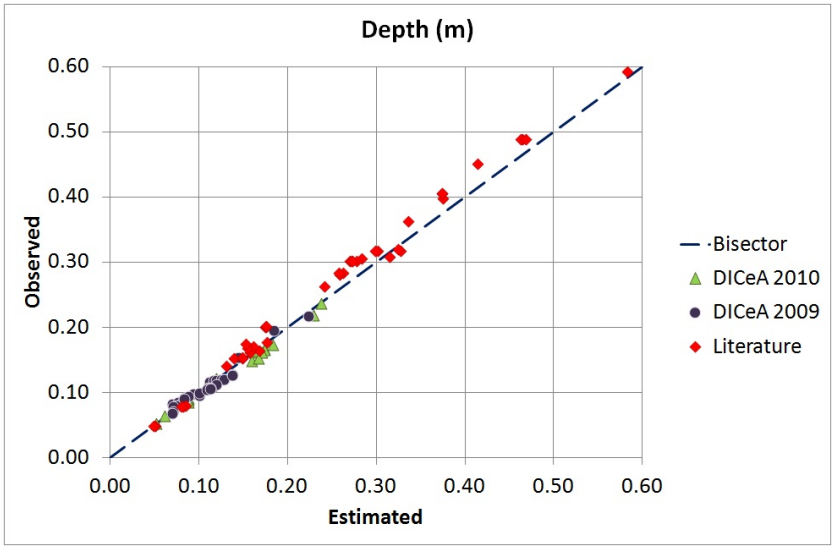

Figure 9.5: Comparison between the depth from the model and the depth observed;

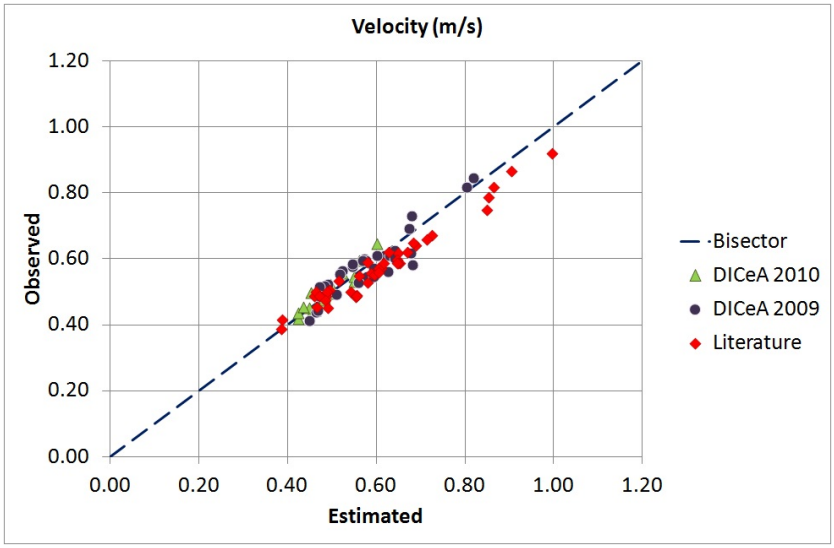

Figure 9.6: Comparison between the mean velocity from the model and the mean velocity observed;

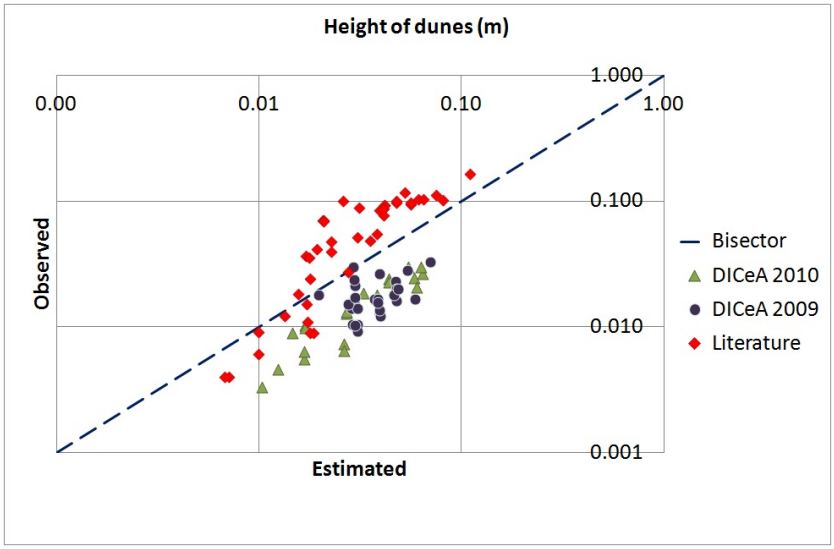

Figure 9.7: Comparison between the dune height from the model and the dune height observed;

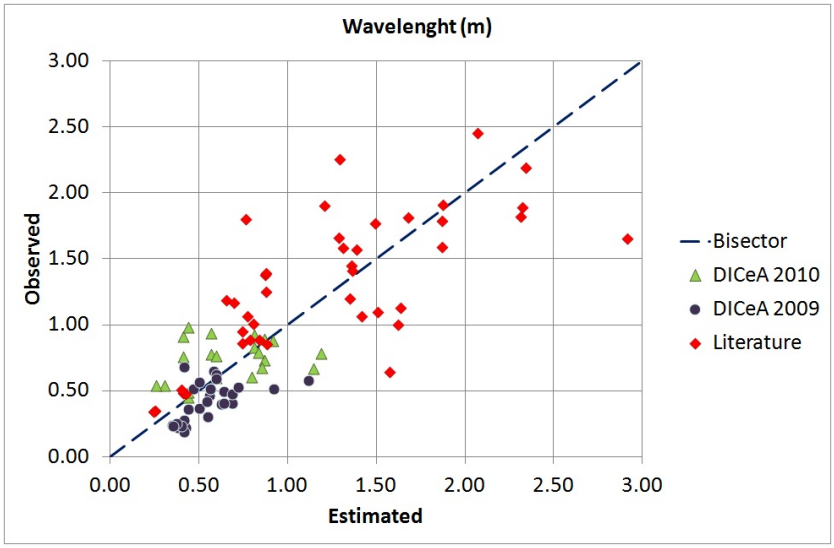

Figure 9.8: Comparison between the wavelength from the model and the wavelength observed;

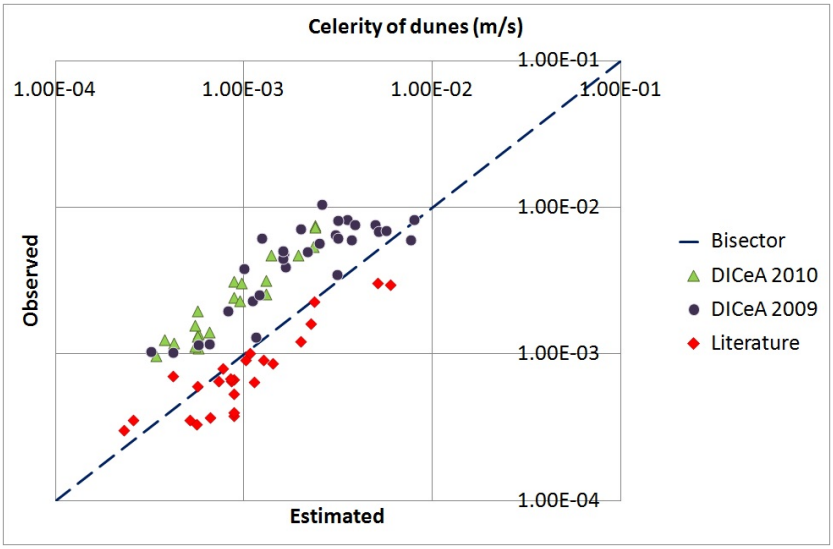

Figure 9.9: Comparison between the celerity from the model and the celerity observed;

9.3 Simulation of experimental runs

The above described model was applied to simulate two experimental runs. By using the same input quantities (independent variables), the outputs provided by the model were compared with the experimental results obtained at the equilibrium phases of the two runs. In the 17-29 sediment B run, the flow discharge is first increased and then decreased in the second part while the sediment supply remains constant (Constant Sediment Supply experiment). In the 1-5 sediment B run the sediment supply is first increased and then decreased while the flow discharge remains constant (Constant Flow Discharge experiment).

Results in terms of predicted and observed values are shown in figures 9.10, 9.11, 9.12 for the 17-29 sediment B run. In particular, figure 9.10, shows the path of the observed slope compared with the predicted slope, when the flow discharge is kept constant. The sequential phases are related to the progressive variation in sediment supply. Figure 9.11 shows the path of the observed dune height and dune celerity compared with the predicted values, and figure 9.12 shows the path of the observed bed shear stress and the effective bed shear stress compared with the predicted values.

Results in terms of predicted and observed values are shown in figures 9.13, 9.14, 9.15 for the 1-5 sediment B run. In particular, figure 9.13, shows the path of the observed slope compared with the predicted slope, when the sediment supply is kept constant. The sequential phases are related to the progressive variation in flow discharge.

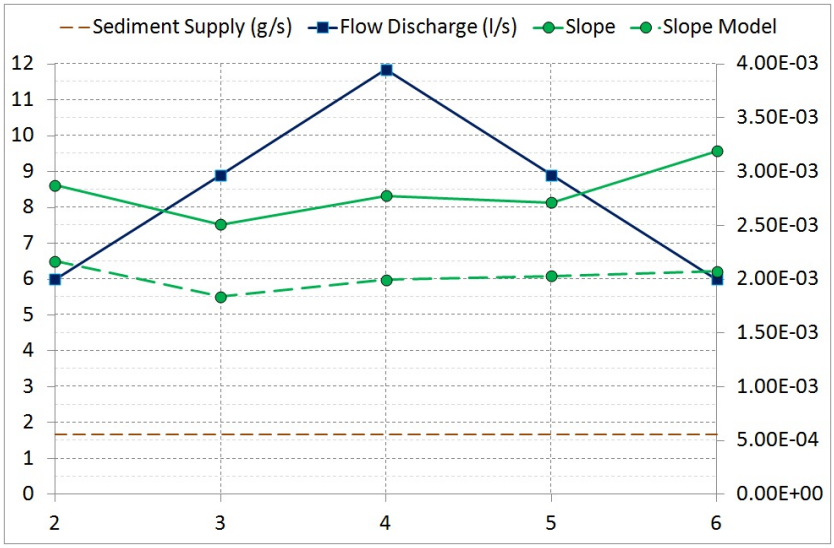

Figure 9.10: C.S.S. cycle-Five equilibrium phases: Flow discharge (left y-axis), Sediment Supply (left y-axis), Slope (right y-axis);

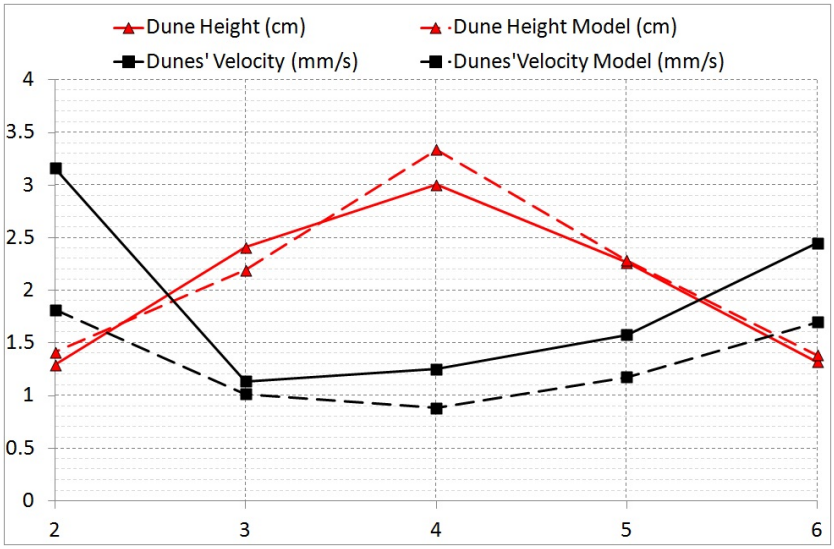

Figure 9.11: C.S.S. cycle-Five equilibrium phases: Dune Velocity and Dune Height;

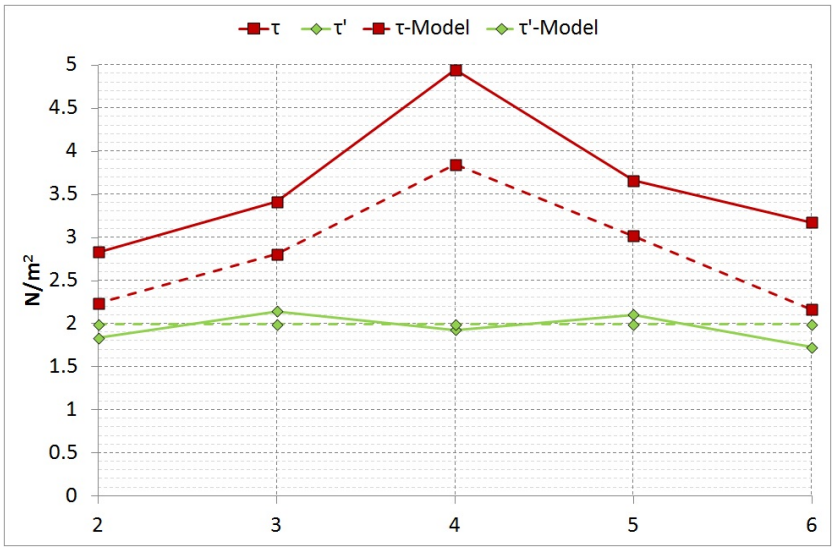

Figure 9.12: C.S.S. cycle-Five equilibrium phases: Total Shear Stress and Effective Shear Stress;

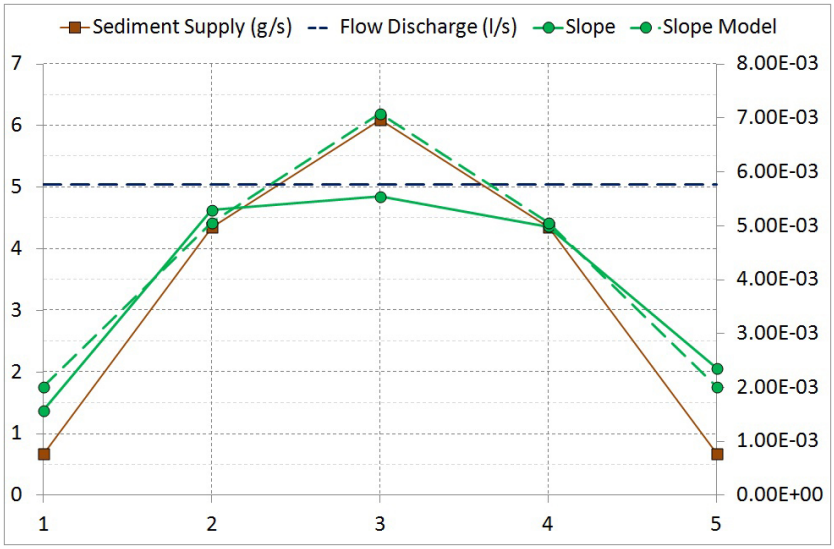

Figure 9.13: C.F.D. cycle-Five equilibrium phases: Flow discharge (left y-axis), Sediment Supply (left y-axis), Slope (right y-axis);

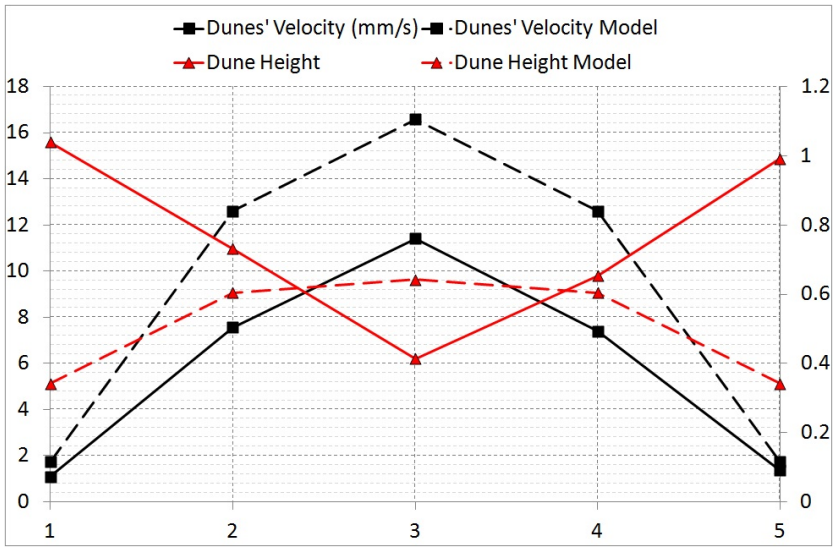

Figure 9.14: C.F.D. cycle-Five equilibrium phases: Dune Velocity (left y-axis), Dune Height (right y-axis);

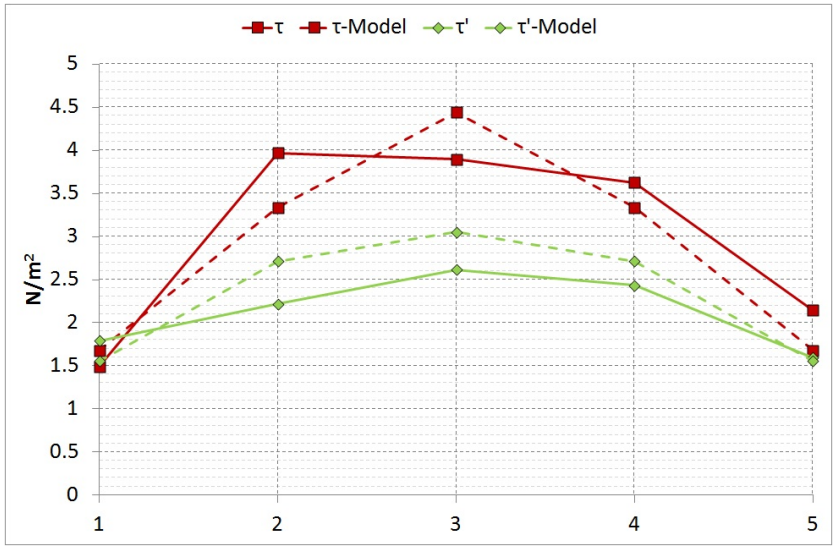

Figure 9.15: C.F.D. cycle-Five equilibrium phases: Total Shear Stress and Effective Shear Stress;

Figure 9.14 shows the path of the observed dune height and dune celerity compared with the predicted values, and figure 9.15 shows the path of the observed bed shear stress and the effective bed shear stress compared with the predicted values.

Chapter 10

Numerical experiments

10.1 Analysis of transition and dune wash out

The proposed model is used to investigate two aspects which can only marginally be experimentally analysed: the field of existence of dunes and the mechanism of dune wash out. The condition of dune washout is well described by several authors (e.g.Nnadi and Wilson (1995) and Engelund and Fredsøe (1974)) and is reported Wang and White (1993) as the condition where the downstream face of the dunes decreases rapidly with an increasing flow strength. This phase consists of a constant degradation of the height of dunes and a reduction of the dunes' steepness, towards the upper plane bed condition. During the laboratory experiments, it was observed that the beginning of the transition condition before dune washout may be attributed to the progressive reduction in (up to the cessation of) the furnishing of sediment at the front of the dune, since the particles on the crest now have sufficient kinetic energy to jump over the stoss side of the following dune. Of course, this interpretation refers to conditions of prevalent bed load transport. In this way the front of the dunes progressively reduces until disappearing in the condition of the upper plan bed. Therefore, the proposed model was developed in order to make it able to simulate the transition and wash out process. In this way, information about the field of existence can also be obtained.

With reference to figure 10.1, grains are transported along the dune stoss-side mainly as bed load.

Once they arrive at the crest, the particle velocity (Vg), may be sufficient to skip the recirculating zone and reach the downstream dune stoss-side. The length of the recirculating zone (Lj) is proportional to the dune height (Δ):

$$Lj = K \cdot \Delta \tag{10.1}$$

For ripples and dunes, Engel (1981) and Karahan and Peterson (1980) suggested that K has a value in the range of 4-10. The particle velocity (Vg)

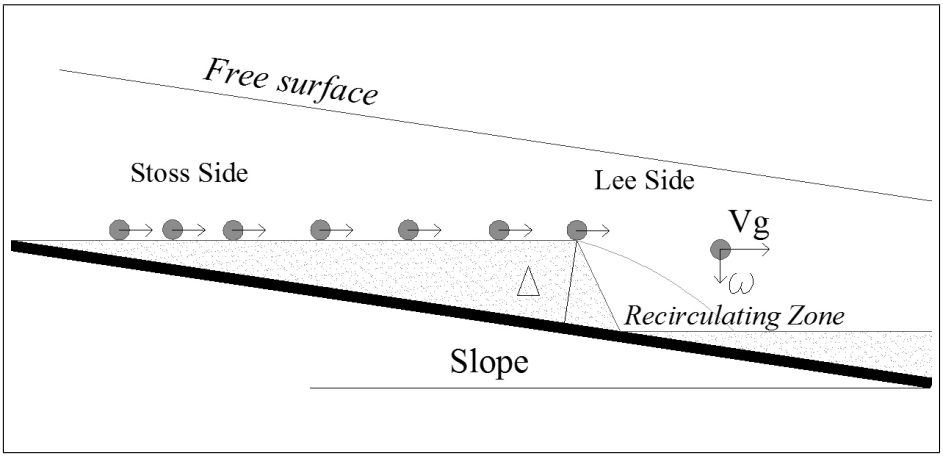

Figure 10.1: Transport over the stoss-side of dunes;

required to jump over the distance Lj can be derived by equating the time to travel the length Lj to the time required to settle over the depth Δ:

$$\frac{K \cdot \Delta}{Vg} = \frac{\Delta}{\omega} \tag{10.2}$$

where ω is the sediment fall velocity.

Hence, the value of Vg for the particles to skip the recirculating zone is:

$$Vg = K \cdot \omega \tag{10.3}$$

Experimental observations have shown that K is in the range:
$2 < K = \frac{Vg}{\omega} < 8$

For this reason, the length of the jump can be assumed proportional to the dimensionless ratio: $\frac{Vg}{\omega}$.

The particle velocity Vg is estimated by using the equation proposed by Fernandez and van Beek (1976):

$$Vg = 11.5 \cdot (u'_* - 0.7 \cdot u_{*cr}) \tag{10.4}$$

The value of Vg sufficient to trigger the transition toward the dune wash out is denoted by Vg_{tr}.

From equations 10.3 and 10.4,the following can be derived:

$$Vg_{tr} = K \cdot \omega = 11.5 \cdot (u'_{*tr} - 0.7 \cdot u_{*cr}) \tag{10.5}$$

From equation 10.5, the value of effective bed shear velocity when transition occurs, u'_{*tr}, can be computed. This value is then introduced into the proposed model in order to find out the correct value of K in agreement with experimental results.

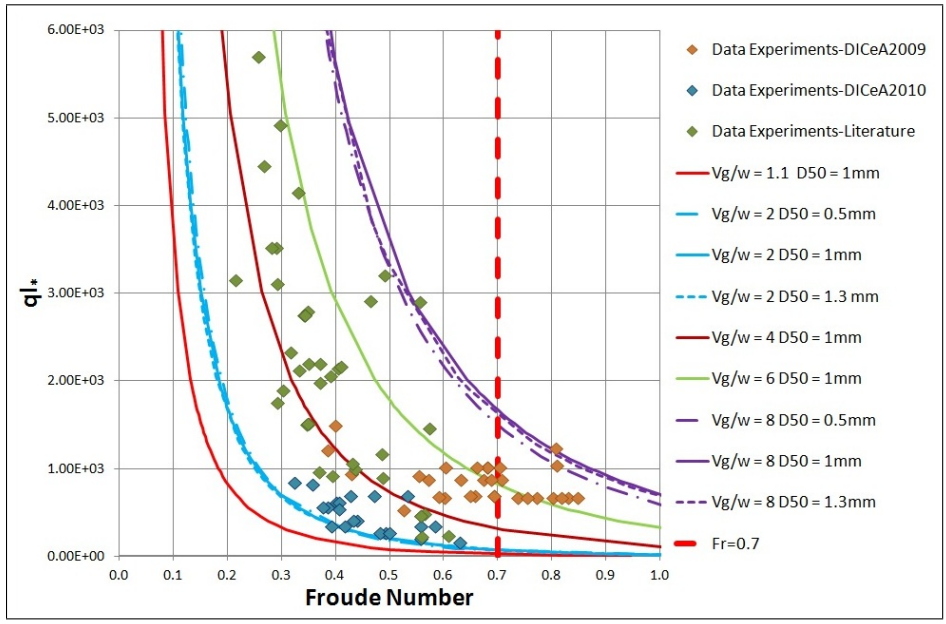

Figure 10.2: Comparison between the experimental data and the model: dimensionless liquid discharge against the Froude number;

In figure 10.2, the dimensionless discharge, ($ql_* = \frac{ql}{\sqrt{g \cdot D_{50}^3}}$) has been plotted against the Froude number for different values of $K = \frac{Vg}{\omega}$ and grain size, D_{50}.

The curves represent the conditions for particles to jump at different values of K. It can be observed, for K = constant, that this condition is likely to occur when the Froude number is increasing even for low discharges. In the same diagram, the available experimental data have been plotted together with the red dashed line Fr=0.7, normally assumed as a limiting value for the dune's existence. It can be seen that all data lies within the computed curves. However, several dune data are present for $Fr > 0.7$, while no data is present in the plot area limited between the line Fr=0.7 and the curve for K=8. Therefore, the proposed criterion for K=8 or dune transition seems to be more representative than the criterion based on the Froude number.

The criterion represented in figure 10.2 provides an upper boundary to the region of existence for dunes. In order to define a lower boundary, experimental data have been plotted in the diagram of figure 10.3, where the variables are the same as the diagram in figure 10.2. The region of existence has been defined by adding two empirical conditions: one referring to the maximum value of the dune height and water depth ratio; the second one expressed in terms of the maximum value of the dune height to the grain size ratio. It can be seen that all experimental data, the values observed in the laboratory experiments and the data collected in literature, are enclosed in the plot area bounded by the

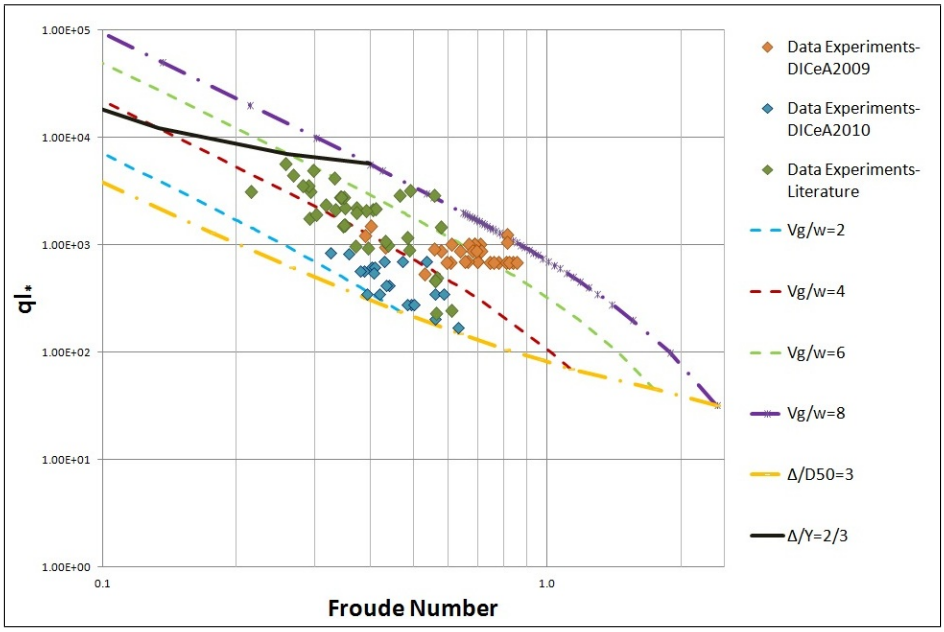

Figure 10.3: Comparison between the experimental data and the model, with a sediment characterization $D_{50} = 1mm$: dimensionless liquid discharge against the Froude number;

transition curve. The dimensionless solid transport is also defined:

$$\Phi = \frac{qs}{\sqrt{(s-1) \cdot g \cdot D_{50}^3}} \tag{10.6}$$

In graph 10.4, the data obtained from experimental observations are plotted; in abscissa the values of the dimensionless solid transport (Φ) and in the ordinate the value of dimensionless dune height with the relative sediment diameter (Δ/D_{50}). Even in this case, it is defined as an area within which all the data are collected: the area is defined by an intersection of 3 lines: the first represents the limit value of the ratio between the dune height and the characteristic particle diameter of the sediment equal to 3; the other line is given by a constant value of Φ near unity and V_g/ω equal to 8, while the last demarcation is presented by the line with dimensionless liquid flow equal to 5000.

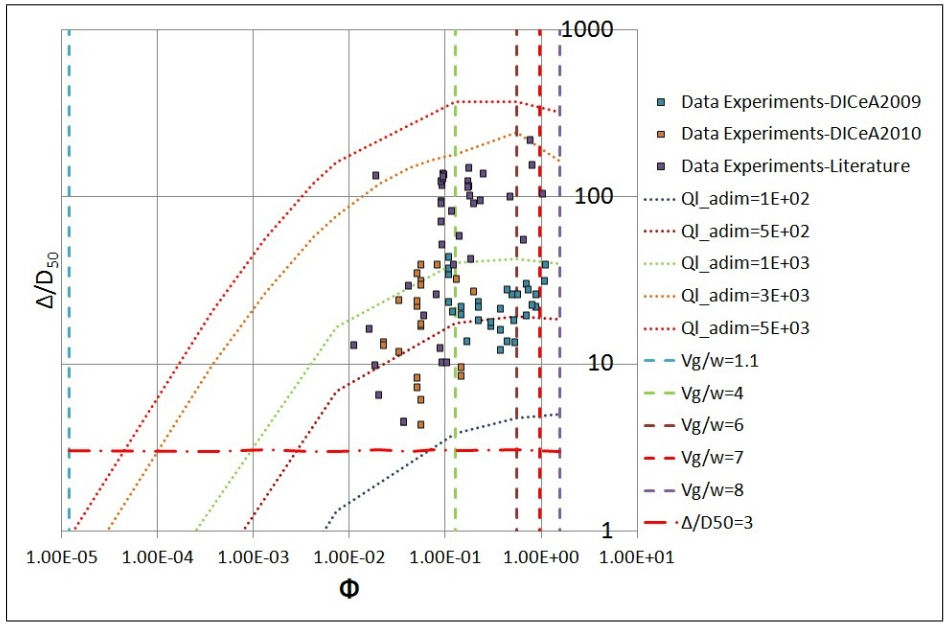

Figure 10.4: Comparison between the experimental data and the model: Dimensionless solid transport against dimensionless dune height;

Part IV

CONCLUSIONS

Several laboratory experimental cycles were conducted in a condition of steps of uniform and subcritical flow without a suspended load and in a straight feed flume. The experimental cycles were carried out to observe the response of the channel to an imposed imbalance. The experimental cycles were conducted in two ways: one in a condition of variation of the sediment supplied, keeping the liquid flow constant, these experimental cycles are called CFD; and the other in a condition of variation of the liquid flow and maintaining the sediment supplied constant, these experimental cycles are called CSS.

It was observed that the response to a variation of sediment supply in a **CFD experimental cycle**, is a prevalent variation of the bed slope and of the dunes' celerity. In particular, when the sediment supply increases, the bed slope and the celerity of the dunes increase, whereas the height of the dunes decreases slightly. In this way, an initial increase of the sediment supply is balanced with an increase of the transport capacity because the bed slope increases and the height of the dunes decreases, decreasing in this way the total bed roughness. The celerity increases because the sediment supply increases and the height of the dunes decreases, in accordance with the continuity equation for sediment 8.5. The opposite happens if a decrease of the sediment supply occurs.

The response of the channel to a variation of the liquid flow in a **CSS experimental cycle**, is predominantly the variation of the height of the dunes whereas the bed slope and the celerity change slowly;

In particular, during an increase of the liquid discharge, the height of the dunes increases and the bed slope and the celerity decrease, but to a lesser extent, so the water channel can reach another sedimentological equilibrium. This is because the sediment transport capacity ceases to increase for the action of the dunes' height which increases the total bed roughness and for the bed slope because it decreases. The dunes' celerity decreases and the height of dunes increases, in accordance with the continuity equation for sediment 8.5, and for this reason the sediment supply remains almost constant. The opposite happens if a decrease of the sediment supply occurs. The characteristics of the bed forms and the bottom of the channel play a significant role in conducting the flume to a new equilibrium. In particular, in the two different experimental cycles, two aspects are immediately evident:

1. the clear differences of behaviour which, in both intensity and trend, the bed slope, the height and the velocity of the dune assume, depending on whether it is conducted a cycle with a variation of sediment supply, CFD or with a variation of the liquid flow, CSS. This is because the bed slope and the speed of the dunes on the one hand and the dune height on the other, interfere in a different way which is complementary with the solid transport capacity, depending on whether this is in excess or in deficit, with respect to the sediment provided.

2. Another evident aspect is the diversity of the time response of the channel to the imbalance, depending on whether this has been caused by a variation in liquid or in solid flow. This is due to the fact that the speed of perturbations

in the CFD cycles is comparable to values of M3, as already shown in figure 8.2, while in CSS cycles the propagation speed of the perturbations is comparable with M1 and M2. Moreover, it is important to note that M1 and M2 are larger than M3 in a subcritical flow condition. A **physically based model** was implemented to reproduce the phenomena observed during the laboratory experiments, and to understand better some mechanisms that occur in a movable bed when the dunes appear. The physically based model reproduces a condition of steady and uniform flow. The model is based both on physical relationships: the continuity sediment equation, the equation of bed load transport and the conservation of momentum applied in the controlled volume upon the dunes, or by using the empirical relation based on the data from experiments. The model has produced data closely comparable with those obtained from the experiments conducted for this study and those collected from literature. The model effectively reproduced the behaviour of the velocity of the dunes and of the bed slope for both cycles but it was able to reproduce the trend of dune height only in CSS cycles. In the last part, the ability to predict the wash out of the dunes was added to the physical based model. This was possible by defining as incompatible the feeding to the lee side of the dune by the previous dune if the shear stress on the crest became too high. Therefore, if the critical value of the shear stress on the dune crest is exceeded, they begin to degrade rapidly, giving rise to the condition of upper plane bed. Defined in this way, the condition of washout of the dune, with the aid also of existence limits of the dunes provided by the literature, the condition of existence of the dunes is established. The field of the adaptive process of the dunes is strongly connected to the field of existence of the dunes. The channel is in the field of the adaptive process of the dunes. In fact, when the channel is the field of adaptive process of the dunes, it can count on achieving an equilibrium, also modifying dune characteristics.

Observations and Outlook

- In spite of the simplification of the phenomena produced in the laboratory, the experimental cycles represented in the channel in this work can have feedbacks in nature. For example, the condition represented by the CSS cycle, i.e. in which the sediment supply is constant, while the liquid flow is variable, may represent the first part of a flood event, thanks to the delay between the liquid and the solid increase. The experimental cycle CFD can represent a condition of a landslide directly in the river, figure 10.5 or the confluence of two rivers where the tributary has a larger sediment transport, figure 10.6.

- As already mentioned, Parker and Wilcock, in their work, Parker and Wilcock (1993), have assumed bed forms effects as negligible. Results obtained in the present study show that the effects of bed forms cannot be neglected since the equilibrium conditions may be greatly affected by bed form characteristics. In particular, the height and speed of the crest can greatly affect the final equilibrium slope. Experiments conducted in this work, have shown that two equilibrium stages can have the same inputs (same liquid and solid flow and the same grain size) but have a significantly different value of the slope of the bed, and the speed and height of the dune crest. This diversity is derived

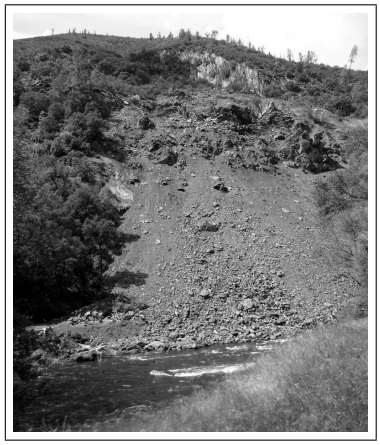

Figure 10.5: Example of a landslide;

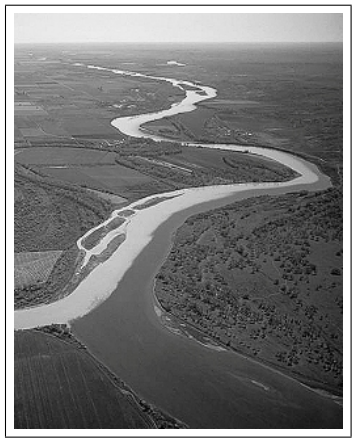

Figure 10.6: Example of a confluence between two rivers with different sediment transports;

exclusively from a variation of the liquid flow rate in the first case, the C.S.S. cycle, and by a solid discharge variation in the second case, the C.F.D. cycle. In these two types of experiments, two different phenomena characterized by very different time scales, are activated. In the case of the C.S.S. cycle, the speed of the perturbations and, consequently, of changes in the channel are much faster than in the C.F.D. cycle.

- The two experimental cycles allowed to highlight the existence of an **"orthogonal behaviour"** when dunes are present. Comparison between literature data, present data and numerical simulations seem to confirm this result.

- The orthogonal behaviour is due to two distinct processes of adjustment. One is commonly reproduced in **recirculating flumes**: the behaviour of dune is in this case **in agreement** with the results of the **CSS cycle** and it is satisfactory predicted by the **numerical simulations**. The second one has been found in the **CFD cycle** and it does not show **any agreement** with the **literature data** and with the values predicted by the **model proposed**.

- So the experimental results appear to disagree with the Parker and Wilcock theory (1993) according to which *the recirculating and the feed flume should conducted to the same equilibrium stage*. Vice versa, from the results it can be inferred that while a **recirculating flume** shows a **unique adjustment** process to reach equilibrium, a **feed flume** is able to generate **two different ways** to reach equilibrium. In particular the behaviour of **dune celerity** and **dune wavelength** do not seem to be dependent on the type of flume and on the experimental cycle but the **dune height** is.

The conclusions reached in this thesis, suggest the results of an experiment that could end and complete the work. The design of the experiment is described in figure 10.7 The experimental test consists of two cycles, one CSS and the other

CFD, conducted in a channel-type feed flume with homogeneous sediment with D_{50} ranging from 0.8 mm to 1.25 mm (approximate range of the sediments analysed). In the experimental cycle CSS, the experiment starts from an initial condition of equilibrium (qs_1_CSS, ql_1_CSS) and it proceeds with other equilibrium stages where the sediment supply is kept constant while the liquid flow for each stage is decreased up to the final value $(qs_1\_CSS, ql_{final}\_CSS)$. In the experimental cycle CFD, the experiment starts from an initial condition of equilibrium (qs_1_CFD, ql_1_CFD) but with a liquid flow, which will remain constant throughout the cycle, lower than the initial liquid flow in the experimental cycle CSS (ql_1_CSS). The cycle CFD proceeds with other equilibrium stages where the liquid flow is kept constant while the sediment supply for each stage is increasing up to the final value $(qs_{final}\_CFD, ql_1\_CFD)$. The final values of liquid and solid flow in the two cycles are the same. Following the conclusions of this work, and in contrast with the literature, the final stages of two cycles should have values significantly different of the bed slope, and the speed and height of the dune crest.

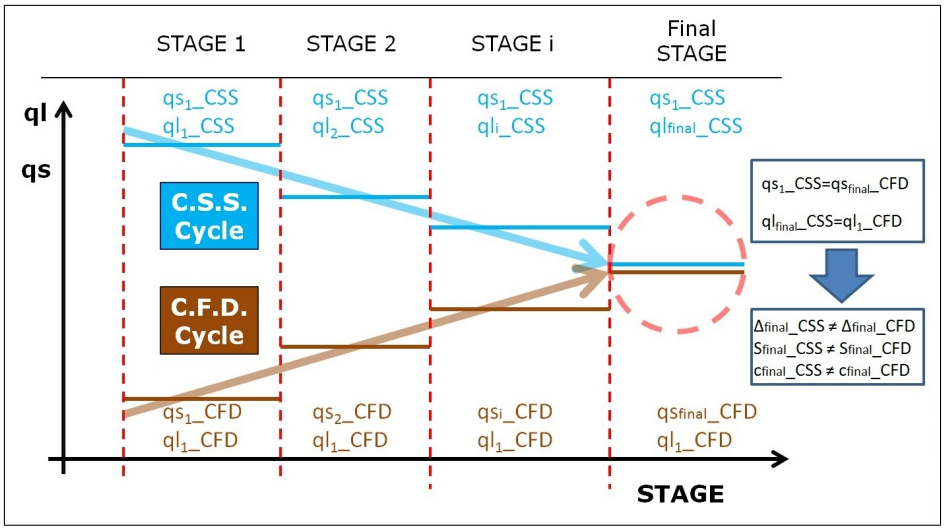

Figure 10.7: Future outlook;

Appendix A

The Measurements-Sediment A

In this appendix the experimental cycle conducted with sediment type A, see section C.1, are represented. Each experimental cycle is described by five/six graphs where the duration of the cycle is set on the x-axis:

1. A dashed line shows the trend of liquid flow value(Q_L, plotted on the left, SX) during the time of the experiments; asterisks plot the values of the mean slope of the movable bed (S, plotted on the right, DX) while a solid line represents the values of the sediment supplied into the flume (M_S, plotted on the left, SX);

2. In this graph, sediment supply and liquid flow are plotted but also the trend of the values of Froude Number in a line with a cross (Fr, plotted on the right, DX) and the values of mean velocity of the water in the flume with a line with squares (U, plotted on the right, DX) are plotted;

3. In this graph, sediment supply and liquid flow are plotted and also the values of the height of the characteristic dune during the cycle (with a Δ symbol, plotted on the right, DX) are plotted with a triangle;

4. In the next graph together with the trend of the sediment supply and liquid flow, plotted with the same symbols of previous diagrams, also the trend of the length of the characteristic dune(with a λ symbol), identified with circles, the velocity of the crest of the characteristic dune, plotted with rhombus, and the mean depth of the water in the flume, plotted with line with circles, are shown;

5. In this graph, sediment supply and liquid flow are shown together with the sediment transport capacity (S.T.C.) of the flume plotted with rhombus and the values of the sediment transport valued on the crest of the dunes,

plotted with squares, and the possible slope of the channel, plotted with dashed and dotted line;

6. In the last graph, the differences of the sediment thickness in the bed, shown during the manual measurements, are plotted: a light grey rectangle represents the altimetric differences of the sediment in the bed of the first three meters of the flume, in a grey rectangle the differences related to the centre part, while in a black rectangle the differences related to the last three meters of the flume are represented. This graph helps to understand when the sedimentological equilibrium has occurred. In fact, when the sediment transport capacity of the flume is equal to the sediment supplied into the flume, there aren't any deposit or erosion phenomena in the bed and the the variations of the flume bottom are irrelevant;

The graphs often display grey rectangles, which are the areas where the morphological balance occurs; in these areas the average values of the tables 5.1 and 5.2, were taken. Moreover, tests often go on for several days, but every day the flume was turned off and then it was turned on the following day; the boundary between one day and the other is represented by a red dotted and dashed vertical line. This explains why after that line, for a transitional period from one hour to two hours, there are very different values from the average slope of the bottom of the previous day.

A.1 Run 2

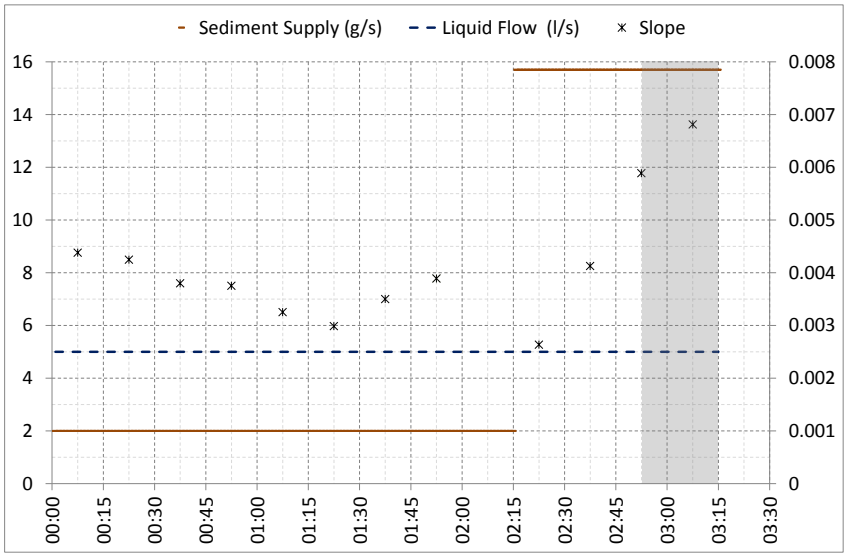

Figure A.1: $M_S(SX)$, $Q_L(SX)$, S(DX);

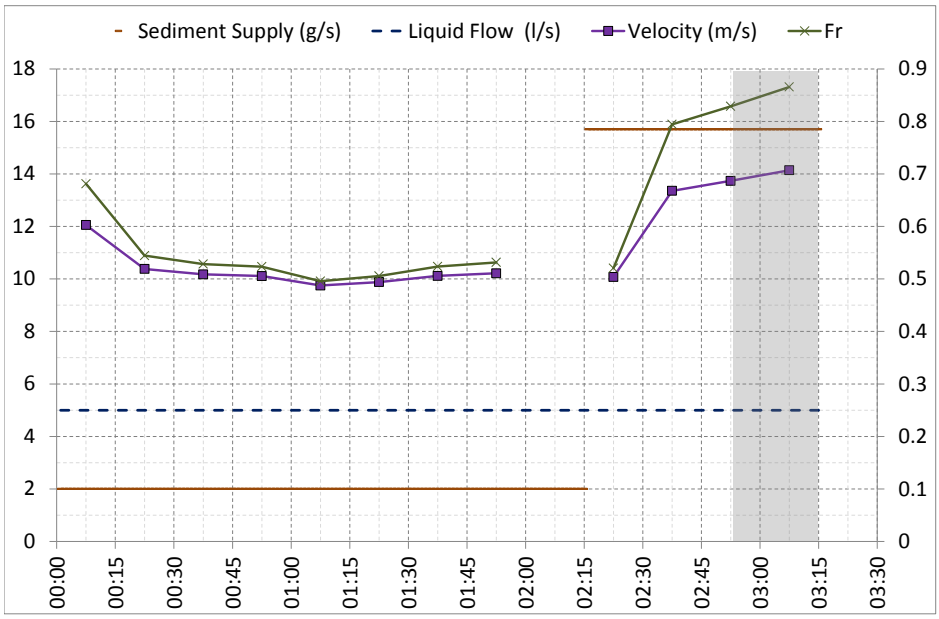

Figure A.2: $M_S(SX)$, $Q_L(SX)$, U(DX), Fr(DX);

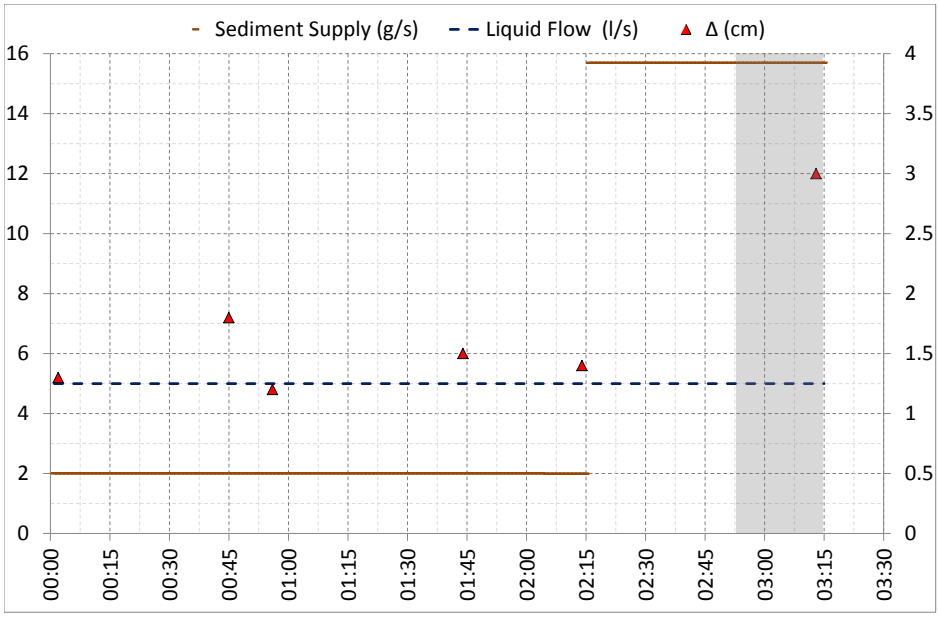

Figure A.3: $M_S(SX)$, $Q_L(SX)$, Dune Height(DX);

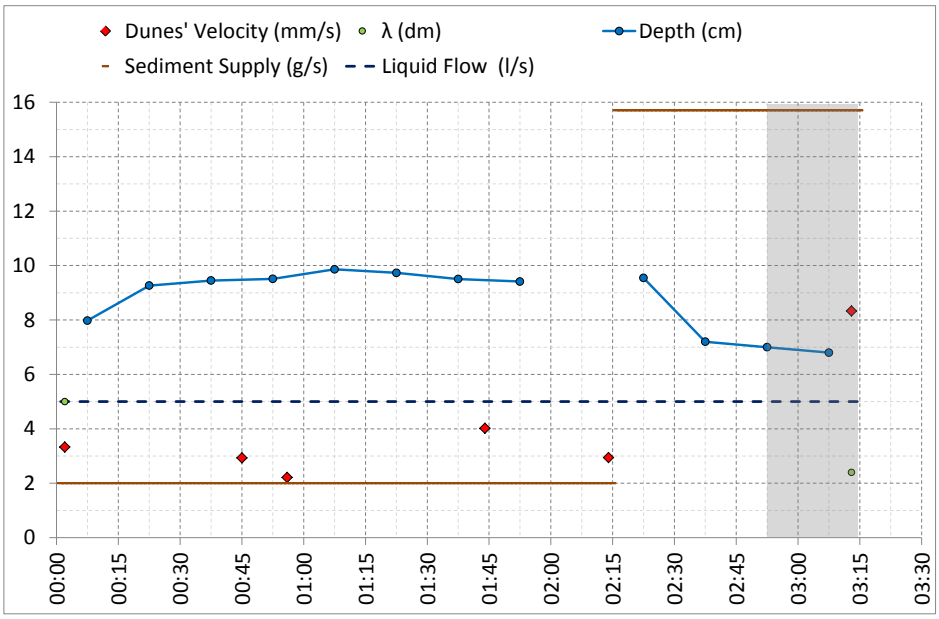

Figure A.4: M_S, Q_L, Dune Velocity, Dune Length, Flow Depth;

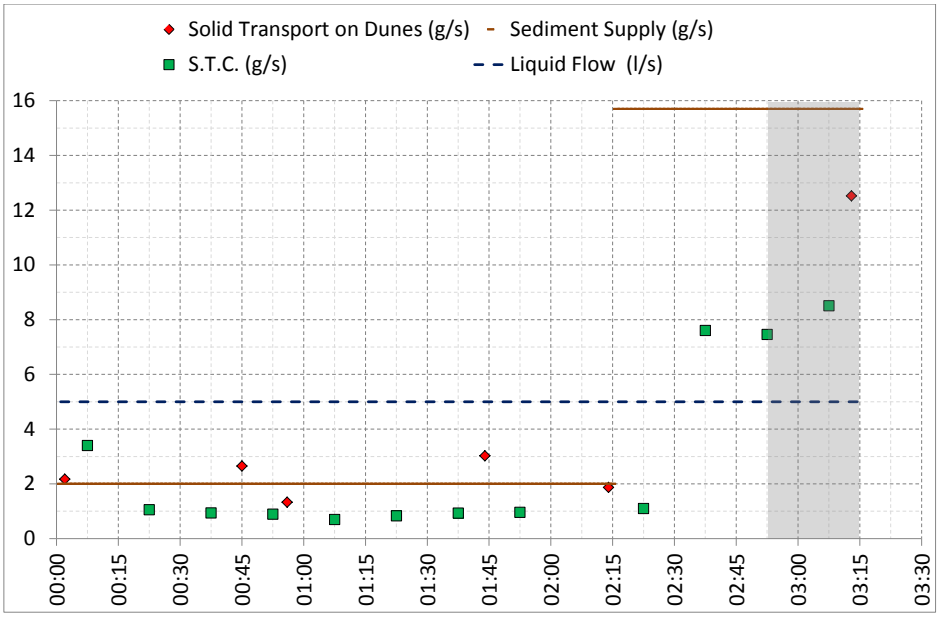

Figure A.5: M_S, Q_L, Solid Transport on Dunes, Solid Transport Capacity;

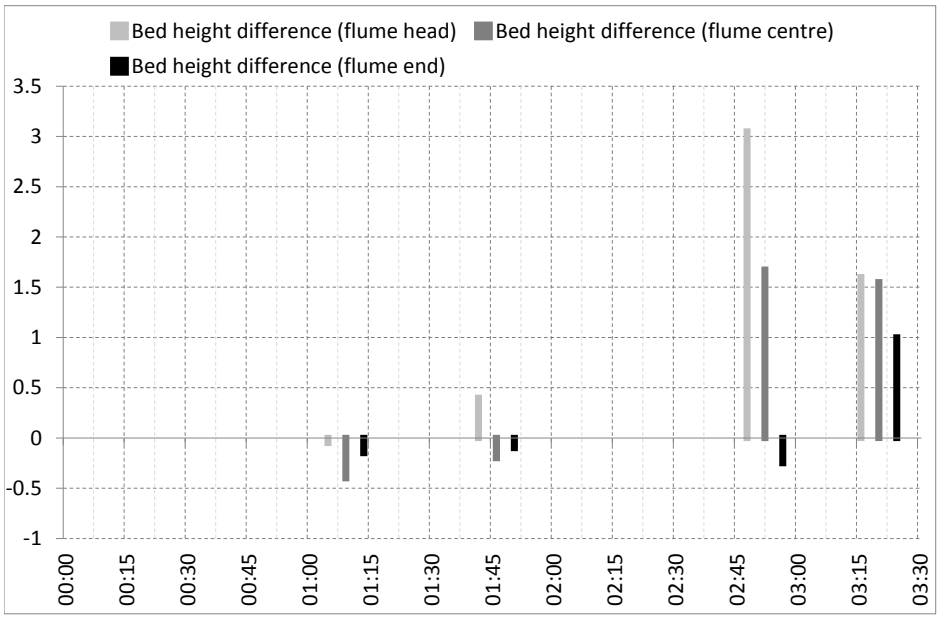

Figure A.6: Bed height difference in several parts of the flume;

A.2 Run 3

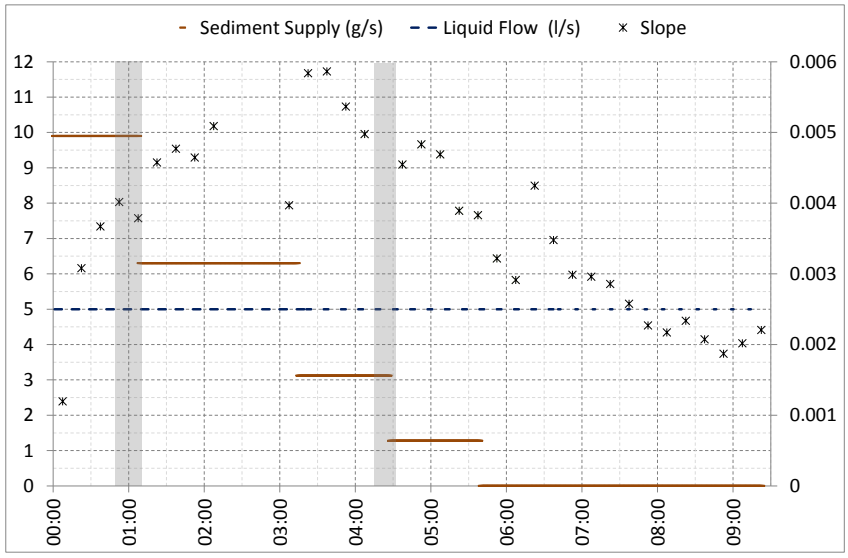

Figure A.7: $M_S(SX)$, $Q_L(SX)$, S(DX);

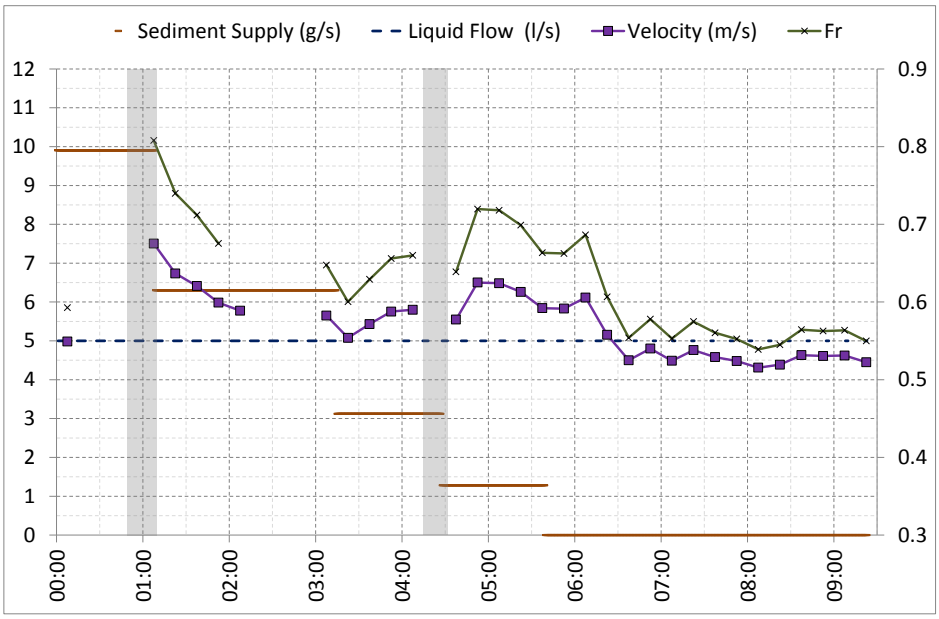

Figure A.8: $M_S(SX)$, $Q_L(SX)$, U(DX), Fr(DX);

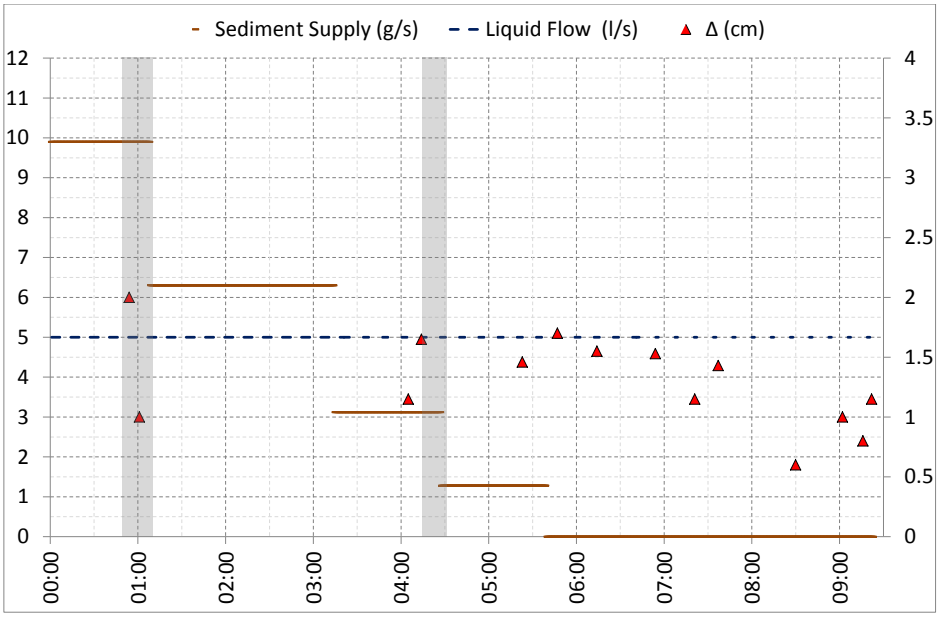

Figure A.9: $M_S(SX)$, $Q_L(SX)$, Dune Height(DX);

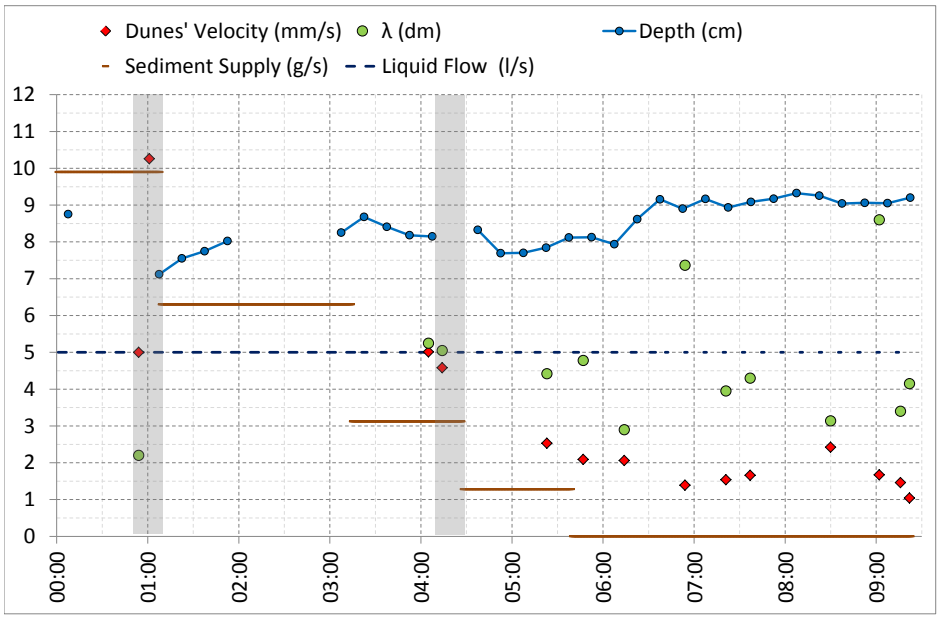

Figure A.10: M_S, Q_L, Dune Velocity, Dune Length, Flow Depth;

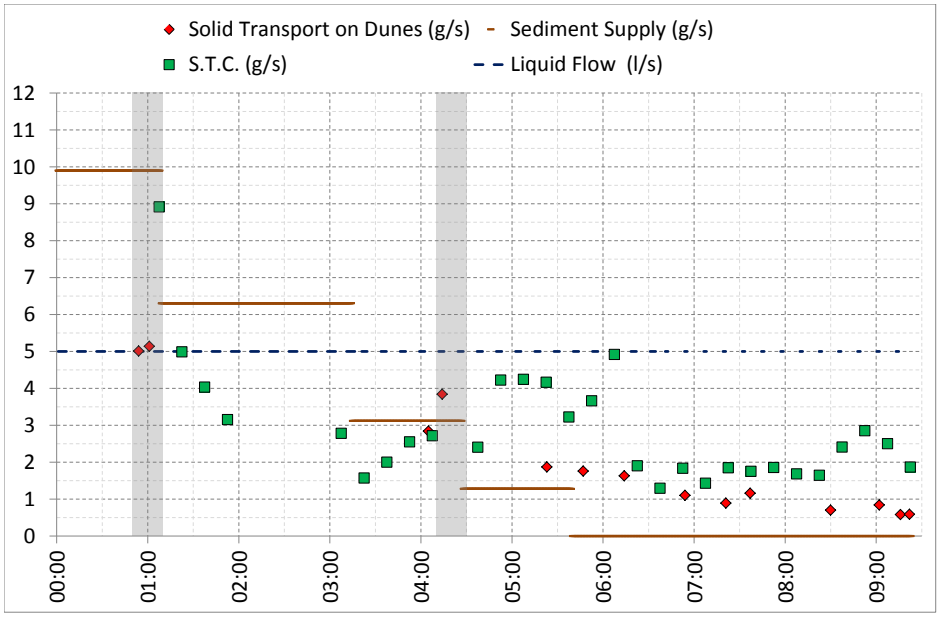

Figure A.11: M_S, Q_L, Solid Transport on Dunes, Solid Transport Capacity;

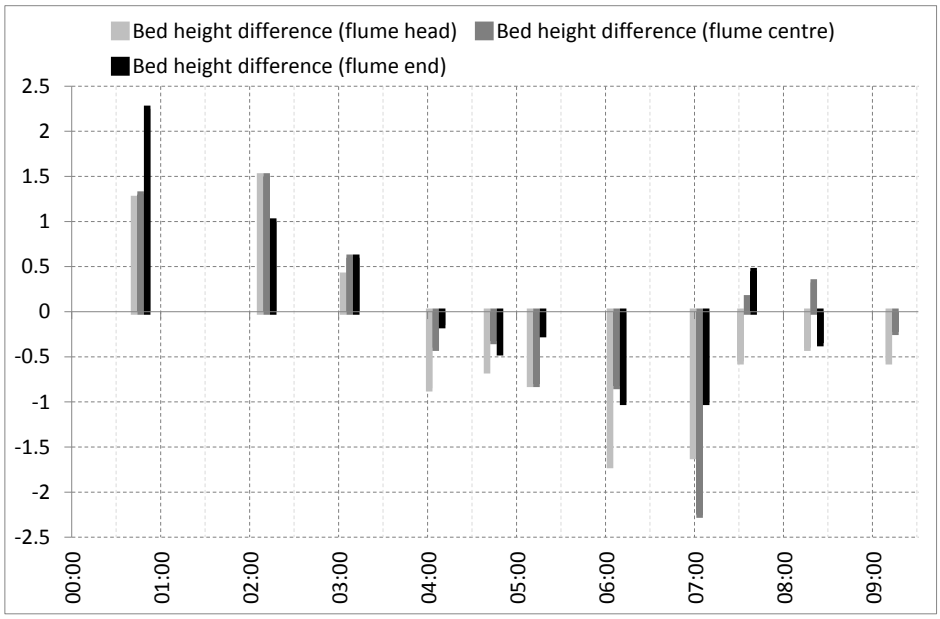

Figure A.12: Bed height difference in several parts of the flume;

A.3 Run 4

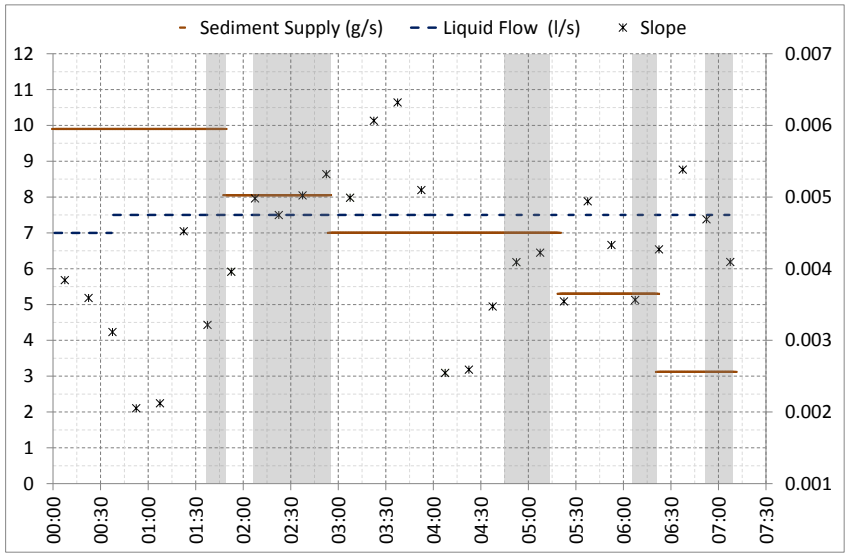

Figure A.13: $M_S(SX)$, $Q_L(SX)$, S(DX);

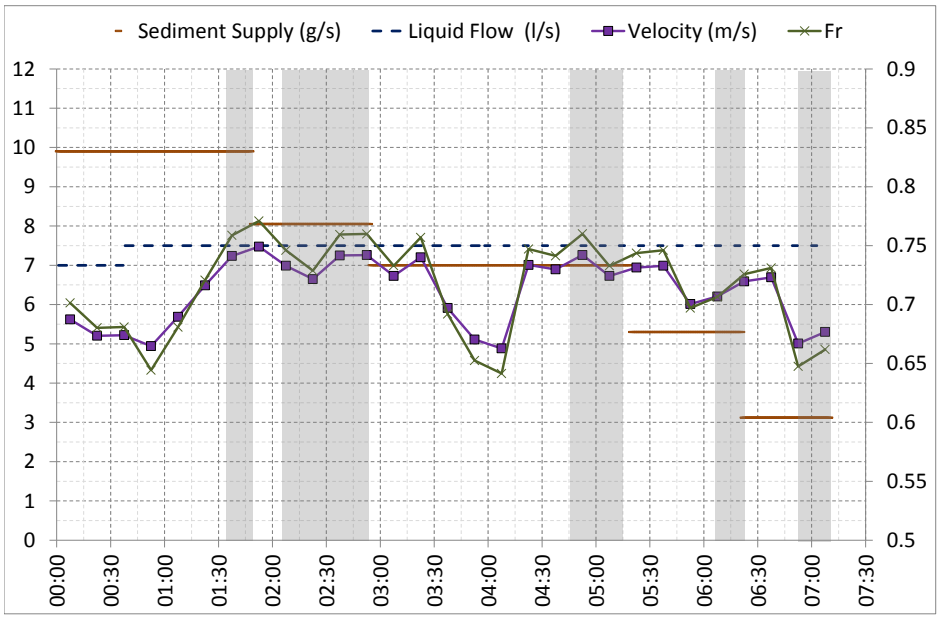

Figure A.14: $M_S(SX)$, $Q_L(SX)$, U(DX), Fr(DX);

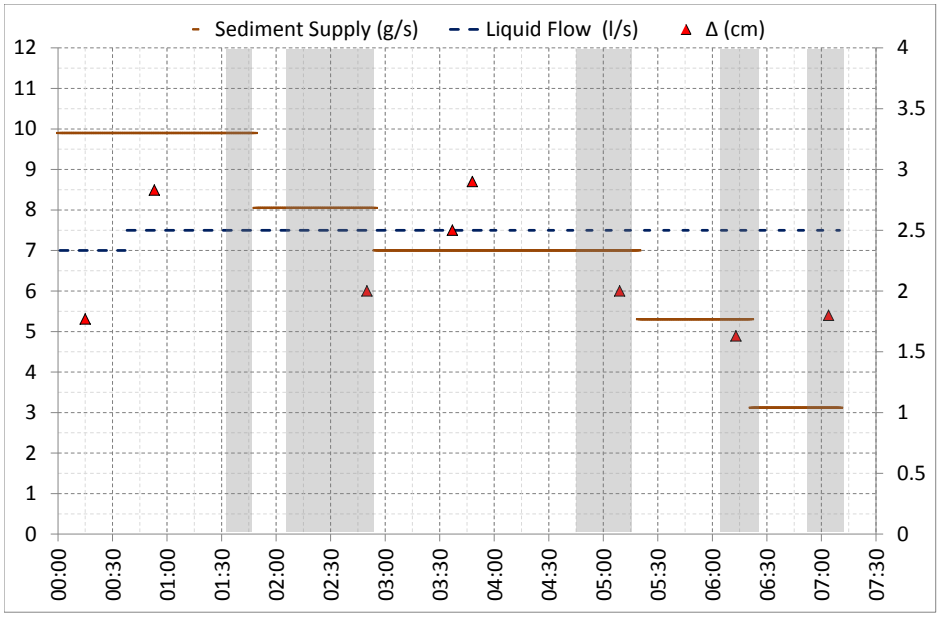

Figure A.15: $M_S(SX)$, $Q_L(SX)$, Dune Height(DX);

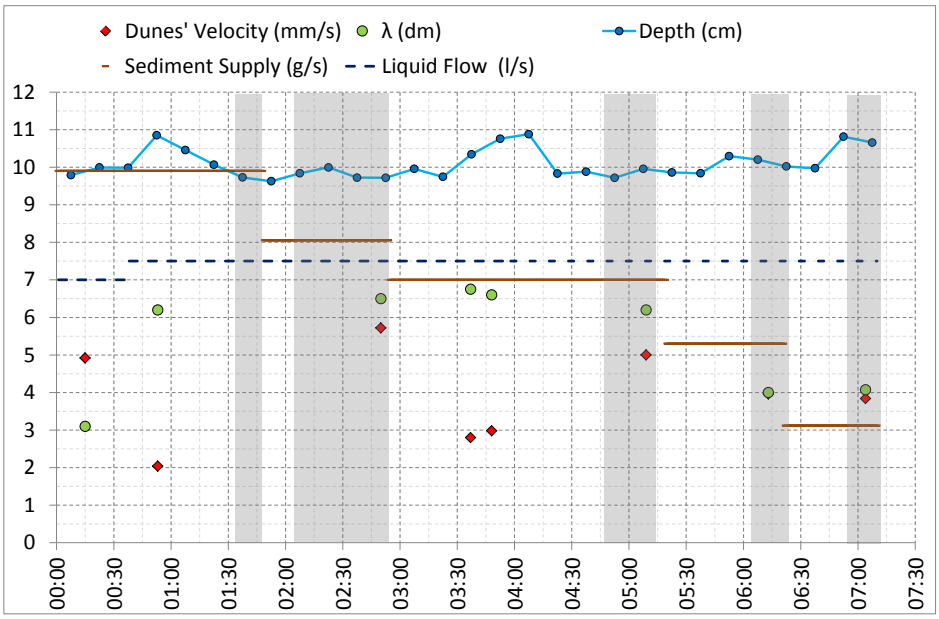

Figure A.16: M_S, Q_L, Dune Velocity, Dune Length, Flow Depth;

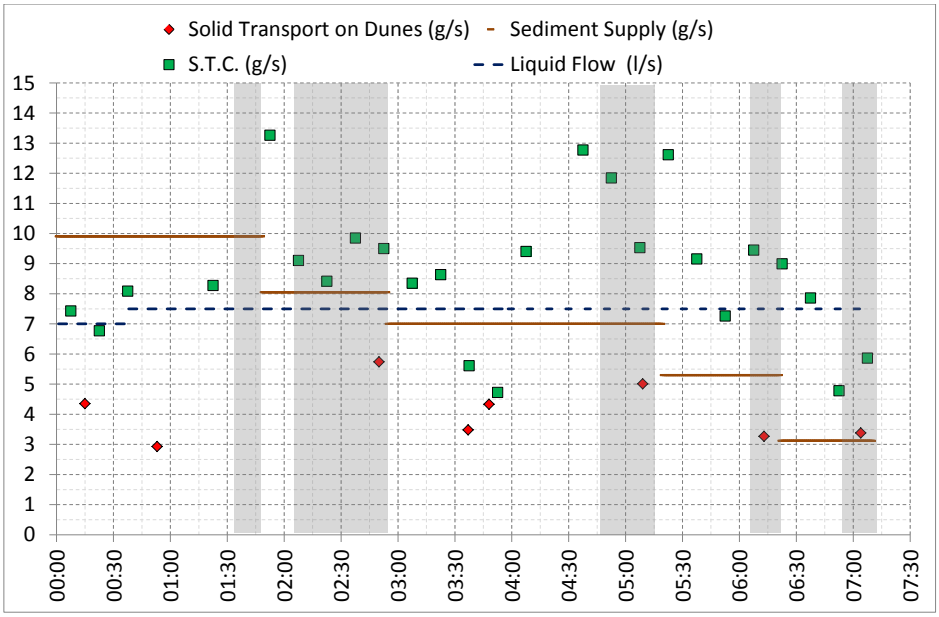

Figure A.17: M_S, Q_L, Solid Transport on Dunes, Solid Transport Capacity;

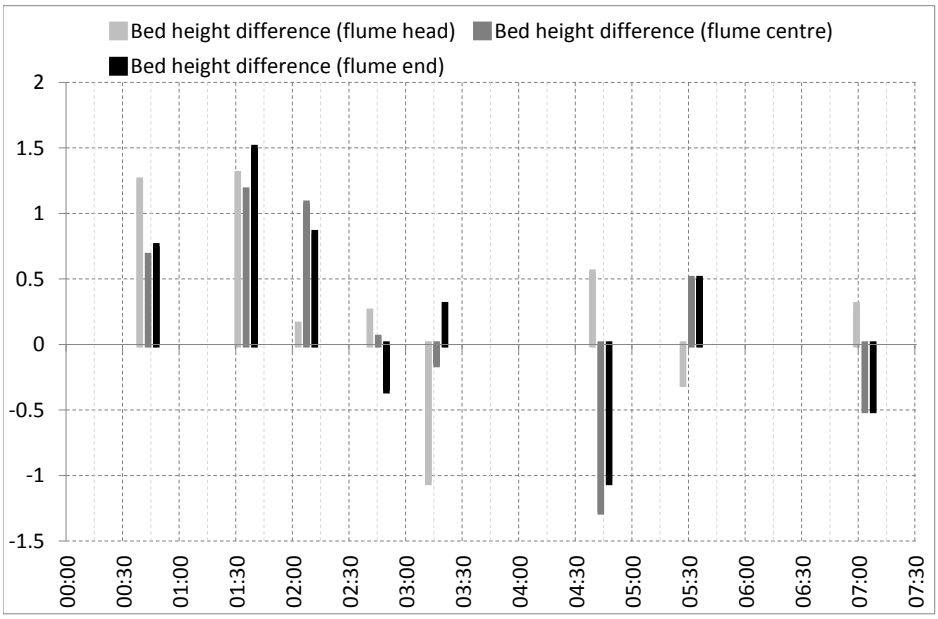

Figure A.18: Bed height difference in several parts of the flume;

A.4 Run 6

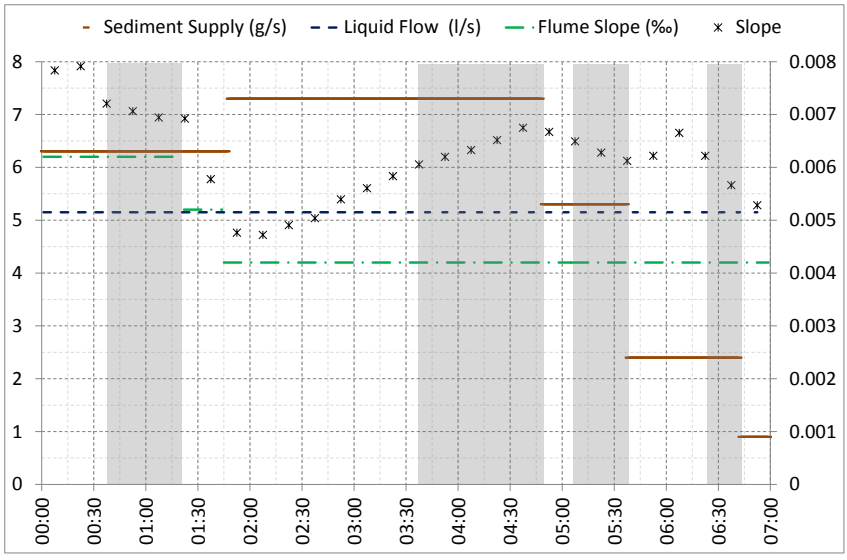

Figure A.19: $M_S(SX)$, $Q_L(SX)$, S(DX);

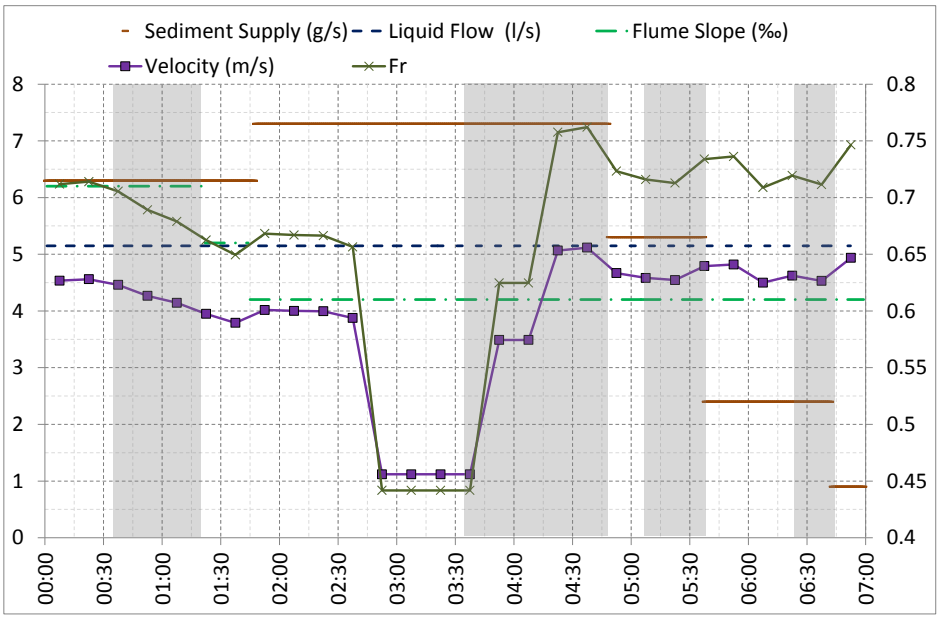

Figure A.20: $M_S(SX)$, $Q_L(SX)$, U(DX), Fr(DX);

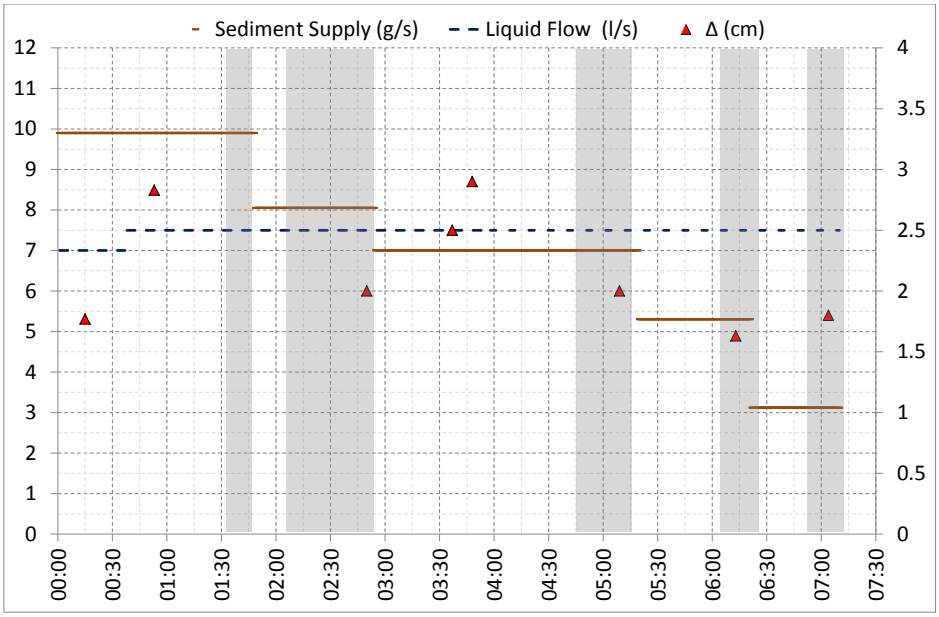

Figure A.21: $M_S(SX)$, $Q_L(SX)$, Dune Height(DX);

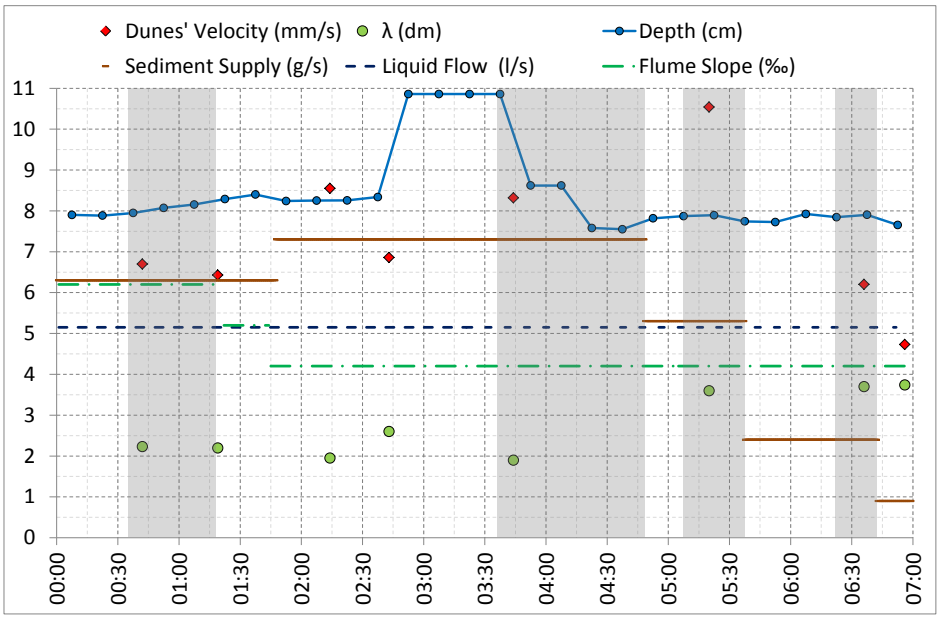

Figure A.22: M_S, Q_L, Dune Velocity, Dune Length, Flow Depth;

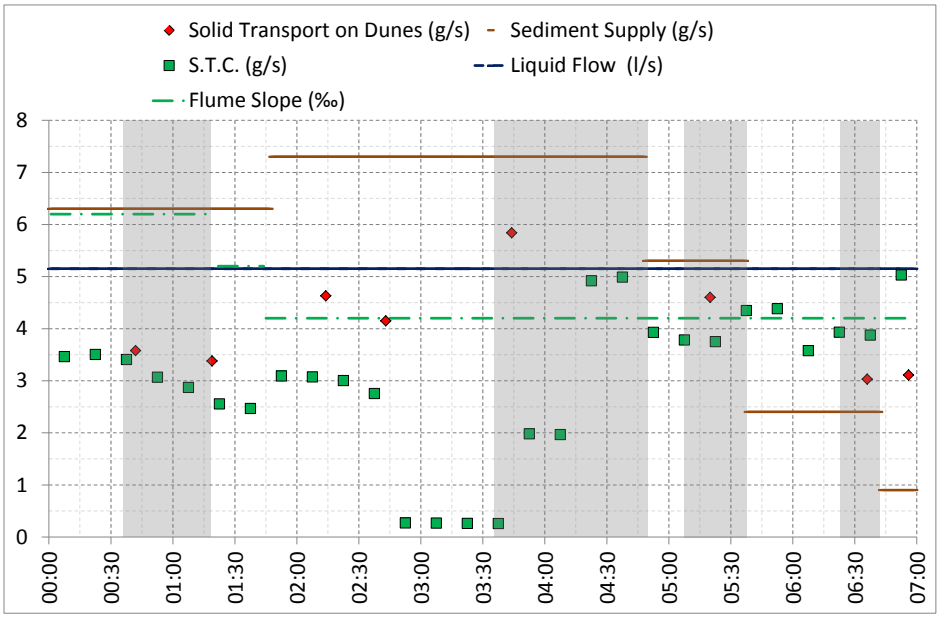

Figure A.23: M_S, Q_L, Solid Transport on Dunes, Solid Transport Capacity;

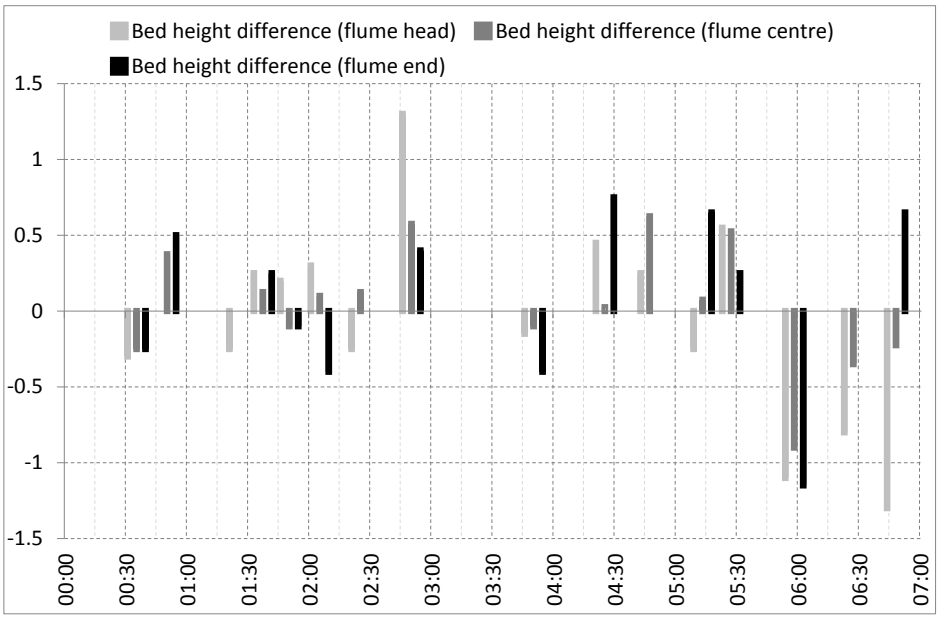

Figure A.24: Bed height difference in several parts of the flume;

A.5 Run 7

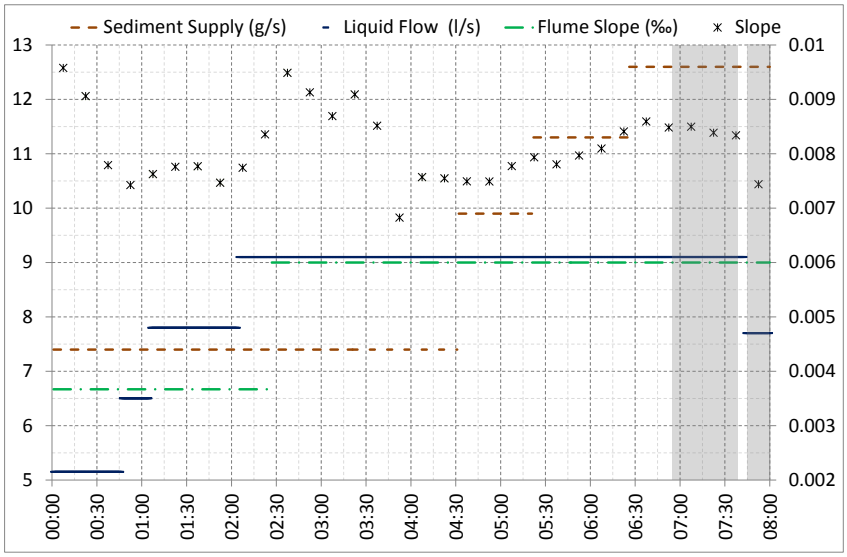

Figure A.25: $M_S(SX)$, $Q_L(SX)$, S(DX);

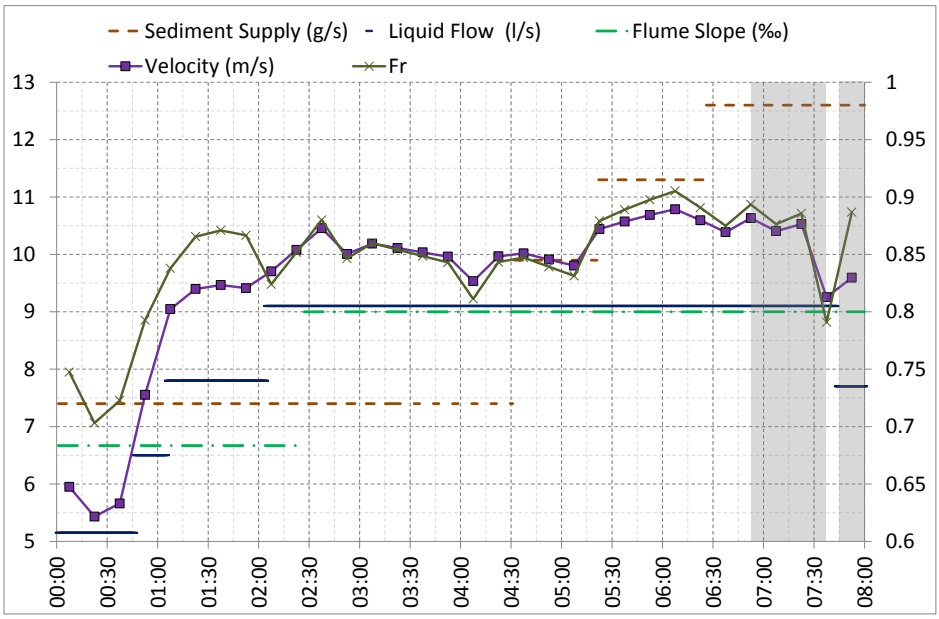

Figure A.26: $M_S(SX)$, $Q_L(SX)$, U(DX), Fr(DX);

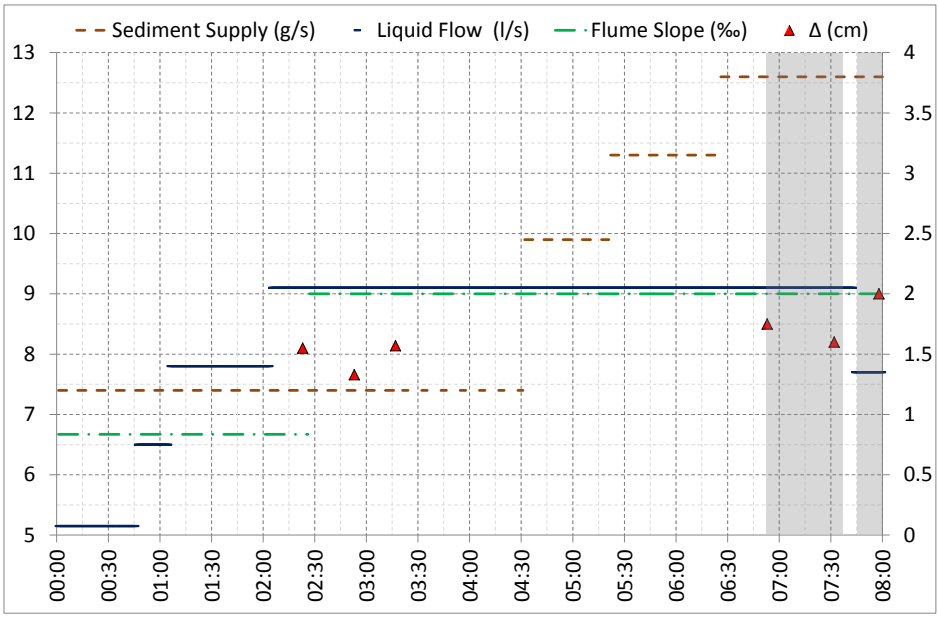

Figure A.27: $M_S(SX)$, $Q_L(SX)$, Dune Height(DX);

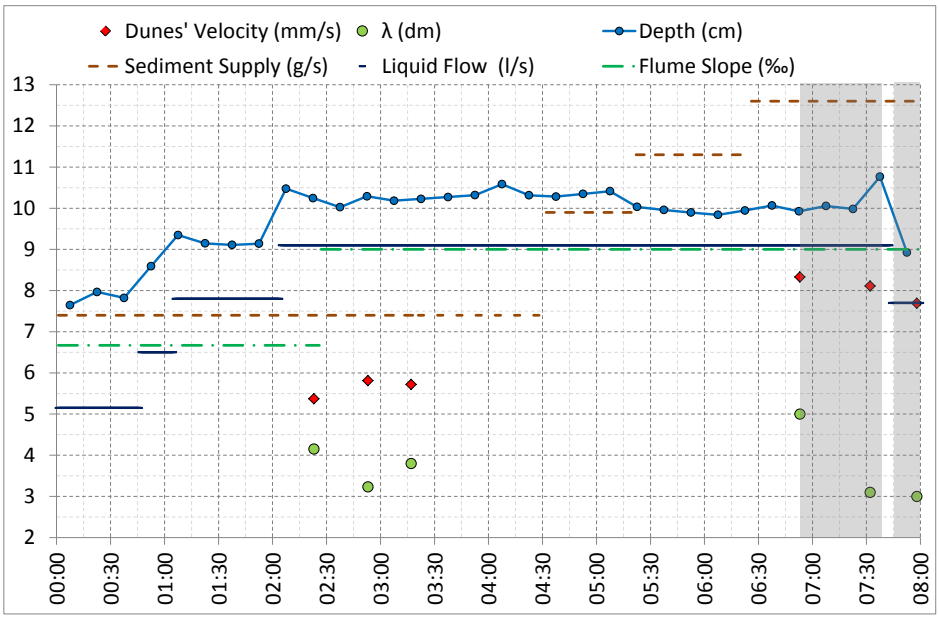

Figure A.28: M_S, Q_L, Dune Velocity, Dune Length, Flow Depth;

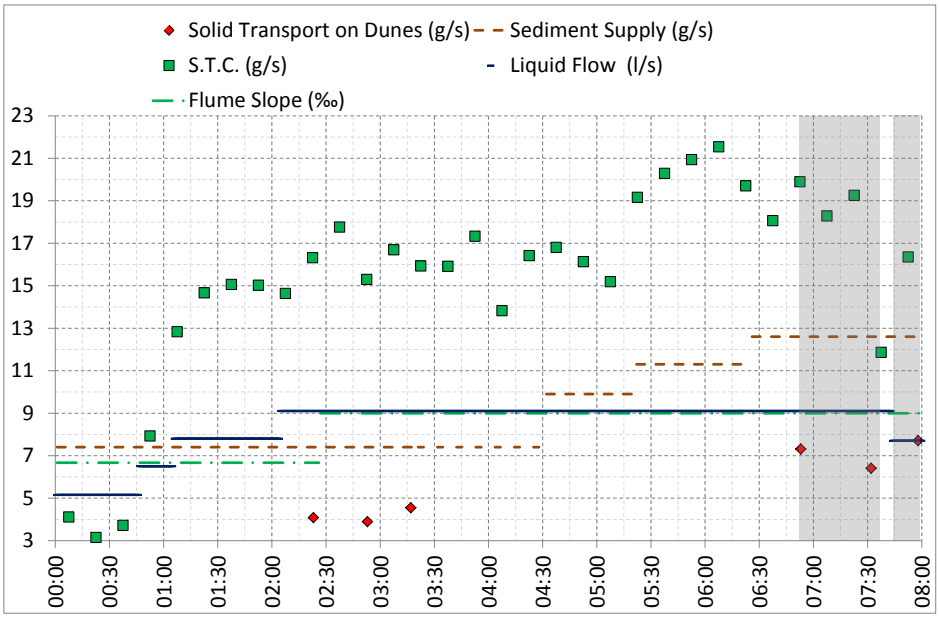

Figure A.29: M_S, Q_L, Solid Transport on Dunes, Solid Transport Capacity;

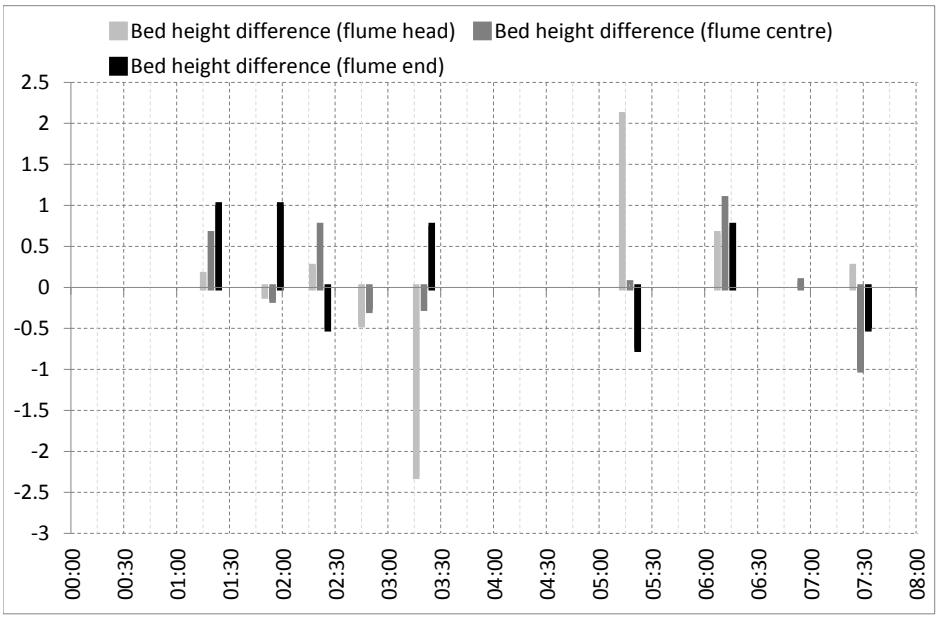

Figure A.30: Bed height difference in several parts of the flume;

A.6 Run 8

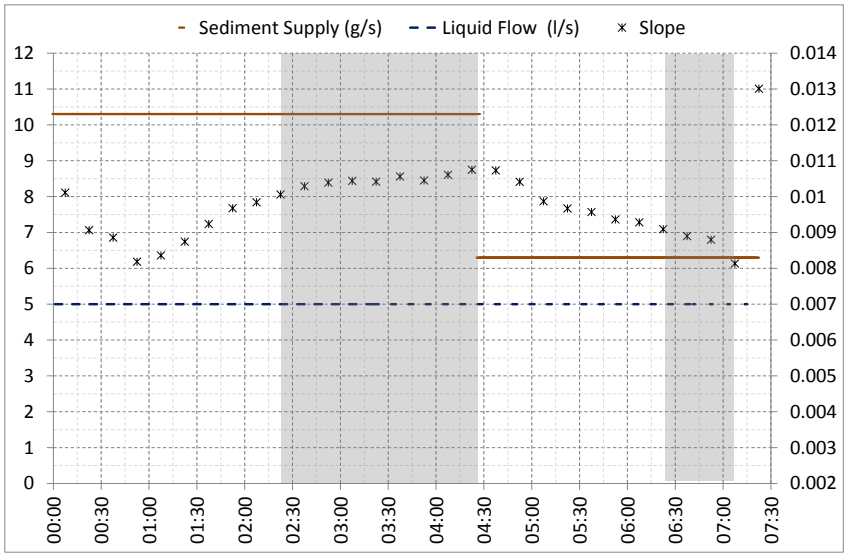

Figure A.31: $M_S(SX)$, $Q_L(SX)$, S(DX);

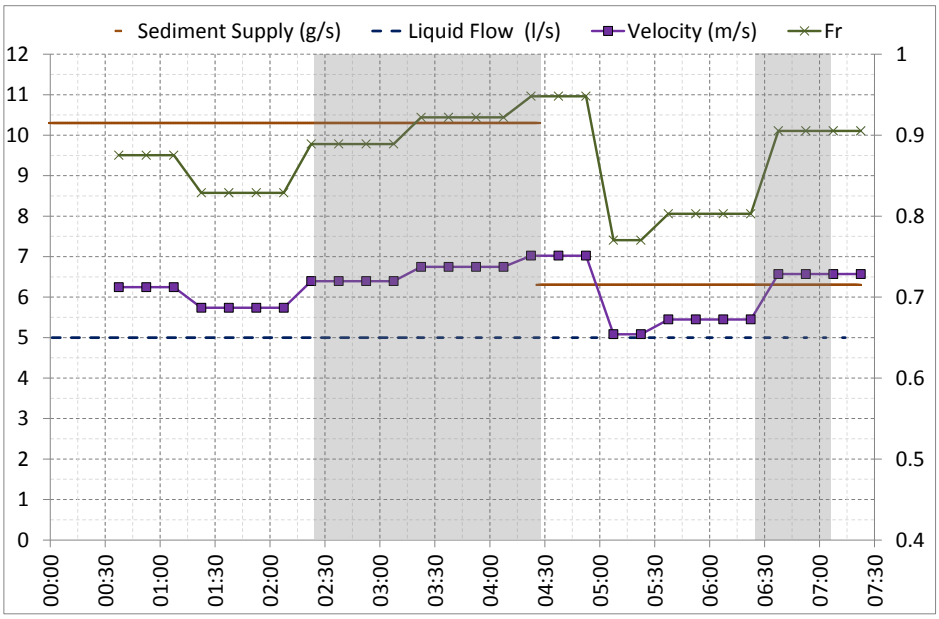

Figure A.32: $M_S(SX)$, $Q_L(SX)$, U(DX), Fr(DX);

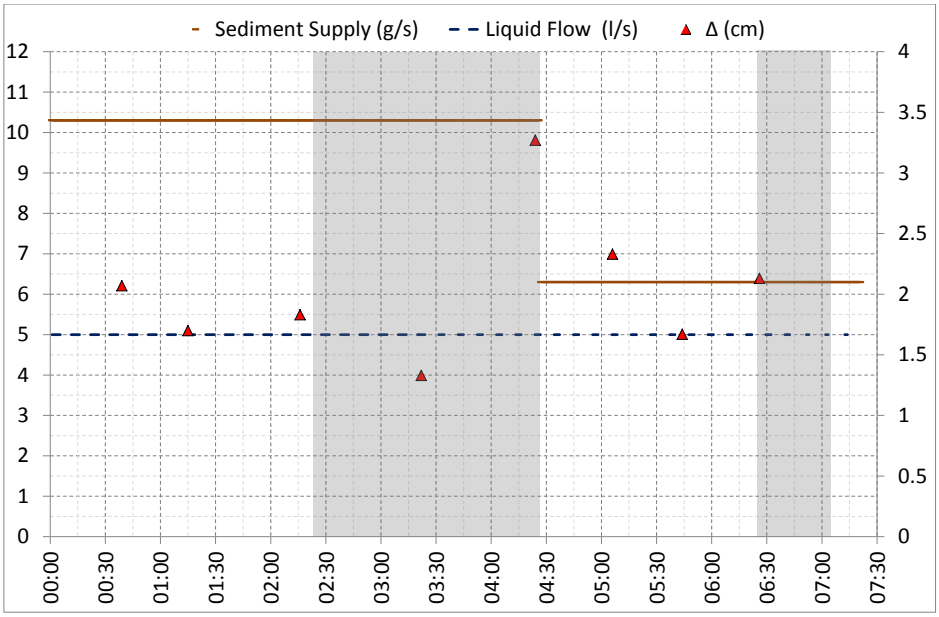

Figure A.33: $M_S(SX)$, $Q_L(SX)$, Dune Height(DX);

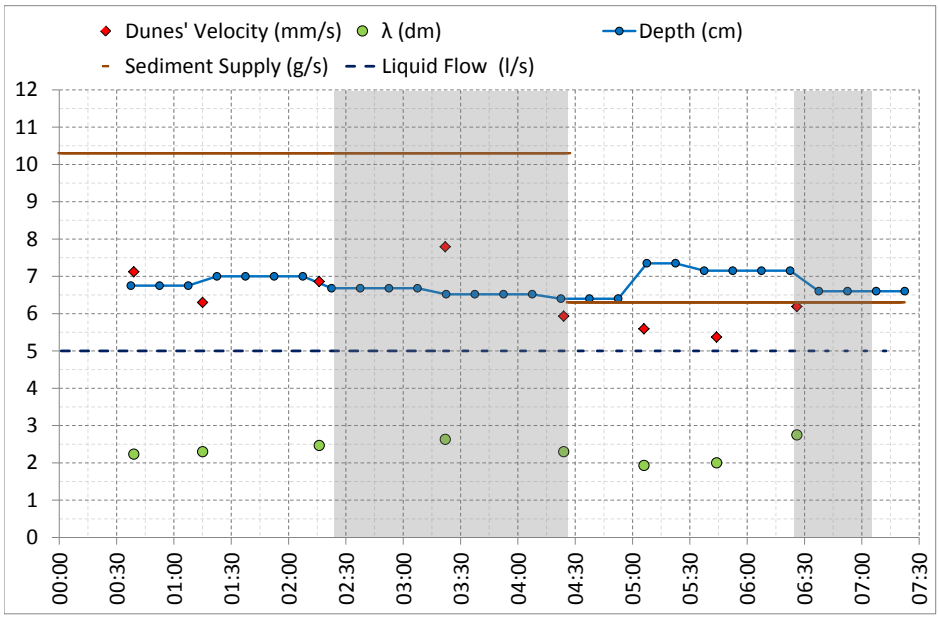

Figure A.34: M_S, Q_L, Dune Velocity, Dune Length, Flow Depth;

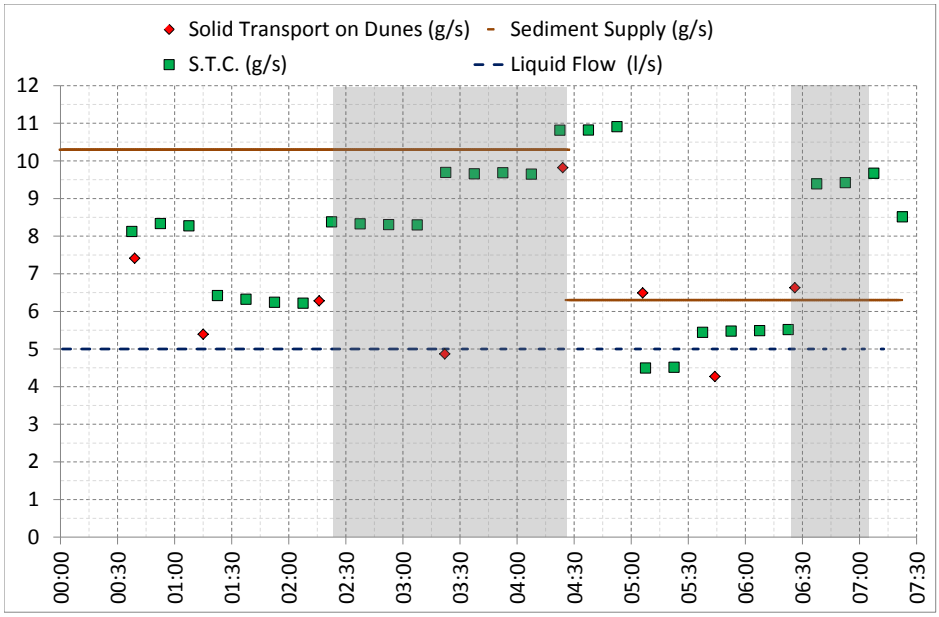

Figure A.35: M_S, Q_L, Solid Transport on Dunes, Solid Transport Capacity;

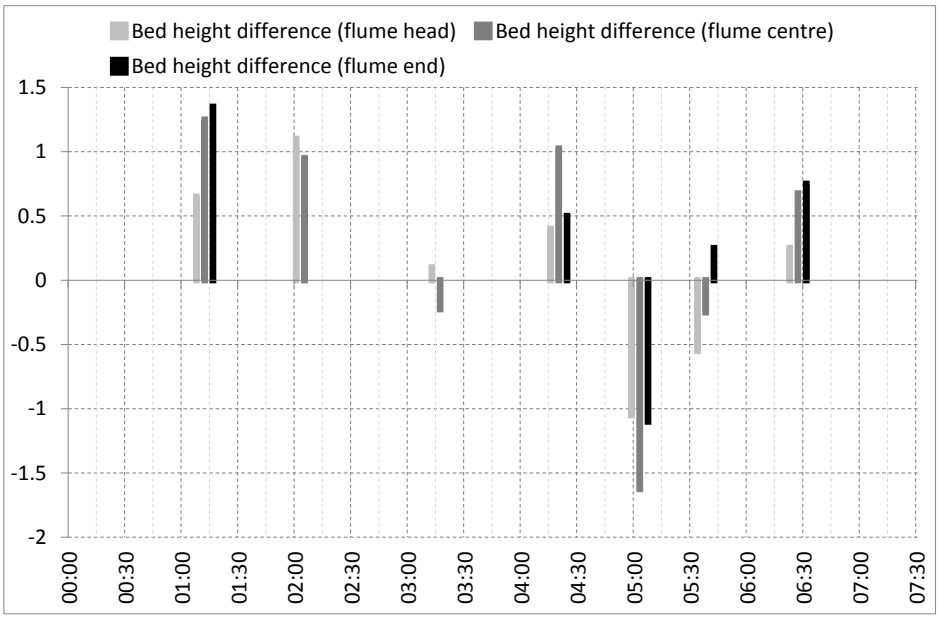

Figure A.36: Bed height difference in several parts of the flume;

A.7 Run 9

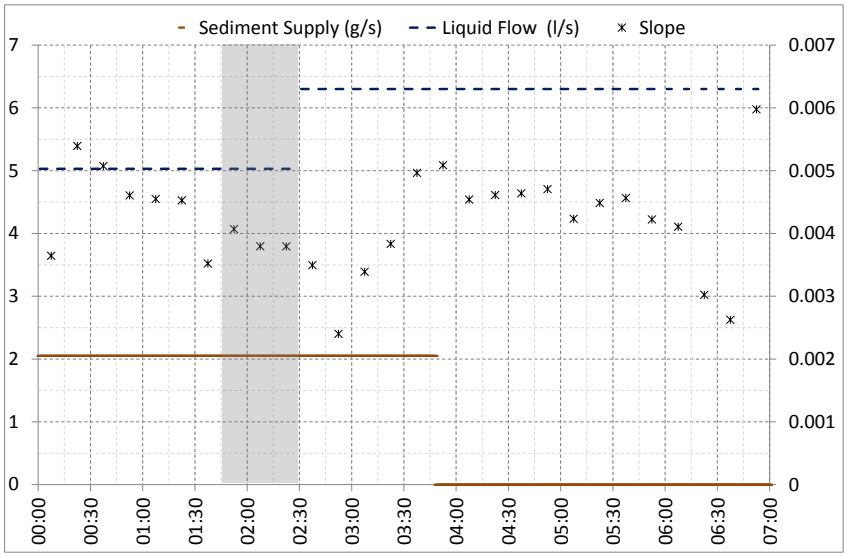

Figure A.37: $M_S(SX)$, $Q_L(SX)$, S(DX);

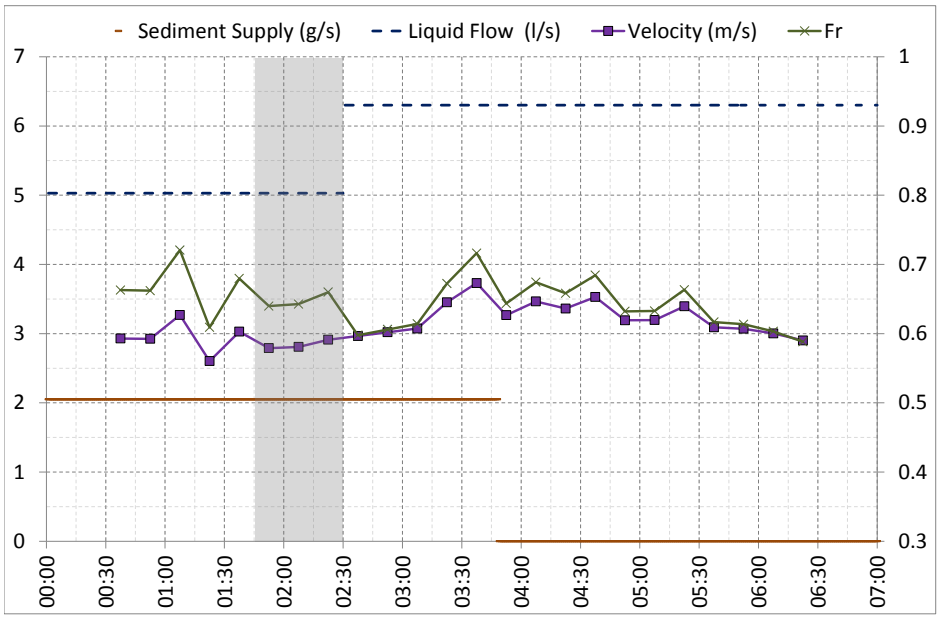

Figure A.38: $M_S(SX)$, $Q_L(SX)$, U(DX), Fr(DX);

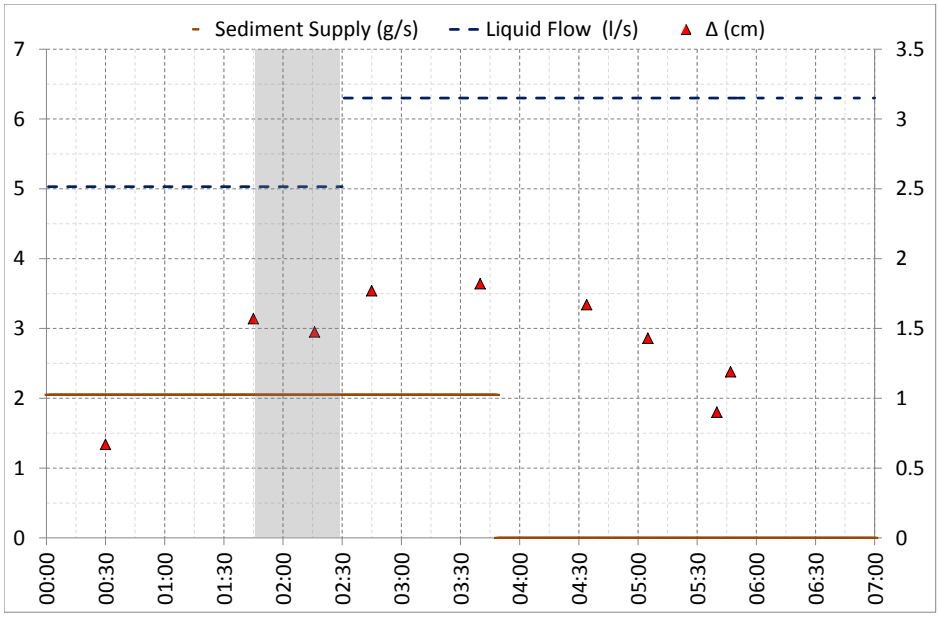

Figure A.39: $M_S(SX)$, $Q_L(SX)$, Dune Height(DX);

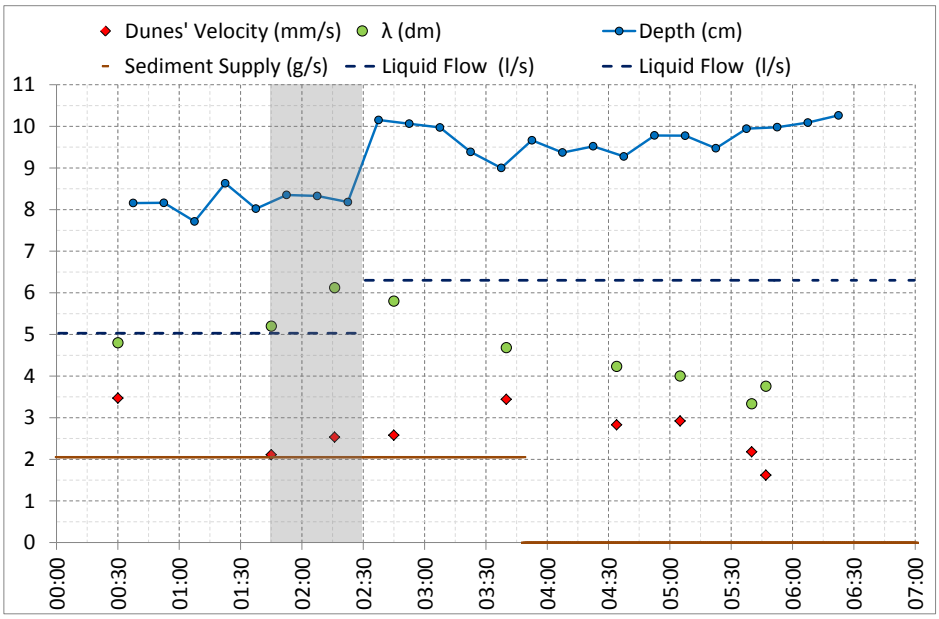

Figure A.40: M_S, Q_L, Dune Velocity, Dune Length, Flow Depth;

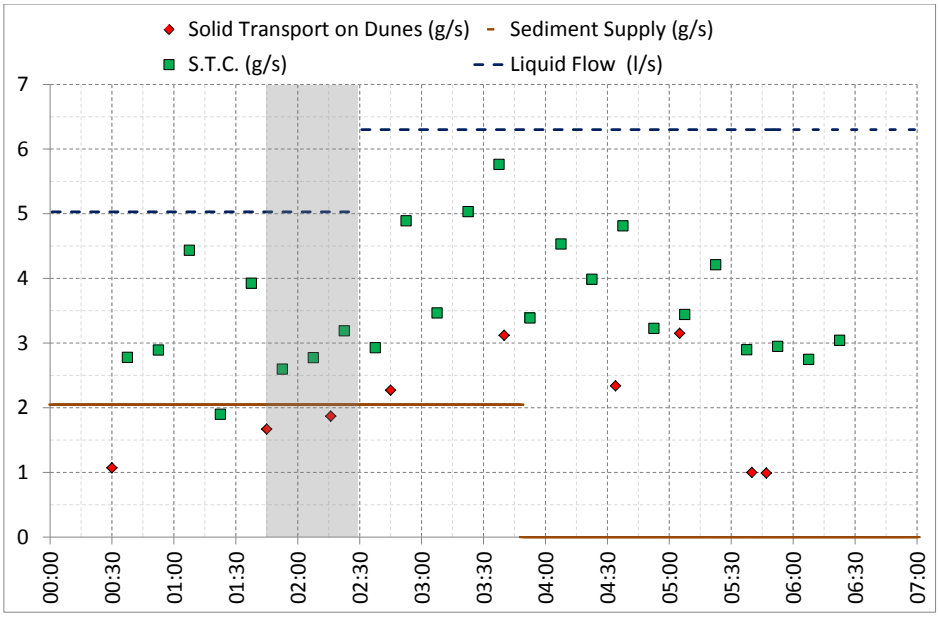

Figure A.41: M_S, Q_L, Solid Transport on Dunes, Solid Transport Capacity;

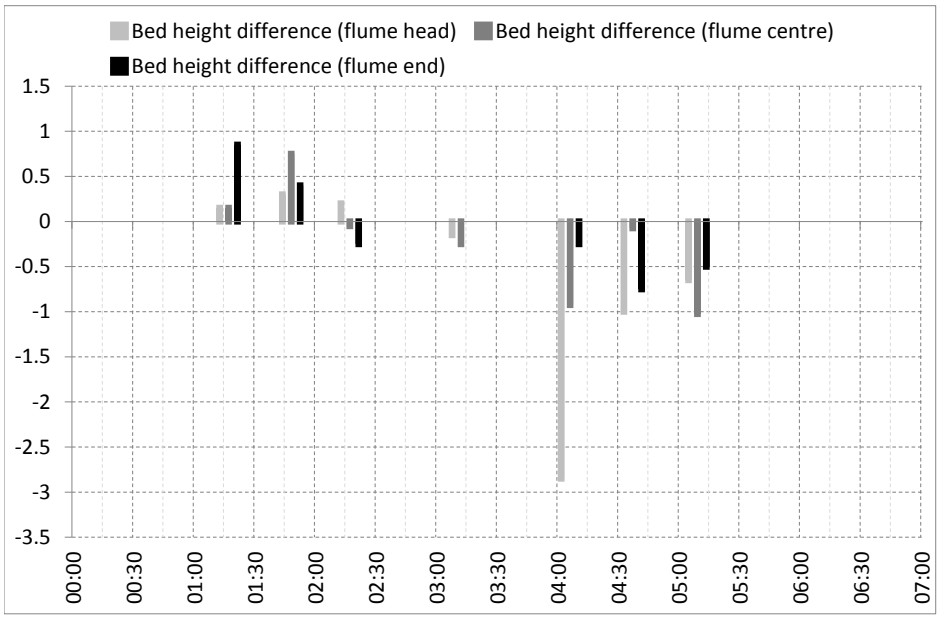

Figure A.42: Bed height difference in several parts of the flume;

A.8 Run 10

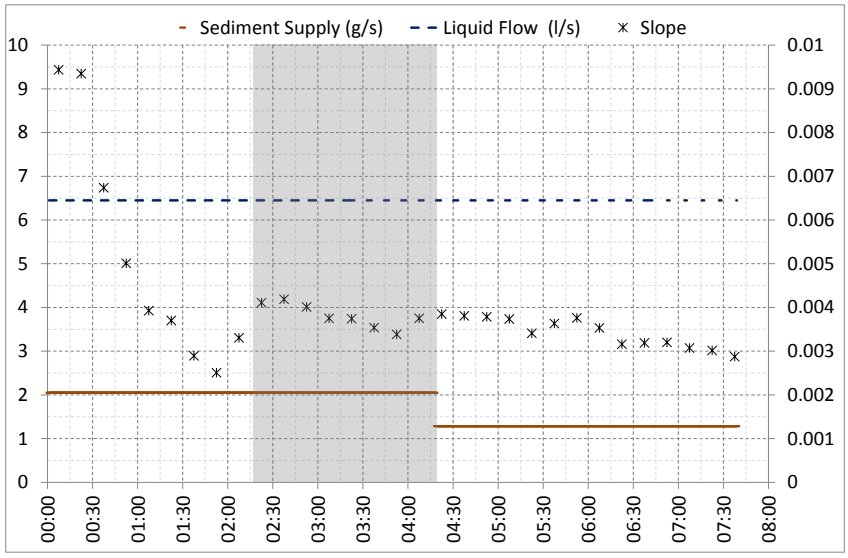

Figure A.43: $M_S(SX)$, $Q_L(SX)$, S(DX);

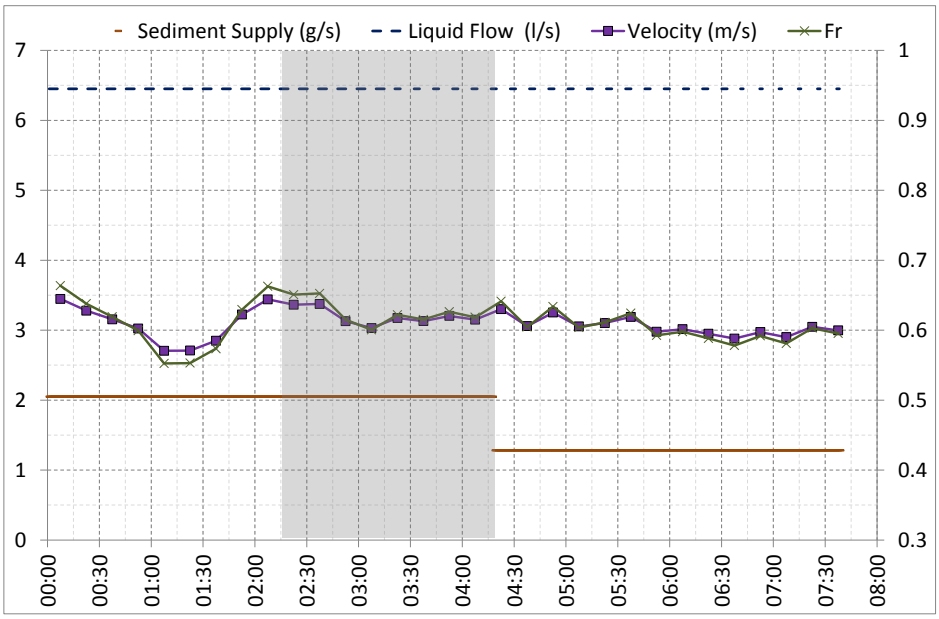

Figure A.44: $M_S(SX)$, $Q_L(SX)$, U(DX), Fr(DX);

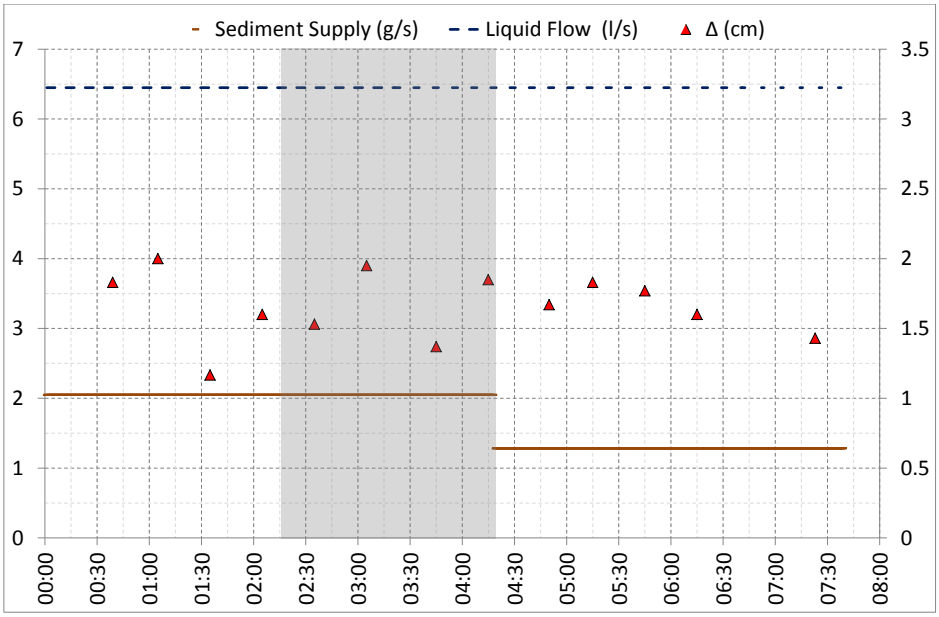

Figure A.45: $M_S(SX)$, $Q_L(SX)$, Dune Height(DX);

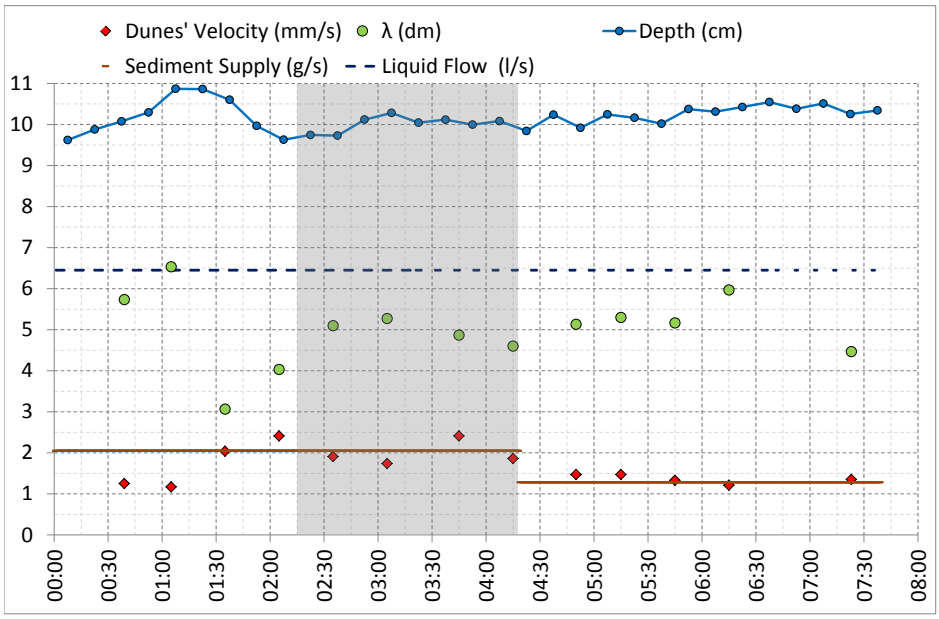

Figure A.46: M_S, Q_L, Dune Velocity, Dune Length, Flow Depth;

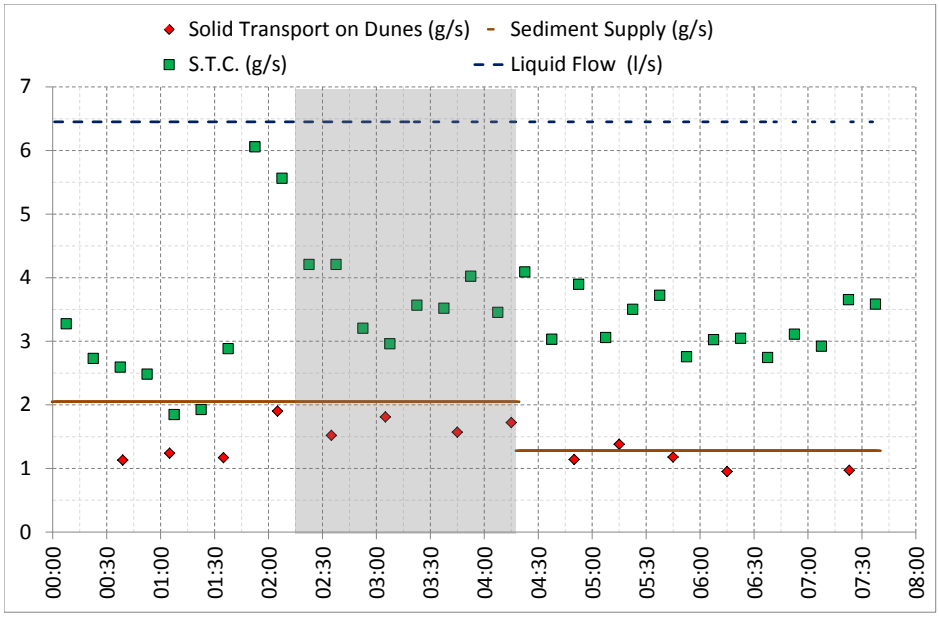

Figure A.47: M_S, Q_L, Solid Transport on Dunes, Solid Transport Capacity;

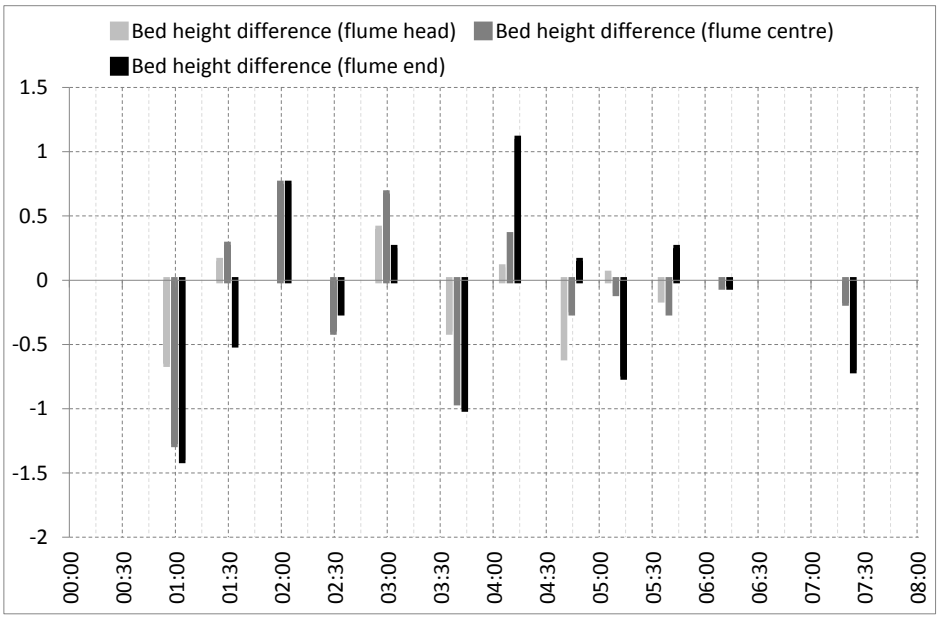

Figure A.48: Bed height difference in several parts of the flume;

A.9 Run 11-18

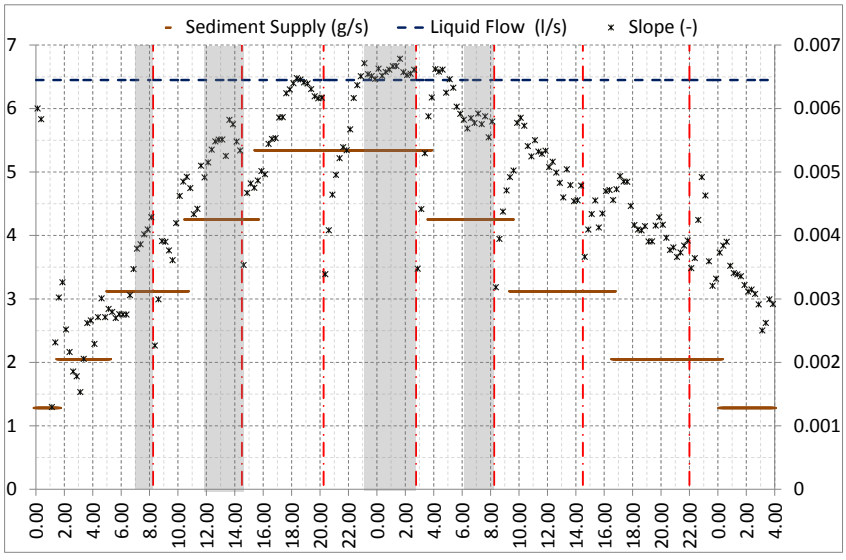

Figure A.49: $M_S(SX)$, $Q_L(SX)$, S(DX);

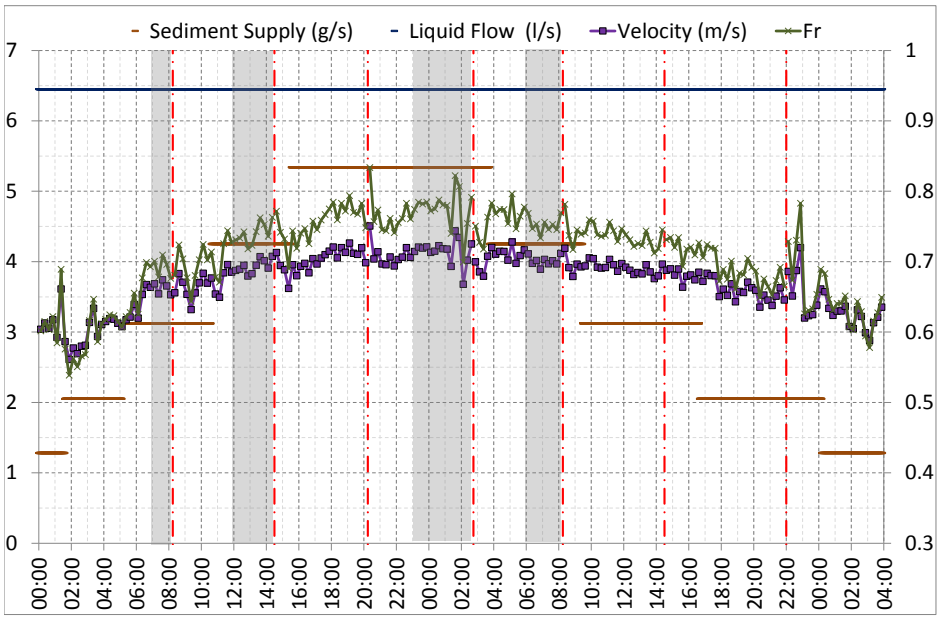

Figure A.50: $M_S(SX)$, $Q_L(SX)$, U(DX), Fr(DX);

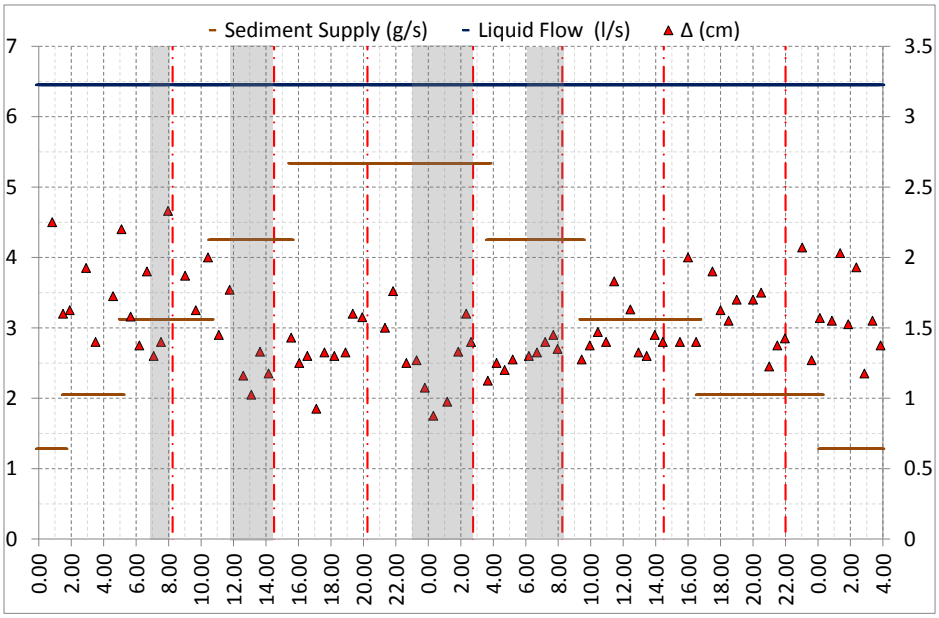

Figure A.51: $M_S(SX)$, $Q_L(SX)$, Dune Height(DX);

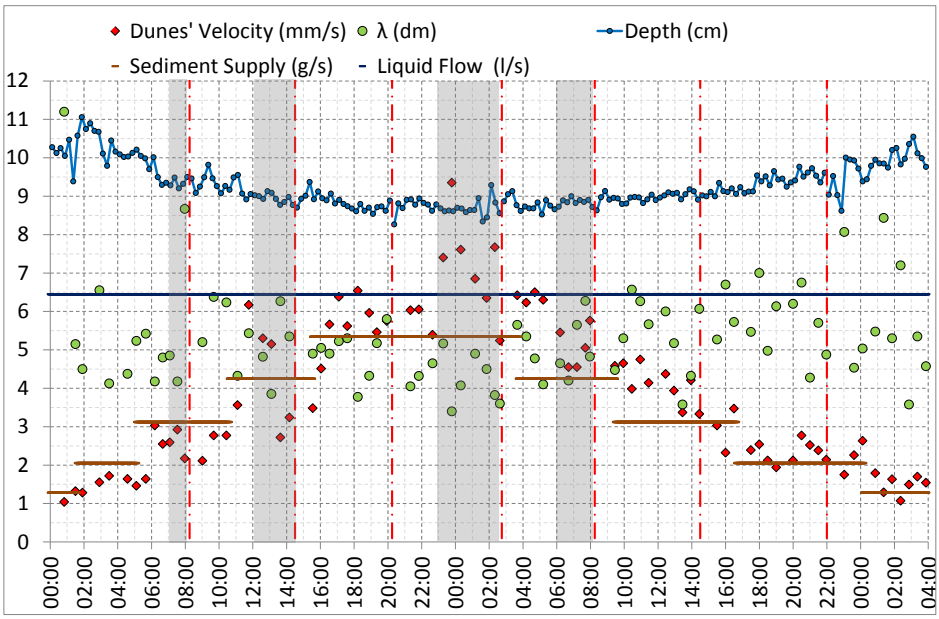

Figure A.52: M_S, Q_L, Dune Velocity, Dune Length, Flow Depth;

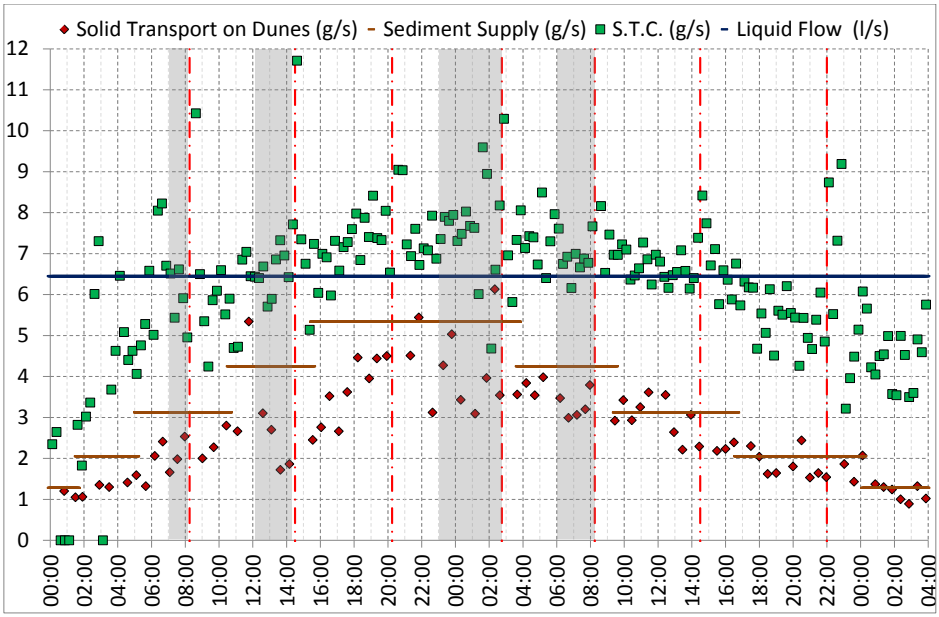

Figure A.53: M_S, Q_L, Solid Transport on Dunes, Solid Transport Capacity;

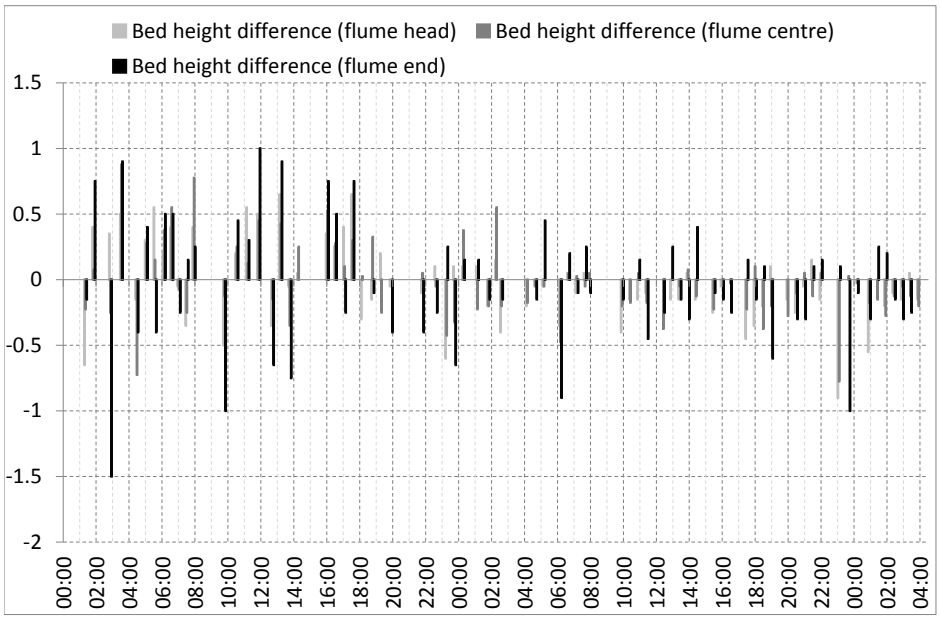

Figure A.54: Bed height difference in several parts of the flume;

A.10 Run 19-20

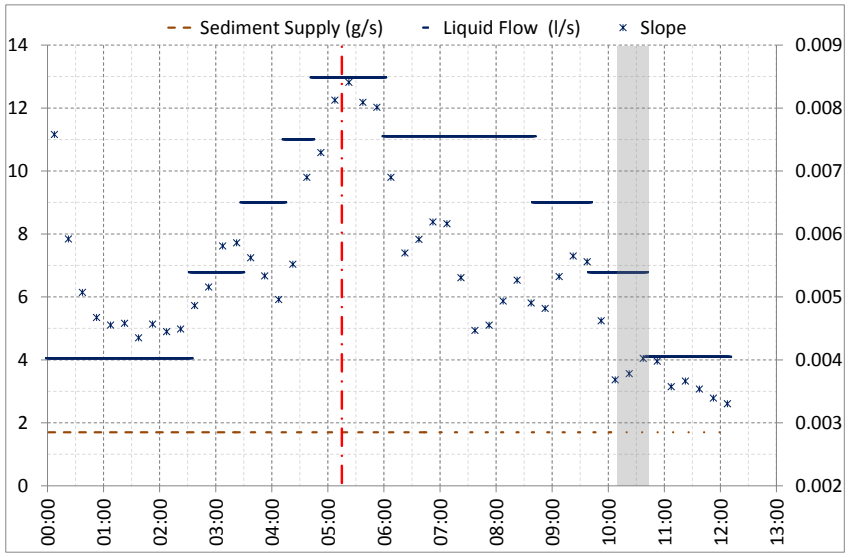

Figure A.55: $M_S(SX)$, $Q_L(SX)$, S(DX);

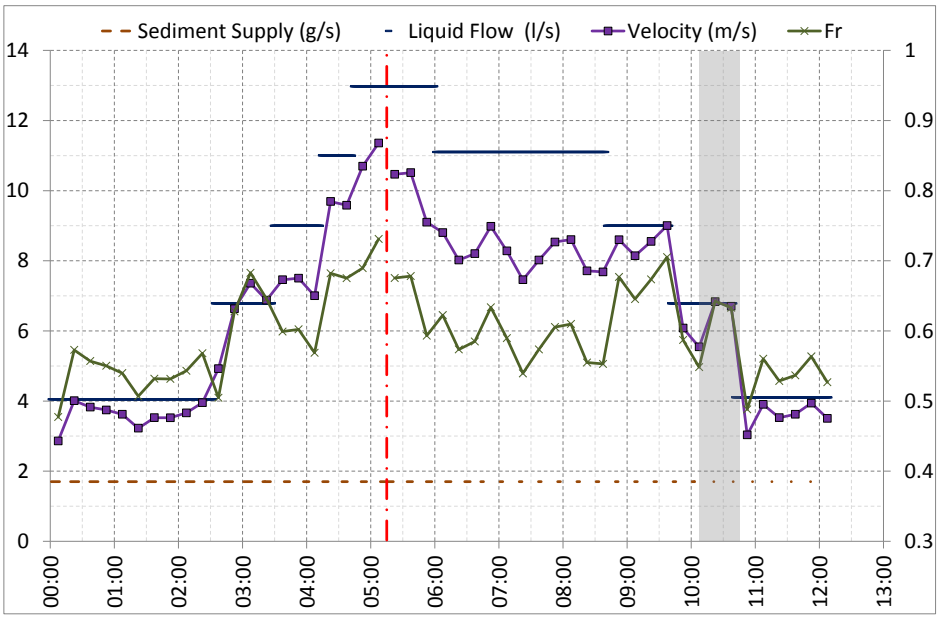

Figure A.56: $M_S(SX)$, $Q_L(SX)$, U(DX), Fr(DX);

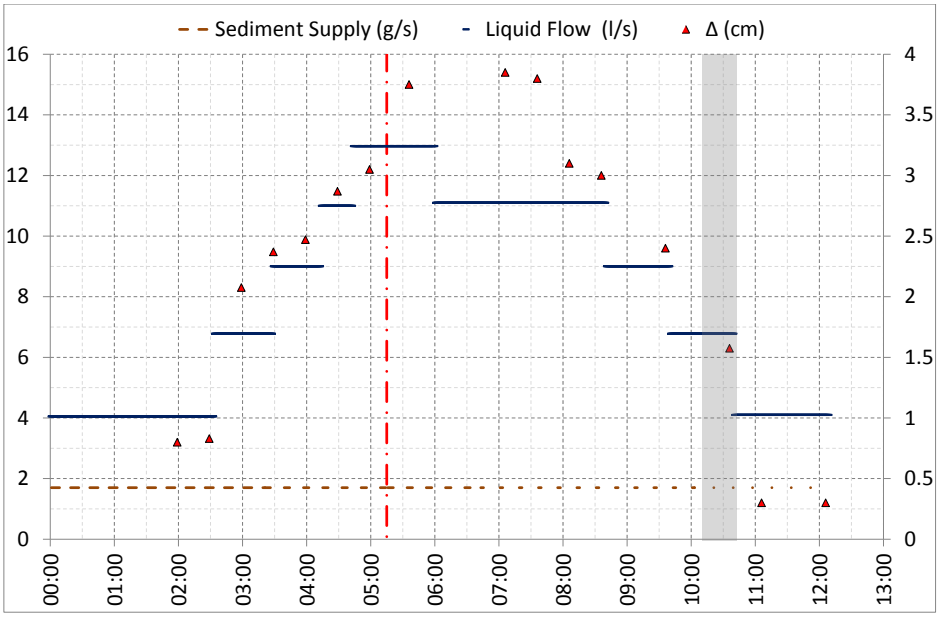

Figure A.57: $M_S(SX)$, $Q_L(SX)$, Dune Height(DX);

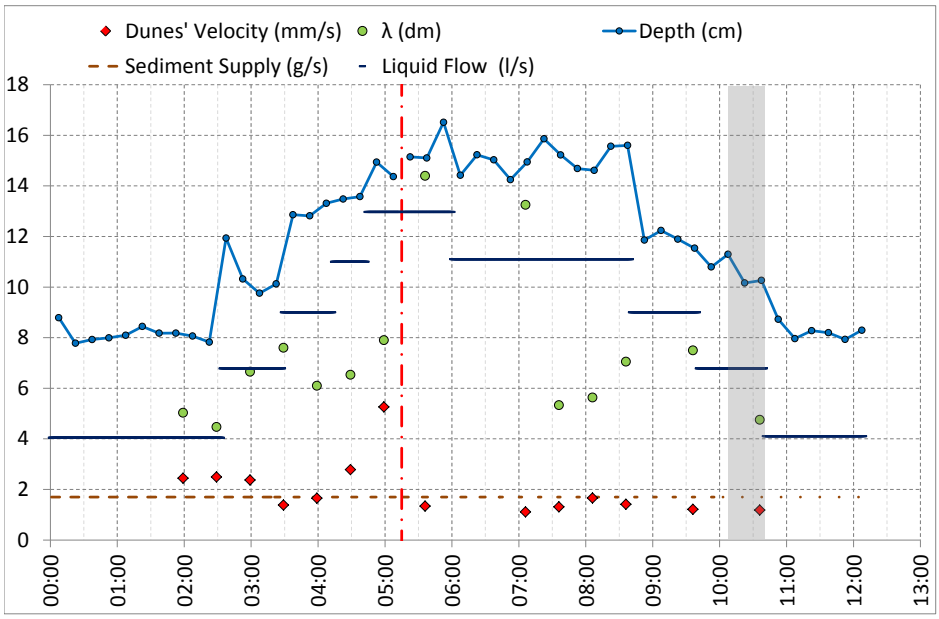

Figure A.58: M_S, Q_L, Dune Velocity, Dune Length, Flow Depth;

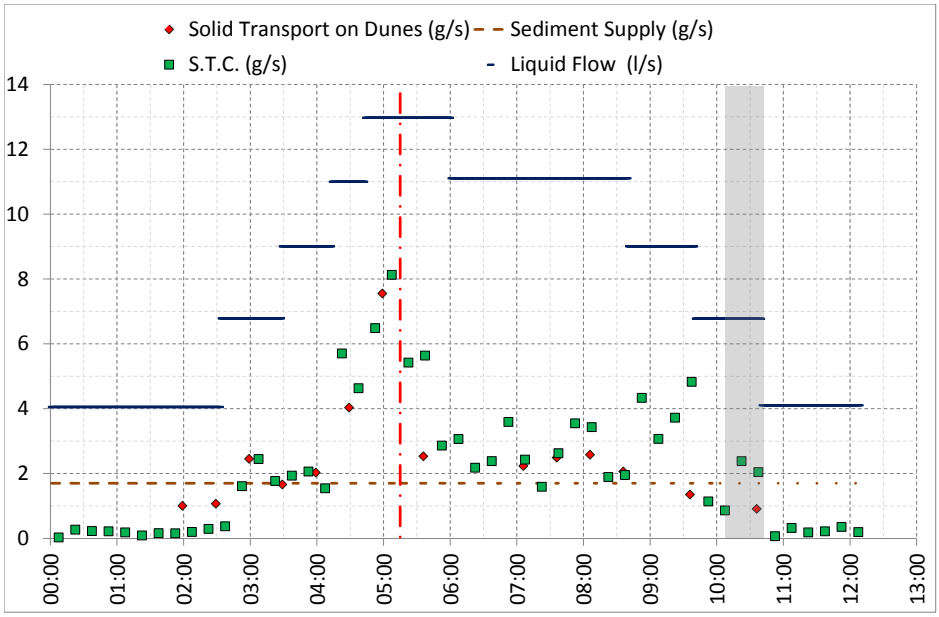

Figure A.59: M_S, Q_L, Solid Transport on Dunes, Solid Transport Capacity;

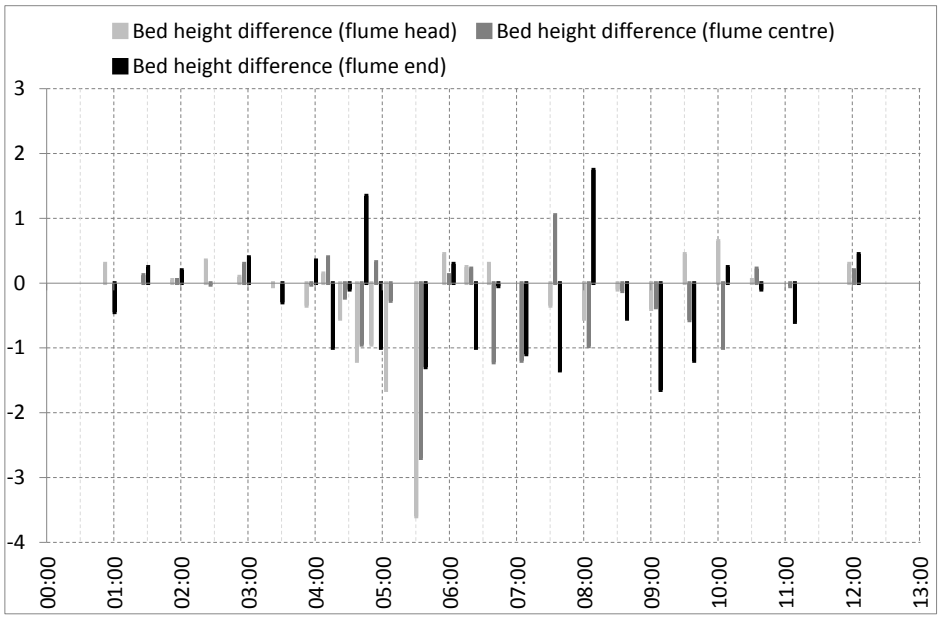

Figure A.60: Bed height difference in several parts of the flume;

A.11 Run 21

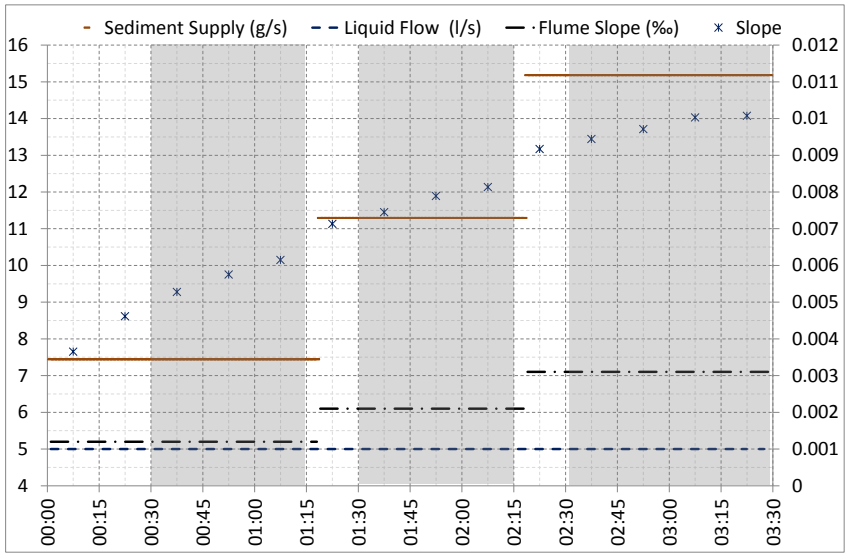

Figure A.61: $M_S(SX)$, $Q_L(SX)$, S(DX);

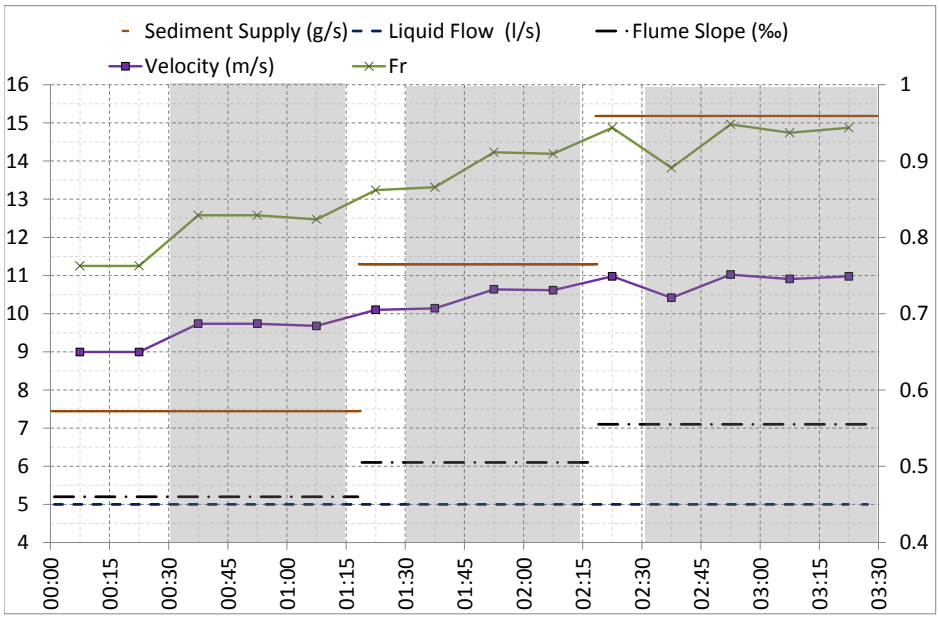

Figure A.62: $M_S(SX)$, $Q_L(SX)$, U(DX), Fr(DX);

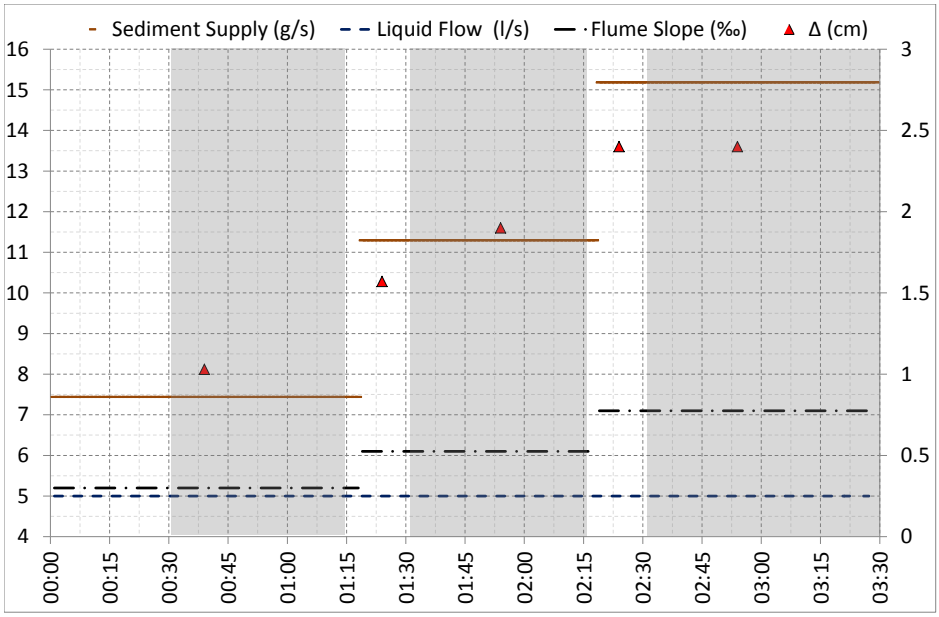

Figure A.63: $M_S(SX)$, $Q_L(SX)$, Dune Height(DX);

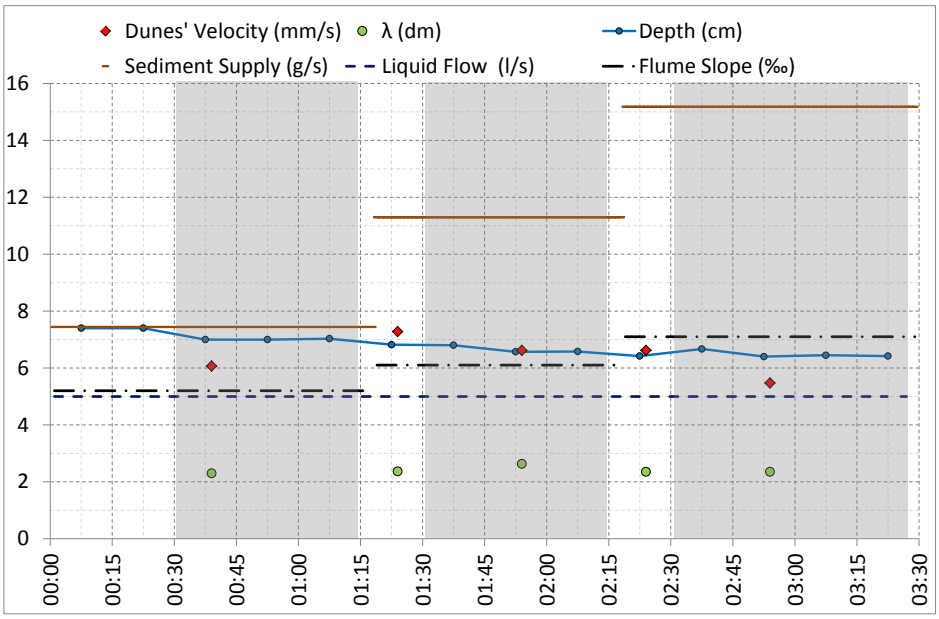

Figure A.64: M_S, Q_L, Dune Velocity, Dune Length, Flow Depth;

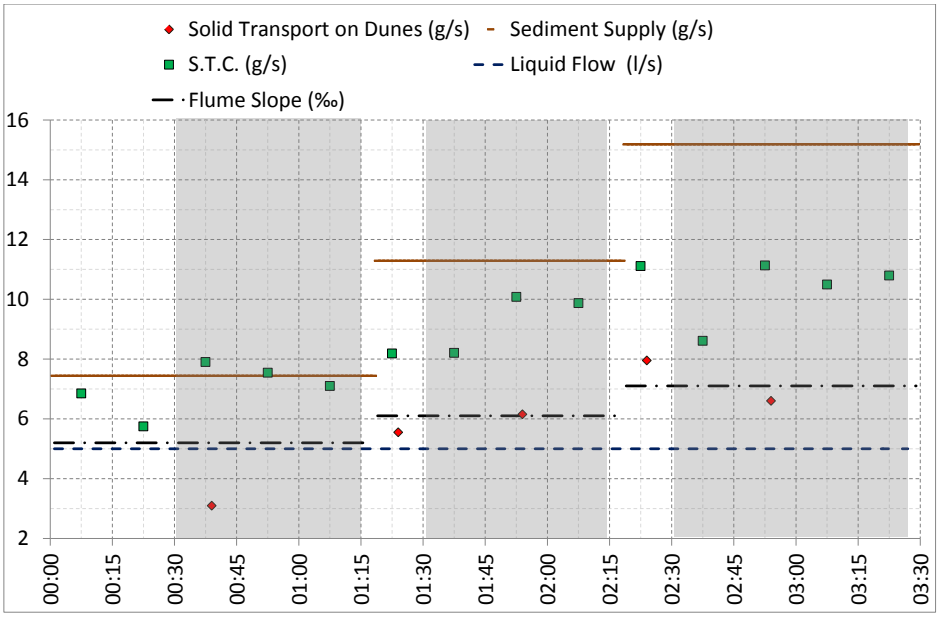

Figure A.65: M_S, Q_L, Solid Transport on Dunes, Solid Transport Capacity;

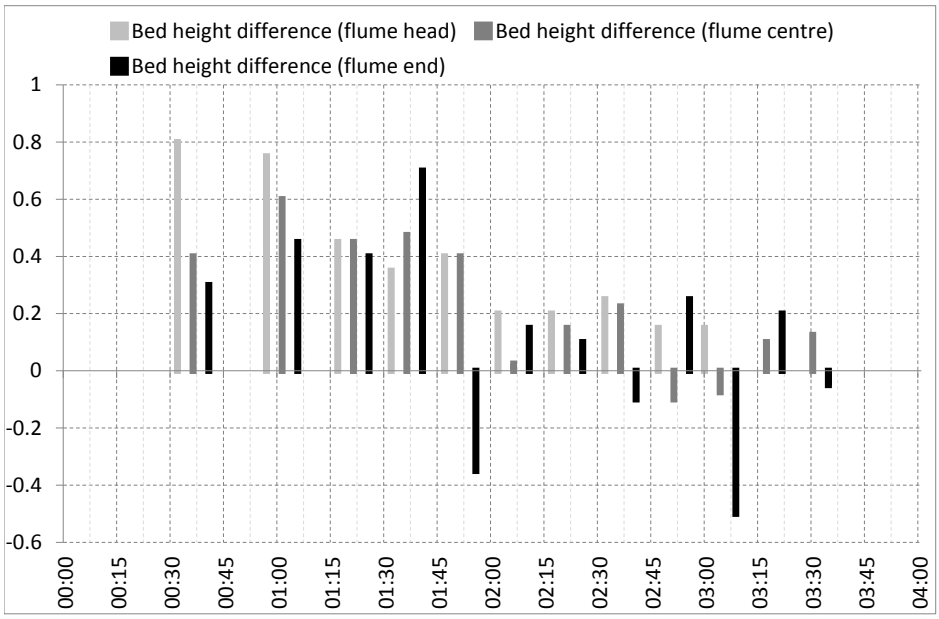

Figure A.66: Bed height difference in several parts of the flume;

A.12 Run 22

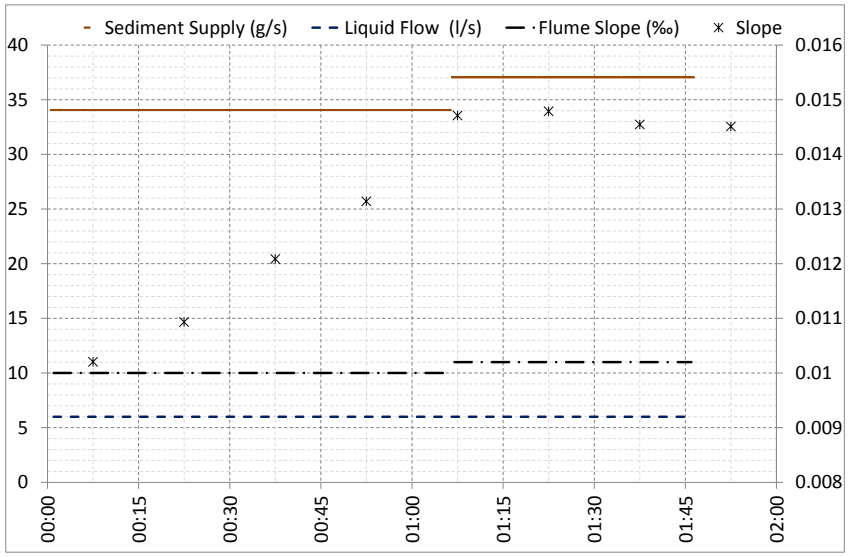

Figure A.67: $M_S(SX)$, $Q_L(SX)$, S(DX);

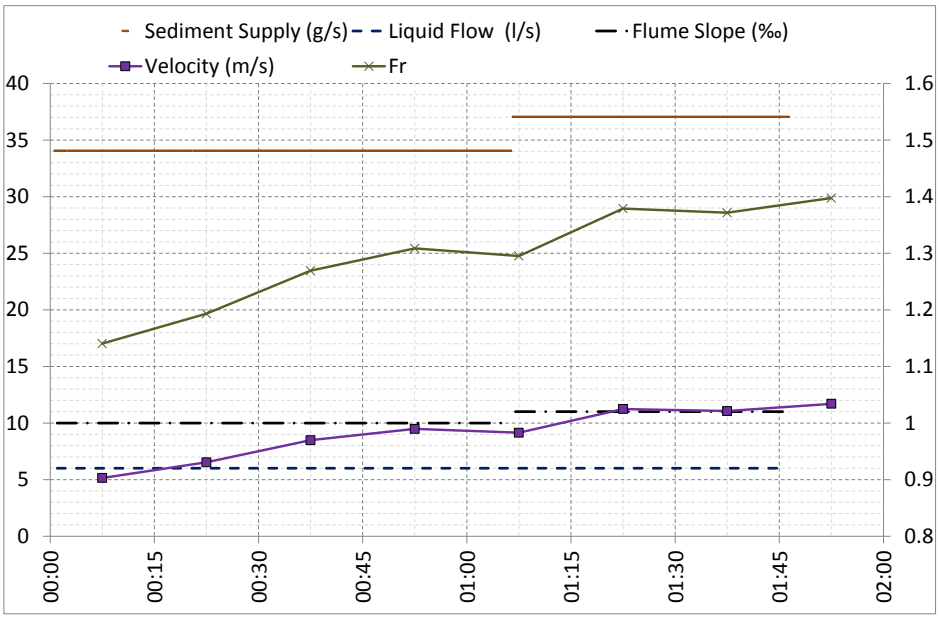

Figure A.68: $M_S(SX)$, $Q_L(SX)$, U(DX), Fr(DX);

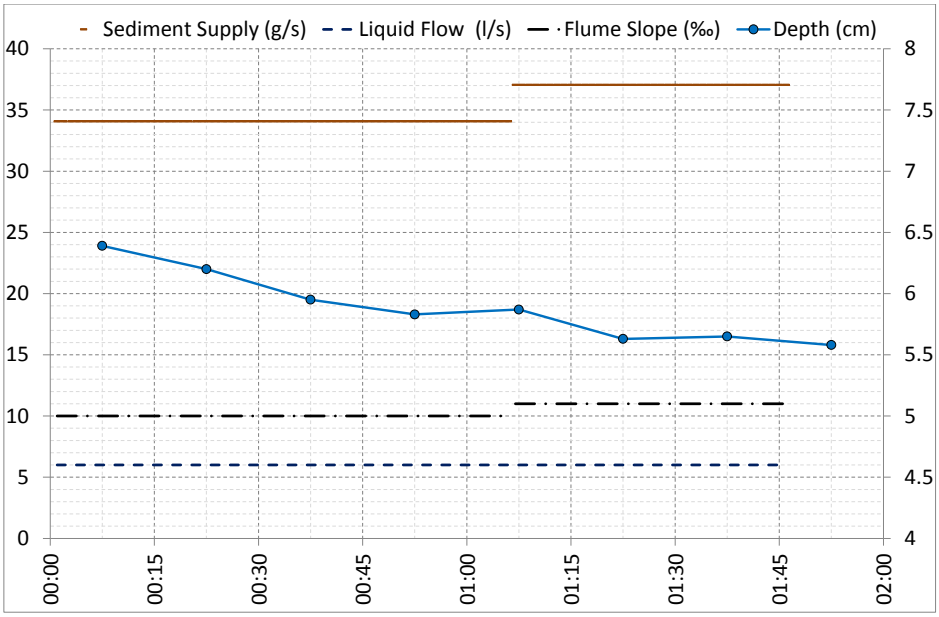

Figure A.69: M_S, Q_L, Dune Velocity, Dune Length, Flow Depth;

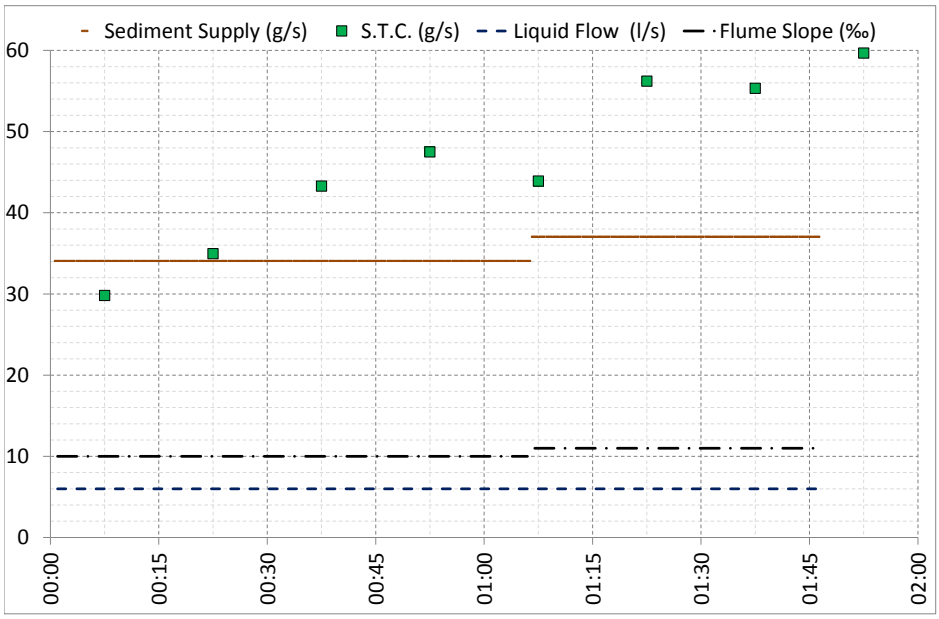

Figure A.70: M_S, Q_L, Solid Transport on Dunes, Solid Transport Capacity;

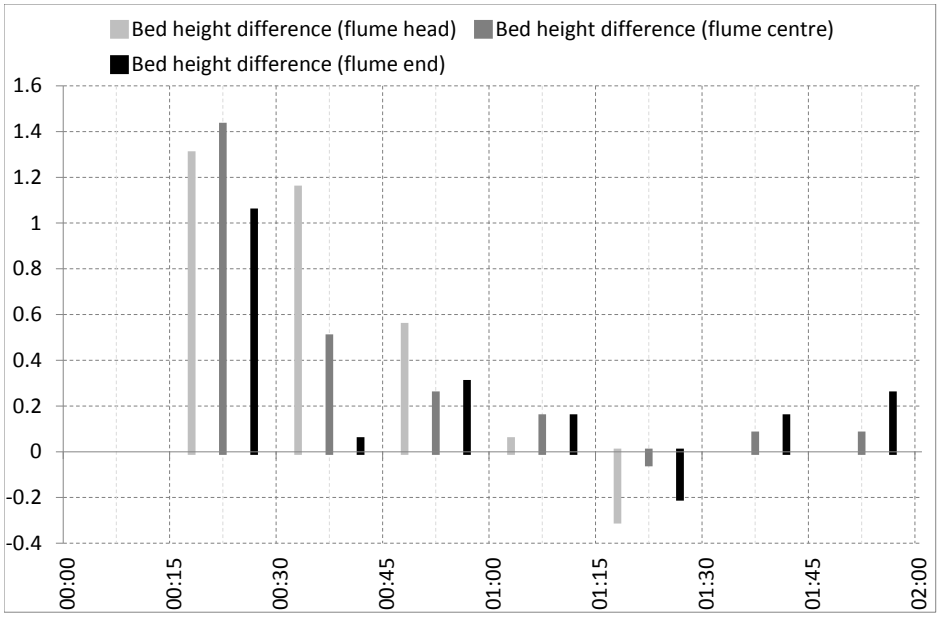

Figure A.71: Bed height difference in several parts of the flume;

A.13 Run 23-32

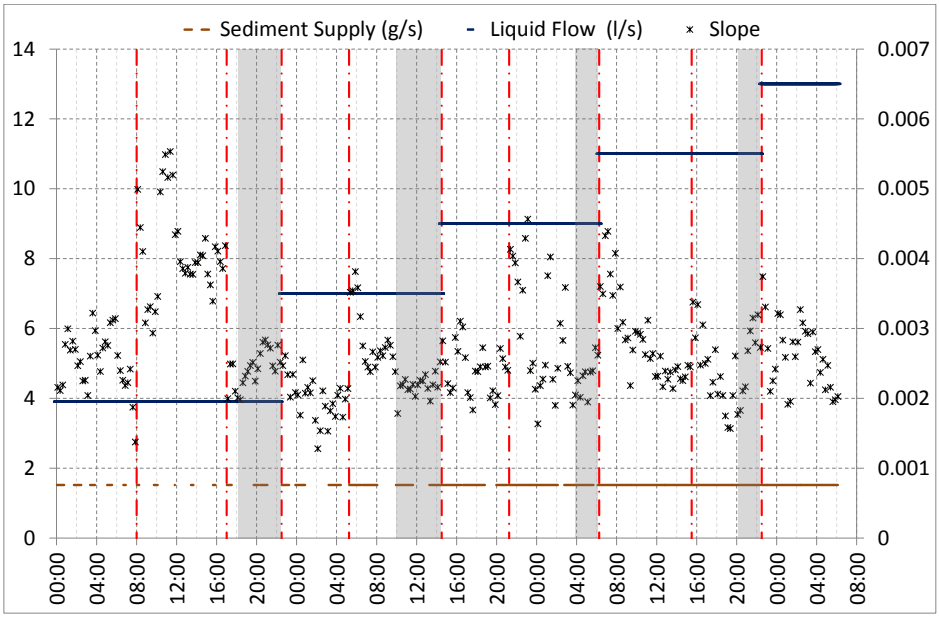

Figure A.72: $M_S(SX)$, $Q_L(SX)$, S(DX);

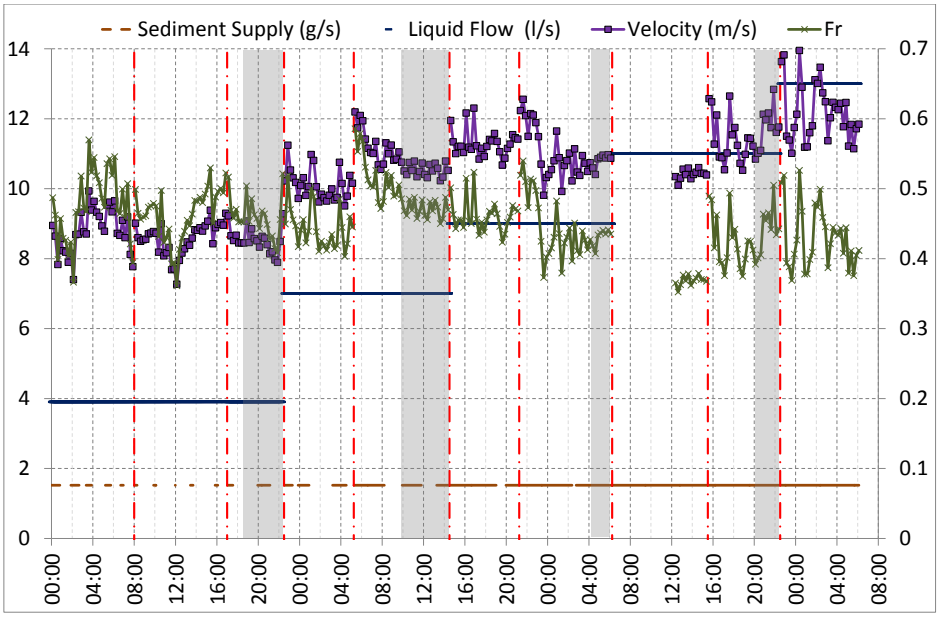

Figure A.73: $M_S(SX)$, $Q_L(SX)$, U(DX), Fr(DX);

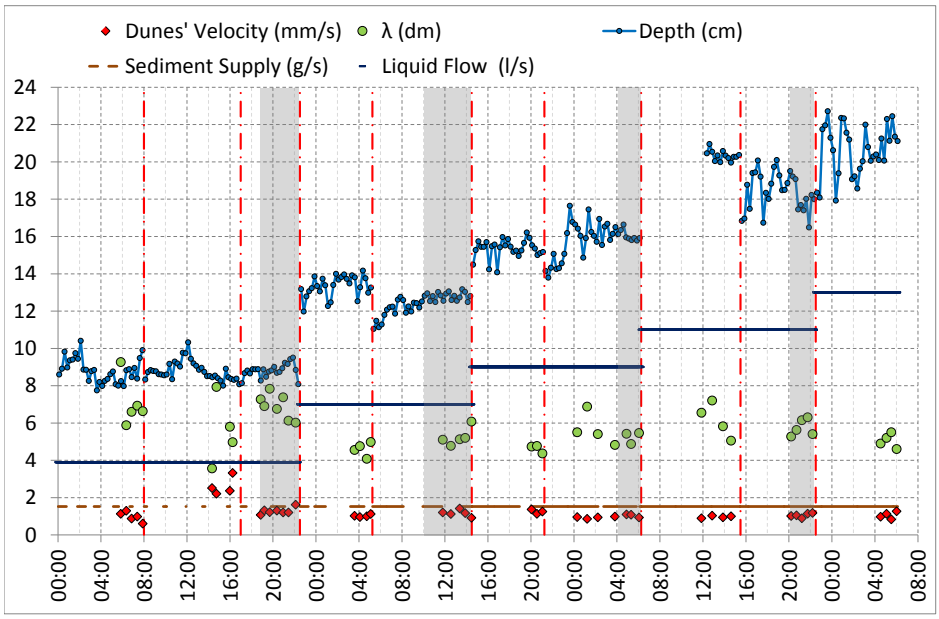

Figure A.74: M_S, Q_L, Dune Velocity, Dune Length, Flow Depth;

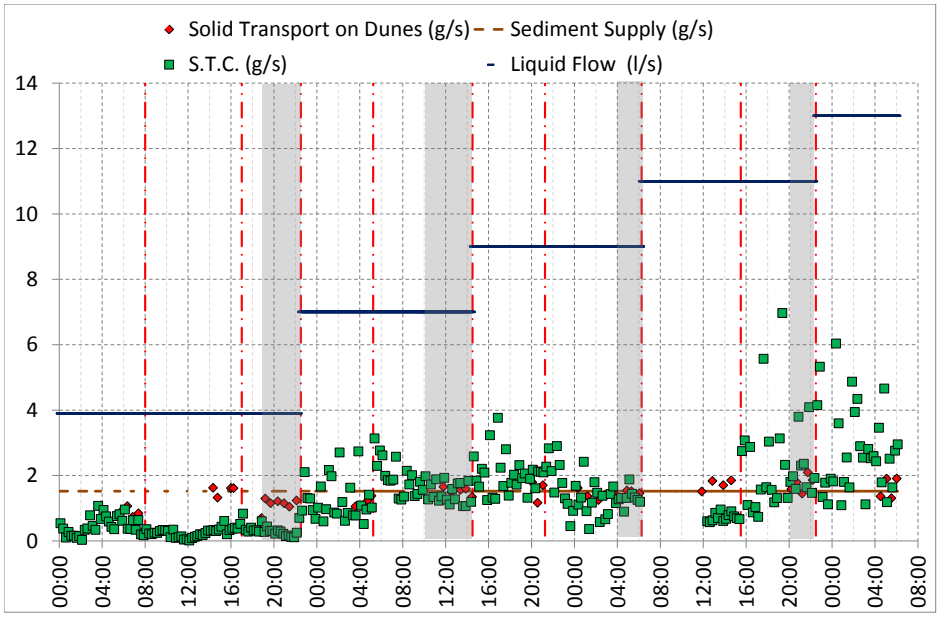

Figure A.75: M_S, Q_L, Solid Transport on Dunes, Solid Transport Capacity;

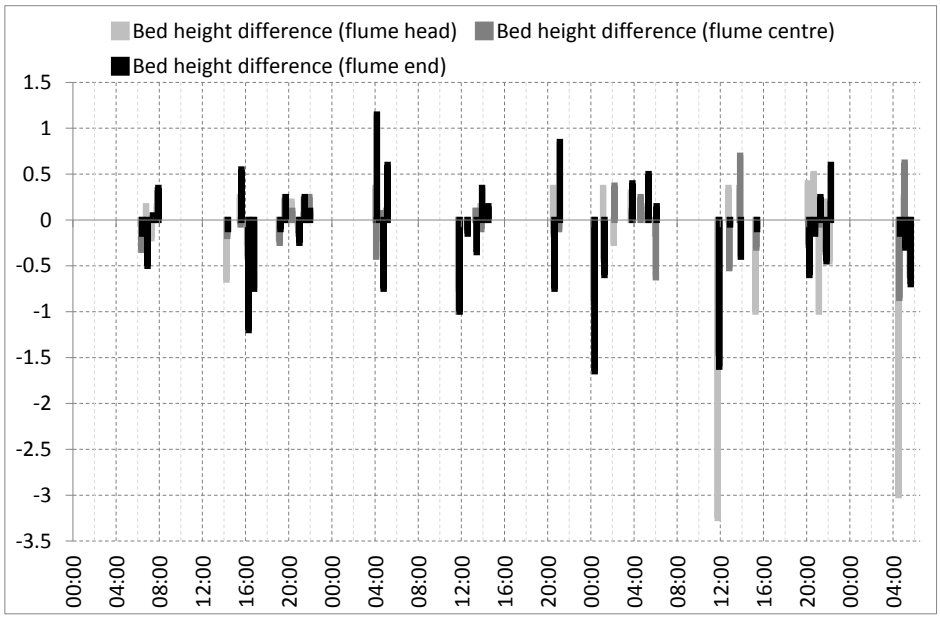

Figure A.76: Bed height difference in several parts of the flume;

Appendix B

The Measurements-Sediment B

The pattern of the representation of the experimental cycle conducted with sediment type B, see section C.2, is the same as that used for the cycles with sediment type A, as has been described in the Appendix A.

B.1 Run 1-5

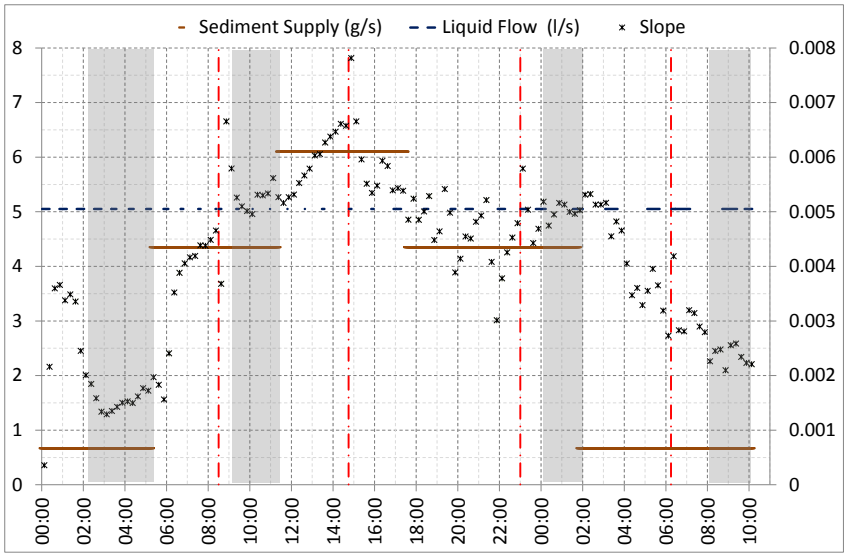

Figure B.1: $M_S(SX)$, $Q_L(SX)$, S(DX);

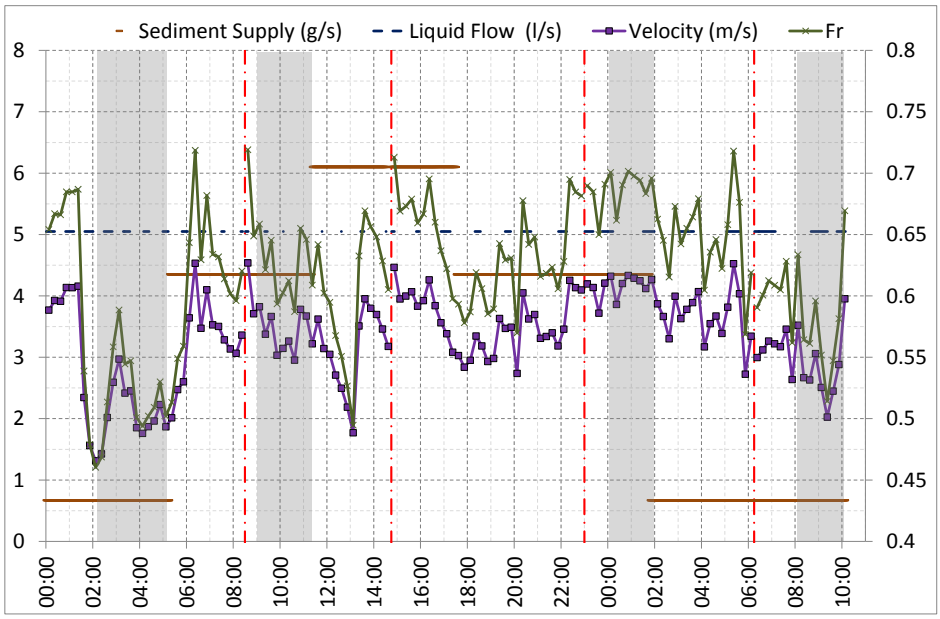

Figure B.2: $M_S(SX)$, $Q_L(SX)$, U(DX), Fr(DX);

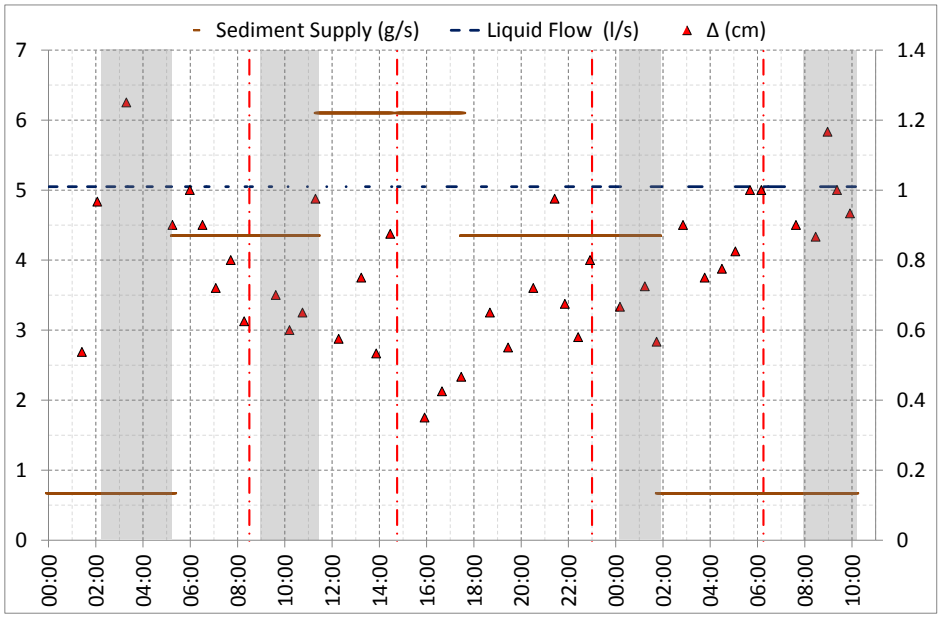

Figure B.3: $M_S(SX)$, $Q_L(SX)$, Dune Height(DX);

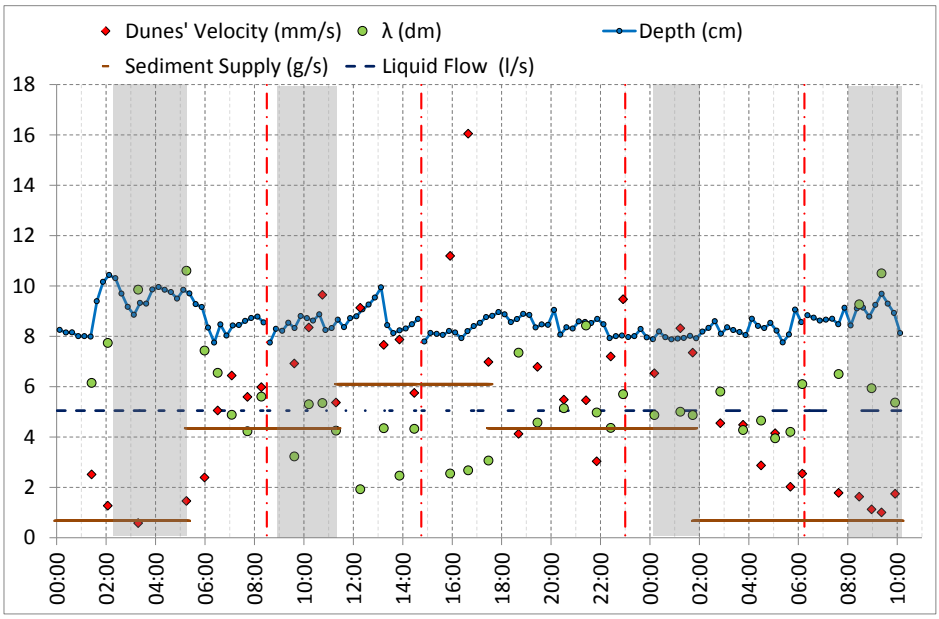

Figure B.4: M_S, Q_L, Dune Velocity, Dune Length, Flow Depth;

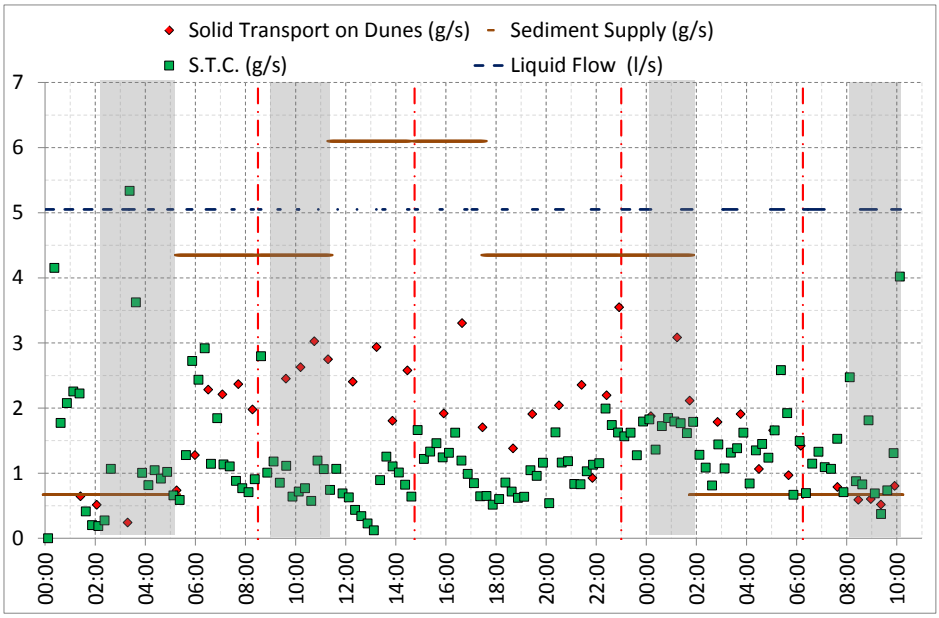

Figure B.5: M_S, Q_L, Solid Transport on Dunes, Solid Transport Capacity;

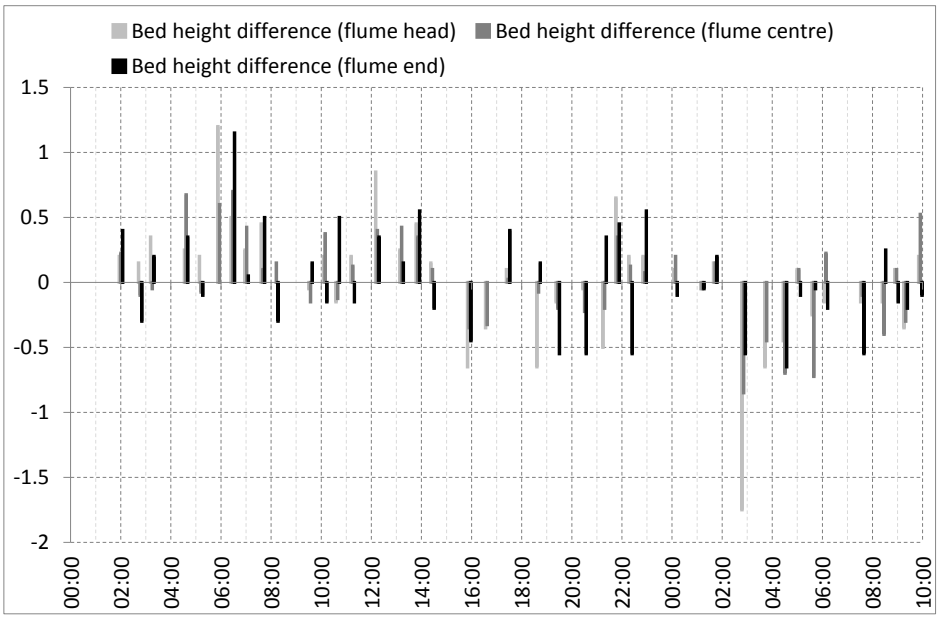

Figure B.6: Bed height difference in several parts of the flume;

B.2 Run 6-12

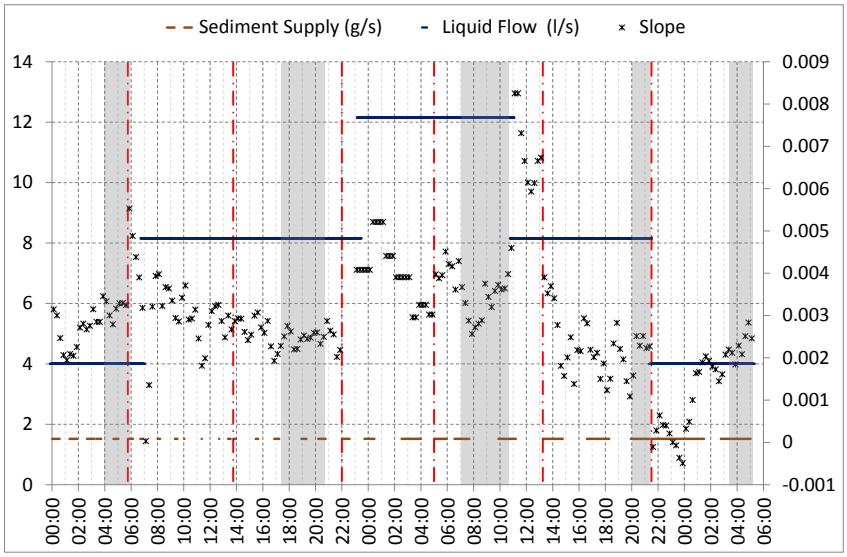

Figure B.7: $M_S(SX)$, $Q_L(SX)$, S(DX);

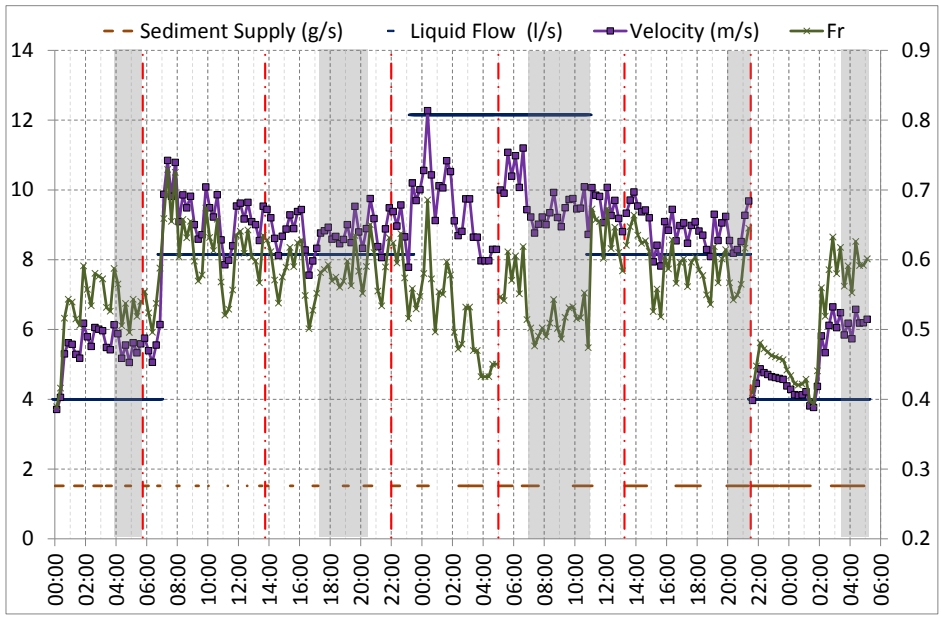

Figure B.8: $M_S(SX)$, $Q_L(SX)$, U(DX), Fr(DX);

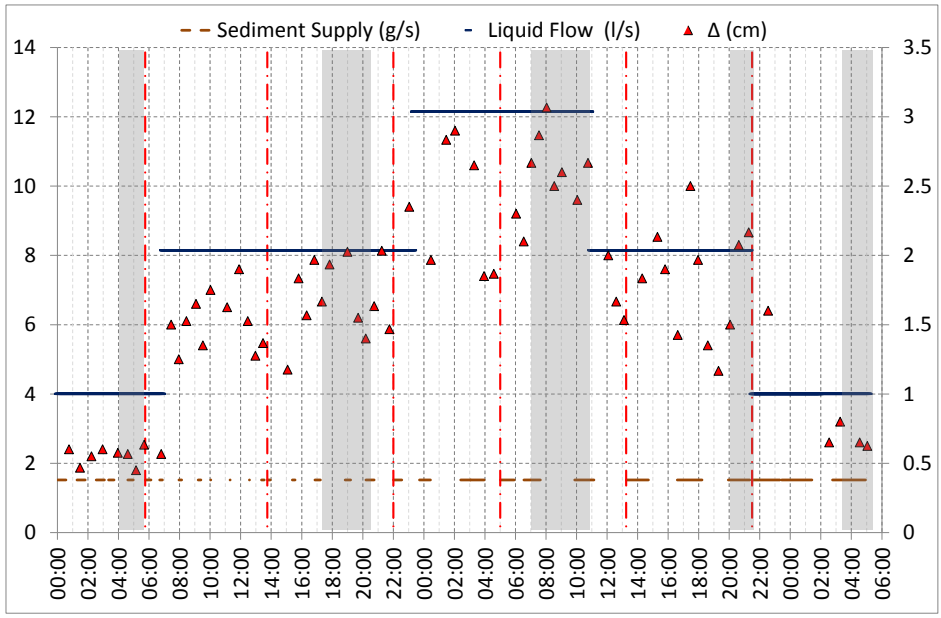

Figure B.9: $M_S(SX)$, $Q_L(SX)$, Dune Height(DX);

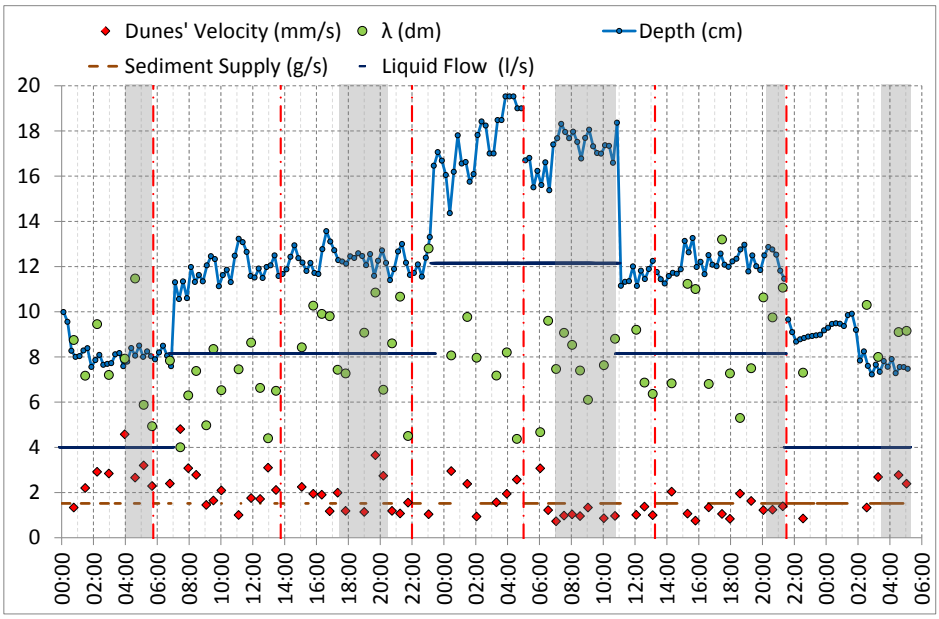

Figure B.10: M_S, Q_L, Dune Velocity, Dune Length, Flow Depth;

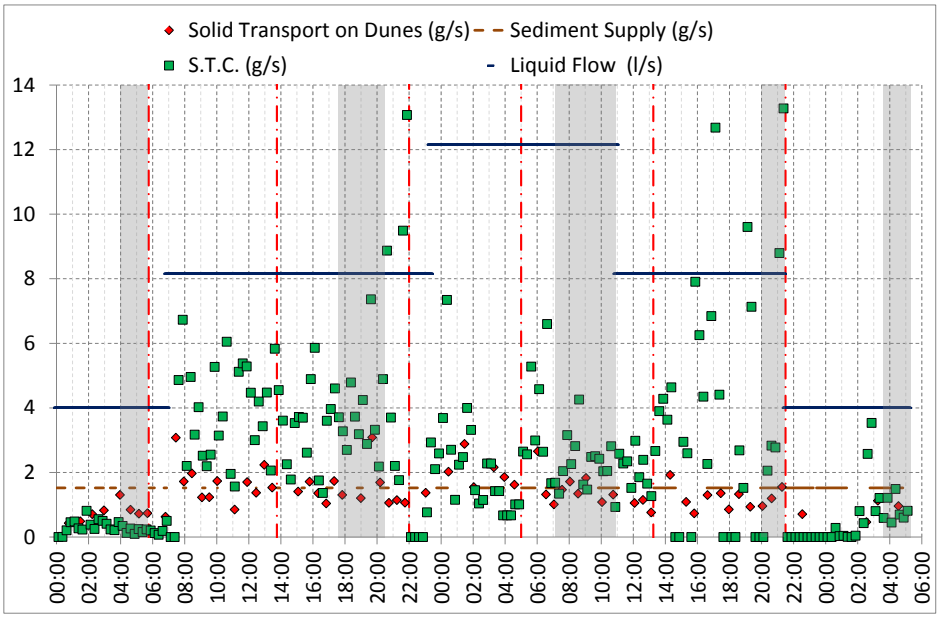

Figure B.11: M_S, Q_L, Solid Transport on Dunes, Solid Transport Capacity;

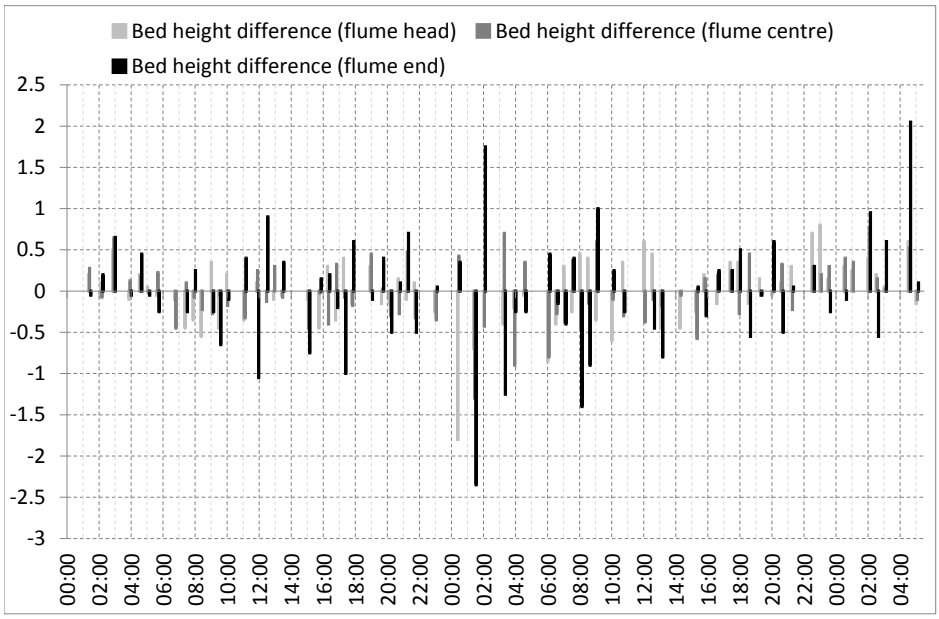

Figure B.12: Bed height difference in several parts of the flume;

B.3 Run 14-15

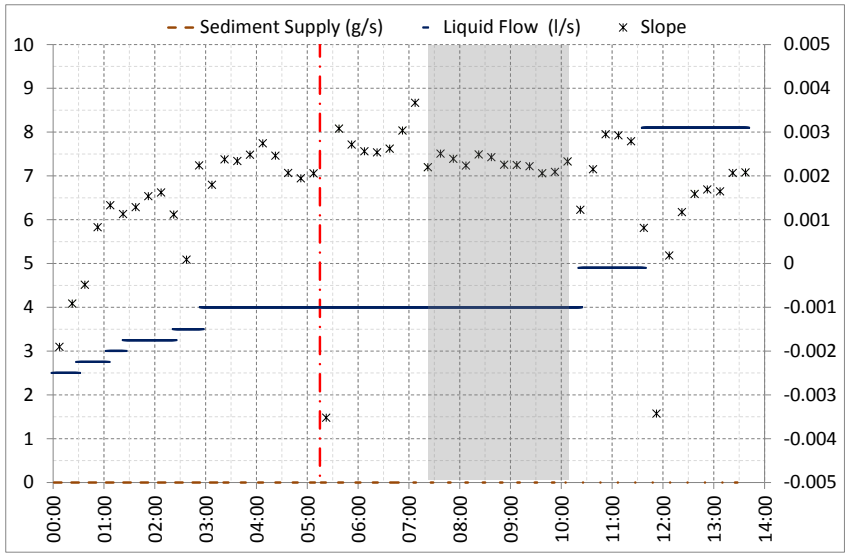

Figure B.13: $M_S(SX)$, $Q_L(SX)$, S(DX);

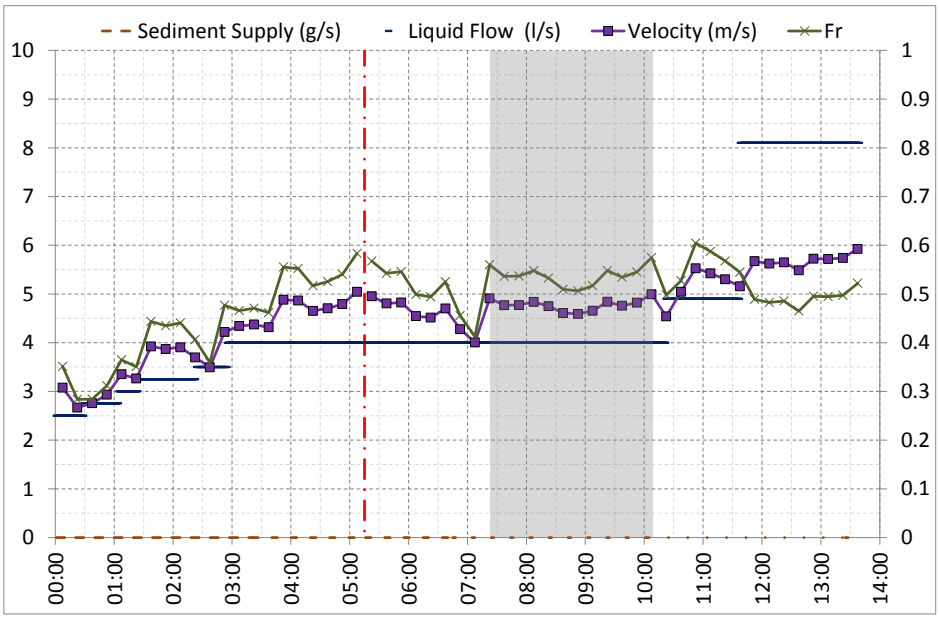

Figure B.14: $M_S(SX)$, $Q_L(SX)$, U(DX), Fr(DX);

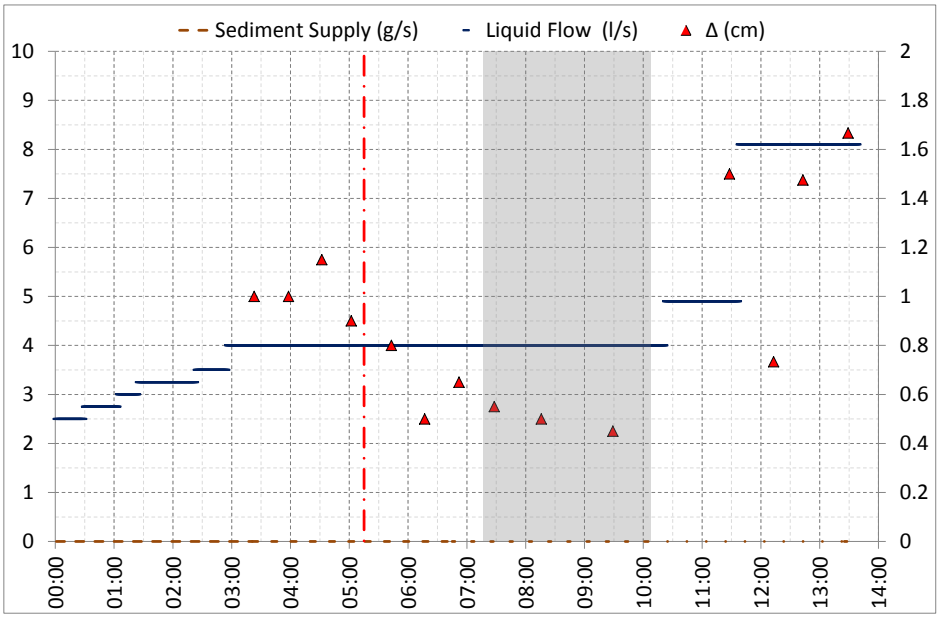

Figure B.15: $M_S(SX)$, $Q_L(SX)$, Dune Height(DX);

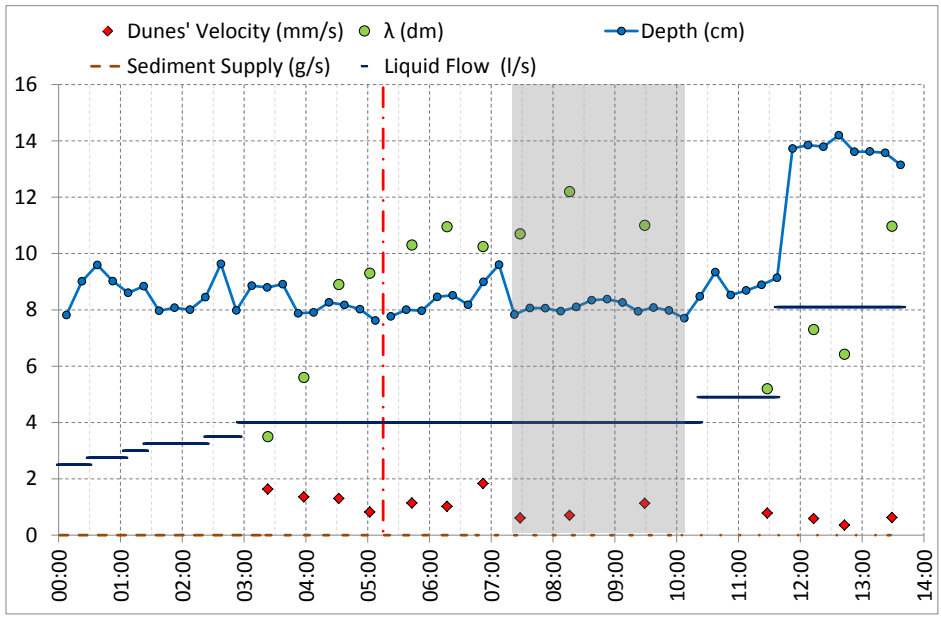

Figure B.16: M_S, Q_L, Dune Velocity, Dune Length, Flow Depth;

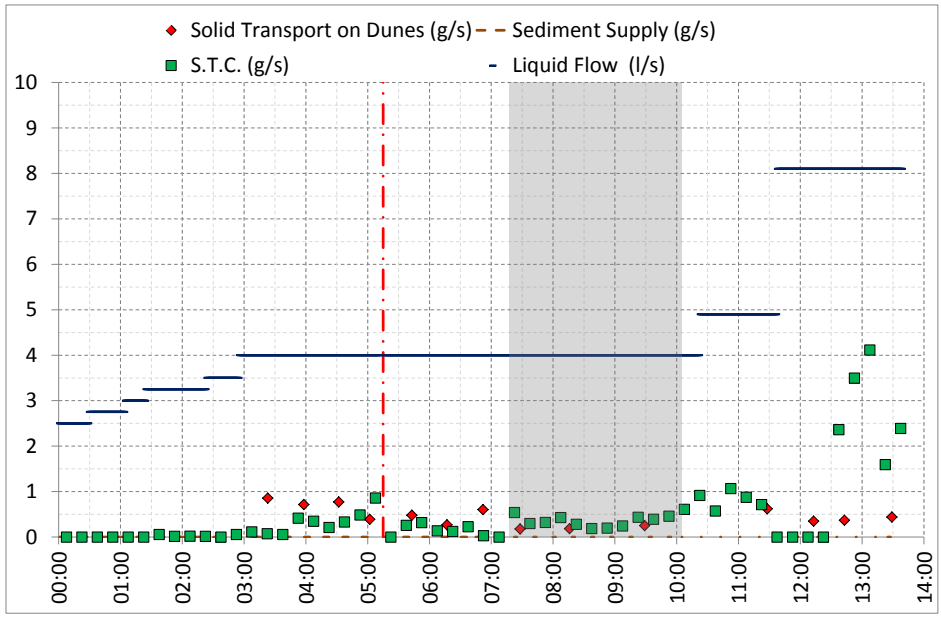

Figure B.17: M_S, Q_L, Solid Transport on Dunes, Solid Transport Capacity;

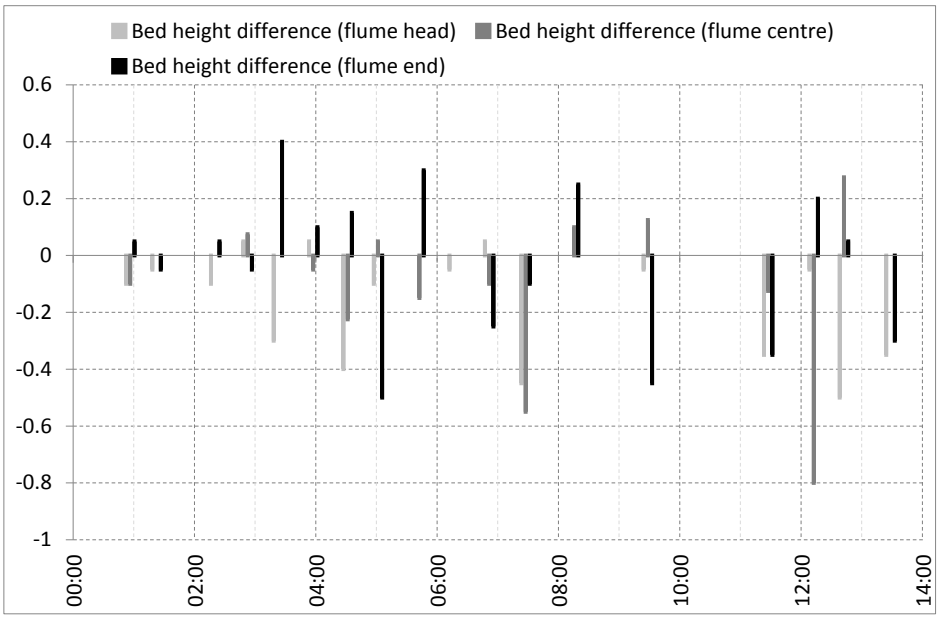

Figure B.18: Bed height difference in several parts of the flume;

B.4 Run 16

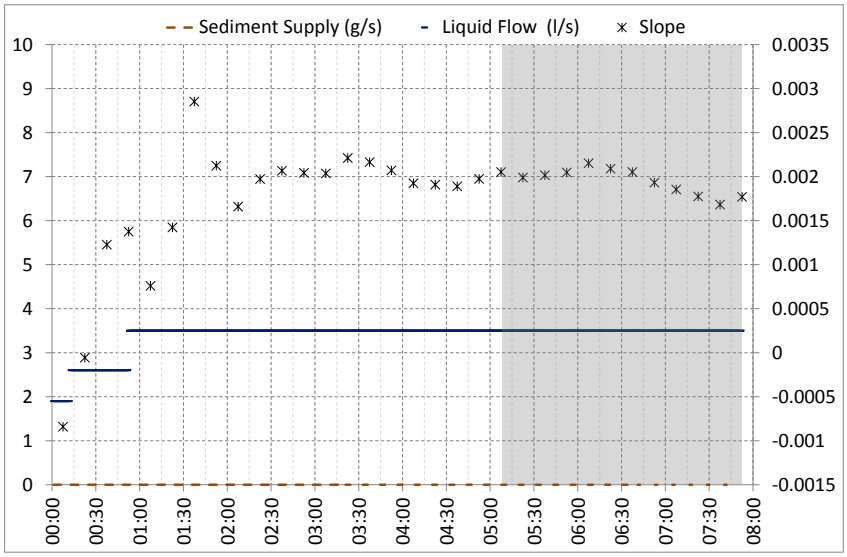

Figure B.19: $M_S(SX)$, $Q_L(SX)$, S(DX);

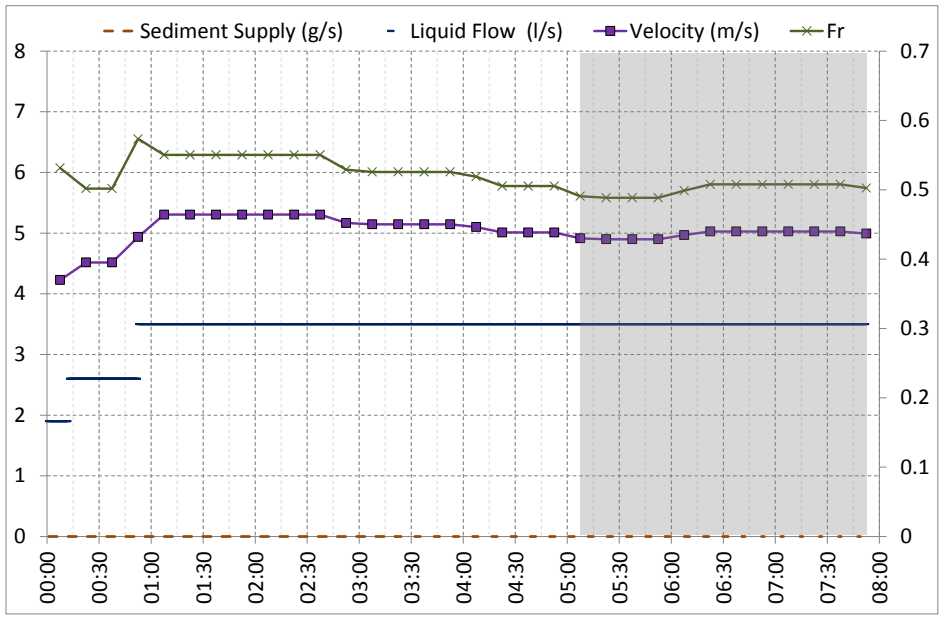

Figure B.20: $M_S(SX)$, $Q_L(SX)$, U(DX), Fr(DX);

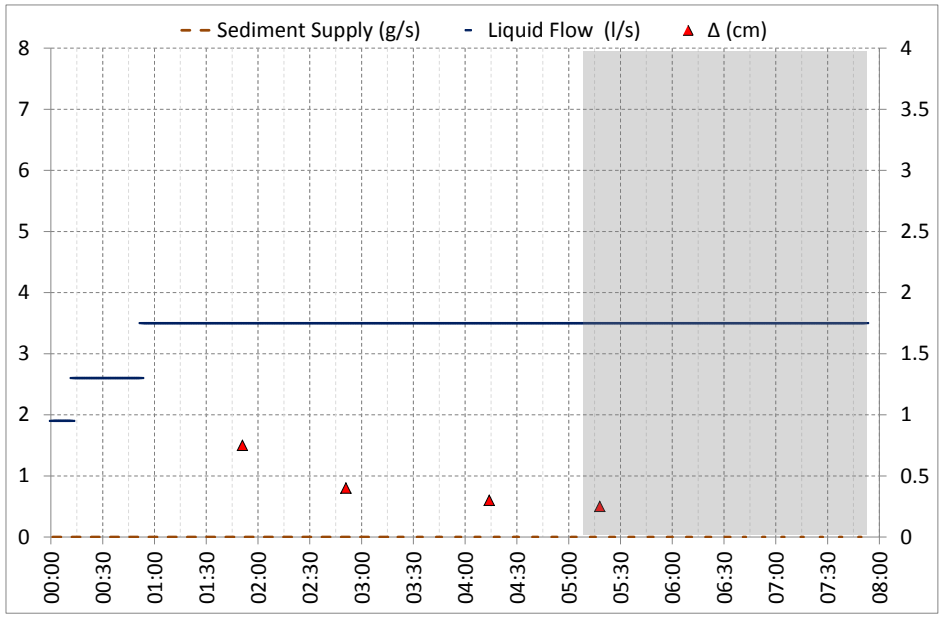

Figure B.21: $M_S(SX)$, $Q_L(SX)$, Dune Height(DX);

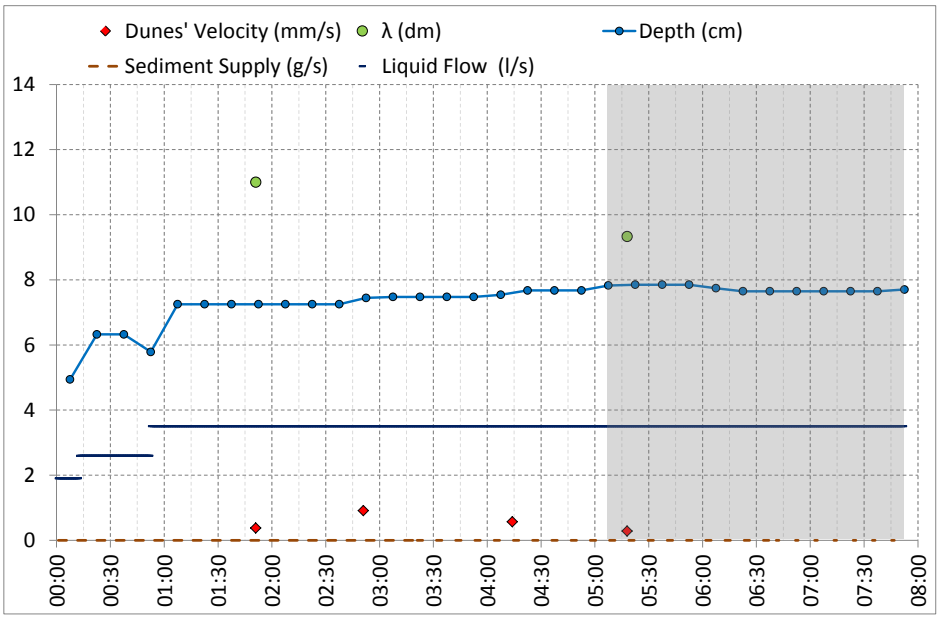

Figure B.22: M_S, Q_L, Dune Velocity, Dune Length, Flow Depth;

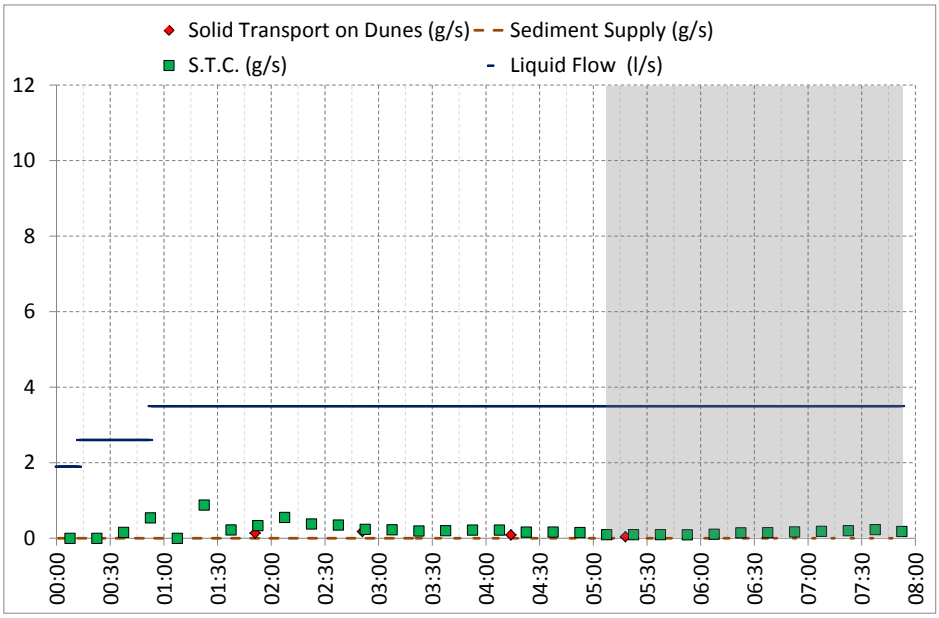

Figure B.23: M_S, Q_L, Solid Transport on Dunes, Solid Transport Capacity;

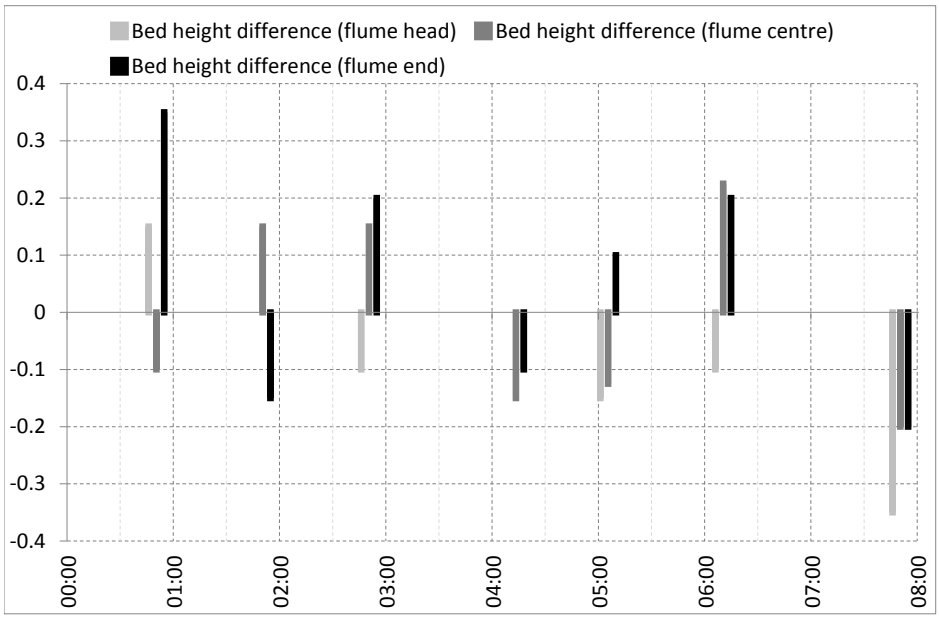

Figure B.24: Bed height difference in several parts of the flume;

B.5 Run 17-29

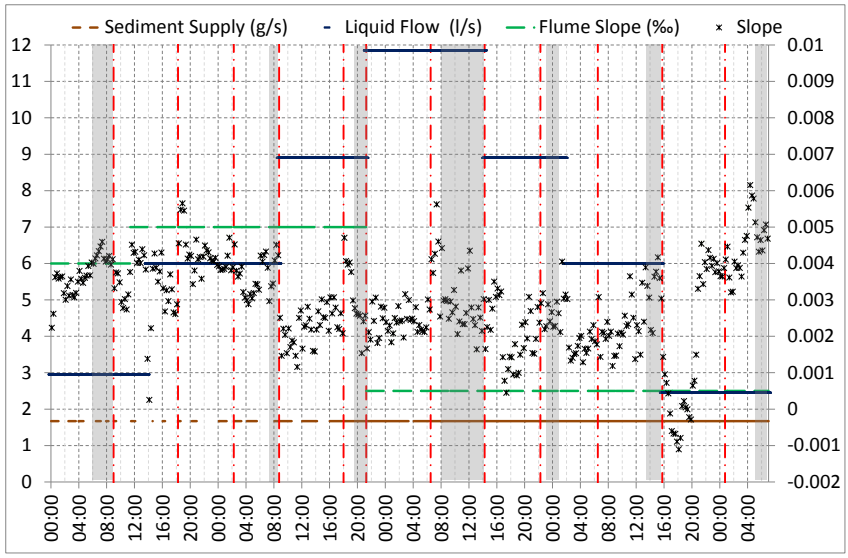

Figure B.25: $M_S(SX)$, $Q_L(SX)$, S(DX);

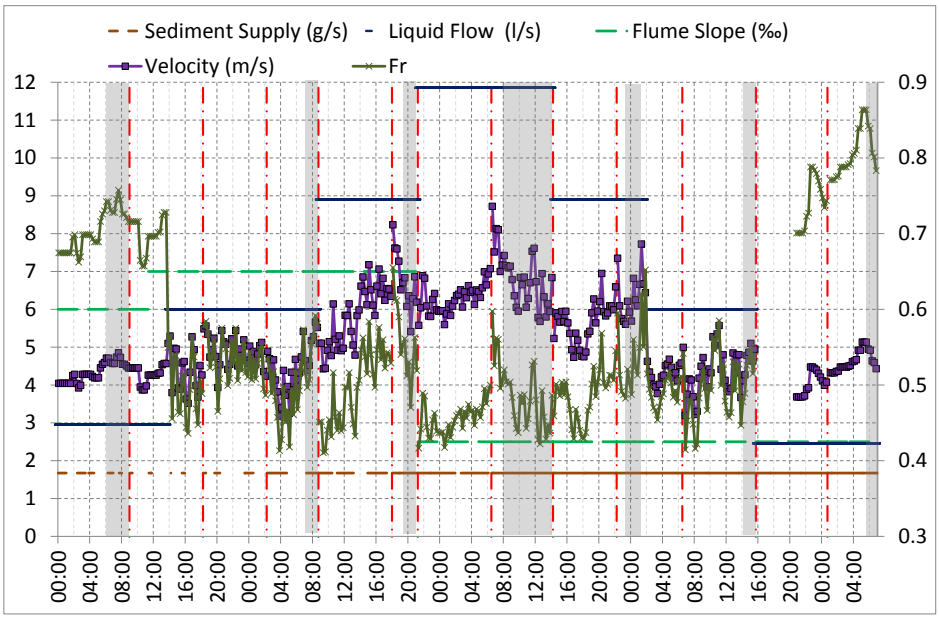

Figure B.26: $M_S(SX)$, $Q_L(SX)$, U(DX), Fr(DX);

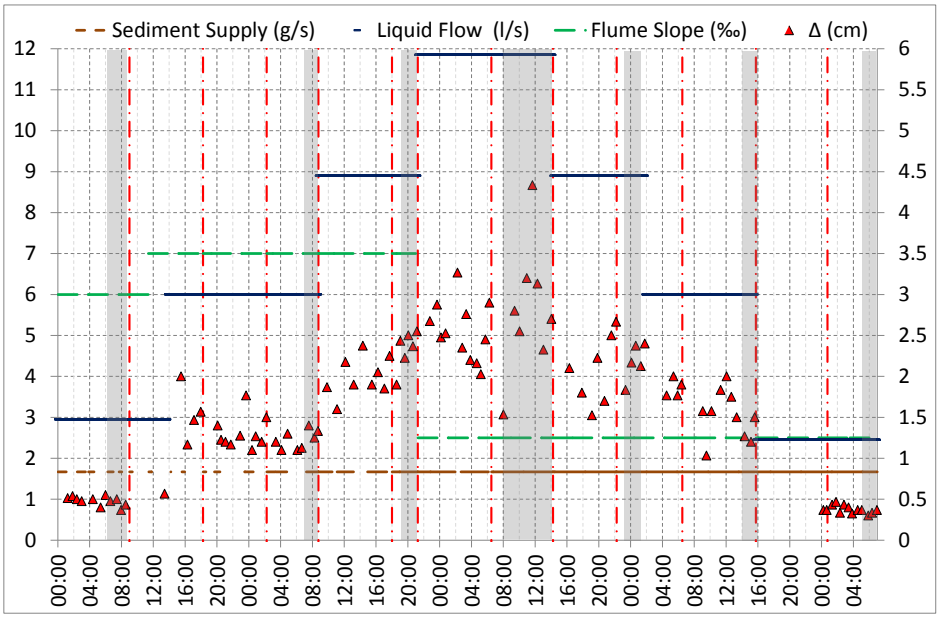

Figure B.27: $M_S(SX)$, $Q_L(SX)$, Dune Height(DX);

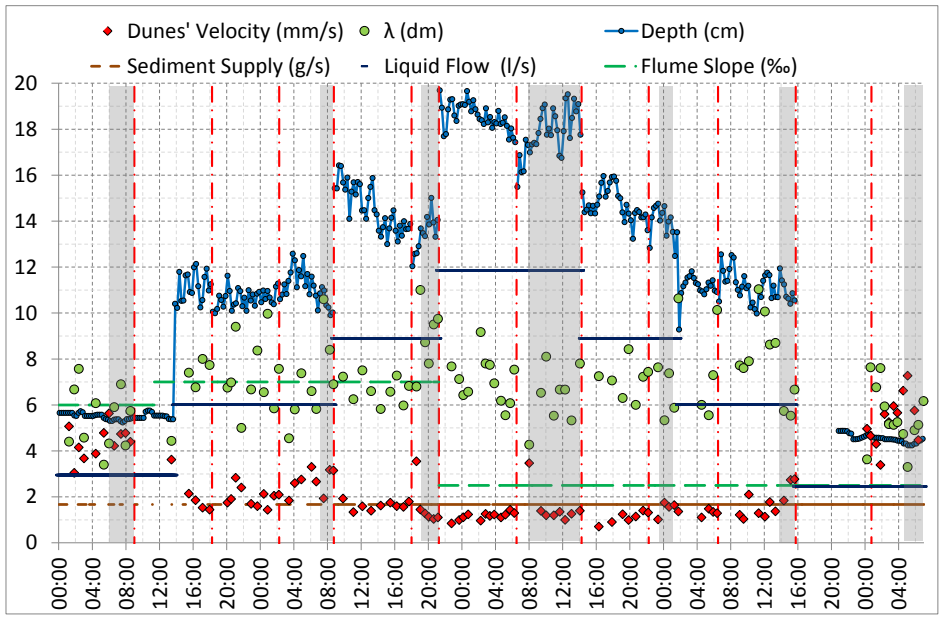

Figure B.28: M_S, Q_L, Dune Velocity, Dune Length, Flow Depth;

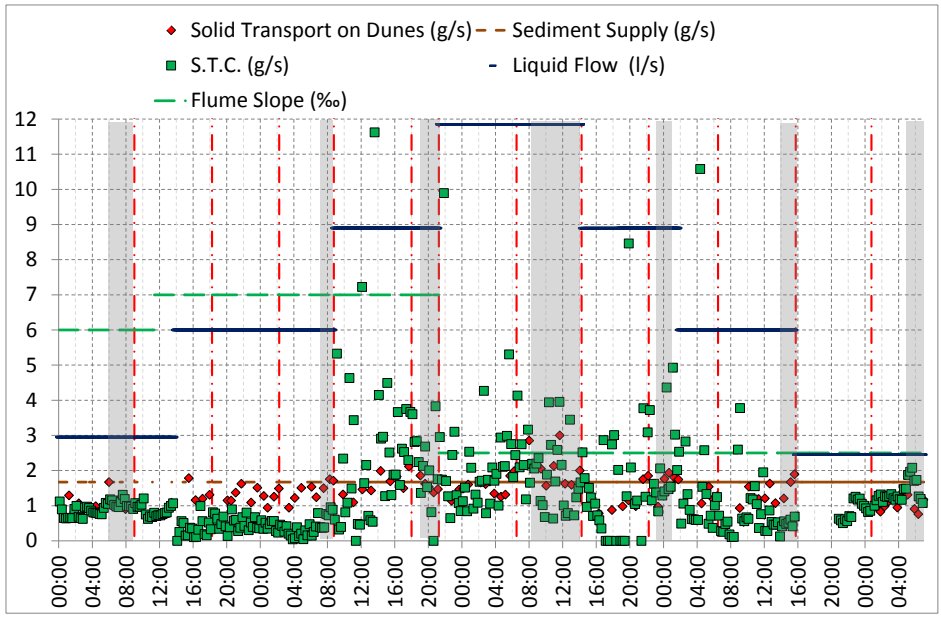

Figure B.29: M_S, Q_L, Solid Transport on Dunes, Solid Transport Capacity;

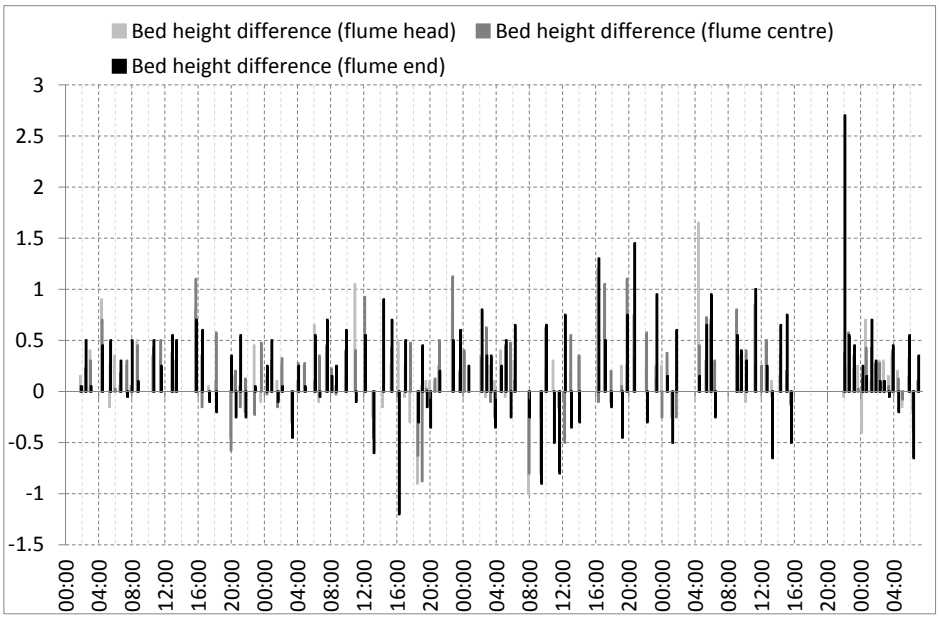

Figure B.30: Bed height difference in several parts of the flume;

B.6 Run 30-36

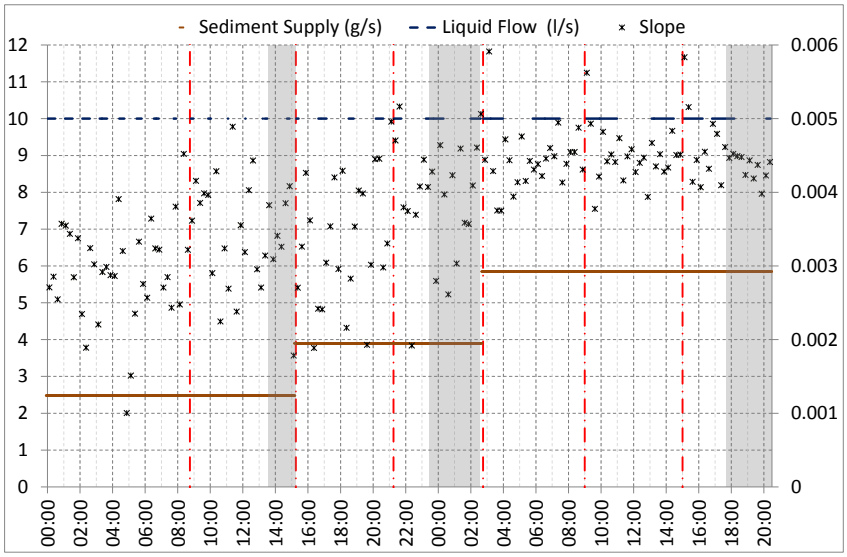

Figure B.31: $M_S(SX)$, $Q_L(SX)$, S(DX);

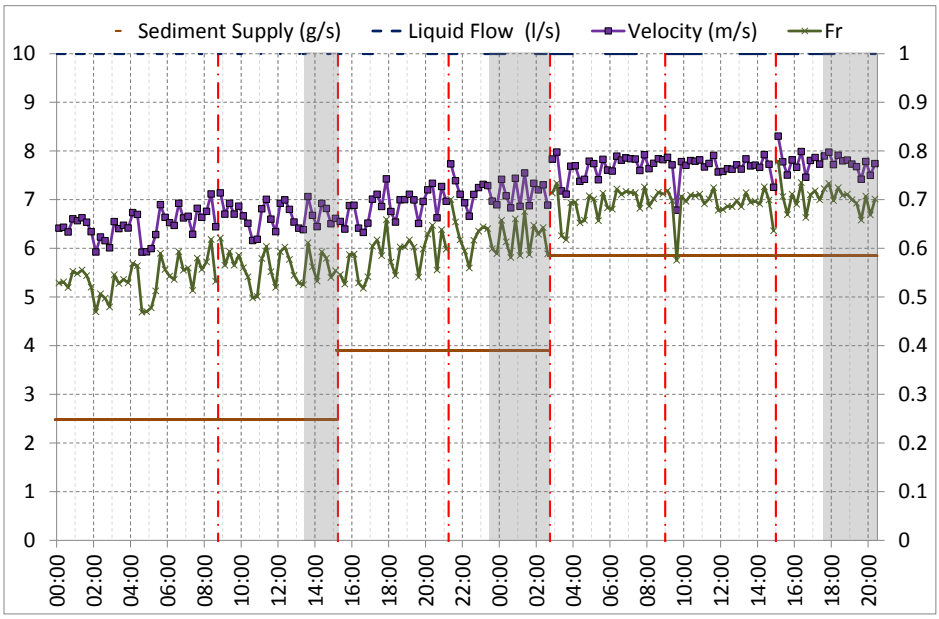

Figure B.32: $M_S(SX)$, $Q_L(SX)$, U(DX), Fr(DX);

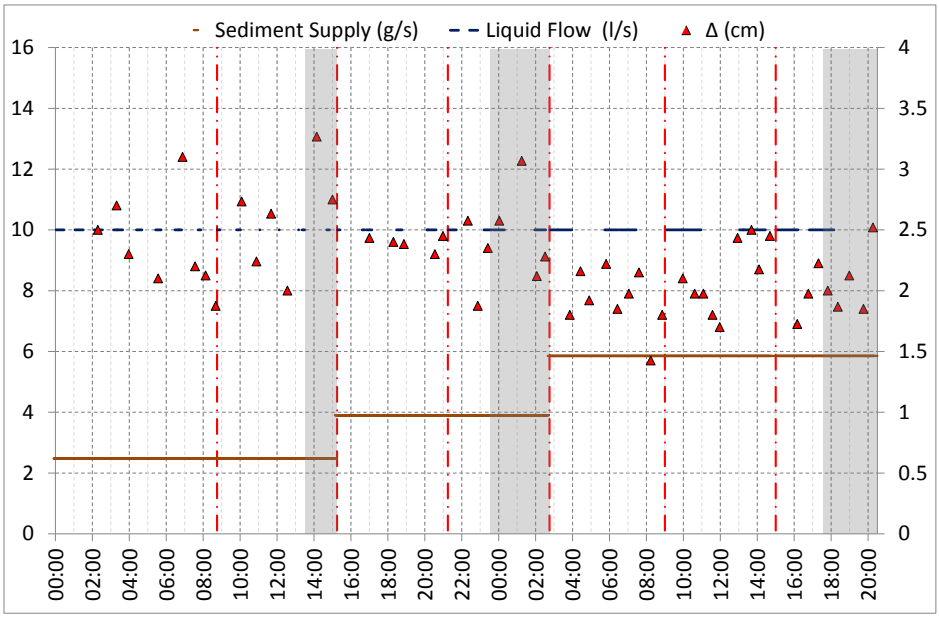

Figure B.33: $M_S(SX)$, $Q_L(SX)$, Dune Height(DX);

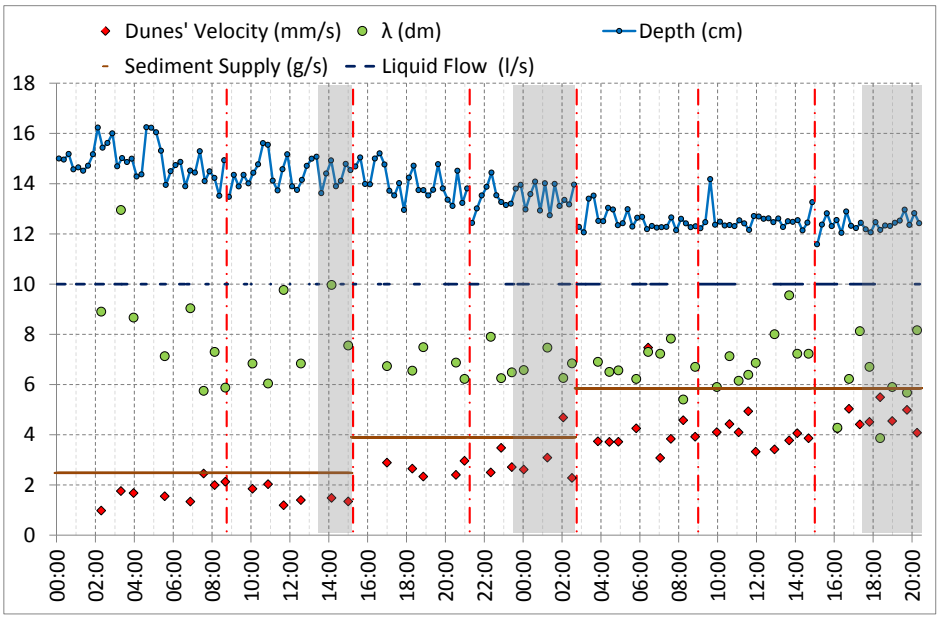

Figure B.34: M_S, Q_L, Dune Velocity, Dune Length, Flow Depth;

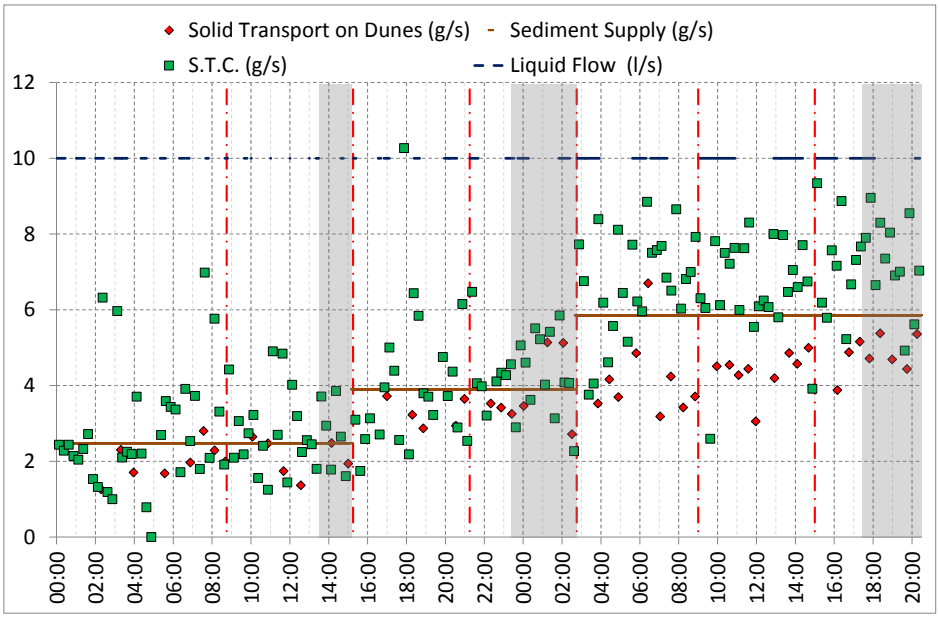

Figure B.35: M_S, Q_L, Solid Transport on Dunes, Solid Transport Capacity;

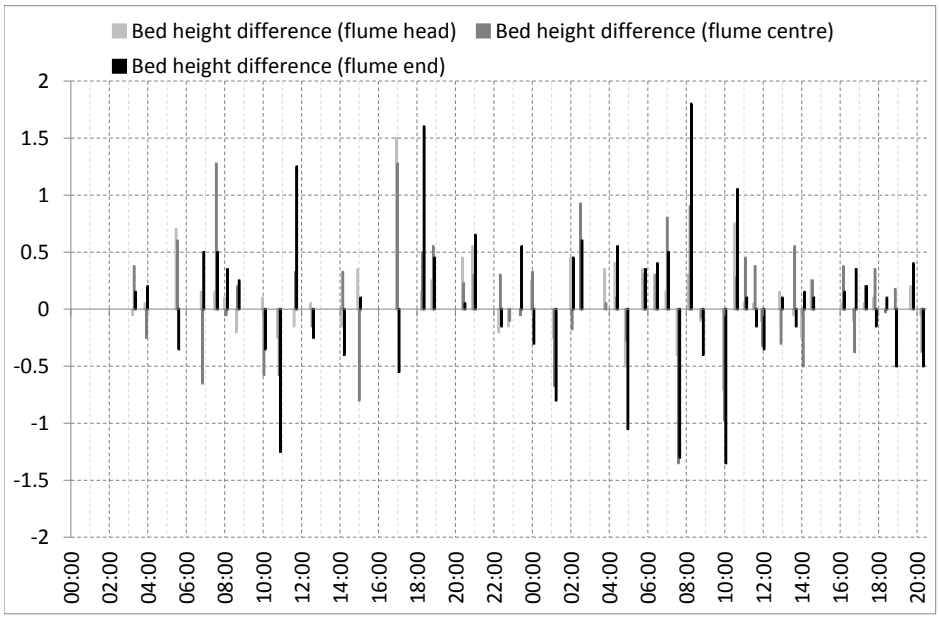

Figure B.36: Bed height difference in several parts of the flume;

B.7 Run 37-40

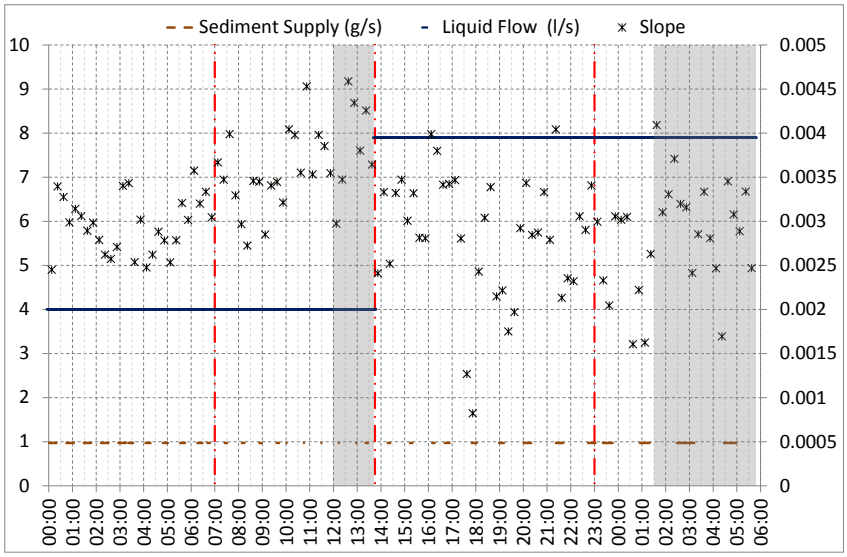

Figure B.37: $M_S(SX)$, $Q_L(SX)$, S(DX);

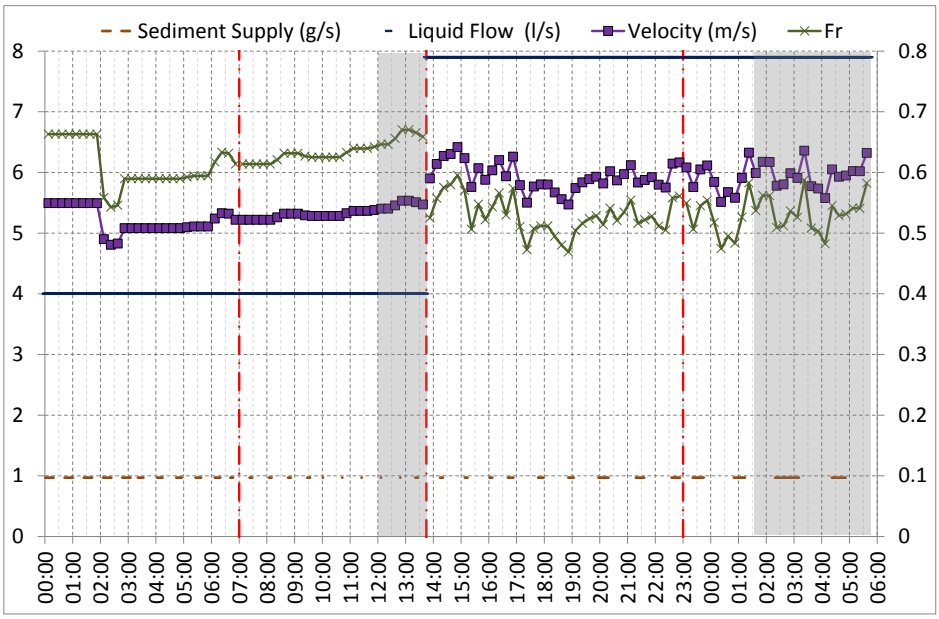

Figure B.38: $M_S(SX)$, $Q_L(SX)$, U(DX), Fr(DX);

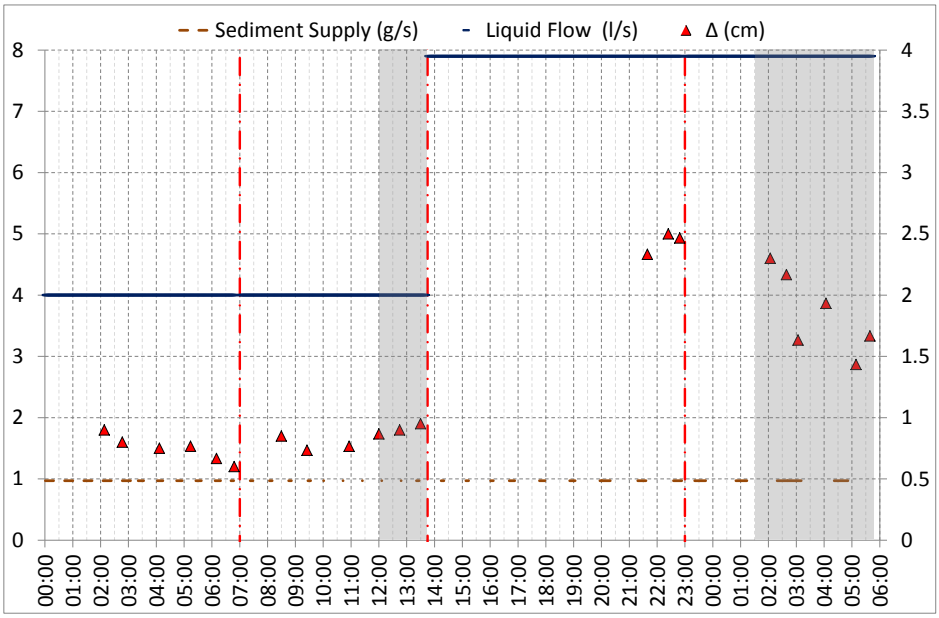

Figure B.39: $M_S(SX)$, $Q_L(SX)$, Dune Height(DX);

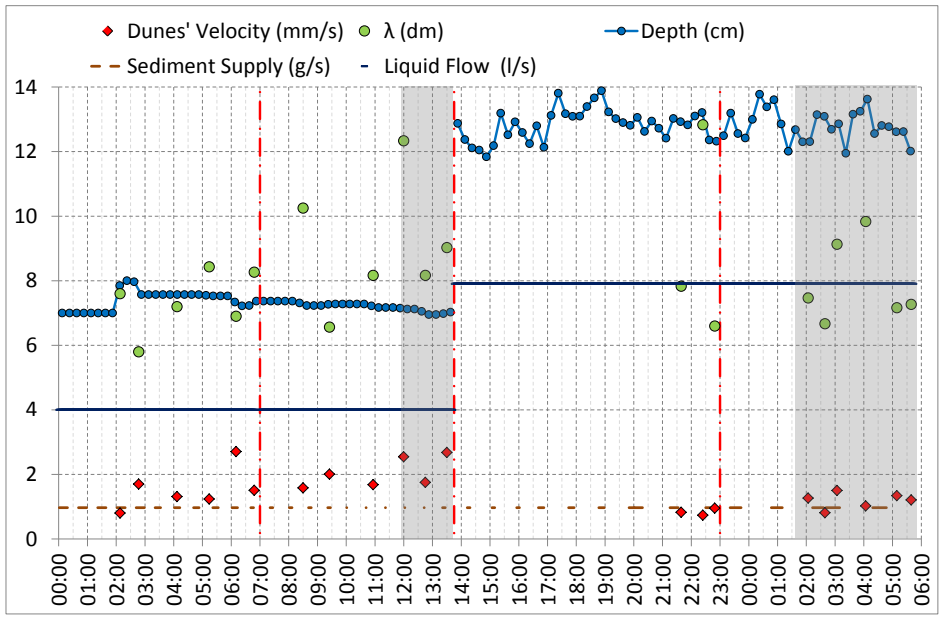

Figure B.40: M_S, Q_L, Dune Velocity, Dune Length, Flow Depth;

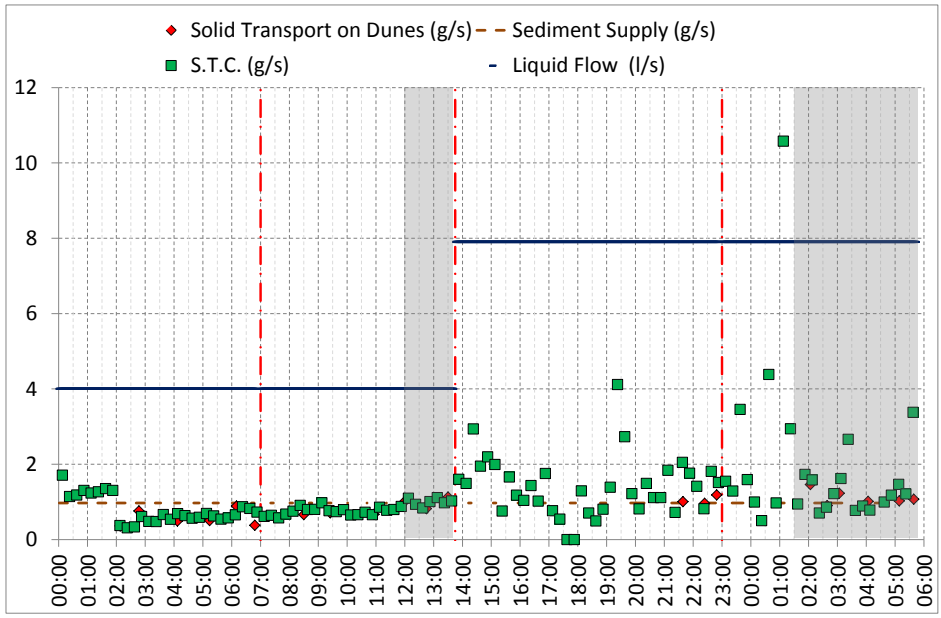

Figure B.41: M_S, Q_L, Solid Transport on Dunes, Solid Transport Capacity;

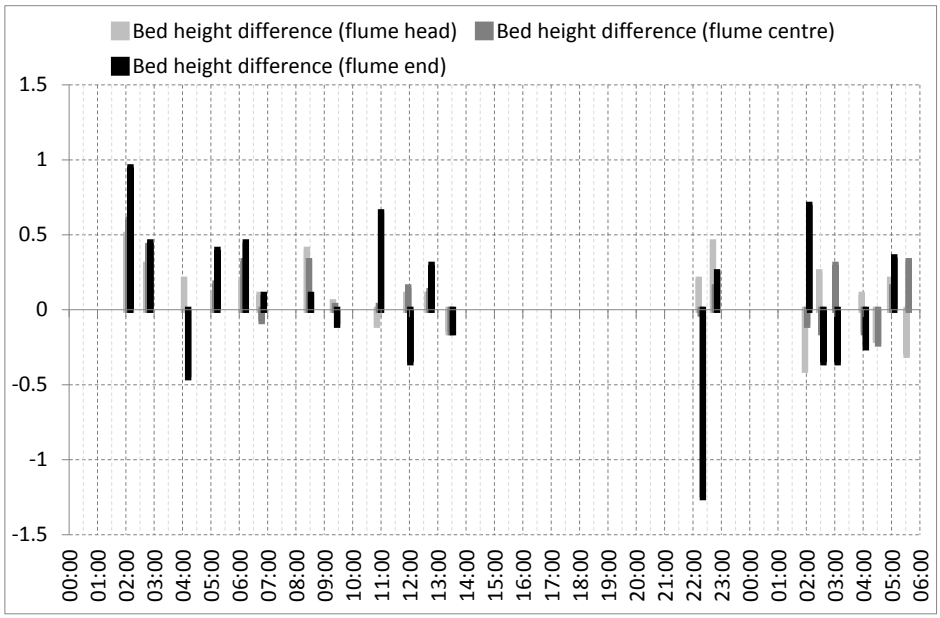

Figure B.42: Bed height difference in several parts of the flume;

Appendix C

Bulk Properties

C.1 Sediment Type A

	Φ	D_{50}
D_{10}	0.8586	0.5515
D_{16}	0.7469	0.5959
D_{25}	0.5793	0.6693
D_{35}	0.4553	0.7294
D_{40}	0.4163	0.7493
D_{50}	0.3384	0.7909
D_{75}	0.1437	0.9052
D_{84}	0.0736	0.9502
D_{90}	0.0269	0.9815
MEAN	0.38	0.7711

STANDARD DEVIATION	0.49
SKEWNESS	1.53
KURTOSIS	0.03
Gravel (%)	0.00
Sand (%)	100.00

Table C.1: Characteristic Diameter: Sediment Type A;

Figure C.1: Sediment Type A;

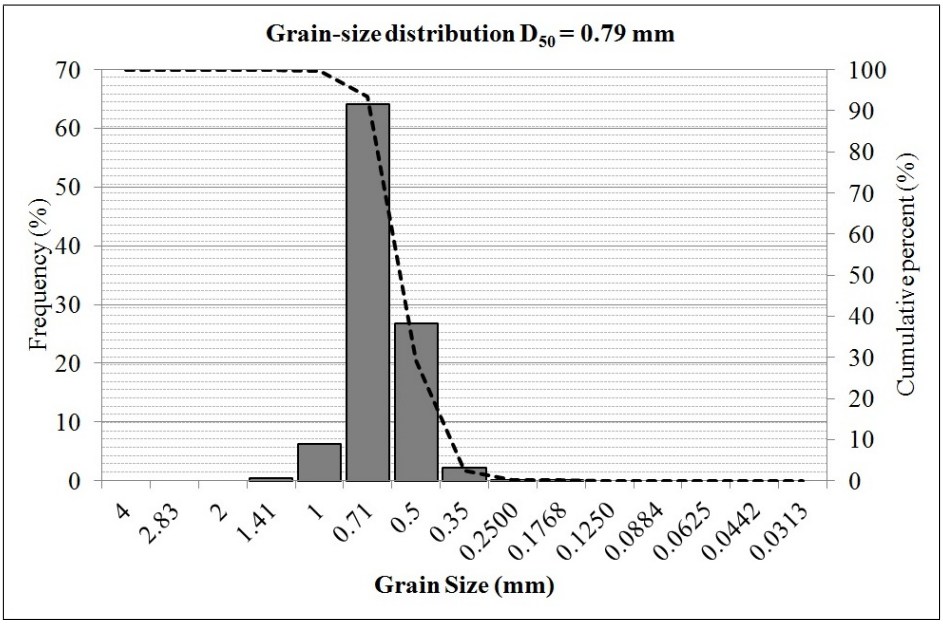

Figure C.2: Grain-size distribution-Sediment Type A;

C.2 Sediment Type B

	Φ	D_{50}
D_{10}	0.3171	0.8027
D_{16}	-0.0131	1.0091
D_{25}	-0.0947	1.0678
D_{35}	-0.1853	1.1371
D_{40}	-0.2306	1.1733
D_{50}	-0.3213	1.2494
D_{75}	-0.5895	1.5047
D_{84}	-0.7420	1.6725
D_{90}	-0.8437	1.7947
MEAN	-0.27	1.2018

STANDARD DEVIATION	0.60
SKEWNESS	0.74
KURTOSIS	3.05
Gravel (%)	0.78
Sand (%)	99.22

Table C.2: Characteristic Diameter: Sediment Type B;

Figure C.3: Sediment Type B;

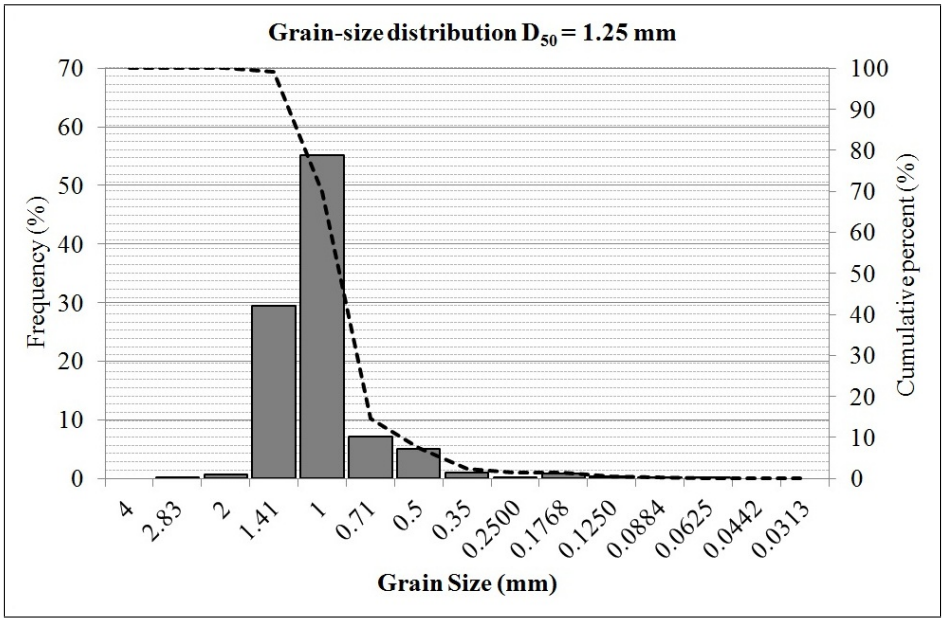

Figure C.4: Grain-size distribution-Sediment Type B;

Appendix D

Some Theoretical Bases

D.1 Side Wall Correction

4 To determine the shear-stress at the bed in the case of unequal bed and side-wall roughness, a correction method must be used, when the width-depth ratio of flow is less than about 5. A method which is frequently used, is that of Vanoni and Brooks (1957):

1. $R = \frac{bh}{b+2h}$ Hydraulic Radius (m)
2. $\bar{u} = \frac{Q}{bh}$ Mean Flow Velocity (m/s)
3. $u_* = \sqrt{gRS}$ Shear Velocity (m/s)
4. $Re = \frac{4\bar{u}R}{\nu}$ Reynolds' number (-)
5. $f = 8(\frac{u_*}{\bar{u}})^2$ Friction coefficient (Darcy Weisbach friction factor) (-)
6. $f_W = 0.0026\left(\log\left(\frac{Re}{f}\right)\right)^2 - 0.0428\left(\log\left(\frac{Re}{f}\right)\right) + 0.1884$ *friction coefficient related to smooth side-wall according to Vanoni-Broooks*$(10^5 \leq (Re/f) \leq 10^8)$(-)
7. $f_b = f + \frac{2h}{b}(f - f_W)$ Friction coefficient Related to the bed (-)
8. $Rb = \frac{f_b}{f}R$ Hydraulic radius related to the bed (m)
9. $u_*b = \sqrt{gR_bS}$ Shear Velocity at the bed (m/s)

D.2 Bed sediment transport estimation with the continuity equation for sediment

An estimate of sediment transport originated from the movement of the dunes can be made starting from the simplified scheme figure D.1, which is considered

to be a succession of dunes with a regular triangular shape moving with constant velocity c (velocity of propagation). Assuming only bed transport, and considering the height of z with respect to a horizontal reference, downstream propagation of the dune form is represented by a wave function that moves, without deformation, forward;

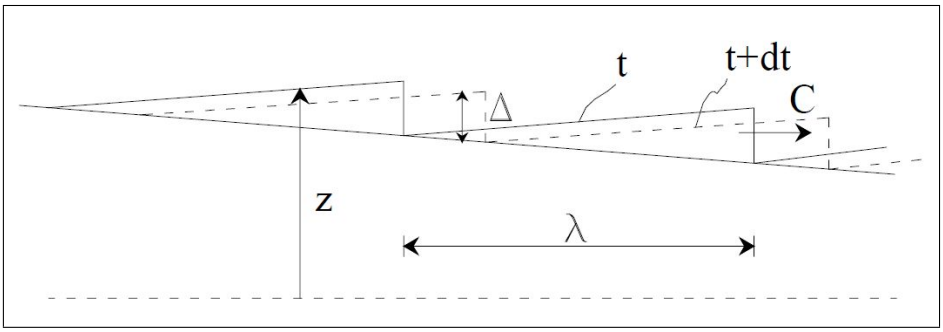

Figure D.1: Bed forms schema;

Assuming:

$$z = f(x,t) \tag{D.1}$$

the total differential of this function must be zero, so:

$$\frac{Dz}{Dt} = \frac{\partial z}{\partial t}dt + \frac{\partial z}{\partial t}dx = 0 \tag{D.2}$$

The speed of propagation is therefore:

$$c = \frac{dx}{dt} = -\frac{\partial z/\partial t}{\partial z/\partial x} \tag{D.3}$$

which yields:

$$\frac{\partial z}{\partial t} = -c \cdot \frac{\partial z}{\partial x} \tag{D.4}$$

From the sediment continuity equation, considering a rectangular and straight channel, with a null lateral supply and a null concentration of suspension material and considering a sufficient wide channel $B/Y > 10$ the equation is:

$$\frac{\partial Q_t}{B\partial x} + \frac{\partial z}{\partial t} \cdot (1-e) = 0 \tag{D.5}$$

where Q_t is the volume of the total sediment load, B is the width of the channel and e is the void ratio of the material at the bottom. Substituting in the equation D.5 the expression in the equation D.4 one obtains:

$$\frac{1}{B(1-e)} \cdot \frac{\partial Q_t}{\partial t} = c \cdot \frac{\partial z}{\partial x} \tag{D.6}$$

Integrating the equation D.6 along the generic length x along the dune, and assuming the width of the riverbed constant, we obtain:

$$\frac{1}{B(1-e)} \cdot \int_0^x \frac{\partial Q_t}{\partial X}\, dx = \int_0^x c \cdot \frac{\partial z}{\partial x}\, dx \Rightarrow Q_s(x) = c \cdot z(c) + Q_0 \tag{D.7}$$

The equation D.7 represents the sediment transport along the dune (varying x), and Q_0 is the value of transport for x=0; it shows that the sediment transport is minimal for x=0, and it varies according to the law increasing x, and reaches a maximum at x equal to λ. Experimentally we observe that, for x=0, next to the throw of the dune, the sediment transport can be considered null and Q_0=0, it is therefore:

$$\frac{1}{B(1-e)} \cdot Q_S(x) = c \cdot z \tag{D.8}$$

Expressing z as a function of the geometrical characteristics of the dune, considering the dunes in a triangular shape the equation D.8 becomes:

$$\frac{1}{B(1-e)} \cdot Q_S(x) = c \cdot \frac{\Delta}{\lambda} \cdot x \tag{D.9}$$

Integrating along the distance λ the sediment transport over dune is obtained:

$$\frac{1}{B \cdot (1-e)} \cdot \frac{1}{\lambda} \cdot \int_0^\lambda Q_S\, dx = \frac{1}{\lambda} \cdot \int_0^\lambda c \cdot \frac{\Delta}{\lambda} \cdot x\, dx = \frac{c \cdot \Delta}{2} \tag{D.10}$$

In this way the volumetric sediment transport over a dune is calculated:

$$Q_S(x) = B \cdot (1-e) \cdot \frac{c \cdot \Delta}{2} \tag{D.11}$$

Bibliography

J.R. Allen. *Current ripples-their relation to patterns of water and sediment motion.* North-Holland Publishing, 1968.

A.S.C.E. Task force: Flow and transport over dunes. *Journal of Hydraulic Engineering*, 128(8):726–728, 2002.

A.S.C.E. *ASCE Manuals and Reports on Engineering Practice No.110-Sedimentation engineering: processes, measurements, modeling, and practice.* American Society of Civil Engineers, 2008.

S.J. Bennet and J.G. Venditti. Spectral analysis of turbulent flow and suspended sediment transport over fixed dunes. *Journal of Geophysical Research*, 105(C9):22, 2000.

S.J. Bennett and J.L. Best. Mean flow and turbulence structure over fixed, two-dimensional dunes: implications for sediment transport and bedform stability. *Sedimentology*, 42:491–513, 1995.

J. Best. The fluid dynamics of river dunes: A review and some future research directions. *Journal of Geophysical Research*, 110:21, 2005.

J. Best and R. Kostaschuk. An experimental study of turbulent flow over a low-angle dune. *Journal of Geophysical Research*, 107:19, 2002.

J.L. Best. *The fluid dynamics of small-scale alluvial bedforms In: Advances in Fluvial Dynamics and Stratigraphy.* Wiley and Sons, 1995.

J.L. Best, R.A. Kostaschuk, and P.V. Villard. Quantitative visualization of flow fields associated with alluvial sand dunes: Results from the laboratory and field using ultrasonic and acoustic doppler anemometry. *Journal of Visualization*, 4(4):373–381, 2001.

J.L. Best, P.J. Ashworth, M.H. Sarker, and J.E. Roden. *Large Rivers: Geomorphlogy and management.* John Wiley, 2007.

A. Blom, J.S. Ribberink, and H.J. de Vriend. Vertical sorting in bed forms: Flume experiments with a natural and a trimodal sediment mixture. *Water Resources Research*, 39(2):13, 2003.

J.S. Bridge. *Rivers and floodplains: forms, processes, and sedimentary record.* pp.491, 2003.

W.R. Brownlie. Compilation of alluvial channel data: Laboratory and field. Technical Report KHR-43B, W. M. Keck Laboratory of Hydraulics and Water Resources, 1981.

P.A. Carling, E. Gölz, H.G. Orr, and A. Radecki-Pawlik. The morphodynamics of fluvial sand dunes in the river Rhine, near Mainz, Germany. I. Sedimentology and morphology. *Sedimentology*, 47(1):227–252, 2000a.

P.A. Carling, J.J. Williams, E. Gölz, and A.D. Kelsey. The morphodynamics of fluvial sand dunes in the river Rhine, near Mainz, Germany. II. Hydrodynamics and sediment transport. *Sedimentology*, 47(1):253–278, 2000b.

M. de Vries. Solving river problems by hydraulic and mathematical models. Technical report, Delft Hydraulics Laboratory, 1969.

W.E. Dietrich, J.W. Kirchner, H. Ikeda, and F. Iseya. Sediment supply and the development of the coarse surface layer in gravel-bedded rivers. *Nature*, 340: 215–217, 1989.

J. Dreano, A. Valance, D. Lague, and C. Cassar. Experimental study on transient and steady-state dynamics of bedforms in supply limited configuration. *Earth Surface Processes and Landforms*, 35:1730–1743, 2010.

J. Driegen. Flume experiments on dunes under steady flow conditions (uniform sand, dm = 0.77 mm). Technical report, Delft Hydraulics, 1986.

P. Engel. Length of flow separation over dunes. *Journal of Hydraulic Division*, 107 (10):1133–1143, 1981.

P. Engel and Y.L. Lau. Computation of bed load using bathymetric data. *Journal of the Hydraulics Division*, 106(3):369–380, 1980.

F. Engelund. Hydraulic resistance of flow over dunes. progress rep. no. 44. Technical report, Institute Hydraulics and Hydraulic Engineering, Tech. Univ., Denmark, 1977.

F. Engelund and J. Fredsøe. *Transition from dunes to plane bed in alluvial channels.* Institute of Hydrodynamics and Hydraulic Engineering, Technical University of Denmark, 1974.

F. Engelund and J. Fredsøe. Sediment ripples and dunes. *Annual Review of Fluid Mechanics*, 14:13–37, 1982.

F. Engelund and E. Hansen. *Monograph on sediment transport in alluvial streams.* Teknisk forlag (Copenhagen), 1967.

J. J. Fedele and M. H. Garcia. Roughness function for alluvial rivers with dunes. In *River, Coastal and Estuarine Morphodynamics*, 2006.

L. R. Fernandez and R. van Beek. Erosion and transport of bedload sediment. *Journal of Hydraulic Research*, 14(2):127–144, 1976.

R. Fernandez, J. Best, and F. Lopez. Mean flow, turbulence structure, and bed form superimposition across the ripple-dune transition. *Water Resources Research*, 42:17, 2006.

S.L. Gabel. Geometry and kinematics of dunes during steady and unsteady flows in the Calamus river, Nebraska, USA. *Sedimentology*, 40(2):237–269, 1993.

R.J. Garde and K.G. Ranga Raju. *Mechanics of sediment transportation and alluvial stream problems*. Wiley Eastern Limited, Roorkee, India, 1985.

M.A. Gill. Height of sand dunes in open channel flows. *Journal of the Hydraulics Division*, 97(12):2067–2074, 1971.

H.P. Guy, D.B. Simons, and E.V. Richardson. Summary of alluvial channel data from flume experiments. Technical Report 462-I, Geological Survey Professional Paper, 1966.

A. Gyr and W. Kinzelbach. Bed forms in turbulent channel flow. *Applied Mechanics Reviews*, 57(1):77–93, 2004.

M. Hino. Equilibrium range spectre of sand waves formed by running water. *Journal of Fluid Mechanics*, 34:565–573, 1969.

R.R Holmes and M. H. Garcia. Flow over bedforms in a large sand-bed river: A field investigation. *Journal of Hydraulic Research*, 46(3):322?333, 2008.

S. Ikeda and G. Parker. *River meandering*. Washington, D.C. : American Geophysical Union, 1989.

D.J. Jerolmack and D. Mohrig. Frozen dynamics of migrating bedforms. *Geology*, 33:57–60, 2005.

P. Y. Julien and J. Wargadalam. Alluvial channel geometry: Theory and applications. *Journal of Hydraulic Engineering*, 121(4):312–325, 1995.

P.Y. Julien and G.J. Klaassen. Sand-dune geometry of large rivers during floods. *Journal of Hydraulic Engineering*, 121:657?663, 1995.

P.Y. Julien, G.J. G. J. Klaassen, W. B. M. Ten Brinke, and A. W. E. Wilbers. Case study: Bed resistance of Rhine river during 1998 flood. *Journal of Hydraulic Engineering*, 128:9, 2002.

A. Kadota and I. Nezu. Three-dimensional structure of space-time correlation on coherent vortices generated behind dune crest. *Journal of Hydraulic Research*, 37(1):59–80, 1999.

M. E. Karahan and A. W. Peterson. Visualization of separation over sand waves. *Journal of the Hydraulics Division*, 106 (8):1345–1352, 1980.

J. F. Kennedy. The mechanics of dunes and antidunes in erodible-bed channels. *Journal of Fluid Mechanics*, 16:521–544, 1963.

J. F. Kennedy. The formation of sediment ripples, dunes, and antidunes. *Annual Review of Fluid Mechanics*, 1:147–168, 1969.

J. F. Kennedy and A. J. Odgaard. Informal monograph on riverine sand dunes. Technical report, Contract Report CERC-91-2, US Army Engineer Waterways Experiment Station, Vicksburg, Mississippi, and Iowa Institute of Hydraulic Research, the University of Iowa, 1991.

G. J. Klaassen, K. Vermeer, and N. Uddin. Sedimentological processes in the jamuna lower brahmaputra! river, bangladesh. In *International Conference on Fluvial Hydraulics, Budapest, Hungary.*, 1988.

G.J. Klaassen. Sediment transport and hydraulic roughness in relation to bed forms. Technical Report No, 213, Delft Hydraulic Laboratory, 1979.

R.A. Kleijwegt. *On sediment transport in circular sewers with non-cohesive deposits.* PhD thesis, Delft University of Technology, 1992.

M.G. Kleinhans and L.C. Van Rijn. Stochastic prediction of sediment transport in sand-gravel bed rivers. *Journal of Hydraulic Engineering*, 128(4):14, 2002.

K. Koll and A. Dittrich. Inflence of sediment transport on armoured surfaces. *International Journal of Sediment Research*, 16:201–206, 2001.

D.M. Kondap and R.J. Garde. Velocity of bed forms in alluvial channels. In *IAHR, 15th Congress, Istambul, Proceedings*, 1973.

R. Kostaschuk and P. Villard. Flow and sediment transport over large subaqueous dunes: Fraser river, canada. *Sedimentology*, 43(5):849–863, 1996.

R. A. Kostaschuk, M. A. Church, and J. L. Luternauer. Bedforms, bed material, and bedload transport in a salt-wedge estuary: Fraser river, british columbia. *Canadian Journal of Earth Sciences*, 26(7):1440–1452, 1989.

R.A. Kostaschuk and M.A. Church. Macroturbulence generated by dunes: Fraser river, Canada. *Sedimentary Geology*, 85:25–37, 1993.

R.A. Kostaschuk and S.A. Ilersich. *Relations between dune migration and sediment transport: Fraser River estuary.* River Geomorphology, 1995.

R.A. Kuhnle, J.K. Horton, S.J. Bennett, and J.L. Best. Bed forms in bimodal sandgravel sediments: laboratory and field analysis. *Sedimentology*, 53(3): 631–654, 2006.

M. R. Leeder. *On the Interactions between Turbulent Flow, Sediment Transport and Bedform Mechanics in Channelized Flows.* Blackwell Publishing Ltd., Oxford, UK., 2009.

D.A. Lyn. Turbulence measurements in openchannel flows over artificial bed forms. *Journal of Hydraulic Engineering*, 119(3):21, 1993.

T.B. Maddux, Nelson J.M., and S. R. McLean. Turbulent flow over three-dimensional dunes: 1. free surface and flow response. *Journal of Geophysical Research*, 108:20, 2003a.

T.B. Maddux, Nelson J.M., and S. R. McLean. Turbulent flow over three-dimensional dunes: 2. fluid and bed stresses. *Journal of Geophysical Research*, 108:17, 2003b.

M. Mancini and G. Menduni. Comportamenti di alvei granulari in condizioni di moto vario. In *Atti del Seminario su Modelli dei Fenomeni Idraulico Fluviali, Bologna*, 1986.

S. R. McLean. The stability of ripples and dunes. *Earth-Science Reviews*, 29: 131–144, 1990.

S. R. McLean, S.R. Wolfe, and J.M. Nelson. Turbulence structure over two-dimensional bed forms: Implications for sediment transport. *Journal of Geophysical Research*, 99(C6):12, 1994.

S. R. McLean, Nelson J.M., and R.L. Shreve. *Flow-sediment interactions in separating flows over bedforms-Coherent Flow Structures in Open Channels.* 1996.

S. R. McLean, S. Wolfe, and J.M. Nelson. Spatially averaged flow over a wavy boundary revisited. *Journal of Geophysical Research*, 104:15, 1999a.

S. R. McLean, S.R. Wolfe, and J.M. Nelson. Predicting boundary shear stress and sediment transport over bed forms. *Journal of Hydraulic Engineering*, 125:12, 1999b.

C. Mendoza and H. W. Shen. Investigation of turbulent flow over dunes. *Journal of Hydraulic Engineering*, 116(4):19, 1990.

D. Mohring and J.D. Smith. Predicting the migration rates of subaqueous dunes. *Water*, 32(10):3207–3217, 1996.

H. Morvan, D. Knight, N. Wright, X. Tang, and A. Crossley. The concept of roughness in fluvial hydraulics and its formulation in 1d, 2d and 3d numerical simulation models. *Journal of Hydraulic Research*, 46:191–208, 2008.

J.M. Nelson and J.D. Smith. Mechanics of flow over ripples and dunes. *Journal of Geophysical Research*, 94:8146–8162, 1989.

J.M. Nelson, S. R. McLean, and S.R. Wolfe. Mean flow and turbulence fields over two-dimensional bed forms. *Water Resources Research*, 29:3935–3953, 1993.

J.M. Nelson, M.W. Schmeeckle, R. L. Shreve, and S. R. McLean. *Sediment entrainment and transport in complex flows in River, coastal, and estuarine morphodynamics*. Springer-Verlag, Berlin, 2001.

F. N. Nnadi and K. C. Wilson. Bed-load motion at hight shear stress: Dune washout and plane-bed flow. *Journal of Hydraulic Engineering*, 121:7, 1995.

H. J. M. Ogink. Hydraulic roughness of single and compound bed forms. Technical report, Delft Hydraulics, 1988.

A. Paarlberg. *Modeling dune evolution and dynamic roughness in rivers*. PhD thesis, University of Twente, 2008.

G. Parker. 1d sediments transport morphodynamics with applications to rivers and turbidity currents-chapter 22: Morphodynamics of recirculating and feed flumes, November 2004.

G. Parker and M. H. Garcia. River, coastal and estuarine morphodynamics:rcem 2005. In *RCEM 2005*, 2006.

G. Parker and P. Wilcock. Sediment feed and recirculating flumes: a fundamental difference. *Journal of Hydraulic Engineering*, 119(11):1192–1204, 1993.

D.R. Parsons, J.L. Best, O. Orfeo, R.J. Hardy, R. Kostaschuk, and S.N. Lane. Morphology and flow fields of three-dimensional dunes, rio paran?,argentina: Results from simultaneous multibeam echosounding and acoustic doppler current profiling. *Journal of Geophysical Research*, 110:9, 2005.

J.J. Peters. Discharge and sand transport in the braided zone of the Zaire estuary. *Netherlands Journal of Sea Research*, 12:273–292, 1978.

Y. Raslan. *Geometrical properties of dunes.* PhD thesis, Colorado State University, Fort Collins., 1991.

A. J. Raudkivi. Bed forms in alluvial channels. *Journal of Fluid Mechanics*, 26: 507–514, 1966.

A. J. Raudkivi. *Loose Boundary Hydraulics*. A.A. Balkema, Rotterdam, 1998.

K.J. Richards. The formation of ripples and dunes on an erodible bed. *Journal of Fluid Mechanics*, 99:597–618, 1980.

A. Robert and W. Uhlman. An experimental study on the rippledune transition. *Earth Surface Processes and Landforms*, 26(6):615–629, 2001.

J.E. Roden. *The sedimentology and dynamics of mega-dunes, Jamuna river, Bangladesh*. PhD thesis, University of Leeds, 1998.

R.J. Schindler and A. Robert. Flow and turbulence structure across the ripple-dune transition: an experiment under mobile bed conditions. *Sedimentology*, 52(3):627–649, 2005.

G. Seminara. Effect of grain sorting on the formation of bedforms. *Applied Mechanics Reviews*, 48:15, 1995.

G. Seminara and P. Blondeaux. *River, coastal, and estuarine morphodynamics.* Springer-Verlag, Berlin, 2001.

H. W. Shen, A. S. Harrison, and A. S. Mellema. Temperature and missouri river stages near omaha. *Journal of the Hydraulics Division*, 104(1):1–20, 1978.

A. Shields. *Anwendung der Aenlichtkeitsmechanik und der Turbulenzforschung auf die Geschiebebewegung.* PhD thesis, Preussische Versuchsanstalt f???r Wasserbau und Schiffbau, Berlin, 1936.

J. B. Southard. Experimental determination of bed-form stability. *Annual Review of Earth and Planetary Sciences*, 19:423, 1991.

J.B. Southard and L.A. Boguchwal. Bed configuration in steady unidirectional water flows; part 2, synthesis of flume data. *Journal of Sedimentary Research*, 60(5):658–679, 1990.

N. Struiksma. Celerity and deformation of bed perturbation travelling over a non-erodible layer. Technical report, Delft Hydraulics, 1985.

A.N. Sukhodolov, J. J. Fedele, and B.L. Rhoads. Structure of flow over alluvial bedforms: an experiment on linking field and laboratory methods. *Earth Surface Processes and Landforms*, 31:1292–1310, 2006.

A.P. Tuijnder. *Sand in short supply : modelling of bedforms, roughness and sediment tansport in rivers under supply-limited conditions.* PhD thesis, University of Twente, 2010.

A.P. Tuijnder, J.S. Ribberink, and S.J.M.H. Hulscher. An experimental study into the geometry of supply-limited dunes. *Sedimentology*, 56:6 (1713–1727), 2009.

J. Udo, M. Bakker, and P. Termes. Sobek-model rijn; hydraulische calibratie. Technical report, HKV Consultants, Lelystad, the Netherlands, 2007.

J.H. Van Den Berg and A. Van Gelder. A new bedform stability diagram, with emphasis on the transition of ripples to plane bed in flows over fine sand and silt. *Special publication of the International Association of Sedimentologists*, 17:11–21, 1993.

C.F. Van der Mark. *Asemi-analytical form drag model for river bedforms.* PhD thesis, University of Twente, Enschede, Netherlands, 2009.

J.J. Van der Zwaard. Roughness aspects of sand transport over fixed bed. In *XVth IAHR-Congress 1973*, 1974.

M. C.L.C. Van Mierlo and J.C.C. de Ruiter. Turbulence measurements above artificial dunes. Technical report, Delft Hydraulics, Delft, Netherlands, 1988.

L.C. van Rijn. Sediment transport, first part: Bed load transport. *Journal of Hydraulic Engineering*, 110(10):1431–1456, 1984a.

L.C. van Rijn. Sediment transport, third part: Bed forms and alluvial roughness. *Journal of Hydraulic Engineering*, 110(12)(Rep. No. S 487-part III):1733–1754, 1984b.

V. Vanoni and L. S. Hwang. Relation between bed form and friction in streams. *Journal of the Hydraulics Division*, 93(HY3):121–144, 1967.

V. A. Vanoni and N. H. Brooks. Laboratory studies of the roughness and suspended load of alluvial streams. Technical report, Sedimentation Laboratory, California Institute of Technology, Pasadena, Calif., 1957.

D.J. Varnes, the International Association of Engineering Geology Commission on Landslides, and Other Mass Movements. Landslide hazard zonation: A review of principles and practice. natural hazards. Technical Report 3, UNESCO, Paris, France, 1984. 63p.

J.G. Venditti. Turbulent flow and drag over fixed two-dimensional and three-dimensional dunes. *Journal of Geophysical Research-Earth Surface*, 112:21, 2007.

J.G. Venditti, M.A. Church, and S.J. Bennet. On the transition between 2d and 3d bedforms. *Sedimentology*, 52:1343–1359, 2005a.

J.G. Venditti, M.A. Church, and S.J. Bennet. Bedform initiation from a flat sand bed. *Journal of Geophysical Research-Earth Surface*, 110:19, 2005b.

P. Villard and R. Kostaschuk. The relation between shear velocity and suspended sediment concentration over dunes: Fraser estuary, canada. *Marine Geology*, 148:71–81, 1998.

C.A. Vionnet and S.G. Serra. Migration of large dunes during extreme floods of the paran river, argentina. In *River, Coastal and Estuarine Morphodynamics: RCEM 2005*, 2005.

S. Wang and W.R. White. Alluvial resistance in transition regime. *Journal of Hydraulic Engineering*, 119(6):558, 1993.

W.R. White, R. Bettess, and E. Paris. Analytical approach to river regime. *Journal of the Hydraulics Division*, 108(10):1179–1193, 1982.

J. H. A. Wijbenga. Flow resistance and bedform dimensions for varying flow conditions-a literature review: main text and annexes. Technical report, Delft Hydraulics, 1990.

J. H. A. Wijbenga and G.J. Klaassen. *Changes in bedforms dimensions under unsteady flow conditions in a straight flume.* Special publication of the International Association of Sedimentologist-Blackwell scientific publications, 1993.

J. H. A. Wijbenga and A.R. Van Nes. Flow resistance and bedform dimensions for varying flow conditions; results of flume experiments with flood waves. Technical report, Delft Hydraulics, Delft, the Netherlands., 1986.

J. H. A. Wijbenga, M.T. Duits, and van Noortwijk J.M. Parameter optimisation for two-dimensional flow modelling. In *Hydrodynamics '98, Copenhagen, Denmark*, 1998.

A. Wilbers. *The development and hydraulic roughness of subaqueous dunes.* Utrecht, Utrecht (Netherlands), 2004.

A.W.E. Wilbers and A.W.M. Ten Brinke. The response of subaqueous dunes to floods in sand and gravel bed reaches of the dutch Rhine. *Sedimentology*, 50: 1013–1034, 2003.

P.R. Wilcock. Critical shear stress of natural sediments. *Journal of Hydraulic Engineering*, 119:4, 1993.

P.R. Wilcock and B.W. McArdell. Partial transport of sand/gravel sediment. *Water Resources Research*, 33(1):235, 1997.

P.R. Wilcock and J. B. Southard. Bed load transport of mixed size sediment: fractional transport rates, bed forms, and the development of a coarse bed surface layer. *Water Resources Research*, 25(7):1629–1641, 1989.

J.J. Williams, P.S. Bell, and P.D. Thorne. Field measurements of flow fields and sediment transport above mobile bed forms. *Journal of Geophysical Research*, 108:36, 2003.

M.S. Yalin. Geometrical properties of sand waves. *Journal of the Hydraulics Division*, HY5:105–119, 1964.

M.S Yalin. *Mechanics of sediment transport.* Pergamon Press, Braunschweig, Germany, 1973.

M.S. Yalin. On the determination of ripple geometry. *Journal of Hydraulic Engineering*, 111(8):8, 1985.

M.S. Yalin. *River Mechanics.* Elsevier, New York, 1992.

M.S. Yalin and A.M.F. da Silva. Fluvial processes solutions manual. Technical report, International Association of Hydraulic Engeneering and Research, Delft, The Netherlands., 2001.

J.Y. Yoon and V.C. Patel. Numerical model of turbulent flow over sand dune. *Journal of Hydraulic Engineering*, 122(10):9, 1996.

N.S. Znamenskaya. Changes in forms of river bed sand dunes with the passage of a flood. *Translated in Soviet Hydrology*, 1963.

Acknowledgements

At first, I would like to thank the professors Enio Paris and Andreas Dittrich for the time they have devoted to my thesis, for their patience and for their suggestions and corrections that have allowed me to improve my work. A heartfelt thanks goes to the two coordinators of international PhD, without whom this beautiful reality of international PhD would not be born, Prof. Claudio Borri and Prof. Udo Peil. I would also like to thank the comrades of Department. of Civil and Environmental Engineering in Florence and also Dr.Ing. Katinka Koll and Dr.Ing. Jochen Aberle, for their availability and their help in every moment of my work in Braunschweig. I also thank Prof. Luigi Montefusco for his helpful advice and availability in the last part of my work. Thanks to the technicians of the laboratory of Hydraulics, University of Florence, Muzio Mascherini and Mauro Gioli, for their invaluable assistance. Many thanks to the secretariat of the doctorate, German and Italian, for the organization of our journey. A special thanks to my fellow travellers, Italians and Germans, who shared with me the experience of the adventure of the doctorate, especially Giuseppe, Laura and "Ninni". Finally, thanks to my family and my friends, who were close to me even when the path was uphill. The biggest thanks goes to my daughter Letizia and to my wife Elisa who fill with joy my days and give me the strength and encouragement to keep going on.

List of Figures

List of Tables